Quarks and Hadrons on the Lattice

Graham John Boyd

Submitted in partial fulfilment of the requirements
for the degree of Master of Science
at the
University of Cape Town

December 17, 1989

Contents

List of Figures

List of Tables

Chapter 1

Introduction

> To be sure, it has been pointed out that the introduction of a space-time continuum may be considered as contrary to nature in view of the molecular structure of everything which happens on a small scale. It is maintained that perhaps the success of the Heisenberg method points to a purely algebraic method of description of nature, that is the elimination of continuum functions from physics. Then, however, we must also give up, by principle, the space-time continuum. It is not unimaginable that human ingenuity will some day find methods which will make it possible to proceed along such a path. ...Albert Einstein (1936)

Quantum Chromodynamics has emerged over the past two decades as the only description of the strong interaction without any manifest defects. It describes the dynamics of quarks and gluons in terms of a local gauge theory based on the $SU_c(3)$ colour symmetry group. It has complemented the success of the other local gauge theory, the electroweak theory of Glashow, Weinberg and Salam [34].

In the Fifties and Sixties a disordered plethora of 'elementary' particles was known. Order was imposed when, extending the SU(2) isospin symmetry between protons and neutrons to $SU_F(3)$ flavour symmetry, Gell-Mann and Ne'eman [67] showed that some of the representations of the group exactly fitted the quantum number structure of the observed hadrons. This led to the prediction of an as yet unobserved hadron to complete the spin $\frac{3}{2}$ decuplet; when the Ω^- was discovered in 1963 in bubble-chamber photographs at Brookhaven, the possible validity of SU(3) was realised.

The next step came in 1964, when they pointed out that all of the representations used to describe the hadrons could be generated by combinations of the fundamental representations of SU(3). Gell-Mann named the entities in this representation 'quarks,' taken from the book *'Finnegan's Wake'* by James Joyce. This is a rather idiosyncratic use of a German word meaning 'curds' or 'slop'. The use of an unusual name for these entities was apt; in order to construct a baryon from three quarks, each had to have some unusual quantum numbers!

Each had baryon number $\frac{1}{3}$ and an electric charge of $\frac{1}{3}$ or $\frac{2}{3}$ in order to satisfy the formula relating charge to isospin and baryon number[1]. Further, to insure that the baryons and mesons had spin $\frac{1}{2}$ and 1 respectively, the quarks were required to have spin $\frac{1}{2}$.

Due to the complete failure to observe free quarks, the physics community was somewhat sceptical about the physical existence of quarks. Quarks were regarded as useful mathematical entities with no physical reality.

[1] $\frac{Q}{e} = (\frac{B}{2} + I_3)$

We have now, from the SLAC and CERN deep inelastic lepton scattering experiments [188], evidence for the existence and correct quantum numbers of both the quarks and the gluons. Using charged leptons, measurements of the structure function F_2 have been made. The measured values were found to be approximately independent of the scattering energy; ie., they were approximately scale invariant. This 'scaling' implies that the constituents of the hadrons are point-like. The neutrino-scattering measurements of F_1 also show point-like constituents.

The measurement of F_3 using the neutrino data [188], shows that the difference between the number of quarks and anti-quarks in the nucleon is 2.81 ± 0.16; consistent with having three valence quarks in the nucleon. Using the Adler sum rule, it was shown that the difference between the no. of u and d quarks in the proton was 1.07 ± 0.20[21]. Finally, from the Gottfried sum rule [98] and the ratio of F_2 measured in muon and neutrino scattering, the charges on the u and d quarks were measured to be 0.64 ± 0.05 and 0.41 ± 0.09 respectively [188].

The hadrons also contain further sub-particles, the gluons. These are the gauge bosons responsible for the interaction between the quarks. The existence of the gluons was confirmed when it was shown that the quarks carry half the momentum of the hadron [22], in the infinite-momentum frame. The 3-jet e^+e^- events [217] showed that the gluons had spin 1 and parity $-$.

Although we now have much evidence indicating that QCD is a good theory of the strong interactions, it has been impossible to use QCD to make predictions from first principles. The reason for this lies in the non-Abelian nature of QCD and in the fact that the coupling is inversely proportional to the energy scale. This means that the perturbative approach, successful in QED, will only work in the high-energy regime of QCD (where some success has been achieved).

In the lower energy regime, the initial approach was via QCD-motivated models. The MIT-Bag [129] was one of the first, followed by Skyrmion models and a number of other indirect attempts.

The most successful approach so far, working from first principles and covering the entire energy spectrum, has been that of Lattice QCD. This approach was initiated by Ken Wilson of Cornell in 1974 [212]. The Lattice form of QCD is not a model, but a first principles approach to solving the theory of the strong interactions; it is a respectable regulation of the theory[2]. The lattice is merely a technique of constructing the theory of Quantum Chromodynamics in a mathematically well-defined manner.

There are three steps in the construction of the lattice version of QCD:

1. A quantum system of fields, described by an Hamiltonian $H = \int d^3x \mathcal{H}(x)$ can be treated as a statistical system, with a partition function, $Z = Tre^{-\beta H}$. This can be re-written as a path-integral:

$$Z(\beta, V) = \int [dA] e^{-\left\{\int_0^\beta \int_V d\tau\, d^3x\, \mathcal{L}[\psi(\vec{x},\tau), A(\vec{x},\tau)]\right\}} \tag{1.1}$$

$$= \int [dA] e^{-S} \tag{1.2}$$

[2]Note that the lattice is *not* automatically U-V finite. One can construct lattice models that suffer from U-V infinities, despite the finite lattice spacing and lattice size [199]. In essence, this is a statement of the fact that there is nothing to prevent an integral over a compact momentum space from diverging; hence simply restricting the momentum space does not guarantee finite integrals.

where β has been sliced into infinitesimal elements $d\tau$ to provide the fourth integral. This is now a path-integral in Euclidean space-time, where 'time' has been Wick rotated, $\tau = it$. S is the action of the system. Note also that time represents the inverse of the temperature of the statistical system [162]. The key point to bear in mind is that Lattice QCD does not have any real time axis; as yet, no questions involving real-time, finite temperature can be answered by the lattice approach. Thus the path integral and statistical mechanics approaches are equivalent, with the exponential of the action playing the role of the Boltzmann factor. The Green functions of field theory are equivalent to the correlation functions of a statistical system.

2. Replace the continuum with a discrete lattice. Usually, the imaginary time axis is Wick rotated, giving an Euclidean, rather than the usual Riemannian, space-time. There are two types of lattice in general use:

   - All 4 dimensions are discrete; used in the Lagrangian formulation [212].
   - The time dimension is left continuous, while the 3 space dimensions are discrete; used in the Hamiltonian formulation [141].

   There are two factors, not expected for any a priori reason, that have made the lattice approach relatively promising. Firstly, small lattices are already giving fairly interesting results. Secondly, the Callan-Symanzik relation (see page 25) connects the scale-change (change in the lattice spacing) and the coupling strength to a good approximation[3]. Thus the calculations are nearing the continuum limit.

3. The final step is to replace the vector potential A_μ by elements of the gauge group:

$$U_{ij} = e^{-i(x_i - x_j)^\mu A_\mu(\frac{x_i + x_j}{2})}$$

   where $x_{(i,j)}$ represents adjacent lattice sites i and j, and the value of A_μ at the mid-point of the link joining the two sites is used.

It can be seen from this that the particles will be defined on the sites, and the gauge fields on the links between the sites. The next simplest object is the plaquette, the smallest possible square of 4 sites and the links joining them. It will be shown later that the plaquette represents the energy density of that region (see page 19.) For example, the field strength in the x direction is found from plaquettes in the xt plane.

A feature useful for QCD is that the lattice generates confinement in the strong coupling limit. Via the Callan-Symazik relation, the strong coupling limit is yielded by a lattice with a large lattice spacing.

In fact, even QED is confined on a coarse lattice! The free theory is only recovered when the lattice spacing (ie., coupling constant) is sufficiently small. The results giving QED confinement have been questioned recently by calculations using non-compact gauge actions; these have not found confinement for QED at any value of the coupling (see section 3.3.2).

Although the lattice is ideally suited to investigations in the strong coupling limit, in which perturbation theory cannot be used, it has also been used in the perturbative regime.

[3] To be accurate, one still needs to use the non-perturbative beta-function; there have been some calculations of this on the lattice recently.

For example, a recent paper [52] calculated the renormalisation coefficients for the energy-momentum tensor in perturbative lattice QED, and showed that the correct anomoly was obtained.

With infinitely many degrees of freedom, field theory is analogous to statistical mechanics. Thus mapping the phase diagram of the equivalent statistical theory leads to an understanding of the field theory. The phase transitions (eg. confined to deconfined) are obviously especially interesting; also, at the critical points the system gains long-range correlations; the lattice origins of the system have negligible effect, and the continuous symmetries of the field theory are re-established.

This gives the impression that QCD is nearly solved; however, there is still dissatisfaction, with both the Lattice approach and QCD itself. Jaffe [128] feels that a deeper meaning should be found in confinement, and that the proof and understanding of it should not be left to a CRAY! There is some activity to prove confinement in a stronger sense; for example, a recent paper [177] shows that, with Dirac quantisation, the Weyl group forbids the propagation of gauge non-singlets, forcing confinement upon the theory.

Furthermore, no satisfactory way has yet been found to put fermions onto a lattice. This has been one of the major stumbling blocks for LQCD, since quarks are manifestly fermions. It is one of the reason for the slow progress in full LQCD with dynamical fermions

QCD itself, as part of the standard model, suffers from the problems of having too many free parameters, and leaving too many questions unanswered, to be the final theory of everything.

The Lattice approach still remains, though, one of the most promising means of determining whether or not QCD really is the theory of the strong interaction; of understanding the dynamics involved when the coupling strength is high; the origins of confinement; and the nature of chiral symmetry breaking (or why the proton mass is much larger than the pion mass).

1.1 Overview of the Thesis

There is a short introduction to the ideas of lattice theory, followed by an equally brief look at pure gauge QCD on the lattice. More details for either of these may be found in the references cited in each section, as well as in [143].

The bulk of this work deals with the problems encountered in placing fermions on to the lattice, and the techniques used for this purpose. The Nielsen-Ninomiya theorem is introduced, with a detailed treatment thereof relegated to an appendix. The two main fermion techniques, due to Wilson (1974); and Kogut and Susskind (1975) are dealt with in some detail. This is followed by a discussion of the construction of hadrons on the lattice, using either Wilson or Kogut-Susskind fermions.

There is a chapter covering the algorithms used in numerical simulations of lattice QCD, with some examples illustrating them.

The thesis concludes with a discussion of the results obtained thus far on the hadron spectrum, in both the quenched approximation as well as those obtained using dynamical quarks.

Chapter 2

Introduction to Lattice Formalism.

2.1 General Conventions and Notations

μ, ν, etc.	Greek letters used to label a component of a space vector, and to indicate a vector of length a in that direction: $x + \mu \equiv x + a\hat{e}_\mu$.
i, j	Roman letters are used for colour indices, and to label specific sites.
N	Lattice size in terms of the number of sites; in cases where the lengths are unequal, each is specified.
x	Used to count lattice sites. $x \in \boldsymbol{Z}$ usually.
t, τ	Strictly, $\tau = it$; however, t is often used to represent the Euclidean time in those cases in which it is obvious whether it is Euclidean or Riemannian time. It is also the inverse temperature in lattice QCD. t is also used, in the chapter on molecular dynamics, to represent the fictitious time.
a	The physical distance between lattice sites. Quantities on a lattice are measured in units of a.
β	Lattice coupling constant, $\beta = \frac{2N}{g^2}$ for SU(N).
$U(x, x+\mu)$	Gauge Field on a specific link, from the site x to $x + \mu$. An element of the fundamental representation of the gauge group. Also written $U_\mu(x)$ and $U_{\mu x}$.
U_p	Product of the gauge fields involved in traversing an elementary plaquette (see fig. 3.1).
dU	Haar measure for the gauge group in question.
$[dU]$	Product of the Haar measure for each link in the lattice, $\prod_{x,\mu} dU_\mu(x)$.
ψ, χ	Fermion variables; elements of the Grassmann algebra.
$[d\chi]$	Product of the Grassmann measure for each variable in the integrand; $\prod_{x,\mu} d\chi(x)$.
Z	The partition function.
$S_{\mathrm{G,F}}$	The gauge and fermion actions respectively.
$F^{\leftarrow}$	The inverse of a homomorphism F between two spaces, or the inverse function if written as $F^{\leftarrow}(x)$.

2.2 Construction of a Lattice

A lattice is a set of points $\vec{x} = (x_1, \cdots, x_d)$ defined in a vector space $\Re^d$. The most common restriction on the set is to define the points to be on the vertices of hypercubes in the space,

with sides of length a_i in the i^{th} direction[212,141]. Hence the point $x_i = a_i n_i$, where $n_i \in \boldsymbol{Z}$. This is more commonly written with x integer; in other words, one writes $a_i x_i$ for the physical value of x_i. I will abide by this convention; hence, unless otherwise stated, any x is integer, and must be multiplied by a to get a physical length. One commonly chooses units such that $a = 1$, thus dropping it from the equations completely.

Note that a is the only parameter in Lattice QCD with dimension. All other quantities are given in terms of this unit of length. For example, mass is given as ma, and one needs to find the physical value of a to get the corresponding value for m.

There have been many other proposals in the literature for the basic polygon to use for tessellating the vector space, with the lattice sites defined on the vertices. For example, the triangle [123] and the hexagon [59], or body-centred hypercubic [57]. There have even been attempts at putting the sites at random positions[62,88,56], in the hope that this would reduce the problem with fermion doubling (discussed in chapter 5.2.)

A general hypercubic lattice will have N_i points, with spacing a_i in the i direction. The length will then be $L_i = a_i N_i$ and the volume of the lattice will be $V = \prod_{i=1}^{d} a N_i$. Hence the total number of sites will be N^d. One can define a link between any two adjacent lattice sites; the number of these nearest neighbour links will be $dN^d - dN^{d-1}$ (without toral boundary conditions), and dN^d with, since each site will give d links in the positive direction, less the number of links from each of the surfaces.

The standard choice for the lattice spacing is to either make $a_i = a \forall i$, or to have the temporal spacing differ. This gives an asymmetric lattice, with asymmetry factor $\xi = \frac{a_\sigma}{a_\tau}$. Asymmetric lattices are used in finite temperature lattice gauge theory.

2.3 Lattice Fourier Transform.

In infinite continuous space, a Fourier Transform can be defined according to standard procedures, using the definitions of a Fourier Series [16]. One can also define a Fourier Transform in a discrete space such as the lattice.

Consider an infinite lattice, with a function $f(x)$ defined at each point x. From the Heisenberg uncertainty relation, $\Delta x \Delta p \geq 1$, we know that if the shortest possible wavelength is $\lambda \sim a$, the largest possible momentum is $p \sim \frac{1}{a}$. Thus the lattice gives a large momentum, or ultra-violet, cut-off[1]. It is equivalent to take p, and any function $f(p)$, to be equal to the continuum function in the range $p \in (-\frac{\pi}{a}, \frac{\pi}{a},]$ and zero elsewhere.

The Fourier Series of a function $\tilde{f}(p)$ is defined to be:

$$\tilde{f}(p) = \sum_n c_n e^{in\pi\frac{p}{L}} \tag{2.1}$$

$$c_n = \frac{1}{2L}\int_{-L}^{L} \tilde{f}(p) e^{in\pi\frac{p}{L}} \tag{2.2}$$

Taking p to have period $2L$, one gets $L = \frac{\pi}{a}$, with $n = x$, a lattice site with $x \in \boldsymbol{Z}$. If we also identify c_x with $f(x)$ we get the Fourier Transform:

$$\tilde{f}(p) = a^4 \sum_x f(ax) e^{ipxa} \tag{2.3}$$

[1] As mentioned in the introduction, the lattice momentum integrals are not constrained to be finite, however.

With inverse transform:

$$f(x) = \int_{\frac{-\pi}{a}}^{\frac{\pi}{a}} \frac{d^4p}{(2\pi)^4} \tilde{f}(p) e^{-ipxa} \tag{2.4}$$

Where the integral restricted to the range $|p| \leq \frac{\pi}{a}$ is the same as the infinite integral, due to the momentum cutoff of the lattice on the function $\tilde{f}(p)$.

The Fourier transform $\tilde{f}(p)$ is only defined if $f(x)$ is integrable in a finite region, and if convergence of the integral implies that $f(x) \to 0$ as $x \to \infty$.

Using the lattice Fourier transform one can also define the delta funtions on the lattice:

$$a^4 \sum_x e^{ipxa} = \delta^4(p) \tag{2.5}$$

$$\int_{\frac{-\pi}{a}}^{\frac{\pi}{a}} \frac{d^4p}{(2\pi)^4} e^{-ipxa} = \delta^4(ax) = \frac{1}{a^4}\delta^4(x) \tag{2.6}$$

2.4 The Metric and other properties of the 4-space.

The usual metric in pseudo-Riemannian space-time is the one with $\mathrm{Tr} g^{\mu\nu} = 2$ or -2. This is an indefinite metric, ie. the length of a vector in the metric space can be negative. The length of a vector $x^\mu = (x_0, \vec{x})$ is defined as $x^\mu x_\mu = x_0^2 - \vec{x}^2$ for $\mathrm{Tr} g^{\mu\nu} = -2$ and $x_\mu = g_{\mu\nu} x^\nu$.

On the Lattice, the usual choice is Euclidean Minkowski space-time, defined with $g^{\mu\nu} = g_{\mu\nu} = \delta^\mu$ and with $\mathrm{Tr} g^{\mu\nu} = 4$. The coordinate vector is defined as $x^\mu = (\vec{x}, x_4)$ where $x_4 = ix_0$. Then the length of a vector is written $x^2 = x_\mu x^\mu = \vec{x}^2 + x_4^2$.

In order to put the Dirac Equation onto the Lattice, a choice of the Dirac gamma matrices must be made. Now these satisfy the anticommutation relation $\{\gamma^\mu, \gamma^\nu\} = 2g^{\mu\nu} \otimes \mathbb{1} = 2\delta^{\mu\nu} \otimes \mathbb{1}$ on a Euclidean Lattice. Thus the square of a γ matrix is positive, hence all are Hermitian; unlike those defined in pseudo-Riemannian space-time, where either the temporal or the spatial γ matrices are anti-Hermitian.

We can construct our Euclidean γ matrices from the standard Riemannian γ matrices (ex Bjorken and Drell) as follows:

$$\begin{aligned} \gamma_{4_E} &= \gamma_{0_R} = \begin{pmatrix} \mathbb{1} & 0 \\ 0 & -\mathbb{1} \end{pmatrix} \\ \vec{\gamma}_E &= -i\vec{\gamma}_R = \begin{pmatrix} 0 & -i\sigma \\ i\sigma & 0 \end{pmatrix} \end{aligned} \tag{2.7}$$

where

$$\sigma_1 = \begin{pmatrix} 0 & 1 \\ 1 & 0 \end{pmatrix} \quad \sigma_2 = \begin{pmatrix} 0 & -i \\ i & 0 \end{pmatrix} \quad \sigma_3 = \begin{pmatrix} 1 & 0 \\ 0 & -1 \end{pmatrix} \tag{2.8}$$

Also

$$\gamma^5 = \gamma_5 = \gamma_1\gamma_2\gamma_3\gamma_4 = \begin{pmatrix} 0 & \mathbb{1} \\ \mathbb{1} & 0 \end{pmatrix} \tag{2.9}$$

This limits our choice of spaces to even-dimensioned ones. This is because the γ_5 matrix commutes with the γ_μ; it is not a linearly independant matrix, since the γ_μ completely span the space.

Chapter 3

Pure Glue on the Lattice

This chapter is intended as a brief introduction to the methods of putting the gluonic sector of QCD onto the lattice. For more details, one of the many excellent reviews may be consulted [192].

The general QCD action consists of the gluonic and fermionic parts, $S_{\rm QCD} = S_{\rm G} + S_{\rm F}$. Let us consider the partition function, eqn. 1.2, with only the gluonic contribution. This is [8]

$$S_{\rm G} = -\frac{1}{4} F_a^{\mu\nu}(x) F^a_{\mu\nu}(x)$$

where

$$F_a^{\mu\nu}(x) = \partial^\mu A_a^\nu(x) - \partial^\nu A_a^\mu(x) + g f_{abc} A_b^\mu(x) A_c^\nu(x)$$

with $A_a^\nu(x)$ being the components of the vector potential, a, b, c are octet colour indices, μ, ν are 4-vector Lorentz indices, f_{abc} is an SU(3) structure function and g is the QCD coupling.

3.1 Local Gauge Invariance, Connections

Before finding a lattice equivalent for the gluonic action, let us consider how the $F_a^{\mu\nu}(x) F^a_{\mu\nu}(x)$ term arises from the principle of local gauge invariance in the continuum.

Local Gauge Invariance restricts one to using quantities that are invariant under an arbitrary colour transformation at each point in space-time. Since one may then be using different colour coordinates at each point, one needs a way of connecting the different reference frames between two separate points, say a and b. The connection enables one to parallel transport[1] a vector from a to b. This is essentially re-writing the vector in the coordinate system at b, allowing one to compare it with another at b. The connection may depend on the path taken from a to b, hence it must be constructed from infinitesimal elements. The infinitesimal connection for moving from a point x in spacetime to $x + dl$ (where dl has components dx^μ) is given in terms of the vector potential by

$$U(x, x+dx) = e^{igT^a A_{a\mu}(x) dx^\mu} \tag{3.1}$$

$$\approx 1 + igT^a A_{a\mu}(x) dx^\mu \tag{3.2}$$

[1] Parallel Transport of a vector means taking a vector along a path, in a space in which the basis vectors may change with position, in such a way as to keep the angle between the vector and the tangent to the path constant. [6].

This is needed, for example, when trying to find the difference between the values of a vector field at two different points, in order to construct the derivative — hence the covariant derivative[2], in which one parallel transports the value at x to $x + dx$ by multiplying with the connection before taking the difference.

The connection for a finite path Γ from points x to y can then be constructed by taking the product of the infinitesimal connections along the path;

$$U(x, y; \Gamma) = \mathrm{P} \prod_{\Gamma} e^{igA.dl} \tag{3.3}$$

which can be re-written as a path integral by using the Baker-Campbell-Hausdorff formula [190], and ignoring the terms of higher order in dl;

$$U(x, y; \Gamma) = \mathrm{P} \left[e^{ig \int_{\Gamma} A.dl} \right] \tag{3.4}$$

where the P indicates path-ordering.

Now consider the connection for a closed path, $U(x, x; \Gamma)$ in the $\mu\nu$ plane of the lattice, with the path chosen to be the perimeter of an elementary plaquette traversed in a clockwise direction;

$$U(x, x; \Gamma_{\mathrm{plaq}}) = e^{igA(x).a_\mu} e^{igA(x+\mu).a_\nu} e^{-igA(x+\mu+\nu).a_\mu} e^{-igA(x+\nu).a_\nu} \tag{3.5}$$

Showing that, in the limit that $a \to 0$, the above tends towards the continuum term in the QCD action has become a part of some texts; see, for example, Cheng and Li, [6], or [19]. It was derived in detail in [143].

There has been some doubt expressed about the suitability of this action except at the limiting point $a = 0$, something which is further discussed in the section on non-compact actions, section 3.3.2. Part of the problem may come from the fact that one is, in effect, using Stokes' theorem to relate the line integral around a path to the surface integral within; however, this theorem does not hold true on a general manifold — much to the annoyance of those involved in General Relativity.

Furthermore, in deriving the continuum limit, one uses the Baker-Campbell-Hausdorff formula to lowest order in a; however, the lowest order term contributing to the action is of order a^4. It may well be that, in these two steps, properties (such as confinement) that may not be part of a pure glue theory are built into the pure gauge action.

3.2 Wilson Action

In LQCD, the particles live on the sites and the gauge fields on the links between the sites. Hence the first step in the construction of the gauge sector is to replace the infinitesimal

[2]The covariant derivative is:

$$\begin{aligned}
\frac{D\underset{\sim}{\lambda}}{\partial x^\nu} &= \lim_{\delta x^\nu \to 0} \frac{\underset{\sim}{\lambda}(x + \delta x^\nu) - U(x, x + \delta x^\nu)\underset{\sim}{\lambda}(x)}{\delta x^\nu} \\
&= \lim_{\delta x^\nu \to 0} \frac{\underset{\sim}{\lambda}(x + \delta x^\nu) - \underset{\sim}{\lambda}(x)(\mathbb{1} + igA_\nu \delta x^\nu)}{\delta x^\nu} \\
&= \frac{\partial \underset{\sim}{\lambda}}{\partial x^\nu} - igA_\nu \underset{\sim}{\lambda}
\end{aligned}$$

connection of the continuum with a lattice connection, dependant upon the sites to which the link is attached. This is a gauge degree of freedom connecting the colour frames at two nearest neighbour sites. The connection from x to the next site in the μ direction is denoted variously as $U_\mu(x)$; or $U_{ij}(x, x+\mu)$ or $U(x, i; x+\mu, j)$ where the i, j denote colour indices (ie., the corresponding matrix element of U) related to the sites at each end of the link. Since one returns to the same site along the same path if one travels forward along a link and then back again, the product of the connections in the forward and backward directions must yield the unit matrix; hence one gets

$$U(x+\mu, x) = U^{-1}(x, x+\mu) = U^\dagger(x, x+\mu)$$

The colour trace of the product of the links around any closed path on the lattice is gauge invariant. This can easily be seen; a gauge transformation at a site x, say V, will left-multiply the connection exiting the point, and the inverse will right-multiply the connection entering. Via the commutative nature of the trace operator, V^{-1} may be commuted until it adjoins V, yielding the unit matrix.

The first Euclidean Yang-Mills action along these lines was proposed by Wilson in 1974 [212], and is the one most commonly used today:

$$S_G = -\frac{1}{g^2} \sum_p Tr(U_p + U_p^\dagger) \tag{3.6}$$

where $\sum_p$ is a sum over elementary plaquettes (see Fig. 3.1), and

$$U_p = U_{x,x+\mu} U_{x+\mu,x+\mu+\nu} U^\dagger_{x+\nu,x+\mu+\nu} U^\dagger_{x,x+\nu}$$

Due to the trace, it is immaterial which corner of the plaquette is taken as the origin; and the inclusion of the hermitian conjugate counts both clockwise and anti-clockwise traversals of the plaquette. This is equivalent to taking the real part of the plaquette.

Since the lattice usually has a toral structure, one requires some sort of boundary condition; in general, periodic or anti-periodic boundary conditions are chosen for the lattice.

This satisfies the following neccessary requirements;

1. That the action preserves all global symmetries of the continuum action that are meaningful on the lattice.
2. That the action possesses local gauge invariance under SU(3).
3. That the action is real and positive semi-definite.
4. That the action yields the correct continuum limit.

The Wilson action per plaquette gives a measure of how far from the vacuum state ($U_p = \mathbb{1}$) the given plaquette is; it is real and positive, and is larger the farther the plaquette is from the vacuum.

Equation 3.6 corresponds to $F_{\mu\nu}$ in the continuum; $F_{\mu\nu}$ is built from the product of the infinitesimal connections involved in traversing an infinitesimal loop (TrPexp($ig \oint A.dl$) + h.c.); the lattice equivalent is built from finite connections involved in traversing the smallest possible loop on the lattice. This can be shown by simply repeating the calculation given above for the continuum.

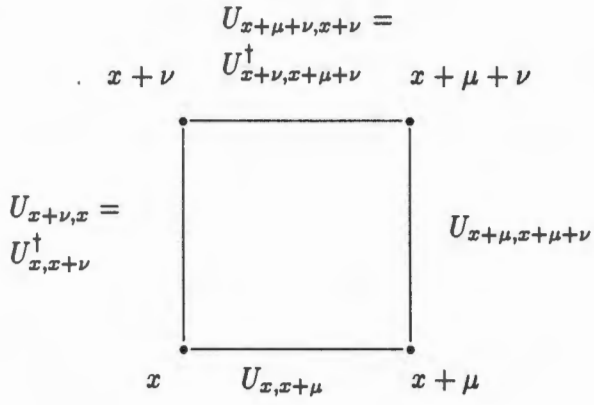

Figure 3.1: An Elementary Plaquette.

One further advantage of the lattice regulation over other methods is the fact that the integral over all gauges is finite. Thus there is no need to introduce, for example, the ghost fields and the Faddeev-Popov determinant.

3.3 Alternative Actions

3.3.1 Compact Actions

The gauge action is not unique. One can propose actions that differ from the Wilson action (whilst still using the full compact gauge group) in an attempt to improve the lattice approximation to some particular aspect of the Gauge sector of QCD, subject to the proviso that it yields the correct Yang-Mills continuum limit.

One possibility is to replace the trace by the characters of the group, the trace of the representation [81,33]. This yields the 'Fundamental-Adjoint mixed action' [81], an action with components from both the fundamental and the adjoint representations of SU(3). The couplings for each are also independent of the other. The limit of zero coupling for the adjoint sector yields the standard Wilson action, while zero coupling for the fundamental sector yields an action for the orthogonal group SO(3).

There are other actions based on the geometry of the Lie group manifold, such as those of Manton [155] and Villain [205,81]. These are useful in the continuum limit, in that they approach the limit more smoothly than the Wilson action. As mentioned earlier, the action per plaquette measures the amount by which the gauge field on the plaquette differs from the continuum. Manton suggested replacing the Wilson action by one involving the shortest

geodesic distance[3] from $\mathbb{1}$ to U_p, viz. $d(U_p)$. The Manton action is then

$$S(U) = \frac{1}{2g^2}\sum_p [d(U_p)]^2 \tag{3.7}$$

This action is, as it needs to be, gauge invariant, real, positive semi-definite, and yields the correct continuum limit. However, this action does have some problems with singularities and multi-valuedness; these problems are solved by the Villain action, in which one adds the periodicity of the group manifold to the action.

One can also use closed loops larger than the elementary plaquette, [210]. The use of lattices with non-hypercubical tesselations of space has also been investigated,

and random lattices.

3.3.2 Non-Compact Actions

A possible problem with the form of discretization of the continuum action proposed by Wilson is that confinement is a universal feature of it. In fact, even QED is confined on the lattice[4]!

This has led people to wonder whether the confinement observed on the lattice for $SU(3)$ is purely a property of QCD, or whether it is already built into the Wilson action.

In an attempt to answer this question there have been a few proposals for so-called non-compact formulations of QCD on the lattice [51,49, and the references contained therein].

In the compact formulations, one uses the full gauge group, preserving an exact gauge symmetry on the lattice, whilst approximating the gauge fields of the continuum. This exact gauge symmetry is not the same as the gauge invariance of the continuum; This is only regained in the continuum limit.

In a non-compact formulation one keeps, as near as possible, the standard continuum construction of the gauge fields, and hence an approximate form of the continuum gauge invariance. However, one then only recovers the full gauge group associated with the invariance in the continuum limit.

In is not clear yet whether the compact approach, with the group elements as variables, is a superior or inferior approach to the problem than is the non-compact when one is working at a finite lattice spacing.

As an example of a non-compact formulation, the gauge fields are placed on the links (constant over the link) and one interpolates linearly across the six plaquettes that have this link as an element. The gauge fields in the $\mu\nu$ plaquette are then given by [49]

$$A^a_\mu(\xi) = \frac{(\nu - \xi_\nu)A^a_\mu(x) + (\xi_\nu)A^a_\mu(x+\nu)}{a} \tag{3.8}$$

with $\xi_\nu \in [0, a]$. Note that the derivative of A will change abruptly across a link from one plaquette to another.

The field strength can then be built up using the standard continuum definition;

$$F^a_{\mu\nu} = \partial_\mu A^a_\nu(x) - \partial_\nu A^a_\mu(x) + g f^{bc}_a A^b_\mu(x) A^c_\nu(x) \tag{3.9}$$

[3]Since we are dealing with compact groups, there are infinitely many geodesics (similar to the surface of the Earth); hence the choice.

[4]QED in 3 dimensions is always confined; in 4 dimensions, using the Wilson action, it is confined in the strong coupling limit ($e \gg 1$) and deconfined in the weak coupling limit ($e \ll 1$), with a phase transition between these two extremes.

and the field action becomes the sum over all plaquettes of the integral over each plaquette of the square of the field strength;

$$S_G = \sum_{p\mu\nu} \frac{a^2}{2} \int d\xi_\mu d\xi_\nu (F_{\mu\nu}(x,\xi))^2 \tag{3.10}$$

In the studies that have been done using this genre of lattice action, confinement has *not* been found for QED at any coupling strength. Furthermore, for SU(2) on 10^4 [49] and 25^4 lattices, although asymptotic freedom was found, confinement was not found! This casts some doubt onto the numerous studies of confinement on the lattice using pure gauge theory in the Wilson formulation.

Two possible resolutions of this [49] are that the quarks play an essential role in the confinement mechanism, and cannot be ignored[5]; or that the non-compact formulation is closer to the continuum at a given lattice spacing, and hence in the asymptotically free phase. The latter comes from the fact that a U(1) theory is not confined, and thus corresponds to our measured U(1) theory, at any coupling.

3.4 Pure Gauge Partition Function

Using one of the above actions for the gauge partition function, one has (from eqn. 1.2)

$$Z_G = \int \{\prod_{\mu,x} dU_\mu(x)\} e^{-S_G(U)} \tag{3.11}$$

$$= \int [dU] e^{-S_G(U)} \tag{3.12}$$

where $dU_\mu(x)$ is the Left-Invariant Haar measure for the Lie Group [7,87] and $\prod_{\mu,x} = [dU]$ represents the product over all links in the lattice.

Whilst the continuum theory is infested with infinities, the lattice partition function is well defined, and yields finite results. This is due to the integral being over a compact Lie group, hence with finite volume, $\int [dU]$. The imposition of gauge invariance on the continuum measure leads to overcounting of the states, and an infinite volume which must be removed by using, for example, Faddeev-Popov ghosts.

[5]The role played by fermions on Aharanov-Bohm type phases has been investigated in the continuum, on the manifold $S^1 \times R^1$. It was found that the vacuum structure was drastically changed upon the addition of fermions to the pure gauge theory.

Chapter 4

The Renormalization Group

Physics describes particles and the local interactions that occur between them. In general, one sets up a Lagrangian to do this. This becomes problematic when one attempts to describe the collective behaviour of large numbers (perhaps of the order of 10^{23}) of these particles, despite the fact that it is the same Lagrangian with local interactions that describes the physics. The reason for this is that systems with many degrees of freedom are dominated by collective behaviour and the nature of the degrees of freedom, whilst the details of the interaction are often unimportant. The renormalization group[1] approach is a technique for dealing with large numbers of DOF.

There are many theories in physics in which quantities can be renormalised, which simply means that one can change parameters in the theory without changing the physical predictions of that theory. Some time after renormalisation was introduced, it was realised that a group structure could be associated with the successive renormalisations of a theory. Using the tools of group theory and renormalisation one is able to extract results from systems with large numbers of degrees of freedom.

One simplifies the theory by integrating out the high-momentum (small scale) degrees of freedom. This results in a renormalisation group transformation of the parameters of the theory.

The most important factor in determining the long-range physics of a system with many DOF is the correlation length, ξ. If the distance between two particles is larger than the correlation length, the particles behave independantly; if it is less, co-operative behaviour will dominate the behaviour of the particles. When the correlation length is of the order of the inter-particle spacing, one may make use of various approximations (such as perturbation theory, virial expansions, etc.); these break down when the correlation length becomes large, especially in the region of, for example, a phase transition, in which the correlation length becomes infinite.

It is just there that the renormalisation group transformations become very simple, for in the region of a phase change the Hamiltonian of the system looks the same before and after the transformation. Hence one is able to repeat the transformation, in much the same way that one, in a perturbative regime of a theory, carry out perturbation theory to very high order.

The Renormalization group approach has two objectives [214];

[1] Note that, strictly speaking, it is not a group; mathematically, it is a semi-group. However, the distinction is of little relevance here, so one usually follows convention and calls it a group.

- To reduce the number of DOF in the initial Hamiltonian ($\mathcal{H}_0$, say), usually by a constant factor (say $\frac{1}{2}$), in steps of such a size that one can compute a new Hamiltonian, $\mathcal{H}_i$, for the reduced system without the loss of essential physics. One repeats the process until the distance between the interacting 'particles' in $\mathcal{H}_i$ is larger than, or approximately equal to, the correlation length of the original system; one is then able to make the standard approximations to reduce the system to approximately 1 DOF. The one requirement for this to work is that the interactions at each stage must remain local, ie., strictly nearest neighbour.

- To explain the qualitative features of co-operative behaviour. In the Renormalization group approach this results from the iterative nature of the transformation τ between successive Hamiltonians: $\tau : \mathcal{H}_{n-1} \mapsto \mathcal{H}_n$. The repeated iterations then magnify or reduce various aspects of the local interactions in $\mathcal{H}_0$, yielding the effective interactions and behaviour of the bulk system.

  The simplest case is if τ has a fixed point $\mathcal{H}^*$, such that $\tau : \mathcal{H}^* \mapsto \mathcal{H}^*$. In general there will be more than one fixed point; this will yield domains in the space of Hamiltonians about each $\mathcal{H}^*$. One may also have an unstable fixed point, such that all transformations in a small subset of the axes of the space take one away from the fixed point. If this is defined by a one parameter manifold, then one will have a 1-parameter trajectory away from the fixed point. This may be an attractive or repulsive trajectory in itself; a local interaction with a repulsive fixed point will have an attractive renormalisation trajectory [172].

  An example of the renormalisation group approach applied to a classical theory of coupled harmonic oscillators can be found in [25]

  Turning to the specific example of QCD, there is an ultra-violet fixed point on the manifold defined by $g = 0$ in the infinite[2] dimensional coupling space. This is unstable in one direction only, and has a 1-parameter trajectory of instability moving away from the UV fixed point.

  This is an attractive trajectory; if one starts with any choice of coupling constants and performs repeated iterations of the renormalisation group transformation, the coupling constants will move closer to the renormalisation trajectory (see fig. 4.1). As can be seen in the figure, the flow lines move closer together, getting arbitrarily close to the renormalisation trajectory with each iteration.

There are two concepts that lie at the root of the renormalization group approach:

Scaling The concept of scaling, as first proposed by Widom, is that functions such as the equation of state can be written as an homogeneous function of one variable in the aymptotic region of the energy. For example, the magnetization M, temperature $t = |T - T_c|$ and magnetic field H are related by $H = M^\delta f(t/M^{1/\beta})$. The indices β and δ are constant and introduce whatever power law behaviour is required in the critical region.

Scaling is conjectured to be due to the irrelevance of all length scales at $T = T_c$, the point at which the correlation length ξ diverges. Consider a spin system — say the Ising

[2]This concept is a generalisation of the two couplings used in the mixed fundamental-adjoint action of the previous chapter; in principle, one can have infinitely many different couplings, and iterations of the renormalisation group can move one in this space, from one initial coupling to many.

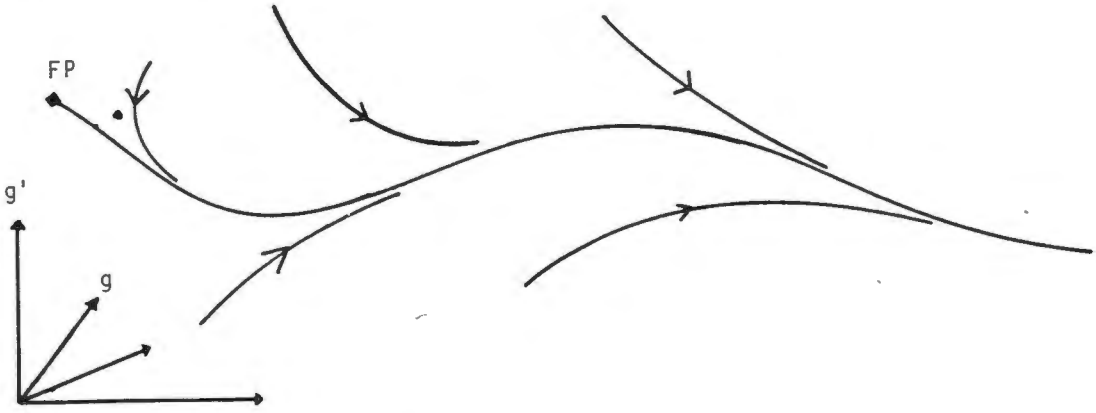

Figure 4.1: The renormalisation trajectory for QCD.

model; at this temperature, the co-operative effects will yield coherent fluctuations in the spin over all length scales. Thus the system will appear identical at all length scales, and is scale invariant. The application of this to Hadron spectroscopy is that the masses of the hadrons should be independent of the choice of coupling constant, given an arbitrary, but fixed renormalization group invariant quark mass and a fixed mass scale Λ.

Universality Universality is the independance of the scaling indices on the exact nature of the interaction. It states that all $\mathcal{H}_0$ in the domain of some $\mathcal{H}^*$ have the same behaviour in the critical region, and that this behaviour is controlled by $\mathcal{H}^*$, with the number of dimensions and the relevant symmetries playing the major role. Universality is based on the fact that behind the renormalized theories lies one, and only one, reality.

4.1 The Renormalisation Group Equations and Scaling.

Consider a theory with some dimensionless coupling constant g, a mass m, a normalization momentum κ and some cutoff Λ; one can obtain partial differential equations [9] in these variables, linking different renormalization schemes. The results obtained must be independant of the specific choice of renormalisation, cutoff etc.; this brings in scaling, since the same physics must be obtained if the cutoff is multiplied by an arbitrary constant.

The first set, the Callan-Symanzik equations link theories renormalised at $\kappa = 0$ with different, but finite, masses. The second set, the renormalisation group equations, link theories with fixed masses, but with freedom in the normalization momentum κ.

If one then renormalises the theory, (hence the coupling and any energy parameter Q), at some κ one will obtain a renormalised coupling, $g_r = g_r(\kappa)$, some function of κ. A function of the energy parameter will then depend on $\frac{Q^2}{\kappa^2}$. The coupling and other parameters must change in some prescribed way with κ, such that the physics is invariant. Thus some observable, based on a function of the coupling and some other parameter, (say $f(q,g)$) must satisfy the renormalisation group equation:

$$\kappa \frac{df}{d\kappa}(q,g) = 0 \tag{4.1}$$

Re-writing the above equation one can get

$$\left[\kappa\frac{\partial}{\partial\kappa}+\beta_{\rm fn}(g)\frac{\partial}{\partial g}\right]f=0 \tag{4.2}$$

For QCD on a finite lattice one has an ultra-violet cutoff given by the lattice spacing and an infra- red cutoff given by the size of the lattice (rather than the continuum normalization momentum κ and UV cutoff Λ). Thus requiring the physics to be independant of the lattice spacing leads to the lattice version of the renormalization group equation:

$$\left[a\frac{\partial}{\partial a}+\beta_{\rm fn}(g)\frac{\partial}{\partial g}\right]f=0 \tag{4.3}$$

with the Callan-Symanzik beta function being given by

$$\beta_{\rm fn}(g)=a\frac{\partial g}{\partial a} \tag{4.4}$$

(In this section, the function will be represented by $\beta_{\rm fn}$ and the inverse coupling by $\beta=\frac{6}{g^2}$.) The beta funtion thus gives the change in the coupling strength with a change in the length scale; hence it is the velocity of flow along the trajectory under the renormalisation group transformations (see fig. 4.1). For QCD, the beta function defined here corresponds to a non-abelian theory with an ultra-violet fixed point at $g_{bare}=0$, for[3] $\beta_{\rm fn}>0$. If some coupling is a fixed point of the Renormalisation group, say g^*, then $\beta(g)=0$; hence, given some bare coupling, $\beta_{\rm fn}$ describes the approach of g_r to g^* with a. This can be writen as a trajectory in the a–g plane by integrating in the small-g limit;

$$\begin{aligned}\frac{a(g)}{a(g_0)} &= \exp\left[\int_{g_0}^{g}\frac{dg'}{\beta_{\rm fn}(g')}\right]\\ &= \exp\left[-\frac{1}{2\beta_0 g^2}-\frac{\beta_1}{2\beta_0^2}\ln\left(g^2\right)+\frac{1}{2\beta_0 g_0^2}+\frac{\beta_1}{2\beta_0^2}\ln\left(g^2\right)\right]\end{aligned} \tag{4.5}$$

Writing

$$\Lambda_L=\frac{1}{a(g_0)}\left(\beta_0 g_0^2\right)^{\frac{\beta_1}{2\beta_0^2}}\exp\left(\frac{\beta_1}{2\beta_0^2 g_0^2}\right) \tag{4.6}$$

with Λ_L the lattice momentum scale, playing the same role as κ above, one then gets

$$a(g)\Lambda_L = \left(\beta_0 g^2\right)^{-\frac{\beta_1}{2\beta_0^2}}\exp\left[\frac{1}{2\beta_0 g^2}\right] \tag{4.7}$$

where the Callan-Symanzik beta function, for an Hamiltonian with an $SU(N)$ interaction and N_f massless fermions, is given by [10]

$$\beta_{\rm fn}(g)=\beta_0 g^3+\beta_1 g^5+\beta_2 g^7 \tag{4.8}$$

The first two terms (ie., to 2-loop level) are renormalisation scheme independant, and have been calculated using perturbation theory [130,55,195]:

$$\beta_0 = \frac{1}{(4\pi)^2}\left[\frac{11}{3}N-\frac{2}{3}N_f\right] \tag{4.9}$$

$$\beta_1 = \frac{1}{(4\pi)^4}\left[\frac{34}{3}N^2-\frac{10}{3}NN_f-\frac{N^2-1}{N}N_f\right] \tag{4.10}$$

[3]Note that some definitions include a $-$ sign in both the beta-function and the differential equation defining it.

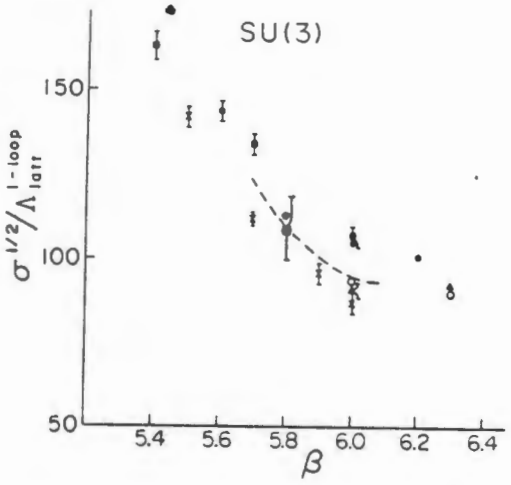

Figure 4.2: Monte Carlo results for the string tension, ex. [118]

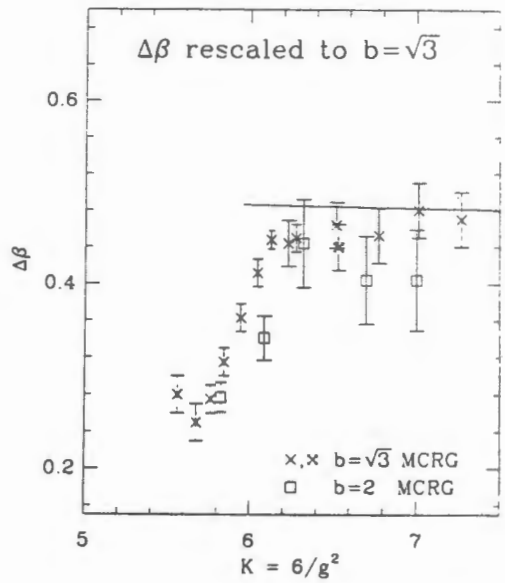

Figure 4.3: The calculations of $\Delta\beta$, with the data for $b = 2$ rescaled to $b = \sqrt{3}$. The solid line is the two-loop perturbative prediction of eqn. 4.13. Ex. [107]

To get the continuum from the lattice results one needs to remove the lattice cutoff a from the results, ie. renormalize the bare g such that the physical quantities are invariant. In the scaling regime, ie. close to the continuum limit, the above scaling relation between a and g will hold, and one can remove the lattice cutoff. This is an essential requirement for any QCD calculation.

However, once sufficient results of numbers such as the string tension (see fig. 4.2) and crossover temperature were available for a range of values of the inverse coupling β, it was found that the asymptotic scaling laws were not satisfied. The results However, whilst the coupling was not yet in the asymptotic region, it might still obey scaling under some non-perturbative beta-function, hence reflecting continuum physics. This was indicated by the fact that, whilst the string tension and crossover temperature were not in the asymptotic scaling region, both behaved in a similar fashion; hence the ratio of the two might be constant before the asymptotic region. This would then be scaling according to some other, non-perturbative beta function.

A number of people then turned towards calculating the beta function on the lattice in order to check whether or not the calculations were in the scaling regime, ie. whether or not the calculations could be used to extract continuum physics.

The function calculated on the lattice is not the beta function itself, but a related quantity $\Delta_b\beta$. The variable b corresponds to the scale change associated with each iteration of the renormalisation group, ie. $a \mapsto ba$. There are two in common use; $b = 2$ and $b = \sqrt{3}$.

The quantity $\Delta_b\beta$ corresponds to the change in β necessary to account for the change in the lattice spacing;

$$\Delta_b\beta = \beta(a) - \beta'(ba) \tag{4.11}$$

and is defined from the beta function by the integral relation;

$$\int_{\beta-\Delta_b\beta}^{\beta} \frac{dx}{x^{3/2}\beta_{\rm fn}(\sqrt{6/x})} = -\frac{2\ln b}{\sqrt{6}} \tag{4.12}$$

The asymptotic value of $\Delta_b\beta$ is given by [107]

$$\Delta_b\beta = \left(\frac{33}{4\pi^2} + \frac{459}{16\pi^4}\frac{1}{\beta}\right)\ln b \tag{4.13}$$

The value of $\Delta_b\beta$ can be calculated very simply on the lattice. One begins with two lattices, one of size $L_1 = L$ and one of size $L_2 = \frac{L}{b}$ with couplings β and β' respectively. One then performs the renormalisation group transformation for a number of iterations, calculating some physical quantity at each stage. Once the coupling on the second lattice has been tuned to give the same value for the chosen physical quantity (usually a Wilson Loop) one can find the value of $\Delta_b\beta$ from the difference between β and β' on L_1 after the nth iteration and L_2 after the $n-1$th iteration. One needs to compare lattices of the same size, and with the same boundary conditions to avoid finite size (Infra-red cutoff) effects. Since, at each comparison the larger lattice has been transformed once more, the two actions are related by the scale factor b. The justification for this is the fact that, after sufficient iterations of the renormalisation group transformation, two actions starting from different couplings can both be arbitrarily close to the remormalisation trajectory; hence in the above case will only differ by one renormalisation step. The result of the various lattice calculations of the beta function are shown in fig. 4.3. It is worth noting the consistent difference between the values calculated using the two different b values, with the $b = 2$ values being 15% below; it is not known why this difference has occured, and further study is being done to determine the non-perturbative beta function more accurately [122].

Note that the renormalisation trajectory (and the UV Fixed Point) depends on the choice of transformation; hence one needs to choose this judicously in order to start the procedure as close to the renormalisation trajectory as possible.

Note that all of this changes once dynamical fermions are introduced onto the lattice. The coupling then depends on the quark mass, decreasing exponentially with it. Furthermore, the virtual $q\bar{q}$ change the Wilson loop dependance from an area law to a perimeter law. To date, there have been no quantitative results for the non-perturbative beta function for full QCD on the lattice. Doubtless these will begin to arrive soon after the discrepancy between the two methods used for the pure gauge theory have been resolved.

The momentum scale Λ is common to renormalisation procedures; the relationship between different renormalisation procedures and the lattice is given in table 4.1, taken in the continuum limit in which the two-loop approximation to the beta function holds. The value of Λ on the lattice is calculated using eqn. 4.7; the value of Λ for the continuum theory is given by an identical equation, excepting that the role of the lattice spacing is replaced by some renormalisation mass, and the coupling is evaluated as a function of that mass [117].

These values can be tied to reality using the recent experimental result from the AMY collaboration, [171]. Using multi-jet events from e^+e^- annihilations, the optimal fitted value of $\Lambda_{\bar{M}S}$ for four fermions was $\Lambda_{\bar{M}S} = 173 \pm 60$ MeV.

4.1.1 Universality

The choice of lattice action is governed by the requirement that it yields the correct continuum limit. This leads to the principle of *Universality*, viz. all actions must produce the same

Table 4.1: Ratio between the lattice scale Λ_L and the scale of other QCD renormalisation schemes.

N_f	$\Lambda^{MOM}_{Feynman}/\Lambda^L$	Λ^{MS}/Λ^L	Λ^{min}/Λ^L	$\Lambda_{\bar{M}S}/\Lambda^L$
	Wilson fermions		Kogut-Susskind Fermions	
0	83.4 [116]	10.8 [58]	7.46 [185]	28.8 [89]
2	96.7 [58]			30.1 "
3	106 [133]	19.2 [58]		56.8 "
4	117 [133]	24.7 [58]	34.44 [185]	76.3 "

Table 4.2: Ratio of string tension to crossover temperature for various actions.

Action	$\sqrt{\sigma}/\Lambda_L$	T_c/Λ_L	$\sqrt{\sigma}/T_c$
Wilson	46.3 ± 1 [54]	42.0 ± 0.5 [30]	1.10 ± 0.7
Fundamental-Adjoint	40.6 ± 2 [36]	42.0 ± 0.5	0.97 ± 0.12
Manton	16.2 ± 0.5 [145]	10.5	1.54 ± 0.05
Villain	48.5 ± 2.6 [145]	27.3	1.78 ± 0.10

physics, and give the same numbers (up to an overall scale factor.) The scale parameter is Λ_L obtained from the Renormalisation goup equations.

Hence, the ratio of two numbers with the same dependance on the cutoff must produce the same number with any action, provided the actions are equivalent and yield the same continuum limit. Two such numbers are the String Tension,[4] $\sqrt{\sigma}$ and the crossover temperature, T_c, at which the deconfining transition occurs.

The following ratios exist for the cutoff of the Manton and Villain actions to the Wilson [144,145]: $\Lambda^M_L = 3.07\Lambda^W_L$ and $\Lambda^M_L = \Lambda^V_L$. For the Fundamental- Adjoint Mixed Action Λ_L is a function of the relative admixtures of the two representations; details can be found in [36].

This is another region in which Monte-Carlo renormalisation group techniques are being used to improve the choice of action used. Since any action must yield the same physics, it makes sense to choose ones that are as close to the renormalisation trajectory as possible. One then needs fewer iterations on a coarse lattice to get results that are in the scaling regime and can be used to extract the continuum limit. This is due to the fact that irrelevant and redundant operators due to finite lattice spacing artefacts are suppressed close to the renormalisation trajectory [172]. An example of this is a recent calculation [110] using a renormalisation group improved Wilson action on a lattice of size $8^3 \times 16$ with lattice spacing $\approx$ 0.15fm. The results obtained were similar to those obtained at $a \approx$ 0.10fm using the normal Wilson action, which gives an indication of the extent of the improvement.

[4]The potential energy between a $q\bar{q}$ pair is of the form $V(r) = \sigma r - \frac{\alpha}{r}$ [72] where σ is the field energy per unit length in the flux tube. The string tension can be found directly in LQCD, and has provided direct evidence for the existence of linear term in the potential, and hence confinement.

4.2 Critical Slowing Down

At a critical point of a system, the Hamiltonian and coupling constant etc. become invariant under the renormalisation group; equivalently, the velocity $\beta(g)$ becomes equal to zero. Thus, as a changes the rate at which g changes will decrease as $g \to g^*$. This can be pictured as a ball rolling into a valley, but with physics such that the velocity rather than the acceleration is given by the slope; as the ball approaches the lowest point, the velocity decreases, with the final few metres of rolling taking infinitely long.

The net result of this is that improvements in the accuracy of a computer simulation of Lattice QCD increase the amount of time taken in a decidedly non-linear fashion as the lattice spacing is decreased by a given fraction. Effectively, the algorithms appear to be slowed down.

The other form of critical slowing down for lattice QCD occurs when the bare mass is decreased. The inverse of the bare mass is the correlation length; hence this will increase. The critical slowing down can be understood as an increase in the number of iterations needed to propagate a change through a correlation length. This also adds a restriction to how low a fermion mass can be used on a given size lattice; manifestly, one cannot use a value for the mass that is so low that the correlation length is a significant proportion of the lattice size!

Chapter 5

Fermions on the Lattice

5.1 Nielsen-Ninomiya No-Go Theorem.

It is well known that there are fundamental problems involved in putting fermion fields onto a lattice; in essence, one cannot put one handed fermion onto the lattice with continuous chiral invariance. It was shown that this is due to the topology of the momentum space of fermions on a lattice by Nielsen and Ninomiya in 1981[164,165]. A proof of this is given in appendix A.

Consider an N component spinor fermion field ψ defined on a lattice in Euclidean 4-space, transforming under some symmetry group (e.g. $SU_c(3) \otimes SU_L(2) \otimes U_{chiral}(1)$, under which the following generic action is invariant in the continuum:

$$S = -\sum_{x,y}\sum_{\mu=1}^{4} \bar{\psi}(x)\gamma^{\mu}H_{\mu}(x,y)\psi(y) \tag{5.1}$$

with $H_\mu(x,y)$ an interaction between the fermion fields. The Nielsen-Ninomiya theorem states that one has either the correct number of fermions, *or* chiral invariance.

This is fatal for any attempt at putting the full standard model onto the lattice, as there is no way of placing handed Weyl fermions (neutrinos) onto the lattice. If one attempts to place a left-handed neutrino and electron with weak hypercharge $Y = \frac{1}{2}$, and a right-handed electron with $Y = 1$ onto the lattice, one automatically creates the chiral partners; viz., a right-handed neutrino and electron with $Y = \frac{1}{2}$ and a left-handed electron with $Y = 1$.

It also poses a problem for QCD, which is believed to have a chiral symmetry in the limit of massless quarks (spontaneously broken by the vacuum). However, in order to have a theory with local chiral symmetry, one is forced to accept spectral doubling on the lattice.

The crux is that it is fundamentally impossible to put the standard model on the lattice with the correct chiral symmetries and the correct number of particles.

5.1.1 Axial Anomaly

This is intimitely tied to the so-called Axial Anomaly, or $U_A(1)$ problem. For a short review of this in the continuum, see Appendix B. The connection between spectral multiplicity and the Axial anomaly was discussed by Karsten and Smit, [132]; further details can be found in [104,185].

Since the Lattice is a mathematically rigorous regulation of the theory from first principles, there is no place in it for anomolies of any sort; thus the Axial current will always be conserved on the Lattice. Hence sôme technique must be found for introducing it in the continuum limit. There are three ways of doing this on the Lattice:

1. Forsaking chiral symmetry on the lattice, and only restoring it in the continuum limit. This is the approach taken by Wilson, in which all traces of the chiral symmetry are lost on the lattice; and by Kogut and Susskind, in which a remnant of chiral symmetry is kept on the lattice.

2. Cancelling the anomaly by doubling the number of fermion species in such a fashion that one has equal numbers of right and left handed fermions; thus making the total chiral charge equal to zero. This is the method implemented in the naive fermion approach.

3. Choosing a non-local derivative, such that the conserved axial current diverges in the continuum limit. This is the approach adopted by the SLAC derivative.

Naive Fermions

The naive fermions remove the Axial anomaly very simply; since all of the symmetries are preserved, the formulation insures that there are no anomolies by simply providing a left-handed partner (with negative chiral (ie., axial) charge) for each right-handed fermion placed on the lattice. This can easily be seen in the table presented in Appendix A, table A.1, by realising that the winding number for each of the fermions is exactly the chiral charge of that fermion[1] ; hence, each fermion with an even number of $\frac{\pi}{a}$ components has a chiral charge of $+1$ whilst those with an odd number have chiral charge -1. Since there are 8 of each variety, the one set cancels the contribution to the anomaly of the other set; hence the lattice manages to neatly avoid the anomaly.

One also needs to consider the interaction between two photons and a Z^0, via either a fermion loop or a triangle diagram (the VVA vertex). The calculation of the vacuum expectation value of this, to one-loop level, was done by Karsten and Smit [132]. They showed that it was anomaly free, satisfied the lattice vector Ward identity and was Lorentz covariant, due to the duplication of particles by the lattice. Some understanding of there being 15 extra fermions, rather than just the one needed for cancelling the anomaly, can be gained by understanding that each dimension can be made discrete independently. If any one dimension is made discrete, a single extra fermion will be introduced to cancel the anomaly; when performed independently, each will introduce fermions to cancel the anomaly.

Wilson Fermions

For the Wilson theory, the 15 extra particles are no longer massless, even in the massless approximation; this removes the spectral degeneracy. Furthermore, the terms decouple in

[1]This can also be found using the more conventional method of determining the axial charge, by considering the axial-vector vertex, $\bar{\psi}\gamma_\mu\gamma_5\psi = \bar{u}\bar{s}(\pi)\gamma_\mu\gamma_5 s(\pi)u$ with u the standard Dirac particle spinor and $s(\pi)$ the spin function introduced in the section on the symmetries of the naive fermions, sec. 5.3. For the 8 fermions with positive axial charge the spin factor turns out to be ± 1, since there are an even number of components of the momentum with magnitude $\frac{\pi}{a}$, and each will introduce a factor of $\gamma_\mu\gamma_5$, whilst it is $\gamma_\mu\gamma_5$ for the other 8, with an odd number of components of the momentum with magnitude $\frac{\pi}{a}$.

the continuum limit, since the masses of the extra 15 go to infinity. One is then left with just the single fermion with chiral charge 1; and a need for the anomaly!

This is, as one would expect if the Wilson fermions are to produce the correct continuum limit, introduced by the extra 15 terms! These add an extra term to the axial Ward identity, which gives the usual anomaly to the vacuum expectation value of the interaction between two photons and a Z^0. Thus the anomaly is introduced into the theory on the lattice by the same r-term that broke the explicit chiral invariance!

Furthermore, upon considering the vacuum polarisation, one finds that all 16 of the fermions contribute on the lattice in order to get a unitary theory; without them the theory is not unitary [132]

Kogut-Susskind Fermions

In the case of the Kogut-Susskind fermions, one has one component fermion fields on the lattice. The consequence of this is that the parity operator is defined for only one component as [104]

$$x_\nu \mapsto -x_\nu \qquad P = (-)^{x_\nu} \tag{5.2}$$

Now the γ_5 operator is also just a sign operator; hence the parity and γ_5 operators now commute instead of anti-commuting, as is required for the γ_5 operator to be correctly identified with the chiral symmetry operator (see appendix B). Now, with the Susskind fermions one does still have a $U_\epsilon(1)$ symmetry (see the section on the symmetries of the Kogut-Susskind action, section 5.4.5) which behaves like γ_5 on the spinor degrees of freedom; however, it acts like $+\gamma_5$ for two species and $-\gamma_5$ for the other two!

Hence, whilst one still has a $U(1)$ symmetry on the lattice, it does not produce the anomaly; the contributions from two of the four fermions cancel those from the other two, exactly as occured for the naive fermions.

SLAC Fermions

The SLAC fermions reproduce the continuum anomaly by insuring that the conserved current diverged in the continuum limit; however, these fermions have severe problems reproducing the correct continuum weak coupling perturbation theory, due to the non-local terms introduced by the derivative.

5.2 Various Formulations of Lattice Fermions.

5.2.1 Continuum Dirac Lagrangian

Before considering quarks on the lattice, one must consider the Dirac Lagrangian in the continuum:

$$\mathcal{L} = \frac{i}{2}\left(\bar{\psi}(x)\gamma_\mu \frac{\partial \psi}{\partial x^\mu}(x) - \frac{\partial \bar{\psi}}{\partial x^\mu}(x)\gamma_\mu \psi(x)\right) - m\bar{\psi}(x)\psi(x) \tag{5.3}$$

which becomes, upon performing the Wick rotation into Euclidean space,

$$\begin{aligned} \mathcal{L}_{\mathrm{E}} &= -\frac{1}{2}\left(\bar{\psi}(x)\gamma_\mu \frac{\partial \psi}{\partial x^\mu}(x) - \frac{\partial \bar{\psi}}{\partial x^\mu}(x)\gamma_\mu \psi(x)\right) - m\bar{\psi}(x)\psi(x) \\ &= -\bar{\psi}(x)[\gamma_\mu \overleftrightarrow{\partial}_\mu + m]\psi(x) \end{aligned} \tag{5.4}$$

where

$$\bar{\psi} \overleftrightarrow{\partial}_\mu \psi = \frac{1}{2} [\bar{\psi}(\partial_\mu \psi) - (\partial_\mu \bar{\psi})\psi] \tag{5.5}$$

5.2.2 Naive Derivatives.

The crucial step in putting the Dirac Equation, and thus fermions, onto the Lattice is to choose a suitable lattice version of the derivative to act on the Grassmann spinor fields describing the fermions. As we shall see, there is no way of constructing a difference equation in such a way as to keep all of the relevant continuum properties of the fermions.

The three obvious approaches towards this goal are the Naive Derivatives;

Forward: $\partial_\mu \psi \mapsto \frac{\psi(x_\mu+a)-\psi(x_\mu)}{a}$

Backward: $\partial_\mu \psi \mapsto \frac{\psi(x_\mu)-\psi(x_\mu-a)}{a}$

Symmetric: $\partial_\mu \psi \mapsto \frac{\psi(x_\mu+a)-\psi(x_\mu-a)}{2a}$ or: $\partial_\mu \mapsto a \sum_{x'} \frac{\delta_{ax',ax+a_\mu}-\delta_{ax',ax-a_\mu}}{2a}$

Note that the forward and backward derivatives yield the same results if one is performing a summation over the entire lattice.

Each of these derivatives suffers from at least one major problem which prevents one from using them on a lattice;

- The forward and backward derivatives generate a non-Hermitian Hamiltonian, thus the action is not real. However, there is no species doubling.
- The symmetric derivative generates an Hermitian Hamiltonian, but suffers from the serious problem of fermion multiplicity, or doubling (it is more than doubling, since one gets 2^d fermions, where d is the dimension of the space-time considered.)

That the Hamiltonian generated by the first two breaks unitarity can be shown by taking the Hermitian Conjugate of the action based on the forward derivative;

$$S_F = -a^4 \sum_x \frac{1}{2} \left[\bar{\psi}(x)\gamma^\mu \frac{\psi(x_\mu + a) - \psi(x_\mu)}{a} - \frac{\bar{\psi}(x_\mu + a) - \bar{\psi}(x_\mu)}{a} \gamma^\mu \psi(x) \right] \tag{5.6}$$

Thus the Hermitian Conjugate is (note that τ is complex, hence $(\partial_4 \psi)^\dagger = -\partial_4 \psi^\dagger$);

$$\begin{aligned} S_F^\dagger &= -a^4 \sum_x \frac{1}{2} \left[-\bar{\psi}(x)\gamma^\mu \frac{\psi(x_\mu + a) - \psi(x_\mu)}{a} + \frac{\bar{\psi}(x_\mu + a) - \bar{\psi}(x_\mu)}{a} \gamma^\mu \psi(x) \right] \\ &= -S_F \end{aligned}$$

Thus $S \neq S^\dagger$; ie., the action is not real. This implies that the energy of the associated field is not real! Since this is unacceptable, we are left with the symmetric derivative; it can be similarly checked that this does generate an hermitian Hamiltonian.

The problem with the symmetric derivative is that it generates unwanted fermions: the fermion doubling problem. The origin of this can be seen from the dispersion relation of

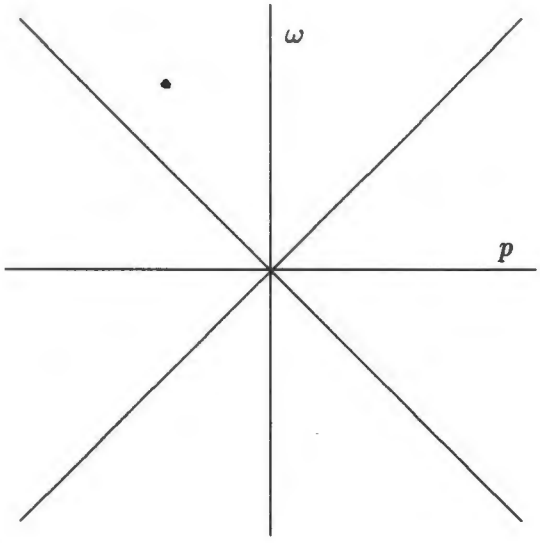

Figure 5.1: Continuum Dispersion Relation

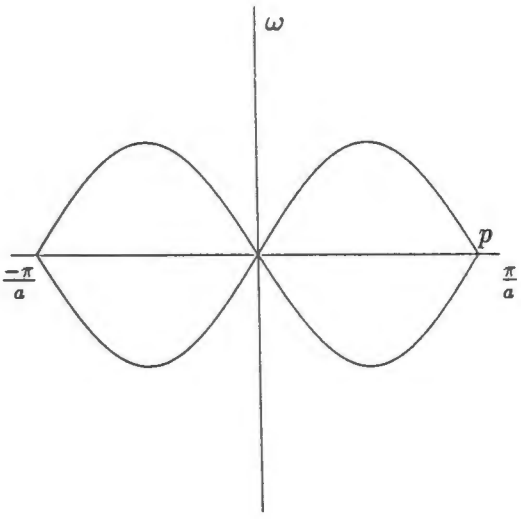

Figure 5.2: Naive Fermion Dispersion Relation

the action using a symmetric derivative, which can be found by using a Fourier Transform (eq. 2.3) to go into momentum space as follows [104]:

$$\partial \mapsto a\sum_{x'} \frac{\delta_{ax',ax+a} - \delta_{ax',ax-a}}{2a} \tag{5.7}$$

$$a\sum_{x=-\infty}^{\infty} \partial e^{ipxa} \mapsto a\sum_{x} a\sum_{x'} \frac{\delta_{ax',ax+a} - \delta_{ax',ax-a}}{2a} e^{ipx'a} \tag{5.8}$$

$$ipa\sum_{x=-\infty}^{\infty} e^{ipxa} \mapsto a\sum_{x}[e^{ip(ax+a)} - e^{ip(ax-a)}] \tag{5.9}$$

$$p \mapsto \frac{\sin(ap)}{a} \tag{5.10}$$

There are two zero-energy momenta[2]; the one we want, representing a massless fermion, at zero momentum, and another at $p = \frac{\pi}{a}$. This is an unwanted addition to our theory! Note that in 4 dimensions, we would get 15 of these unwanted fermions, at $(0,0,0,\frac{\pi}{a}) \cdots (\frac{\pi}{a},\frac{\pi}{a},\frac{\pi}{a},\frac{\pi}{a})$.

If we compare the dispersion relations of the continuum Dirac equation in one spatial dimension ($\omega = \pm p$, where the $+$ and $-$ refer to right and left moving particles respectively), and the naive discretization of it ($a\omega = \sin(ap)$), the problem is easily seen. (See figures 5.1 and 5.2)

[2]That the forward derivative does not suffer from spectral multiplicity is easily checked, using the same procedure. One finds

$$p_\mu \mapsto \frac{2}{a}\sin(\frac{pa}{2})e^{ipa/2} \tag{5.11}$$

Thus there is only the pole at 0 inside the first Brillouin zone; the other poles of the symmetric deriyative, where $p_\mu = \frac{\pi}{a}$ are all of order $O(\frac{1}{a})$. However, the energy is a complex quantity!

Even an attempt to populate only the zero-momentum state will not work; the other modes will be excited by vacuum fluctuations and scattering processes. These fall into two categories;

- those resulting in a scattered momentum outside the Brillouin zone ('umklapp processes') (the fact that momentum is only conserved modulo $2\pi/a$ is explicity used). These get transformed back into the Brillouin zone as low-energy particles moving in the opposite direction.
- since momentum is only defined modulo 2π, any particle-antiparticle scattering is likely to convert an incoming pair near $p = 0$ to a pair near $p = \pi$. Also, virtual fluctuations treat each on an equal footing.

Since hermiticity is an essential requirement for a physical action, we are forced to choose the symmetric derivative to define our naive fermionic action:

$$\begin{aligned} S_F &= -a^4 \sum_x \sum_\mu \frac{1}{2} \left[\bar{\psi}(x)\gamma^\mu \frac{\psi(x_\mu + a) - \psi(x_\mu - a)}{2a} - \frac{\bar{\psi}(x_\mu + a) - \bar{\psi}(x_\mu - a)}{2a} \gamma^\mu \psi(x) \right] \\ &\quad + m \sum_x \bar{\psi}(x)\psi(x) \\ &= -a^4 \sum_x \sum_\mu \frac{1}{2a} \left[\bar{\psi}(x)\gamma_\mu \psi(x + \mu) - \bar{\psi}(x + \mu)\gamma_\mu \psi(x) \right] \\ &\quad + m \sum_x \bar{\psi}(x)\psi(x) \end{aligned} \tag{5.12}$$

There is no difference between the different poles of the propagator; the action is symmetric under a 32 element group of transformations (16 linearly independant elements [15]), isomorphic to the Clifford group, mapping one pole of the propagator into another.

However, since reality lacks the spectral doubling of the naive derivative, some method must be found to remove these unwanted fermions. There have been many various, and more or less devious, methods proposed. The two most often used these days are the Wilson fermions [212] and the Staggered, or Kogut-Susskind, fermions [141].

In both of these, Chiral symmetry is sacrificed; completely, in the Wilson case, where it is only recovered in the continuum limit, and partially in the Staggered case, where a remnant remains on the lattice. In the following, these two cases, and some of the other proposals, will be examined in more detail.

5.3 Symmetries of the Naive Fermion Action

The fermion action based on the naive derivative, eqn. 5.12 is symmetric under the group of 16 transformations, isomorphic to the Clifford group, $\psi(x) \mapsto T(x)\psi(x)$, $\bar{\psi}(x) \mapsto \bar{\psi}(x)T^{-1}(x)$ with $T(x) = 1, (-)^{x_\mu a}\gamma_\mu\gamma_5$ or any product of these transformations.

These transformations relate the different points at which the propagator has poles, ie. the various points π; $(-)^{x_1 a}\gamma_1\gamma_5$ maps p_1 to $p_1 + \frac{\pi}{a}$ modulo $\frac{2\pi}{a}$. This can be shown by considering the Fourier transform of ψ; from section 2.3 one has:

$$a^4 \sum_x e^{ipxa}(-)^{x_\mu}\gamma_\mu\gamma_5\psi(x) = \gamma_\mu\gamma_5 a^4 \sum_x e^{ipxa} e^{1\pi x_\mu a}\psi(x) \tag{5.13}$$

$$= \gamma_\mu\gamma_5 \tilde{\psi}\left(p + \frac{\pi_\mu}{a}\right) \tag{5.14}$$

Thus, the transformation will shift the desired pole at $(0,0,0,0)$ to one of the other 15, with a spin factor of $\gamma_\mu\gamma_5$ included.

5.4 Kogut-Susskind Fermions

This method was introduced by Kogut and Susskind in 1975 [141]. Unlike the Wilson fermions, it succeeds in retaining a vestige of chiral symmetry; however, it still suffers from some of the spectral multiplicity of the naive derivative.

5.4.1 Removing Doubling via constraining ψ in configuration space

Consider the naive fermion action, eqn. 5.12, in the limit $m = 0$. It is symmetric under a symmetry group, $\mathcal{G}$ say, that contains elements not present in the continuum; $\mathcal{G}$ is isomorphic to the 32 element Clifford group, with occasional position-dependent sign factors $(-)^{x_\mu}$. The generators of $\mathcal{G}$ are:

$$\begin{array}{rcll} \psi & \mapsto & i(-)^{x_\mu}\gamma_5\gamma_\mu\psi & \text{No summation over } \mu \\ & & & \mu \text{ is identical to the } \mu \text{ of each term in eqn.5.12.} \\ \psi & \mapsto & i(-)^{x_\nu}\gamma_\nu\psi & \text{No summation over } \nu \\ & & & \nu \neq \mu \text{ in eqn.5.12.} \end{array} \tag{5.15}$$

Secondly, consider the role played by invariance under the Lorentz group. In the continuum, the spin representation [15] of the Lorentz group is given by the Dirac matrices; the commutation relations of these are preserved under a Lorentz transformation. Hence, the requirement of Lorentz-invariance for theory involving particles described by spinors, determines the number of components in the spinor. This must be the same as the dimension of the Dirac matrices[3]. However, by introducing the lattice in the first place one explicitly destroys Lorentz invariance[4] anyway! There is thus no neccessity for a many-component spinor to describe spin-$\frac{1}{2}$ particles.

The approach taken by Kogut and Susskind to decrease the spectral multiplicity involves taking advantage of both of the above properties of the lattice. The idea is to place a field with one component per site (as in the scalar case) whilst still retaining as much information about the spin as possible.

Firstly, note that the group $\mathcal{G}$ above has an abelian subgroup (say $\mathcal{H}$) [94] with generators $i\gamma_5\gamma_3$ and $i\gamma_1\gamma_2$. These are both diagonal unitary matrices, with diagonal elements $(1,-1,-1,1)$ and $(-1,1,-1,1)$ respectively. If we now constrain the ψ by requiring that $\psi = h\psi$ and $\bar{\psi} = \bar{\psi}h^\dagger$ for all $h \in \mathcal{H}$ we decrease the number of degrees of freedom[5] by a factor of 2 for each generator in the group $\mathcal{H}$; this leaves us with 4 of the original 16 unwanted fermions.

---

[3]This is $2^{[d/2]}$ for d space-time dimensions, where [] represents the integer part of the argument. One is also restricted to even d, if chirality is required, by the fact that γ_5 is not one of the linearly independent monomials of the Clifford algebra in odd d.

[4]The dangers of this have been pointed out by [59]; it is usually assumed that Lorentz invariance will be regained in the continuum limit. This is not always the case, as some of the doubled fermions lead to non-Lorentz invariant Green functions in the continuum limit of some lattice theories (eg. the massive Schwinger model). This is not the case for either the Wilson or the Kogut- Susskind approach; the removal of the doublers also removes the problematic Green functions.

[5]It can be shown using the above representation for the two generators of H that the first and second

This is due to the fact that the subgroup $\mathcal{F}$ of $\mathcal{G}$ is the only part of $\mathcal{G}$ under which the action is non-trivially invariant. This subgroup is obtained from the remainder of $\mathcal{G}$ after $\mathcal{H}$ has been excluded; ie.,*

$$\mathcal{G} = \mathcal{F} \cup \mathcal{H}$$

If one introduces an additional factor of $(-)^{x_\mu}$ to the generators, the 4 fermions are again split slightly, with two appearing on the sites with $\sum x_\mu$ positive, and two on the odd sites. It must be mentioned that the original Lagrangian is only invariant under transformations with this factor included, if one does not impose the constraint of H-invariance on the spinors.

Under this situation one can also re-write ψ as $u\chi$ with u a normal c-number spinor, subject to the constraint required of ψ above, as well as the normalisation $u^\dagger u = 1$, and χ a single Grassmann variable. These two constraints, and the obvious one of requiring $\psi = u\chi$, leaves 1 degree of freedom for u and χ at each point in the continuum; hence 16 at each site on the lattice. Since one needs 4 DOF in order to construct a spinor, the even/odd site splitting introduced above leads to 8 DOF, or two fermions, per site in order to construct the 4 fermions.

There are 2 generators of $\mathcal{H}$ for the Dirac matrices in four dimensions; each decreases the number of DOF by a factor of 2. One way of further decreasing the number of DOF is to increase the size of $\mathcal{G}$, by adding another internal symmetry of the ψ to $\mathcal{G}$. If, for example, one adds the isospin symmetry, a further generator is obtained for $\mathcal{H}$, leading to the interpretation of the remaining two fermions as u and d quarks. However, this addition will not be made in what follows; an interpretation of the 4 fermions remaining as belonging to the first two families of quarks will be made.

5.4.2 Removing doubling by diagonalising the Dirac matrix

In the previous subsection, the spectral degeneracy was lifted by explicitly making the ψ invariant under the abelian subgroup of $\mathcal{G}$; ie, under a transformation by a diagonal matrix. Consider now an alternative; transform the Dirac matrices into a diagonal form [138]. Construct a 4×4 matrix T, with an associated Grassmann spinor χ, with the following transformation of ψ,

$$\psi(x) = T(x)\psi(x) \quad \bar{\psi}(x) = \bar{\psi}(x)T^\dagger(x) \tag{5.17}$$

such that these T matrices simultaneously diagonalise the γ matrices appearing in the naive fermion action, eqn 5.12

$$T^\dagger(x)\gamma_\mu T(x+\mu) = \Delta_\mu(x) \tag{5.18}$$

where Δ_μ is a diagonal unitary matrix,

$$\Delta_\mu = U(1) \otimes U(1) \otimes U(1) \otimes U(1) \tag{5.19}$$

for four dimensional space-time. In general dimensions, it will be $2^{[\frac{d}{2}]}$ direct products of $U(1)$.

---

generators constrain ψ to

$$\psi = \begin{pmatrix} \psi_1 \\ 0 \\ 0 \\ \psi_4 \end{pmatrix} \qquad \text{and} \qquad \psi = \begin{pmatrix} 0 \\ \psi_3 \\ 0 \\ \psi_4 \end{pmatrix} \tag{5.16}$$

respectively.

This results in eqn. 5.12 becoming, setting $m = 0$;

$$S_F = -a^4 \sum_x \sum_\mu \frac{1}{2a} \left[\bar{\chi}(x)\Delta_\mu(x)\chi(x+\mu) - \bar{\chi}(x+\mu)\Delta_\mu^\dagger(x)\chi(x)\right] \tag{5.20}$$

The most usual choice made these days is to take $\Delta_\mu(x) = \pm\mathbb{1}$. The question then arises as to whether there are any restrictions on the choice. To answer this, one must consider consider the product around an elementary plaquette of the Δ_μ;

$$\begin{aligned} T^\dagger(x)\gamma_\mu T(x &+ \mu)T^\dagger(x+\mu)\gamma_\nu T(x+\mu+\nu)T^\dagger(x+\mu+\nu)\gamma_\mu T(x+\nu)A^\dagger(x+\nu)\gamma_\nu T(x) \\ &= T^\dagger(x)\gamma_\mu\gamma_\nu\gamma_\mu\gamma_\nu T(x) \\ &= -\mathbb{1} \end{aligned} \tag{5.21}$$

It can be shown [138] that all choices subject to this restriction are equivalent, since each yields eqn. 5.20

Since the square of any Dirac matrix is in the form wanted, $\mathbb{1}$, a reasonable ansatz is to choose $T(x)$ to be some polynomial in the Dirac matrices, such as

$$T(x) = \gamma_1^{x_1}\gamma_2^{x_2}\gamma_3^{x_3}\gamma_4^{x_4} \tag{5.22}$$

Since the only important factor is whether the Dirac matrix is raised to an even or an odd power, the $T(x)$ are chosen from amongst the following 16 T^A matrices;

$$T^A = \gamma_1^{A_1}\gamma_2^{A_2}\gamma_3^{A_3}\gamma_4^{A_4} \tag{5.23}$$

where A is a four-vector, $A_\mu = x_\mu \mathrm{mod} 2 = 0, 1$.

This results in the Fermion action, with $m = 0$, taking on the following form:

$$S_F = -a^4 \sum_x \sum_\mu \frac{1}{2a} [\bar{\chi}(x)\eta_\mu(x)\chi(x+\mu) - \bar{\chi}(x+\mu)\eta_\mu(x)\chi(x)] \tag{5.24}$$

where the $\eta_\mu(x)$ are given by

$$\left.\begin{aligned} \eta_\mu(x) &= T^\dagger(x)\gamma_\mu T(x) \\ \eta_1(x) &= 1\mathbb{1} \\ \eta_2(x) &= (-1)^{x_1}\mathbb{1} \\ \eta_3(x) &= (-1)^{x_1+x_2}\mathbb{1} \\ \eta_4(x) &= (-1)^{x_1+x_2+x_3}\mathbb{1} \end{aligned}\right\} \tag{5.25}$$

With $\chi(x)$ a four component spinor, the action becomes

$$\begin{aligned} S_F = -a^4 \sum_x \sum_\mu \frac{1}{2a} \Bigg[&(-)^0 \sum_{\alpha=1}^4 [\bar{\chi}_\alpha(x)\chi_\alpha(x+\mu) - \bar{\chi}_\alpha(x+\mu)\chi_\alpha(x)] \\ &+ (-)^{x_1} \sum_{\alpha=1}^4 [\bar{\chi}_\alpha(x)\cdots\chi_\alpha(x)] + (-)^{x_1+x_2} \sum_{\alpha=1}^4 [\bar{\chi}_\alpha(x)\cdots\chi_\alpha(x)] \\ &+ (-)^{x_1+x_2+x_3} \sum_{\alpha=1}^4 [\bar{\chi}_\alpha(x)\chi_\alpha(x+\mu) - \bar{\chi}_\alpha(x+\mu)\chi_\alpha(x)] \Bigg] \end{aligned} \tag{5.26}$$

The Greek index counts the spinor components.

This is, in essence, the sum of four identical fermion actions; hence one imposes the additional constraint

$$\chi_\mu = \frac{1}{4}\chi_1 \tag{5.27}$$

which is equivalent to taking the $\chi(x)$ to be a one-component Grassmann variable, on each of the lattice sites, with the $\eta_\mu(x)$ given by eqn. 5.25 sans the identity matrix. Note that Lorentz invariance, the original reason for taking the fermion spinor to be a 4-component field, is no longer present on the lattice; hence one might just as well take $\chi(x)$ to be a one-component field.

Hence the Kogut-Susskind action, *with χ a one-component field*, is given by

$$\begin{aligned} S_{\mathrm{F}} &= -a^4 \sum_x \sum_{ij} \Bigg\{ \sum_\mu \frac{1}{2a} \eta_\mu(x) \left[\bar{\chi}_i(x) U_{ij}(x, x+\mu) \chi_j(x+\mu) \right. \\ &\qquad \left. - \bar{\chi}_i(x+\mu) U^\dagger_{ij}(x, x+\mu) \chi_j(x) \right] + m \bar{\chi}_i(x) \chi_j(x) \delta_{ij} \Bigg\} \end{aligned} \tag{5.28}$$

The gauge field U (the connection between adjacent lattice sites) has been explicitly included, as has the mass. The Roman indices represent the colour variables.

In another notation, more closely resembling the usual form of the continuum equation, one gets

$$S_{\mathrm{F}} = -a^4 \sum_{x,y} \bar{\chi}_i(x) K(x, i; y, j) \chi_j(y) \tag{5.29}$$

where the Kogut-Susskind 'hopping parameter', or fermion matrix, which describes the movement of fermions from one site to another, is given by

$$K(x, i; y, j) = m \delta_{x,y} \delta^{ij} + \frac{1}{2a} \sum_\mu \eta_{x,\mu} (U^{ij}_{x,\mu} \delta_{y,x+\mu} - U^{\dagger ji}_{x,\mu} \delta_{x,y+\mu}) \tag{5.30}$$

This reduces the number of degrees of freedom by a factor of 4. We began in the continuum with 4 DOF; these were multiplied by 16 upon moving to the lattice, resulting in 64 DOF. One is now left with 16 DOF again, spread over the sites constituting a tesseract by the even/odd spliting of the η; hence the spinor for each of the four fermions will be constructed from the χ on each of four sites in a tesseract.

The problem with this method of lifting the spectral degeneracy is the fact that the symmetries of the action that remain, including flavour symmetry, become mixed with the lattice translations.

5.4.3 Removing doubling in momentum space by constraining ψ

The above formulations of the Kogut-Susskind fermions are grounded in configuration space. Another approach is to assign different regions in the momentum space to different flavours, hence eliminating the multiplicity. This approach was used by Sharatchandra et al. [185] and later, using a different and more transparent technique, by Golterman and Smit [204,96].

The first step is to use the Fourier Transform, page 2.3, to re-write the naive fermion action (eqn. 5.12) in momentum space as follows:

$$S_{\mathrm{F}} = -a^4 \sum_x \Bigg\{ \sum_\mu \Bigg[\left(\int_{-\frac{\pi}{a}}^{\frac{\pi}{a}} \frac{d^4k}{(2\pi)^4} e^{-ikxa} \tilde{\psi}(k) \right) \gamma_\mu \left(\int_{-\frac{\pi}{a}}^{\frac{\pi}{a}} \frac{d^4k'}{(2\pi)^4} e^{ik'(x+\mu)a} \tilde{\psi}(k') \right)$$

$$
\begin{aligned}
&\quad - \left(\int_{-\frac{\pi}{a}}^{\frac{\pi}{a}} \frac{d^4k}{(2\pi)^4} e^{-ik(x+\mu)a} \tilde{\bar{\psi}}(k) \right) \gamma_\mu \left(\int_{-\frac{\pi}{a}}^{\frac{\pi}{a}} \frac{d^4k'}{(2\pi)^4} e^{ik'xa} \tilde{\psi}(k') \right) \Bigg] \\
&\quad + m \int_{-\frac{\pi}{a}}^{\frac{\pi}{a}} \frac{d^4k}{(2\pi)^4} e^{-ikxa} \tilde{\bar{\psi}}(k) \int_{-\frac{\pi}{a}}^{\frac{\pi}{a}} \frac{d^4k'}{(2\pi)^4} e^{ik'xa} \tilde{\psi}(k') \Bigg\} \\
= & - \int_{-\frac{\pi}{a}}^{\frac{\pi}{a}} \frac{d^4k}{(2\pi)^4} \int_{-\frac{\pi}{a}}^{\frac{\pi}{a}} \frac{d^4k'}{(2\pi)^4} a^4 \sum_x e^{i(k'-k)xa} \Bigg\{ \sum_\mu \left[\tilde{\bar{\psi}}(k) \gamma_\mu (e^{ik'_\mu a} - e^{-ik_\mu a}) \tilde{\psi}(k') \right] \\
&\qquad + m \tilde{\bar{\psi}}(k) \tilde{\psi}(k') \Bigg\} \\
= & - \int_{-\frac{\pi}{a}}^{\frac{\pi}{a}} \frac{d^4k}{(2\pi)^4} \left[\tilde{\bar{\psi}}(k) S(k)^{-1} \tilde{\psi}(k) \right] \qquad (5.31)
\end{aligned}
$$

where the Feynman Propagator is given by

$$
S(k) = \frac{1}{\sum_\mu \left(\frac{i}{a} \gamma_\mu \sin(k_\mu a) \right) + m} \qquad (5.32)
$$

One has periodicity of $\frac{2\pi}{a}$ in the momentum in each of the four directions. The momentum space can thus be restricted to the domain

$$
D = \left\{ k | \frac{-\pi}{a} < k_\mu \leq \frac{\pi}{a} \quad , \quad \mu = 1,2,3,4 \right\} \qquad (5.33)
$$

The essence of the momentum-space approach to eliminating the spectral multiplicity is to subdivide the Brillouin zone into 16 independant regions, with independant Grassmann variables in each. (These will later be identified with different flavours.)

The first step in the process is to construct a set (G, say) containing 16 elements, each being an ordered set of indices, one of which is the empty set

$$
G = \{ g | g = (\mu_1, \cdots, \mu_s), 1 \leq \mu_1 < \cdots < \mu_s \leq 4 \} \qquad (5.34)
$$

with an Abelian group structure given by the following algebra for $g, g' \in G$:

$$
\begin{aligned}
& gg' = g'' \in G \\
& \mu \in g'' \Rightarrow \mu \in g \cup g', \mu \notin g \cap g'
\end{aligned} \qquad (5.35)
$$

G is now isomorphic to the linearly independant subgroup of the Clifford group, and hence to the group $\mathcal{G}$ introduced in section 5.4.1. The connection between this approach and the one presented here will be made clearer below.

Thus to each element of G one can associate a vector π_g, one of $(0,0,0,0)$ through to $(\frac{\pi}{a}, \frac{\pi}{a}, \frac{\pi}{a}, \frac{\pi}{a})$, as follows:

$$
(\pi_g)_\mu = \begin{cases} \frac{\pi}{a}, & \mu \in g \\ 0 & \text{otherwise} \end{cases} \qquad (5.36)
$$

These then acquire the following property due to the abelian nature of G:

$$
\begin{aligned}
\pi_g + \pi_{g'} &= \pi_{gg'} \mathrm{mod} \left(\frac{2\pi}{a} \right) \qquad (5.37) \\
&= \pi_{g''}
\end{aligned}
$$

Hence one can decompose the domain D into subdomains D_g according to $D = \bigcup_{g\in G} D_g$ where

$$\left.\begin{array}{rcl} {}^{\bullet}D_g & = & \{k|k = (k_\phi + \pi_g), k_\phi \in D_\phi, g \in G\} \\ D_\phi & = & \{k|\frac{-\pi}{2a} < k_\mu \leq \frac{\pi}{2a}, \mu = 1,2,3,4\} \end{array}\right\} \tag{5.38}$$

The action is invariant under the following 16-element group $\mathcal{G}$, isomorphic to the Clifford group (see appendix C, with the transformations

$$\begin{array}{ll} \psi(k) \mapsto e^{ix\pi_g} M_g \psi(k+\pi_g) & \bar{\psi}(k) \mapsto e^{ix\pi_g} \bar{\psi}(k+\pi_g) M_g^\dagger \\ \tilde{\psi}(k) \mapsto M_g \tilde{\psi}(k+\pi_g) & \bar{\tilde{\psi}}(k) \mapsto \bar{\tilde{\psi}}(k+\pi_g) M_g^\dagger \end{array} \tag{5.39}$$

where M_g is given by

$$M_g = M_{\mu_1} \cdots M_{\mu_s}, \mu_i \in g \tag{5.40}$$

$$M_\mu = i\gamma_5\gamma_\mu \tag{5.41}$$

with

$$M_g^\dagger M_g = \mathbb{1} \quad M_g^\dagger \gamma_\mu M_g = e^{ia\hat{\mu}\pi_g}\gamma_\mu \tag{5.42}$$

At this point one can construct 16 new fields (not linearly independant) from the $\tilde{\psi}(k)$, one in each of the D_g;

$$\begin{array}{l} \tilde{q}^g(k) = M_g\tilde{\psi}(k+\pi_g) \quad \bar{\tilde{q}}^g(k) = \bar{\tilde{\psi}}(k+\pi_g)M_g^\dagger \\ k \in D_\phi \end{array} \tag{5.43}$$

Thus the naive fermion action, eqn. 5.12 can be re-written as

$$S_F = -\int_{-\frac{\pi}{a}}^{\frac{\pi}{a}} \frac{d^4k}{(2\pi)^4} \bar{\tilde{q}}_0(k-\pi_0) M_0 S(k)^{-1} M_0^\dagger \tilde{q}_0(k-\pi_0) \tag{5.44}$$

where the element $g = 0$ has been chosen to avoid overcounting. Now the q fields are only independant[6] in the restricted range of the momentum D_ϕ. One can then restrict the integral to the domain D_ϕ, and introduce a sum over G, by making the substitution

$$\tilde{q}_0(k') \; = \tilde{q}_0(k+\pi_g) \; = M_0 M_{0g}^\dagger \tilde{q}_{0g}(k) \; = M_g^\dagger \tilde{q}_g(k) \tag{5.46}$$

for some $g \in G$ and $k \in D_\phi$, $k' \in D$, but $k' \notin D_\phi$.

Thus

$$S_F = -\sum_{g\in G} \int_{-\frac{\pi}{2a}}^{\frac{\pi}{2a}} \frac{d^4k}{(2\pi)^4} \bar{\tilde{q}}_g(k) M_g S(k)^{-1} M_g^\dagger \tilde{q}_g(k) \tag{5.47}$$

with $M_g S(k)^{-1} M_g^\dagger = -\sum_\mu \left(\frac{i}{a} e^{ia\hat{\mu}\pi_g}\gamma_\mu \sin(k_\mu a)\right) + m$.

In order to reduce the spectral degeneracy from 16-fold to 4-fold one now chooses a subgroup H, $H \subset G$, such that

$$[M_h, M_{h'}] = 0 \forall h, h' \in H \tag{5.48}$$

---

[6] If $k \in D, k \notin D \cap D_\phi$ then $\tilde{q}^g(k) = \tilde{q}^{g''}(k'), k' \in D_\phi$

$$\tilde{q}^g(k) = \tilde{q}^g(k' + \pi_{g'}) = M_g\tilde{\psi}(k' + \pi_{g'} + \pi_g) = M_g\tilde{\psi}(k' + \pi_{g''}) = M_g M_{g''}^\dagger \tilde{q}^{g''}(k') \tag{5.45}$$

using eqn. 5.35 and eqn. 5.37

Hence one has chosen the subgroup $\mathcal{H} \subset \mathcal{G}$ of section 5.4.1; following the same procedure, one constrains the $\tilde{\psi}(k)$ by imposing the condition

$$\tilde{\psi}(k) = M_h \tilde{\psi}(k + \pi_h) \quad \tilde{\bar{\psi}}(k) = \tilde{\bar{\psi}}(k + \pi_h) M_h^\dagger \tag{5.49}$$

If one chooses the generators of $\mathcal{H}$ as before, then the group H has generators $\{3\}$ and $\{1,2\}$. This leaves just four of the G as non-trivial symmetries of the action (with independant $\tilde{q}^g$ associated with each); these form the subgroup F,

$$F = \{(1),(4),(1,4),()\} \tag{5.50}$$

with $G = F \cup H$.

Not all the $\tilde{q}^g(k)$ are independant, but only those for which $g \in F$. All other $g'' \notin F$ are mapped onto some f by the imposition of invariance of $\tilde{q}^g(k)$ under H; all g can be written fh. This can easily be seen by examining the effect on π_g:

$$\pi_g \mapsto \pi_g + \pi_{h_1} + \pi_{h_2} = \pi_f \forall g \in G \tag{5.51}$$

with only 4 elements in F, the fermion action in momentum space then becomes

$$S_{\mathrm{F}} = -4 \sum_{f \in F} \int_{-\frac{\pi}{2a}}^{\frac{\pi}{2a}} \frac{d^4k}{(2\pi)^4} \tilde{q}^f(k) M_f S(k)^{-1} M_F^\dagger \tilde{q}^f(k) \tag{5.52}$$

Where the factor 4 can be removed by normalizing the expression, which manifestly describes four fermions, each of which can be interpreted as a flavour.

5.4.4 Removing the doubling in momentum space by constraining the Dirac Matrices

Just as in the configuration space approach to reducing the spectral degeneracy, one has many possible choices of constraint. The method that is the momentum-space complement of the T matrices used to diagonalise the Dirac matrices in section 5.4.2 is presented below [96,204]; it has the same form as the method presented above, with the added advantage that the symmetries of the action are more easily seen.

One begins with the fermion action presented in eqn. 5.28 and transforms to momentum space using the Fourier transform of section 2.3 with

$$\eta_\mu(x) = e^{i\pi_{\eta_\mu} x a} \tag{5.53}$$

with $\pi_{\eta_{1,2,3,4}} = (0,0,0,0),(\frac{\pi}{a},0,0,0),(\frac{\pi}{a},\frac{\pi}{a},0,0),(\frac{\pi}{a},\frac{\pi}{a},\frac{\pi}{a},0)$ respectively. If we consider the 16-element set G above, with the following order imposed

$$\begin{aligned} G \;=\; & \{\{\,\},\{1\},\{12\},\{2\},\{123\},\{23\},\{3\},\{13\}, \\ & \{1234\},\{234\},\{34\},\{134\},\{4\},\{14\},\{124\},\{24\}\} \end{aligned} \tag{5.54}$$

with the first element numbered zero. Then $\pi_{\eta_\mu} = \pi_g$ for $g = 1,2,4$ respectively.

Repeating the calculation of eqn. 5.31, eqn. 5.28 becomes

$$S_{\mathrm{F}} = -\int_{\frac{-\pi}{a}}^{\frac{\pi}{a}} \frac{d^4k}{(2\pi)^4} \int_{\frac{-\pi}{a}}^{\frac{\pi}{a}} \frac{d^4k'}{(2\pi)^4} \tilde{\bar{\chi}}(k) S^{-1}(k,k') \tilde{\chi}(k') \tag{5.55}$$

with the Fermion propagator for Kogut-Susskind fermions given by

$$S(k,k') = \frac{1}{\frac{i}{a}\sum_\mu \delta^4(k-k'+\pi_{\eta_\mu})\sin(k_\mu a)+m} \tag{5.56}$$

Divide momentum space into 16 regions according to the prescription of eqn. 5.38. Construct a 16-component field in momentum space, $\tilde{\phi}(p)$, with components

$$\begin{aligned} \tilde{\phi}_g(p) &= \tilde{\chi}(p+\pi_g) & \bar{\tilde{\phi}}_g(p) &= \bar{\tilde{\chi}}(p+\pi_g) \\ \phi_g(x) &= \int_{\frac{-\pi}{2a}}^{\frac{\pi}{2a}} \frac{d^4p}{\pi^4} e^{-ipxa}\tilde{\phi}(p) & \bar{\phi}_g(x) &= \int_{\frac{-\pi}{2a}}^{\frac{\pi}{2a}} \frac{d^4p}{\pi^4} e^{-ipxa}\bar{\tilde{\phi}}(p) \end{aligned} \tag{5.57}$$

The Susskind action can be re-written in terms of the 16-component field; firstly, one needs to construct 16 16 × 16 matrices $\hat{\pi}_g$ from the π_g according to the prescription

$$(\hat{\pi}_g)_{g'g''} = \begin{cases} 1 \text{ for } \pi_g + \pi_{g'} + \pi_{g''} = \pi_0 = 0 \\ 0 \text{ otherwise} \end{cases} \tag{5.58}$$

These matrices[7] are symmetric under any permutation of g, g', g'' and are abelian. Each of the $\hat{\pi}_g$ contains only one non-zero element in each row and column; since the π_g form a basis, as well as a group, the sum of any two gives uniquely a third element. If one considers the addition law for the π_g, one can see that

$$\begin{aligned} \pi_{g'} + \pi_{g''} &= \pi_g \\ &= \sum_{g'''} (\hat{\pi_{g'}})_{gg'''}\pi_{g'''} \\ &= \sum_{g'''} (\hat{\pi_{g''}})_{gg'''}\pi_{g'''} \end{aligned} \tag{5.60}$$

One can also construct generalised sign factors

$$S_g^\mu = e^{i\pi_g a\hat{\mu}}$$

with a 16 × 16 diagonal sign matrix S^μ given by

$$(S^\mu)_{gg'} = S_0^\mu \otimes S_1^\mu \otimes \cdots \otimes S_{15}^\mu \tag{5.61}$$

[7]Some explicit examples of the $\hat{\pi}_g$ are;

$$\hat{\pi}_{\eta_1} = \hat{\pi}_0 = \begin{pmatrix} 1 & 0 & 0 & & 0 \\ 0 & 1 & 0 & & 0 \\ 0 & 0 & 1 & & 0 \\ & & & \ddots & \\ 0 & 0 & 0 & 0 & 1 \end{pmatrix} \quad \hat{\pi}_{\eta_3} = \hat{\pi}_2 = \begin{pmatrix} 0 & 0 & 1 & 0 & & & & & & 0 \\ 0 & 0 & 0 & 1 & & & & & & 0 \\ 1 & 0 & 0 & 0 & & & & & & 0 \\ 0 & 1 & 0 & 0 & & & & & & 0 \\ & & & & 0 & 0 & 1 & 0 & & 0 \\ & & & & 0 & 0 & 0 & 1 & & 0 \\ & & & & 1 & 0 & 0 & 0 & & 0 \\ & & & & 0 & 1 & 0 & 0 & & 0 \\ & & & & & & & & \ddots & 0 \\ 0 & 0 & 0 & 0 & 0 & 0 & 0 & 0 & 0 & 0 \end{pmatrix} \tag{5.59}$$

The commutation relations of the S^μ and $\hat{\pi}_g$ can be determined by considering the requirements for individual elements; consider the element ab of $\hat{\pi}_g$ to be non-zero. We then have $(\hat{\pi}_g S^\mu)_{ab} = {}^\bullet S^\mu_b$ and $(S^\mu \hat{\pi}_g)_{ab} = S^\mu_a$. Since $S^\mu_a \times S^\mu_a = 1$, and $S^\mu_a \times S^\mu_b = expi[\pi_{a_\mu} + \pi_{b_\mu}] = exp[i\pi_{g_\mu}] = S_{g_\mu}$. Hence we get the commutation relation

$$\hat{\pi}_g S^\mu = S^\mu \hat{\pi}_g S_{g_\mu} \tag{5.62}$$

The fermion action can then be written in terms of this field as follows:

$$S_{\mathrm{F}} = -\sum_{gg'} \int_{\frac{-\pi}{2a}}^{\frac{\pi}{2a}} \frac{d^4p}{(\pi)^4} \int_{\frac{-\pi}{2a}}^{\frac{\pi}{2a}} \frac{d^4p'}{(\pi)^4} \bar{\tilde{\chi}}(p+\pi_g) S^{-1}(p+\pi_g, p'+\pi_{g'}) \tilde{\chi}(p'+\pi_{g'}) \tag{5.63}$$

with $p, p' \in D_\phi$. Consider now the inverse propagator;

$$\begin{aligned} S^{-1}_{gg'} &= \sum_\mu \delta^4(p-p'+\pi_g-\pi_{g'}+\pi_{\eta_\mu}) \frac{i}{a} \sin((p+\pi_g)_\mu a) + m\delta_{gg'} && (5.64) \\ &= \sum_\mu \delta^4(p-p'+\pi_g+\pi_{g'}+\pi_{\eta_\mu}) \frac{i}{a} \cos(\pi_{g_\mu} a)_\mu \sin(p_\mu a) + m\delta_{gg'} && (5.65) \\ & && (5.66) \end{aligned}$$

Since $\pi_g \notin D_\phi$ the only way for the δ function to hold is if $\pi_g + \pi_{g'} + \pi_{\eta_\mu} = (0,0,0,0) = \pi_0$. This constraint can be taken out of the δ, and the cos written as the sign function given above, yielding the expression

$$\begin{aligned} S^{-1}_{gg'} &= \sum_\mu \delta^4(p-p')(\hat{\pi_{\eta_\mu}})_{gg'} S^\mu_g \sin(p_\mu a) + m\delta_{gg'} && (5.67) \\ &= \sum_\mu \delta^4(p-p')(S^\mu \hat{\pi_{\eta_\mu}})_{gg'} \sin(p_\mu a) + m\delta_{gg'} && (5.68) \end{aligned}$$

Which is essentially a 16×16 matrix; hence the Kogut-Susskind action becomes, as a matrix equation,

$$S_{\mathrm{F}} = -\int_{\frac{-\pi}{2a}}^{\frac{\pi}{2a}} \frac{d^4p}{(\pi)^4} \int_{\frac{-\pi}{2a}}^{\frac{\pi}{2a}} \frac{d^4p'}{(\pi)^4} \bar{\tilde{\phi}}(p) S^{-1}(p,p') \tilde{\phi}(p') \tag{5.69}$$

One can then use this 16-component field to construct four Dirac spinors on the lattice, describing 4 flavours of fermions.

Before one can attempt this, however, an understanding must be gained of the symmetries of the lattice action. The method of distinguishing the different flavours is intimitely related to the manner in which the continuum symmetries manifest themslves on the lattice; in particular, the fact that the discrete, internal symmetries become mixed with the translational symmetries.

5.4.5 Symmetries of the Lattice Dirac Action

The following symmetries exist on the lattice for the Dirac Action:

In Coordinate Space

1. Shift Invariance
   Note that this is note the same as the usual translation invariance of the Poincaré invariance in the continuum; the translation operator is introduced further on in the text, as the product two successive shift operators.

$$\mathcal{S}_\mu : \chi(x) \mapsto \zeta_\mu(x)\chi(x+\mu) \quad \mathcal{S}_\mu : \bar{\chi}(x) \mapsto \bar{\chi}(x+\mu)\zeta_\mu(x) \tag{5.70}$$

   with

$$\begin{aligned} \zeta_\mu &= (-)^{\sum_{\nu>\mu} x_\nu} && (5.71)\\ &= e^{i\pi\zeta_\mu x a} && (5.72) \end{aligned}$$

   By substituting this into eqn. 5.28 one can easily show[8] that this gives the correct transformation for the η_μ. Taking the ordering of G given above, one has $\pi_{\zeta_{1,2,3,4}} = \pi_g$ with $g = 9,10,11,0$ respectively.

2. Rotational Invariance; Rotations under multiples of $\frac{\pi}{2}$

$$R_{\mu\nu} : \chi(x) \mapsto S_R(R^{\leftarrow}x)\chi(R^{\leftarrow}x) \quad R_{\mu\nu} : \bar{\chi}(x) \mapsto S_R(R^{\leftarrow}x)\bar{\chi}(R^{\leftarrow}x) \tag{5.76}$$

   where $R_{\mu\nu}$ is the rotation $x_\mu \mapsto x_\nu, x_\nu \mapsto -x_\mu, x_\rho \mapsto x_\rho$ for $\rho \neq \mu,\nu$. with

$$S_{R_{\mu\nu}}(x) = \tfrac{1}{2}(1 \pm \zeta_\mu(x)\zeta_\nu(x) \mp \eta_\mu(x)\eta_\nu(x) + \zeta_\mu(x)\zeta_\nu(x)\eta_\mu(x)\eta_\nu(x) \quad \mu \lesseqgtr \nu \tag{5.77}$$

   It can also be shown (relegated to the end of this section, for the sake of clarity here), albeit less trivially than for shift invariance, that the action is invariant under this transformation.

3. Axis Reversal

$$I^\mu : \chi \mapsto (-)^{x_\mu}\chi(I^{\leftarrow}x) \tag{5.78}$$

   where $I = I^\mu$ is the axis reversal $x_\mu \mapsto -x_\mu, x_\rho \mapsto x_\rho$ for $\rho \neq \mu$. One interesting point here is that γ_5 can no longer be associated with the chiral operator; the chiral and parity operators must anti-commute, whilst γ_5 and a position dependant sign factor will commute [104].

---

[8] One wants $\bar{\chi}(x+\rho)\zeta_\rho(x)\eta_\mu(x)\zeta_\rho(x)\bar{\chi}(x+\mu+\rho) = \bar{\chi}(x+\rho)\eta_\mu(x+\rho)\bar{\chi}(x+\mu+\rho)$, or, equivalently,

$$\zeta_\rho(x)\eta_\mu(x)\zeta_\rho(x) = \eta_\mu(x+\rho); \quad \eta_\mu(x+\rho) = \begin{cases} (-)^{\sum_{\nu<\rho} x_\nu+1} = -\eta_\mu(x) & \rho < \mu \\ (-)^{\sum_{\nu<\mu} x_\nu} = \eta_\mu(x) & \rho \geq \mu \end{cases} \tag{5.73}$$

Now

$$\zeta_\rho(x)\eta_\mu(x)\zeta_\rho(x) = (-)^{\sum_{\nu<\rho} x_\nu}(-)^{\sum_{\nu<\mu} x_\nu}(-)^{\sum_{\nu<\rho}(x+1)_\nu} \tag{5.74}$$

Since the last factor on the RHS is

$$(-)^{\sum_{\nu<\rho}(x+1)_\nu} = \begin{cases} -\zeta_\mu(x) & \mu > \rho \\ \zeta_\mu(x) & \mu \leq \rho \end{cases} \tag{5.75}$$

we have exactly the form desired.

4. $U_\alpha(1)$ Invariance; Baryon number conservation.

$$u : \chi(x) \mapsto e^{i\alpha}\chi(x) \tag{5.79}$$

for $u \in U(1), u(\alpha) = e^{i\alpha}$

5. $U_\epsilon(1)$ Invariance; A Chiral-like symmetry
This $U(1)$ symmetry is generated by:

$$u : \chi(x) \mapsto e^{i\beta\epsilon(x)}\chi(x) \tag{5.80}$$

for $u \in U(1), u(\beta) = e^{i\beta\epsilon(x)}$ with

$$\begin{aligned} \epsilon(x) &= (-)^{x_1+x_2+x_3+x_4} \\ &= e^{i\pi_\epsilon x_a} && (5.81) \\ \pi_\epsilon &= \pi_8 && (5.82) \end{aligned}$$

This is not the true axial symmetry (see the section on the axial anomoly on the lattice, section 5.1.1) since, whilst it acts like γ_5 on the spinors, it does so with + sign for two of the flavours and - sign for the other two; thus, since one has four flavours on the lattice, the generator of this symmetry is also a member of the group $SU_L(4) \otimes SU_R(4)$, as well as of the subgroup $SU_{L-R}(4)$, the axial group (see appendix B).

This is of great importance to QCD on the lattice; as discussed in appendix B the pion is a pseudo-Goldstone boson created by the spontaneous breakdown of $SU_L(4) \otimes SU_R(4)$ to $SU_{L+R}(4)$, the vector group, by the vacuum. Since one only has one of the generators of the broken $SU_{L-R}(4)$ symmetry on the lattice, one can only expect to get one pion. The other two should appear in the continuum limit.

6. Interchange of χ and $\bar{\chi}$, or charge conjugation

$$\begin{aligned} C : \chi &\mapsto \epsilon(x)\bar{\chi}(x) \\ C : \bar{\chi}(x) &\mapsto -\epsilon(x)\chi(x) \end{aligned} \tag{5.83}$$

One can re-write these in momentum space following the method given below.

In Momentum Space

Firstly, one needs two more sets of 16×16 matrices, Γ_μ and Ξ_μ, defined as follows:

$$\Gamma_\mu = S_\mu \hat{\pi}_{\eta_\mu}, \quad \Xi_\mu = S_\mu \hat{\pi}_{\zeta_\mu} \tag{5.84}$$

The commutation relations can be derived using the results given in eqn. 5.62, yielding

$$\begin{aligned} \{\Gamma_\mu, \Gamma_\nu\} &= S_\mu \hat{\pi}_{\eta_\mu} S_\nu \hat{\pi}_{\eta_\nu} + S_\nu \hat{\pi}_{\eta_\nu} S_\mu \hat{\pi}_{\eta_\mu} && (5.85) \\ &= S_\mu S_\nu S^\nu_{\eta_\mu} \hat{\pi}_{\eta_\mu} \hat{\pi}_{\eta_\nu} + S_\nu S_\mu S^\mu_{\eta_\nu} \hat{\pi}_{\eta_\nu} \hat{\pi}_{\eta_\mu} && (5.86) \\ &= 2\delta_{\mu\nu} \otimes \mathbb{1}_{16} && (5.87) \end{aligned}$$

since we have, from the definition of S^g_μ, and the fact that $(\pi_{\eta_\mu})_\nu = 0$ for $\nu \geq \mu$ and π otherwise; (vice-versa for $(\pi_{\zeta_\mu})_\nu$).

$$S^{\eta_\mu}_\nu = S^{\zeta_\mu}_\nu = \begin{cases} 1, & \mu \leq \nu, \\ -1, & \mu > \nu \end{cases} \tag{5.88}$$

Similarly, one can show that

$$\begin{aligned} \{\Xi_\mu, \Xi_\nu\} = 2\delta_{\mu\nu} \otimes \mathbb{1}_{16}, \quad [\Gamma_\mu, \Xi_\nu] = 0 \\ \Gamma_\mu = \Gamma^*_\mu = \Gamma^T_\mu, \qquad \Xi_\mu = \Xi^*_\mu = \Xi^T_\mu \end{aligned} \tag{5.89}$$

The symmetries then become, in momentum space;

1. Shift Invariance
$$\mathcal{S}_\mu : \tilde{\phi}_g(p) \mapsto e^{ip_\mu a}(\Xi_\mu)_{gg'}\tilde{\phi}_{g'}(p) \tag{5.90}$$
Which can be obtained from the form in configuration space as follows, performing a Fourier transform (eqn. 2.3) first:
$$\begin{aligned} \mathcal{S}_\mu : \tilde{\chi}(k) &\mapsto a^4 \sum_x \chi(x) e^{i(k+\pi_{\zeta_\rho})(x-\rho)} \\ &\mapsto e^{ik_\rho a}\tilde{\chi}(k + \pi_{\zeta_\rho}) \\ \mathcal{S}_\mu : \tilde{\phi}_g(p) &\mapsto e^{ip_\rho a + i(\pi_g)_\rho a}(\hat{\pi}_{\zeta_\rho})_{gg'}\tilde{\phi}_{g'}(p) \\ &\mapsto e^{ip_\rho a} S^\rho_g (\hat{\pi}_{\zeta_\rho})_{gg'}\tilde{\phi}_{g'}(p) \end{aligned} \tag{5.91}$$
(5.92)
where
$$\pi_{\zeta_\rho} + \pi_g = \pi_{g'} = (\hat{\pi}_{\zeta_\rho})_{gg'}\pi_{g'} \tag{5.93}$$

2. Rotational Invariance Following the same procedure as for the previous item, but with more in the calculation, one obtains the following form for the $\frac{\pi}{2}$ rotation in momentum space;
$$R_{\mu\nu} : \tilde{\chi}(p) \mapsto e^{\frac{\pi}{4}\Gamma_\mu\Gamma_\nu} e^{\frac{\pi}{4}\Xi_\mu\Xi_\nu}\tilde{\chi}(R^{\leftarrow}p) \tag{5.94}$$

3. Axis Reversal
$$I_\mu : \tilde{\chi}(p) \mapsto \Gamma_\mu\Gamma_5\Xi_\mu\Xi_5\tilde{\chi}(Ip) \tag{5.95}$$
where $\Gamma_5 = -\Gamma_1\Gamma_2\Gamma_3\Gamma_4$ and $\Xi_5 = -\Xi_1\Xi_2\Xi_3\Xi_4$

4. $U_\alpha(1)$ Invariance remains as before:
$$u : \chi(\tilde{p}) \mapsto e^{i\alpha}\chi(\tilde{p}) \tag{5.96}$$

5. $U_\epsilon(1)$ Invariance
$$u : \tilde{\chi}(p) \mapsto e^{i\beta\Xi_5\Gamma_5}\tilde{\chi}(p) \tag{5.97}$$
Using the relation $\Gamma_5\Xi_5 = \hat{\pi}_\epsilon$ which can be obtained by using the commutation relations given above and an explicit representation for the $\hat{\pi}$ matrices.

6. Charge Conjugation
$$\tilde{\chi}(p) \mapsto \tilde{\bar{\chi}}^T(-p) \quad \tilde{\bar{\chi}}(p) \mapsto \tilde{\chi}^T(-p) \tag{5.98}$$

Note that these symmetries only hold if one has periodic or anti-periodic boundary conditions, ie. $(\mathcal{S}_\mu)^{N_\mu} : \chi(x) \mapsto \pm\chi(x)$ with N_μ being the length of the lattice in the μ direction, which is required to be even for anti-periodic boundary conditions. (Screw boundary conditions, for example, would not yield these symmetries.)

From the continuous Poincaré group, we now have the 384 element group (W_4, [137]) of discrete rotations and reflections of the hypercube, with the shift symmetries. The proper rotations form a group of 192 elements, SW_4. Shifts and inversions transform as expected under an element of W_4; however, the differences between Lattice fermions and scalars becomes apparent when one considers the commutation of shift operators; for $\mu > \nu$ we have

$$\mathcal{S}_\mu\mathcal{S}_\nu : \chi(x) \mapsto \zeta_\mu(x+\nu)\zeta_\nu(x)\chi(x+\nu+\mu) = \zeta_\mu(x)\zeta_\nu(x)\chi(x+\nu+\mu) \quad (5.99)$$

$$\mathcal{S}_\nu\mathcal{S}_\mu : \chi(x) \mapsto \zeta_\nu(x+\mu)\zeta_\mu(x)\chi(x+\mu+\nu) = -\zeta_\mu(x)\zeta_\nu(x)\chi(x+\nu+\mu) \quad (5.100)$$

One can, however, construct operators $\mathcal{T}_\mu = \mathcal{S}_\mu^2$ that do commute.

Proof of Rotation Invariance

What is required here is that, for $R_{[\alpha\beta]}$ with $\alpha > \beta$,

$$\begin{aligned}&\textstyle\sum_{x,\mu}[\bar\chi(R^{\leftarrow}x)S_R(R^{\leftarrow}x)\eta_\nu(x)S_R(R^{\leftarrow}(x+\nu))\chi(R^{\leftarrow}(x+\nu))\\ &\qquad - \bar\chi(R^{\leftarrow}(x+\nu))S_R(R^{\leftarrow}(x+\nu))\eta_\nu(x)S_R(R^{\leftarrow}x)\chi(R^{\leftarrow}(x)) \\ &= \textstyle\sum_{x,\nu}[\bar\chi(R^{\leftarrow}x)\eta_\nu(R^{\leftarrow}x)\chi(R^{\leftarrow}(x+\nu)) - \bar\chi(R^{\leftarrow}(x+\nu))\eta_\nu(R^{\leftarrow}x)\chi(R^{\leftarrow}(x)\end{aligned} \quad (5.101)$$

In the continuum [15], a rotation affects the Dirac matrices via the commutator $G_{[\alpha\beta]} = \frac{1}{4}[\gamma_\alpha, \gamma_\beta]$. The rotation operator for a finite rotation of ϕ in the $\alpha\beta$ plane is given by $exp[G_{[\alpha\beta]}\phi] = cos(\frac{\phi}{2}) - 2G_{[\alpha\beta]}sin(\frac{\phi}{2})$. For a rotation given by $R_{[\alpha\beta]}$ we then have $R_{[\alpha\beta]} : \gamma_\alpha \mapsto \gamma_\beta$ and $R_{[\alpha\beta]} : \gamma_\beta \mapsto -\gamma_\alpha$; hence the same transformation must apply to the η_μ. To determine the effects of $S_R(R^{\leftarrow}x)$ on *eta* one needs the following results:

$$\eta_\mu(R^{\leftarrow}x) = \begin{cases} \eta_\mu(x) & \alpha \geq \mu, \beta \geq \mu \\ \eta_\mu(x) & \alpha < \mu, \beta < \mu \\ \eta_\mu(x)(-)^{x_\alpha+x_\beta}\{ & \alpha \geq \mu, \beta < \mu \\ & \alpha < \mu, \beta \geq \mu \end{cases} \quad (5.102)$$

$$\zeta_\mu(R^{\leftarrow}x) = \begin{cases} \zeta_\mu(x) & \alpha \leq \mu, \beta \leq \mu \quad 1 \\ \zeta_\mu(x) & \alpha > \mu, \beta > \mu \quad 2 \\ \zeta_\mu(x)(-)^{x_\alpha+x_\beta}\{ & \alpha \leq \mu, \beta > \mu \quad 3 \\ & \alpha > \mu, \beta \leq \mu \quad 4 \end{cases} \quad (5.103)$$

In evaluating $S_R(R^{\leftarrow}x)\eta_\nu(x)S_R(R^{\leftarrow}(x+\nu))$ one begins by using the above relations to re-write $S_R(R^{\leftarrow}x)$ i.t.o. x, yielding

$$S_R(R^{\leftarrow}x) = \frac{1}{2}\Big[1 - \eta_\alpha(x)(-)^{x_\alpha+x_\beta}\eta_\beta(x) + \zeta_\alpha(x)\zeta_\beta(x)(-)^{x_\alpha+x_\beta} \quad (5.104)$$

$$+ \eta_\alpha(x)\eta_\beta(x)\zeta_\alpha(x)\zeta_\beta(x)\Big] \quad (5.105)$$

For $S_R(R^{\leftarrow}(x+\nu))$ one has four cases: (1) $\nu < \beta$; (2) $\nu = \beta$; (3) $\nu = \beta$; (4) $\nu > \beta$. That the second case yields the correct result will be demonstrated below; the others can be

derived similarly.

$$\begin{aligned} S_R(R^{\leftarrow}(x+\nu)) &= \frac{1}{2}\Big[1-\eta_\alpha(x+\nu)(-)^{x_\alpha+x_\beta}\eta_\beta(x+\nu)+\zeta_\alpha(x+\nu)\zeta_\beta(x+\nu)(-)^{x_\alpha+x_\beta+1} \\ &\quad +\eta_\alpha(x)\eta_\beta(x)\zeta_\alpha(x)\zeta_\beta(x)(-)\Big] \\ &= \frac{1}{2}\Big[1-\eta_\alpha(x)(-)^{x_\alpha+x_\beta}\eta_\beta(x)+\zeta_\alpha(x)\zeta_\beta(x)(-)^{x_\alpha+x_\beta+1} \\ &\quad +\eta_\alpha(x)\eta_\beta(x)\zeta_\alpha(x)\zeta_\beta(x)(-)\Big] \end{aligned} \tag{5.106}$$

Since the S are merely numbers, they commute with the η; taking the product of eqns. 5.104 and 5.106 one has:

$$\begin{aligned} S_R(R^{\leftarrow}x)\eta_\nu(x)S_R(R^{\leftarrow}(x+\nu)) &= -\eta_\nu(x)\eta_\alpha(x)\eta_\beta(x)(-)^{x_\alpha+x_\beta} \\ &= -\eta_\alpha(x)(-)^{x_\alpha+x_\beta} \qquad (5.107) \\ &= -\eta_\alpha(R^{\leftarrow}x) \qquad (5.108) \end{aligned}$$

For a rotation in the $\alpha\beta$ plane the terms in the action not invoving either of these indices are manifestly invariant; performing the above transformation on the two relevant terms yields

$$\begin{aligned} &\textstyle\sum_x[\bar\chi(R^{\leftarrow}x)(-)\eta_\alpha(R^{\leftarrow}x)\chi(R^{\leftarrow}(x+\beta)) - \bar\chi(R^{\leftarrow}(x+\beta)(-)\eta_\alpha(R^{\leftarrow}x)\chi(R^{\leftarrow}(x) \\ &\quad +\bar\chi(R^{\leftarrow}x)\eta_\beta(R^{\leftarrow}x)\chi(R^{\leftarrow}(x+\alpha)) - \bar\chi(R^{\leftarrow}(x+\alpha))\eta_\beta(R^{\leftarrow}x)\chi(R^{\leftarrow}(x)] \\ &=\textstyle\sum_x[\bar\chi(R^{\leftarrow}x)(-)\eta_\alpha(R^{\leftarrow}x)\chi(R^{\leftarrow}(x)-\alpha) - \bar\chi(R^{\leftarrow}(x)-\alpha)(-)\eta_\alpha(R^{\leftarrow}x)\chi(R^{\leftarrow}(x) \\ &\quad +\bar\chi(R^{\leftarrow}x)\eta_\beta(R^{\leftarrow}x)\chi(R^{\leftarrow}(x)+\beta) - \bar\chi(R^{\leftarrow}(x)+\beta))\eta_\beta(R^{\leftarrow}x)\chi(R^{\leftarrow}(x)] \\ &=\textstyle\sum_x[\bar\chi(R^{\leftarrow}x)\eta_\alpha(R^{\leftarrow}x)\chi(R^{\leftarrow}(x)+\alpha) - \bar\chi(R^{\leftarrow}(x)+\alpha)\eta_\alpha(R^{\leftarrow}x)\chi(R^{\leftarrow}(x) \\ &\quad +\bar\chi(R^{\leftarrow}x)\eta_\beta(R^{\leftarrow}x)\chi(R^{\leftarrow}(x)+\beta) - \bar\chi(R^{\leftarrow}(x)+\beta))\eta_\beta(R^{\leftarrow}x)\chi(R^{\leftarrow}(x)] \end{aligned} \tag{5.109}$$

Thus giving the rotational invariance desired!

5.4.6 Construction of Flavoured Quark Fields

One can define 4 flavoured quark fields, each with the requisite number of Dirac components, from the 16 χ defined on the corners of a tesseract [138,93,139,35]. In the text below, these will be constructed following the definitions of [35,138], in configuration space[9].

One begins by defining the physical lattice, $\{y\}$ with lattice spacing $2a$, from the existing lattice $\{x\}$ with lattice spacing a:

$$x_\mu = 2y_\mu + A_\mu \tag{5.110}$$

where the 16 A_μ are 0 or 1, as defined in section 5.4.2. Thus these A_μ define the corners of the tesseract with origin at the point $x = 2y$.

[9] One can also construct the quark fields in momentum space; in that case, one usually takes the 16 different regions of momentum space to define the requisite degrees of freedom. The construction in momentum space can be related to the one in configuration space [74]

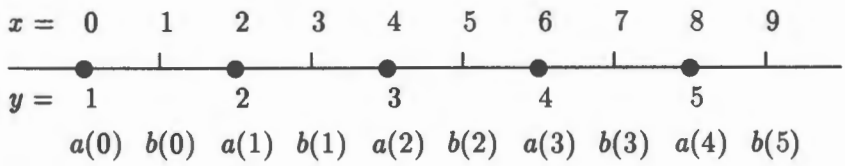

Figure 5.3: Blocked lattice in 1 dimension

One then defines the 4 flavours of quarks as follows:

$$q_i^{\alpha a}(y) = \frac{1}{8}\sum_A \Gamma_A^{\alpha a} U^{ij}(y,A)\chi_j(2y+A) \tag{5.111}$$

$$\bar{q}_i^{\alpha a}(y) = \frac{1}{8}\sum_A \bar{\chi}_j(2y+A)U^{\dagger ij}(y,A)\Gamma_A^{*\alpha a} \tag{5.112}$$

with α the Dirac index, a the flavour index, i,j colour indices and $\Gamma_A^{\alpha a}$ the αa component of the matrix Γ_A, one of the 16 independent matrices representing the Clifford Group (see appendix C for the explicit construction of the matrices), constructed identically to the $T(x)$ used as the transformation matrices in section 5.4.2. One may choose the basis vectors $(1,0,0,0),(0,1,0,0),(0,0,1,0),(0,0,0,1)$ for the u,d,s,c quarks respectively.

Finally, the $U^{ij}(y,A)$ are the products of the connections from $x = 2y$ to $x = 2y + A$ along some path linking the two corners of the tesseract. One possible choice is

$$U^{ij}(y,A) = [U_1(y)]^{A_1}[U_2(y)]^{A_2}[U_3(y)]^{A_3}[U_4(y)]^{A_4} \tag{5.113}$$

in which the exponent of A_μ insures that the connection corresponding to any direction that does not contribute to the destination corner yields the unit matrix.

To begin with, one may consider the effect that 'blocking' the lattice in this fashion has upon the form of the action. Consider a one dimensional lattice, blocked in this fashion to yield the physical lattice, with new variables defined on the physical lattice as follows (note that this construction [139] differs from that commonly used today on the lattice [35]; it is, however, pedagogically clearer):

$$a(y) = \chi(2y) \quad b(y) = \chi(2y+1) \tag{5.114}$$

as depicted in figure 5.3. Now the one-dimensional fermion action can then be written as follows:

$$\sum_y \bar{a}(y)\frac{b(y)-b(y-1)}{2a} + \bar{b}(y)\frac{a(y+1)-a(y)}{2a} \tag{5.115}$$

which can be re-expressed in terms of forward and backward derivatives:

$$\sum_y \bar{a}(y)\Delta^- b(y) + \bar{b}(y)\Delta^+ a(y) \tag{5.116}$$

Notice now that these derivatives are *not* on the original lattice, but are on the physical lattice. The backward derivative is a difference between the current block and the previous

one, whilst the forward derivative is a difference between the next block and the current one. Further, note that the intrinsic lattice spacing has now become $2a$.

One can define two further derivatives on the physical lattice, ∂ and ∂^2 as

$$\begin{aligned} \partial f(y) &= \frac{1}{2}[\Delta^+ + \Delta^-]f(y) \\ &= \frac{f(y+1) - f(y-1)}{4a} \end{aligned} \tag{5.117}$$

$$\begin{aligned} \partial^2 f(y) &= \frac{1}{2a}[\Delta^+ - \Delta^-]f(y) \\ &= \frac{f(y+1) - 2f(y) + f(y-1)}{4a^2} \end{aligned} \tag{5.118}$$

Using these, one can write the action as

$$\sum_y \Big\{\bar{a}(y)[\partial b(y) - 2a\partial^2 b(y)] + \bar{b}(y)[\partial a(y) + 2a\partial^2 a(y)]\Big\} \tag{5.119}$$

which has two components:

1. A naive symmetric derivative on the physical lattice, between two adjacent blocks.
2. A second derivative, linking the current, past and future blocks. This term is responsible for lifting the fermion degeneracy, and vanishes in the limit $a \to 0$. This is similar to the Wilson method, in that one adds a term that resembles a second derivative as well. Note the difference in the relative sign between the first and second derivatives in each square bracket; this is essentially a flavour effect, and carries through into the full four-dimensional approach.

As a final step towards identifying the different flavours, write

$$a(y) = \tfrac{1}{2}[u(y) + d(y)] \quad b(y) = \tfrac{1}{2}[u(y) - d(y)] \tag{5.120}$$

where the two variables now represent different flavours. One can now regard the two flavours of fermions as existing on the physical lattice, composed of components from the fundamental lattice that have been 'smeared out' across the block. The two-dimensional action then reads

$$\begin{aligned} \textstyle\sum_y \{&[\bar{u}(y)\partial u(y) + \bar{d}(y)\partial d(y) + m_u\bar{u}(y)u(y) + m_d\bar{d}(y)d(y)] \\ &+ 2a[\bar{d}(y)\partial^2 d(y) - \bar{d}(y)\partial^2 u(y)]\} \end{aligned} \tag{5.121}$$

into which explicit mass terms have been added.

It is clear that this will become the standard Dirac equation for two independent fermions in the continuum limit, since the terms in the second bracket that are responsible for both lifting the degeneracy and the flavour mixing will vanish.

Returning now to the 4 dimensional case, one proceeds as follows in the explicit construction of the field for an up quark, $q_i^{\alpha 1}$, in the non-interacting limit $U = \mathbb{1}$. one then obtains:

$$q_i(y) = \frac{1}{8}\sum_A \Gamma_A \begin{pmatrix} 1 \\ 0 \\ 0 \\ 0 \end{pmatrix} \chi_i(2y + A) \tag{5.122}$$

$$
\begin{aligned}
q_i(y) &= \frac{1}{8}\left[\begin{pmatrix}1\\0\\0\\0\end{pmatrix}\chi_i(2y)+\begin{pmatrix}0\\0\\0\\i\end{pmatrix}\chi_i(2y+(1,0,0,0))+\cdots+\begin{pmatrix}0\\0\\1\\0\end{pmatrix}\chi_i(2y+(1,1,1,1))\right] \\
&= \frac{1}{8}\begin{pmatrix}
\chi_i(2y) & + & \chi_i(2y+\hat{t}) \\
i\chi_i(2y+\hat{y}+\hat{z}) & + & \chi_i(2y+\hat{x}+\hat{z} \\
i\chi_i(2y+\hat{z}) & + & i\chi_i(2y+\hat{z}+\hat{t}) \\
i\chi_i(2y+\hat{x}+) & - & \chi_i(2y+\hat{y}) \\
+\quad i\chi_i(2y+\hat{x}+\hat{y}) & + & i\chi_i(2y+\hat{x}+\hat{y}+\hat{t}) \\
+\quad \chi_i(2y+\hat{x}+\hat{z}+\hat{t}) & + & i\chi_i(2y+\hat{y}+\hat{z}+\hat{t}) \\
-\quad \chi_i(2y+\hat{x}+\hat{y}) & + & \chi_i(2y+\hat{x}+\hat{y}+\hat{z}+\hat{t}) \\
+\quad i\chi_i(2y+\hat{x}+\hat{t}) & - & \chi_i(2y+\hat{y}+\hat{t})
\end{pmatrix}
\end{aligned}
\tag{5.123}
$$

This gives the four Dirac components of the up quark, again in terms of the fundamental lattice variables 'smeared out' over the block. The full fermion action can be written, in analogy with the method used, as follows:

$$
\begin{aligned}
S_F &= (2a)^4 \sum_y \bar{q}_i^{\alpha a}[(\gamma_\mu \partial^\mu)_{\alpha\alpha'} \mathbb{1}_{aa'} + \mathbb{1}_{\alpha\alpha'} m_{aa'}] q_i^{\alpha' a'} \\
&\quad a\bar{q}_i^{\alpha a}[(\gamma_5^\dagger)_{\alpha\alpha'}(\gamma_\mu^\dagger \partial_\mu^2 \gamma_5^\dagger)_{aa'}] q_i^{\alpha' a'}
\end{aligned}
\tag{5.124}
$$

with implicit summation over all repeated indices. The mass matrix has also been made explicit, with the possibility of different masses for the different flavours.

The derivatives are defined in the same way as those above, with

$$
\partial_\mu f(y) = \frac{1}{4a}[f(y+\mu) - f(y-\mu)] \stackrel{a\to 0}{\longrightarrow} \partial_\mu f(y) \tag{5.125}
$$

$$
\partial_\mu^2 f(y) = \frac{1}{4a}[f(y+\mu) + f(y-\mu) - 2f(y)] \stackrel{a\to 0}{\longrightarrow} \partial_\mu^2 f(y) \tag{5.126}
$$

The re-appearance of the Dirac matrices in this formulation, after they were removed by the spin diagonalisation, is due to the appearance of Γ in the definition of the flavours. One can also do this in two stages, by firstly obtaining four independent Dirac spinors and then re-defining each component such that they have the correct behaviour under the Dirac matrix [139].

Whilst with the original Kogut-Susskind fermions the symmetries were broken by the transformation into one-component variables per site, in this formulation the first term has the full symmetry. It is the second term, vanishing in the continuum limit, that breaks the symmetries down to those given earlier.

Since the symmetry breaking term is now manifestly proportional to the lattice spacing in this formulation, as well as in the Wilson formulation, it is plausible that the full symmetry group of QCD is restored in the continuum limit.

5.4.7 Flavour in Momentum Space

The relationship between the flavoured quarks in momentum space and configuration space was elucidated by Daniel and Kieu [74]. The essential difference is that the fields are flavour diagonal in configuration space, but contain flavour mixing terms in momentum space. The

mixing in momentum space is due to the fact that the seperation of degrees of freedom is done by treating the 16 regions of the Brillouin zone as independent. This is discontinuous at the boundary of the Brillouin zone, which implies non-locality in the corresponding configuration space.

There is also a transformation from the configuration and momentum space interpretations, that tends towards the identity in the continuum limit. Thus, in the continuum limit the two formulations are identical (a fact that was demonstrated by the restoration of flavour symmetry in the continuum limit [41]) .

However, each is useful in different areas on the lattice. The configuration space formulation, being local, is suited to numerical work on, for example, the hadron masses. However, the momentum space interpretation is ideally suited to weak-coupling perturbation theory.

In general, one can say that both forms are, away from the continuum limit, merely rules for associating spin and flavour quantum numbers to the requisite hadrons on the lattice.

5.5 Wilson Fermions

5.5.1 Definition

The essence of Wilson's Method [212,189,134] is to add a term of the form $ar(\partial_\mu^{\mathrm{fwd}}\bar{\psi})(\partial_\mu^{\mathrm{fwd}}\psi)$, with ∂^{fwd} being the forward difference introduced in section 2, and $0 < r \leq 1$, to the naive fermion action, equation 5.12. This term vanishes in the continuum limit for the desired fermion, since it is proportional to the lattice spacing (the forward difference is finite); it adds a mass term of order $\frac{r}{a}$ to the unwanted fermions (since the forward difference is of order $O\left(\frac{1}{a}\right)$), hence they no longer exist as real particles.

This is illustrated in the dispersion relations for Wilson fermions, using different values of the parameter r; (see figs. 5.4 and 5.5). The choice $r = 1$ corresponds to Wilson's original choice.

In detail, the Wilson approach is as follows: add a term

$$\begin{aligned} & ra^4 \sum_{x,\mu} \frac{1}{2a}[\bar{\psi}(x+\mu) - \bar{\psi}(x)][\psi(x+\mu) - \psi(x)] \\ & \quad = ra^4 \textstyle\sum_{x,\mu} \frac{1}{2a}[-\bar{\psi}(x+\mu)\psi(x) - \bar{\psi}(x)\psi(x+\mu) + 2\bar{\psi}(x)\psi(x) \end{aligned} \tag{5.127}$$

to the naive fermion action, eqn. 5.12. This can then be written as

$$\begin{aligned} S_{\mathrm{F}} &= -a^4 \sum_{x,\mu} \frac{1}{2a}[\bar{\psi}(x)(\gamma_\mu - r)\psi(x+\mu) + \bar{\psi}(x+\mu)(r+\gamma_\mu)\psi(x)] \\ &\quad + a^4 \sum_x [m\bar{\psi}(x)\psi(x) + 4\frac{r}{a}\bar{\psi}(x)\psi(x)] \end{aligned} \tag{5.128}$$

Should one want more than one flavour on the lattice, one simply adds a summation over the flavour index to the above equation.

This can be re-written in another form, using a re-scaling of the ψ: $\psi(x) \mapsto \psi_x = (2ma+8r)^{-1/2}\psi(x)$. The action is then written in terms of the so-called 'hopping parameter,' $\kappa = \frac{1}{2ma+8r}$. The hopping parameter gives the probability for a quark to move from one site to a neighbouring site. Hence eqn. 5.128 becomes

$$S_{\mathrm{F}} = -a^4 \sum_{x,\mu} \frac{1}{2a}[\bar{\psi}(x)(\gamma_\mu - r)\psi(x+\mu) + \bar{\psi}(x+\mu)(r+\gamma_\mu)\psi(x)]$$

$$
\begin{aligned}
&+ a^4 \sum_x \frac{1}{2a}(2ma + 8r)\bar{\psi}(x)\psi(x) \\
= \; & -a^4 \sum_{x,\mu} \frac{1}{2a} \frac{1}{(2ma + 8r)} [\bar{\psi}_x(\gamma_\mu - r)\psi_{x+\mu} + \bar{\psi}_{x+\mu}(r + \gamma_\mu)\psi_x] \\
&+ a^4 \sum_x \frac{1}{2a} \bar{\psi}_x \psi_x \\
= \; & -a^4 \sum_x \sum_{ij} \sum_{f=1}^{N_f} \frac{1}{2a} \left\{ \kappa^f \sum_\mu [\bar{\psi}^f_{ix}(\gamma_\mu - r) U_{\mu ij}(x) \psi^f_{j,x+\mu} \right. \\
&\left. + \bar{\psi}^f_{i,x+\mu}(r + \gamma_\mu) U^\dagger_{\mu ij}(x) \psi^f_{j,x}] + \bar{\psi}^f_{i,x} \psi^f_{j,x} \delta_{ij} \right\}
\end{aligned}
\tag{5.129}
$$

with explicit flavour index f running from 1 to N_f. In the last line the gauge fields (connections between x and $x + \mu$) have been included explicitly, as have the colour (i, j) indices. Note that each spinor still carries a Dirac index, which has been suppressed.

This can be re-written in a form closer to the continuum form for the Dirac equation:

$$
S_{\mathrm{F}} = -a^4 \sum_{x,\mu} [\bar{\psi}^{fi}_\alpha(x) K^f(\alpha, i, x; \beta, j, y) \psi^{fj}_\beta(y)] \tag{5.130}
$$

with the fermion matrix, given by

$$
\begin{aligned}
K^f(\alpha, i, x; \beta, j, y) \; = \; & \frac{1}{2a} \left\{ \kappa^f \sum_\mu \left[\; \delta_{x+\mu,y} U^\dagger_{\mu ij}(x)(\gamma_\mu - r)_{\alpha\beta} \right. \right. \\
& \left. \left. + \delta_{x-\mu,y} U_{\mu ij}(y)(r + \gamma_\mu)_{\alpha\beta} \right] + \delta_{\alpha\beta} \delta_{ij} \delta_{x,y} \right\}
\end{aligned}
\tag{5.131}
$$

with the Greek letters being Dirac indices, i, j colour indices and the gauge variables explicitly included.

5.5.2 Wilson Propagator

The propagator can be obtained by, as usual, performing a Fourier transform on eqn. 5.128. This yields

$$
S^{-1}(p) = \sum_\mu \left[\frac{i}{a} \gamma_\mu \sin(p_\mu a) \right] + m + \sum_\mu \frac{r}{a} [1 - \cos(p_\mu a)] \tag{5.132}
$$

or, using the variety with the hopping parameter,

$$
S^{-1}(p) = 1 - \kappa \sum_\mu [i\gamma_\mu \sin(p_\mu a) + r \cos(p_\mu a)] \tag{5.133}
$$

Looking at eqn. 5.132 one can see that this has yielded a mass term consisting of the bare mass and a term that is non-zero at the points in momentum space originally responsible for the spectral multiplicity. This term is also of order $O(\frac{1}{a})$, and thus the spurious mass terms go to infinity in the continuum limit.

One can get an idea of the method by considering the dispersion relation, and comparing with that for the naive fermions (figure 5.2). Consider a two-dimensional space, with time

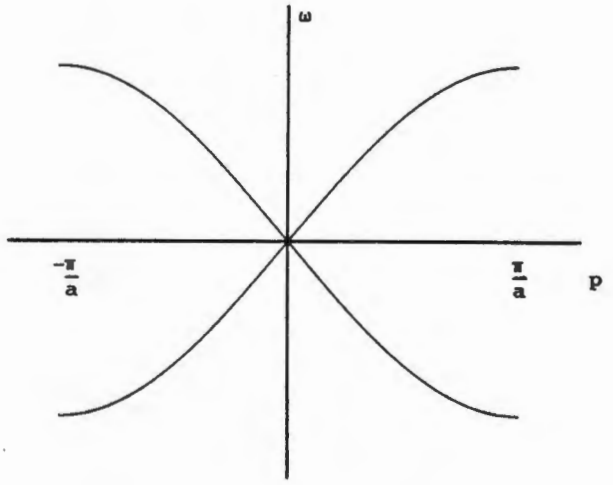

Figure 5.4: Dispersion relation for Wilson fermions, $r = 1$.

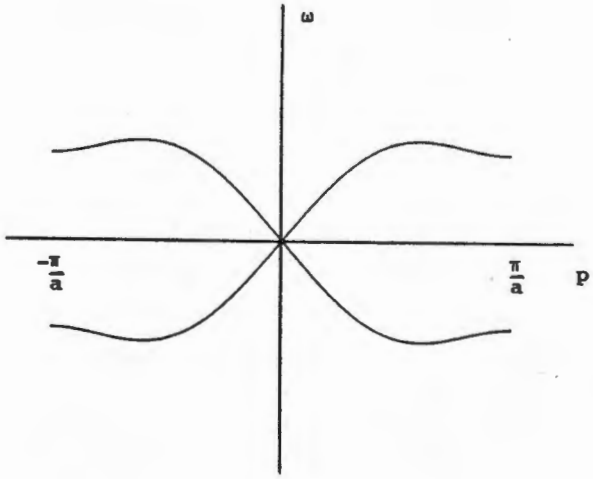

Figure 5.5: Dispersion relation for Wilson fermions, $r = 0.5$.

left continuous[10] ; the Dirac action for Wilson fermions is then

$$S_F = -\int d\tau a \sum_x \int d\tau a' \sum_{x'} \bar{\psi}(\tau', x') \left\{ \gamma_4 \delta_{\tau',\tau} \partial_{\tau'} + \frac{(\gamma_1 - r)\delta_{x',x+1} + (r + \gamma_1)\delta_{x',x-1}}{2a} + \left(m + \frac{r}{a}\right) \delta_{\tau',\tau} \delta_{x',x} \right\} \psi(t, x) \tag{5.134}$$

with the following choice of gamma matrices:

$$\gamma_4 = \begin{pmatrix} 0 & -1 \\ 1 & 0 \end{pmatrix} \quad \gamma_1 = \begin{pmatrix} 0 & 1 \\ 1 & 0 \end{pmatrix} \tag{5.135}$$

The Fermion propagator is then given by

$$S^{-1} = i\gamma_4 \omega + \frac{i}{a}\gamma_1 \sin(pa) + \left[\frac{r}{a}(1 - \cos(pa)\right] \tag{5.136}$$

The dispersion relation is obtained from the poles of the propagator, and thus is given by (after multiplying by the complex conjugate):

$$a^2\omega^2 = \sin^2(pa) + a^2 \left[m + \frac{r}{a}(1 - \cos(pa)\right]^2 \tag{5.137}$$

This is plotted in fig. 5.4 and 5.5 for $a = 1$, $r = 1$ and $r = 0.5$ respectively.

[10] Note that this is now in the Hamiltonian formulation, and we have diag$g^{\mu\nu} = (1, -1)$ with $\{\gamma_\mu, \gamma_\nu\} = 2g^{\mu\nu}$.

5.5.3 The Hopping Parameter

Turning to the version of the fermion propagator containing the hopping parameter, eqn. 5.133, and looking at the continuum limit, one gets

$$\begin{aligned} S^{-1} &\xrightarrow{a\to 0} 1 - 2\kappa \sum_{\mu} i\gamma_\mu p_\mu a - 8r\kappa \\ &= 2\kappa a \left(\frac{1 - 8\kappa r}{2\kappa a} - i\gamma_\mu p_\mu a \right) \end{aligned} \tag{5.138}$$

This gives one the Dirac equation, up to a normalisation constant of $2\kappa a$, provided one takes as the mass of the fermion the value

$$m = \frac{1 - 8\kappa r}{2\kappa a} \tag{5.139}$$

One can then take two different limits; the chiral limit, with zero mass fermions, gives $\kappa = \frac{1}{8}$; and the continuum limit. For the latter to make sense, one obviously wants the above fraction to approach the constant value of the mass of the relevant fermion in the continuum; since $a \to 0$, the numerator must also tend to 0. This gives the continuum, or critical, value of the hopping parameter, as

$$\kappa_c = \frac{1}{8} \tag{5.140}$$

One can then write the mass of the fermion (say a quark) as

$$\begin{aligned} m_q &= \ln \left[1 + \frac{1}{2} \left(\frac{1}{\kappa} - \frac{1}{\kappa_c} \right) \right] \\ &\xrightarrow{\kappa \to \kappa_c} \frac{1}{2} \left(\frac{1}{\kappa} - \frac{1}{\kappa_c} \right) \end{aligned} \tag{5.141}$$

The continuum value of the hopping parameter is found in hadron spectrum calculation by extrapolating the mass of the pion to zero; this corresponds to the critical hopping parameter, or the zero quark mass limit. (The pion mass tends to zero with the quark mass, since it is a pseudo Goldstone boson, as discussed in appendix B.)

A clearer idea of the effect of taking the continuum limit on the mass term can be gained by considering the first version of the propagator, eqn. 5.132, at the tree-graph level. This has a mass-like term of the form $M = m + \frac{4r}{a} = \frac{1}{2a\kappa}$. Regarding m as the physical mass, the requirement that m must be independent of a leads to the necessary behaviour of aM; viz., $aM \xrightarrow{a\to 0} 4r$.

At any order one thus expects that aM is required to approach a critical value, in such a fashion that the physical mass remains finite in the continuum limit. Karsten and Smit showed that the r-dependence of the higher-order terms can be re-absorbed into the coupling constant, mass and wave-function renormalisation, yielding $aM_c = 4r + O(g^2)$. This leads to one of the drawbacks of the Wilson formulation, as compared to the Kogut-Susskind; one needs mass counter-terms (of order $\frac{1}{a}$) in order to insure that the physical mass remains constant as one approaches the continuum limit.

The further requirement one has of the Wilson mass terms is that the effect that they have on the wanted fermion must vanish in the continuum limit, in order that one regains chiral symmetry for massless quarks.

5.5.4 Relationship between Wilson and Kogut-Susskind fermions

A priori, any lattice formulation of physics must give the same continuum limit; there is, after all, only one continuum physics that is measured!

It was shown by Kawamoto and Smit [134] that one could move from the Wilson approach to the Kogut-Susskind approach by taking the limit as $r \to 0$ and applying the standard techniques of Kogut-Susskind. Hence one expects both methods to give the same results away from the continuum limit, (except in anything concerning chiral symmetry, in which only the Kogut-Susskind approach can give any information).

This enables one to use the two different methods to check the validity of a calculation away from the continuum limit; the two versions must be coherent, up to some transformation from one to the other that vanishes in the continuum limit.

5.5.5 Symmetries of the Wilson Action

The Wilson action has one advantage over the Kogut-Susskind action, in that it does not mix translational and internal symmetry groups, and carries over the symmetries of the continuum directly.

The Wilson fermion action then has invariance under: translation in units of the lattice spacing, rotation in multiples of $\frac{\pi}{2}$, axis inversion, charge conjugation, flavour SU(N_f) (assuming N_f flavours have been placed on the lattice) and U(1) invariance.

Since the details of the Wilson fermion symmetries are similar to those of the Kogut-Susskind fermions, up to the difference between even and odd lattice sites in the latter case, the discussion of these symmetries has been omitted for brevity. (Remember that this difference is caused by the method used to retain some chiral symmetry.)

5.6 Recent Fermion Proposals

5.6.1 Disordered Fermion Couplings

This approach to constructing fermions on the lattice does not have spectral multiplicity. It satisfies the Nielsen-Ninomiya theorem (see appendix A) by breaking the requirements of translational invariance and hermiticity.

The basic idea is to add forward and backward derivatives, with a random coupling between them. This fermionic interaction term is very similar in construction to the Wilson term, and also vanishes in the continuum limit. The fermion action is then given by:

$$\begin{aligned} S_F &= a^d \sum_x \sum_\mu \frac{1}{2a}[\bar{\psi}(x)\gamma_\mu\psi(x+\mu) - \bar{\psi}(x+\mu)\gamma_\mu\psi(x)] + a^d \sum_x [m\bar{\psi}(x)\psi(x) \\ &+\lambda \left(a^d \sum_x \sum_\mu \frac{1}{a}\bar{\psi}(x) z_\mu(x)\gamma_\mu[\psi(x+\mu) - \psi(x)] \right. \qquad (5.142) \\ &\left. + a^d \sum_x \sum_\mu \frac{1}{a}\bar{\psi}(x) z_\mu(x-\mu)\gamma_\mu[\psi(x-\mu) - \psi(x)] \right) \qquad (5.143) \end{aligned}$$

with λ a term governing the hermiticity of the interaction. For $\lambda = 1$ the interaction is purely hermitian, and with $\lambda = i$ the interaction term is purely anti-hermitian. The disorder field $z_\mu(x)$ is a Gaussian random field with width σ.

This approach was first proposed by Parisi and Zhang in 1983 [170], with negative results; they found that the required elimination of species doubling did not occur. However, a recent calculation [32] has shown that the elimination of spectral doubling is dependant on the ratio of the width of the disorder field and the fermionic mass. If the width is small, compared to the quark mass, then one obtains doubling, in agreement with the result of [170].

If the width is large compared to the quark mass, then one does not obtain doubling [32]. There is also an intermediate crossover region, in which the propagator diverges.

In the large disorder region, the behaviour is completely different to that of the naive fermions. Firstly, analysis of a function of the momentum shows that there is no spurious pole in momentum space. Secondly, and only for the case of the anti-hermitian coupling, the correct ratio between the pion and rho mass, and the correct scaling of the masses against the quark mass is obtained.

Thus only the anti-hermitian form has any potential applicability.

There are, however, two serious problems. Firstly, one requires considerably more CPU time for the inversion of the fermion matrix than is required for the Wilson or Kogut-Susskind fermions. Since that is already the major factor in full QCD simulations, it prohibits any implementation of this algorithm. Secondly, this approach has only been simulated for 2 dimensions; it is believed [32] that the behaviour in higher dimensions will not necessarily follow the same patterns.

Hence, at the moment, it does not appear to be a useful method of placing fermions on the lattice.

5.6.2 Renormalisation Group Improvements

By making use of the renormalisation group equation, one can move from a theory close to the phase transition (and hence with a large correlation length) to one further away. By doing this, one can either obtain an action that is faster to evaluate near the phase transition, or one that is relatively closer to the continuum than before without any change in the lattice spacing.

An improved fermion action has been obtained by, for example, Gusken et al. [111]. The effective action was generated by 'blocking' a large lattice. This consists of dividing the lattice into blocks of, say, 2^4 sites and integrating out the high frequency modes within the block[11]. This results in a more complex fermionic action with next to nearest neighbour couplings. However, the long-distance behaviour is preserved and is easier to evaluate.

In a study [13] of the hadron masses on a $24^3 \times 48$ lattice, twice blocked with a scale factor of 2, and in the quenched approximation, the signal to noise ratio was improved and smaller quark masses could be reached, as compared to lattices of comparable size to the final blocked lattice. Another study was made on a lattice of the same size, using the $\sqrt{3}$ transformation, [77], see section 8. This study achieved results very close to the physical spectrum.

An idea proposed by Wilcek [211] along similar lines involved thinning out the fermion degrees of freedom, whilst retaining the fine structure of the gluon degrees of freedom. Treating the gluons on a finer lattice than the quarks makes sense physically. The numerical value of the β function is dominated by gluon contributions. The glueball spectrum begins at around 2 GeV, and becomes steadily more important as the length scale decreases.

[11] This application of the renormalisation group is in the same spirit as that used to evaluate the non-perturbative β-function on page 4.1; hence one can also use blocks of linear size other than 2.

It is plausible then to include the quarks accurately only at large distances, where the glueballs have negligible effect. This would reduce the computational time required considerably, since proportionately less time would be spent on the computationally intensive fermion sector.

5.6.3 Random Lattices

The use of random lattices has been a proposed method of solving the fermion problem from the early days of lattice QCD. However, it is hampered by the vast increase in computer time required. This is due to the fact that detailed information needs to be stored on the connection between each pair of lattice sites. There are two types of random lattices in use; the so-called random lattice, which has a triangle as a basic unit cell, and the random block lattice which has a rectangle as the basic unit cell. The random block lattice is the prefered type, since it is more efficient to implement on a parallel supercomputer.

In the random block lattice, one takes over the usual naive Dirac lagrangian, with the modification that all references to a are replaced by the seperation between the two sites referred to at any point in the summation.

A random lattice breaks translational invariance, and in this fashion enables the construction of undoubled chiral fermions. The massless fermion propagator on a two dimensional lattice was shown [181] to consist of either left or right moving fermions in the continuum limit. Translational invariance is regained by summing over an ensemble of random lattices. On the random lattice, the fermion doubles acquire masses of the order of a^{-1} and thus decouple in the continuum limit.

A study of interacting fermion on a random lattice [174] came to the conclusion that the problem of the doubles becomes manifest again when one introduces the interaction. It was found that the doubles enter into the one-loop calculations, and that they do affect the finite part. This has the undesirable consequence of breaking the chiral invariance of the wanted fermion via the radiative mass corrections.

The net result is the need for mass counterterms, and fine tuning in lattice QCD on a random lattice; just as is required for Wilson fermions.

Chiu [60] has studied the Schwinger model on a random block lattice. Since this has no divergence in the one-loop diagrams, the problems described above do not affect it. A short discussion of the results obtained is presented in section 9.6.

There has also been an investigation of fractal lattices [191]. The conclusions were negative, in that the usual problem of fermion doubling was found.

5.6.4 Smeared Fermions

This is an approach taken by Trivedi [199,198]. It is based on the idea that the problems with fermion doubling are due to treating space-time in an unjustifiably overlocalized fashion. The first point to realise is the fact that the lattice does *not* provide a foolproof UV cutoff. It is possible to construct a lattice theory with UV infinities, despite the finite lattice spacing.

An example of this was given in [199], using a Yukawa coupling, $\phi\bar{\psi}\psi$ of scalar and fermion fields. It was shown that the one-loop correction to both the scalar and fermion propagators had integrands of the form p^{2n}/p^4; and hence diverge in any dimension $n \geq 2$.

Motivation for the solution to this problem, and also to that of fermion doubling, came from the observation that the Nielsen-Ninomiya theorem applies to the physical universe as

well as the lattice approximation to it. Namely, the observation of a chiral fermion with finite range coupling in the physical universe leads incontrovertably to the conclusion that spacetime has no lattice structure on any scale whatsoever! However, one expects a question on the lattice structure of spacetime to be answered by an experiment conducted at the scale of the structure itself; certainly not at a macroscopic level far above any structure.

There is also reason to believe that the fermion doubling problem lies less with the essential nature of fermions than it does with the general kinematics of spacetime itself. This is due to the discovery that spin 2 gravitons in the lattice Einstein Lagrangian are also doubled, to the same extent as for the fermions; there are 16 lattice gravitons to each continuum graviton [158]. There is also evidence of doubling in the time dependent Schrödinger equation.

Trivedi posits that the doubling problem is due to the following overlocalized elements of the theory on the lattice:

1. The lattice derivatives act in a single direction, and are infinitely sharp in the transverse direction.

2. Observables are taken to exist as sharply localized functions of a single lattice site, ignoring the possibility of quantum interference from neighbouring sites.

3. The final UV behaviour of a theory depends upon how 'smeared' the interacting theory is with respect to the free theory.

The remedy suggested for curing the doubling disease is 'smearing'. A smeared operator on the lattice is one that includes contributions to any given site from the neighbouring sites, subject to the condition that it reduces to the identity in the continuum limit.

The operators introduced by Trivedi to accomplish this on the lattice are composed of the translation operators $\hat{t}^{\pm}_{\mu} = \sum_{x'} \delta_{x',x\pm 1}$ that move objects to the right or left by one site. The operators used, and the eigenvalues of each, are

$$\begin{aligned} \hat{a}_\mu &= \tfrac{1}{2}(\hat{t}^{+}_{\mu} + 1) & a_\mu &= \tfrac{1}{2}(e^{-iak_\mu} + 1) \\ \hat{s}_\mu &= \tfrac{i}{2a}(\hat{t}^{+}_{\mu} - \hat{t}^{-}_{\mu}) & s_\mu &= \tfrac{1}{a}\sin(ak_\mu) \\ \hat{c}_\mu &= \tfrac{1}{4}(\hat{t}^{+}_{\mu} + 2 + \hat{t}^{-}_{\mu}) & c_\mu &= \cos^2(\tfrac{1}{2}ak_\mu) \end{aligned} \tag{5.144}$$

The first corresponds to taking an average over the current site and next site in the specified direction. The second is simply the symmetric derivative given in section 5.2. The third corresponds to taking an average over the present, previous and next sites. The eigenvalues of each can easily be derived by following the procedure given in eqn. 5.7.

These smeared operators on the lattice are simply a more localised version of the proposal of Dong [80] to use 'fuzzy mathematics' on the lattice. One can define a function $\mu(x)$ for an x that may, or may not, be a member of the set A;

$$\mu(x) = \begin{cases} 1 & \text{if and only if } \; x \in A \\ 0 & \text{if and only if } \; x \notin A \end{cases} \tag{5.145}$$

Fuzzy mathematics is an extension of this usual concept of membership of a set; $\mu(x)$ can take any value along the real line from 0 to 1, such that the closer the value is to 1 the more x belongs to A. Dong's idea was to extend each lattice site by including the continuum around it, with a Guassian membership function. Thus the further a point was from the lattice site

the less the likelyhood of it contributing to the lattice action. It was shown that a Fourier Transform can be defined, and that the particle spectrum is free of spectral multiplicity. Furthermore, the correct Axial anomaly occurs.

This idea is also similar to that proposed by Bender et al. [28] who suggested using finite element methods to construct fermion theory free of spectral multiplicity. However, that idea appears to have proven impossible to extend to more than two dimensions!

The first step is to use these smeared operators to create a derivative on the lattice that is smeared in the transverse direction, subject to the requirement that it reduces to the continuum derivative in the continuum limit. This circumvents the Nielsen-Ninomiya theorem by virtue of the fact that the theorem is only proven true for a time derivative that is not multi-directional. (It does hold true if the spatial derivatives alone are smeared.) The derivative constructed is a product of the normal symmetric derivative, and an average over sites transverse to the direction of the derivative.

$$\partial_\mu \mapsto \hat{z}_{mu} = \frac{i}{2a}(\hat{t}_\mu^+ - \hat{t}_\mu^-) \prod_{\nu \neq \mu} \frac{1}{4}(\hat{t}_\mu^+ + 2 + \hat{t}_\mu^-) \tag{5.146}$$

One then constructs the Dirac Lagrangian from this;

$$\mathcal{L} = \bar{\psi}(x) \left(\gamma^\mu \hat{z}_\mu - m \prod_\mu \hat{c}_\mu \right) \psi(x) \tag{5.147}$$

This tends towards the correct continuum limit, since the smearing terms will tend towards the identity in this limit.

It now remains to check the form of the dispersion relation for this equation. For simplicity consider the two-dimensional form of the equation, similar to the early example of Susskind, [193].

$$\begin{aligned} \gamma_0 z_0 &= \gamma_1 z_1 + m \prod_\mu c_\mu \\ \frac{1}{a}\sin(ak_0)\cos^2(\tfrac{1}{2}ak_1) &= \pm\frac{1}{a}\sin(ak_1)\cos^2(\tfrac{1}{2}ak_0) + m\cos^2(\tfrac{1}{2}ak_0)\cos^2(\tfrac{1}{2}ak_1) \\ \frac{2}{a}\tan(\tfrac{1}{2}ak_0) &= \frac{2}{a}\tan(\tfrac{1}{2}ak_1) + m \end{aligned} \tag{5.148}$$

One can bring this to a form identical to the continuum form through the use of the transformation

$$\frac{2}{a}\tan(\tfrac{1}{2}ak_\mu) \mapsto p_\mu \tag{5.149}$$

The spectrum now lacks the particle doubling of the naive derivative. The momentum behaves as

$$\frac{2}{a}\tan(\tfrac{1}{2}ak_1) = \begin{cases} -\infty & k_1 = -\frac{\pi}{a} \\ 0 & k_1 = 0 \\ \infty & k_1 = \frac{\pi}{a} \end{cases} \tag{5.150}$$

Thus smearing of the lattice operators leads to a lattice Dirac action that is hermitian (As shown in section 5.2 the use of the symmetric derivative leads to an hermitian action), local (in terms of only involving nearest neighbour interactions) and chiral, without any symptoms of the particle multiplicity that infects the standard lattice versions of the Dirac action.

5.7 Full QCD Partition Function

Re-writing equation 1.2 with the fermion action explicitly included, one gets

$$Z = \int [dU][d\bar{\psi}][d\psi] \exp\left[-S_G + \bar{\psi} K \psi\right] \tag{5.151}$$

with K the fermion matrix. Although this has been written in the notation of the Wilson fermions, it applies equally to the Kogut-Susskind fermions.

The fermions are represented by Grassmann variables. The techniques for performing the integral over the Grassmann variables are well known [183,182]. The result of use here is

$$\det K = \int [d\bar{\psi}][d\psi] \exp\left[\bar{\psi} K \psi\right] \tag{5.152}$$

If there are n_f flavours on the lattice, there will be n_f terms in the exponential. Thus, after performing the fermion integration, one has the partition function for an abritrary number of flavours:

$$Z = \int [dU] (\det K)^{n_f} e^{-S_G} \tag{5.153}$$

The integral over the gauge variables is then done numerically. One of the major factors in a numerical simulation is the evaluation of the fermion determinant (itself still a function of U). This is discussed in more detail in the remaining chapters.

Chapter 6

Lattice Observables

6.1 Implementing Lattice QCD on Computer

The correlation length ξ determines the behaviour of the theory in the continuum limit. The correlation length increases near a phase transition (to some characteristic length, in a first order transition, and to infinity in a second order transition). All lattice observables are calculated in terms of the correlation length; for example, masses are of the form $m = \text{Const}/\xi$ with xi expressed in terms of the lattice spacing a: $\xi = af(g)$ with $f(g)$ a dimensionless function of the coupling constants alone. In order for the continuum limit to have a meaningful, finite solution, one needs to have $f \stackrel{a \to 0}{\longrightarrow} \infty$. This means that the coupling must tend to some g_c such that

$$\lim_{g \to g_c} f(g) = \infty \tag{6.1}$$

There are only two input parameters in LQCD for the hadron spectrum; the lattice spacing a and the quark mass m_q. Typical values for these in current simulations are:

$$\begin{aligned} a &= 0.5 \to 0.1\text{fm} \\ am_q &= 0.1 \to 0.025 \Rightarrow m_q = 40 \to 10\text{MeV} \end{aligned}$$

Note that the Callan-Symanzik equation (see section4) links the coupling constant and the lattice spacing, and hence they are not independent parameters.

In practice, one calculates all quantities in terms of the lattice spacing and the quark mass. Once hadronic spectra have been calculated, these two are fixed using the experimental mass for two of the hadrons as input.

For a lattice with n sites in each direction, one uses a Monte-Carlo routine to generate values for the gauge field on each of the links, with a probability for the ith link

$$P(U_i) = \frac{1}{Z}(\det K)^{n_f} e^{-S_G}$$

This yields a configuration of the set of links $\{U_i\}$.

To calculate hadron masses we need to place a valence quark on the lattice; the simulations to date have used between 1 and 10 quarks. These are δ-functions in spacetime and colour (remember that in the Kogut-Susskind formulation the fields carry only a colour index).

6.2 Operators on the Lattice

The expectation value of an operator is given by

$$\langle O \rangle = \frac{1}{Z} \int [dU] O (\det K)^{n_f} e^{-S_G} \tag{6.2}$$

with Z the partition function eqn. 5.153 and n_f the number of continuum fermions placed on the lattice. This becomes, using a number of generated gauge configurations $\{U\}_i$, (where i runs from one to N, the number of independent configurations generated), just the average of $O(U)$ over the number of configurations;

$$\langle O \rangle = \frac{1}{N} \sum_i O(U) \tag{6.3}$$

To determine the masses of mesons and baryons, one measures the expectation value of the zero-momentum propagators, for the corresponding meson or baryon. For infinite continuum 4-space the propagator is the vacuum expectation value of the time-ordered product of the creation and annihilation operators $O(x)$ for the field of the particles concerned.

These are replaced on a finite lattice by correlation functions, defined as follows:

$$C(x) = \langle O(x) O(0) \rangle \tag{6.4}$$

$$= \mathrm{Tr}[S^{-1} O(0) S O(0)] \tag{6.5}$$

where the S are translation operators (see section 5.4.5) on the lattice. These become the normal 2-point Green functions in the limit that the lattice size goes to infinity. If one considers purely time translation, the 2-point Green function is;

$$\langle 0 | O(t) O(0) | 0 \rangle \tag{6.6}$$

which becomes, after inserting a complete set of energy eigenstates $|n\rangle\langle n|$;

$$\sum_{n=0}^{\infty} |\langle 0 | O(0) | 0 \rangle|^2 e^{-E_n t} \tag{6.7}$$

For a large enough t, the ground state will dominate, hence one expects the correlation function to behave as an exponential,

$$C(x) \approx c e^{-E_0 t} \tag{6.8}$$

where the constant c is due to the fact that one projects onto the ground state, and gives the fraction of the correlation function due to the ground state.

6.2.1 Meson Propagators and Masses

In the continuum the field operator for a meson [209] is given by

$$M_g^{ff'}(x) = \bar{\psi}^f(x) \Gamma_g \psi^{f'}(x) \tag{6.9}$$

where f, f' represent the flavours of the quarks involved, and Γ_g yield the requisite continuum quantum numbers for the particle. (The choice of notation for Γ_g is as given in appendix C; this choice will be used throughout this section.) For example, the pion is given by $\Gamma_g = \gamma_5$ and the rho by $\Gamma_g = \gamma_\mu$.

Kogut-Susskind fermions

Using the flavour interpretation given in section 5.4.6 one may construct the meson operators [138,35,93];

$$M_{ab}(y) = \bar{q}^{\alpha a}(y)\,(\Gamma_a)_{\alpha\beta}\,(\Gamma_b)^*_{ab}\,q^{\beta b}(y) \tag{6.10}$$

in which the Greek letters refer to the Dirac indices, and the Roman letters refer to the flavour indices. The second Γ matrix is introduced to yield the correct flavour quantum numbers for the particle concerned. For calculational purposes it is more convenient to work with the original Kogut-Susskind variables. Hence this equation becomes

$$M_{ab}(y) = \sum_{\theta\xi} \bar{\chi}(2y+\theta)\left(\Gamma^\dagger_\theta\right)^{a\alpha}(\Gamma_a)_{\alpha\beta}\,(\Gamma_b)^*_{ab}\,(\Gamma_\xi)^{\beta b}\,\chi(2y+\xi) \tag{6.11}$$

with θ, ξ labeling the different corners of the tesseract. This can be re-written by taking the trace of the Γ matrices explicitly;

$$\begin{aligned} M_{ab}(y) &= \frac{1}{64}\sum_{\theta\xi}\bar{\chi}(2y+\theta)\chi(2y+\xi)\mathrm{Tr}[\Gamma^\dagger_\theta\Gamma_a\Gamma_\xi\Gamma^\dagger_b] \\ &= \sum_{\theta\xi}\bar{\chi}(2y+\theta)\chi(2y+\xi)(-)^{\Xi\bar{A}+\Theta\bar{\Theta}+B\bar{B}+\Theta\Xi+A\bar{B}+\Theta\bar{A}+\Theta\bar{B}+\Xi\bar{A}+\Xi\bar{B}} \\ &\qquad \times \mathrm{Tr}[\Gamma_{\theta+\xi+a+b}] \end{aligned} \tag{6.12}$$

(See appendix C for the relationship between lower and upper case letters in this context.)

Since the only Γ matrix that is not traceless is the unit matrix Γ_0, one gets

$$\sum_{\theta\xi}\mathrm{Tr}\cdots[\Gamma_{\theta+\xi+a+b}] = 4\sum_{\theta}\cdots \tag{6.13}$$

with the condition that $\theta+\xi+a+b=0$. Define, for convenience, the group element $c=a+b$.

Thus the meson operator becomes

$$\begin{aligned} M_{ab}(y) &= \frac{1}{16}\sum_{\theta}(-)^{(\Theta+C)\bar{A}+\Theta\bar{C}+(A+B)\bar{B}+A(\bar{A}+\bar{B})+B(\bar{A}+\bar{B})}\bar{\chi}(2y+\theta)\chi(2y+(\theta+c)) \\ &= \frac{1}{16}\sum_{\theta}(-)^{\Theta(\bar{A}+\bar{C})+C(\bar{A}+\bar{A})}\bar{\chi}(2y+\theta)\chi(2y+(\theta+c)) \end{aligned} \tag{6.14}$$

This is a non-local operator, and yields mesons with mixed flavours, as well as the true flavours. One can restrict these to local operators, by requiring that $\theta=\xi \Leftrightarrow \theta+\xi=0$. This implies, via the condition given above, that $c=0$. This means, if one looks at the original definition of the meson operator, that the Γ matrices giving the Dirac and flavour content must be identical. This results in there being no mixing of the different meson quantum numbers.

One then gets

$$M_{aa}(y) = \frac{1}{16}\sum_{\theta}(-)^{\Theta\bar{A}}\bar{\chi}(2y+\theta)\chi(2y+\theta) \tag{6.15}$$

One can also derive the effects of the various symmetry operators on the meson operator, as was done for the Kogut-Susskind fermions earlier. As an example, consider inversion of one of the axis. $I^\mu : y^\nu \mapsto y'^\nu = -y^\nu$, for $\nu=\mu$. In terms of the blocked lattice one gets

$$I^\mu : (2y+\zeta)^\nu \mapsto \begin{cases} [-2y+(\zeta+1)\mathrm{mod}2]^\nu & \nu=\mu \\ [2y+\zeta]^\nu & \nu\neq\mu \end{cases} \tag{6.16}$$

The reason for the unusual form of the change in the μ direction is that the canonical inversion flips the direction of the block, ie. space itself would not have inversion symmetry. One needs to add the unit vector in the μ direction to restore inversion symmetry to space-time, by flipping the direction of the block from $2y'^{\nu} - \zeta$ to $2y'^{\nu} + \zeta'$.

In the sign factor in the meson operator, it makes no difference whether one takes $(\zeta + 1)\mathrm{mod}2$ or $\zeta + 1$, hence one might as well take the latter for ease of computation. Performing the calculation, one gets

$$M_{aa}(y) = \frac{1}{16}\sum_{\theta}(-)^{\Theta\tilde{A}+\tilde{A}_\mu}\bar{\chi}[I^\mu(2y+\theta)]\chi[I^\mu(2y+\theta)] \tag{6.17}$$

If one repeats the inversion for futher directions, one will simply add terms of the nature of $\tilde{A}_\mu$ to the sign factor. Hence the operator transforms under the parity operation ($I^{\mathrm{P}} = I^1 I^2 I^3$) as

$$I^{\mathrm{P}} M_{aa}(y) = \frac{1}{16}\sum_{\theta}(-)^{\Theta\tilde{A}+A_4}\bar{\chi}[I^{\mathrm{P}}(2y+\theta)]\chi[I^{\mathrm{P}}(2y+\theta)] \tag{6.18}$$

since $\tilde{A}_1\tilde{A}_2\tilde{A}_3 = A_4$. Thus there is an overall sign factor of $(-)^{A_4}$.

The transformations under the other symmetry groups of the lattice can be checked in similar fashion. The relationship of the Γ matrices to the physical mesons is given below;

Γ_a	meson
Γ_0	ϵ
Γ_{12}	$\tilde{\epsilon}$
Γ_8	π
Γ_4	$\tilde{\pi}$
$\Gamma_{1,3,6}$	ρ
$\Gamma_{13,15,10}$	$\tilde{\rho}$
$\Gamma_{9,11,14}$	a_1
$\Gamma_{2,5,7}$	b_1

(6.19)

Note that the first 3 particles occur in pairs. This is a lattice artifact, arising from the Kogut-Susskind formulation of the quarks. These pairs are degenerate in the continuum limit.

One can check that the pion, for example, has the correct parity. The pion correspons to $a = 8$ or $A = (1,1,1,1)$. Hence $A_4 = 1$ and the pion has negative parity, as expected.

The two-point Green function for a spinor ψ, $G(x,x') = \langle\bar{\psi}(x)\psi(x')\rangle$ is the propagator describing movement of the particle from x to x'. In the formulation of the Kogut-Susskind fermions in terms of a hopping parameter (eqn. 5.30) this can be written as

$$G(x,i;x',j) = \frac{1}{K(x,i;x',j)} \tag{6.20}$$

where the possible effect of the gauge field on the colour degree of freedom has been explicitly included by the colour variables i,j.

The meson propagator on the lattice [35], using Kogut-Susskind fermions, is given by

$$M(y,0) = \langle M_{ab}(y)M_{cd}(0)\rangle \tag{6.21}$$

Whilst this form of the propagator gives the flavour content of the meson, it is not the easiest form to implement on the lattice.

If one works with local operators, without any flavour mixing, one can re-write these in terms of the Green function of the original Kogut-Susskind variables as

$$M_{aa}(x,0) = \sum_{i,j} W_{aa}(x) \frac{1}{K(0,i;x,j)} \frac{1}{K(x,j;0,i)} \tag{6.22}$$

where 0 is the source point and x is the sink point. Note that, due to the one-component formulation of the Kogut-Susskind fermions, the Γ matrices become weight factors $W_{aa}(x) = (-)^{\Theta \tilde{A}}$ and have position dependance.

These weight factors can be obtained explicitly in terms of the fine lattice, x, rather than the physical lattice y, for each of the mesons described on the lattice.

In the end one is after the mass of the meson in question. Since this is simply the energy of the zero momentum meson (see eqn. 6.7), one removes the position dependence of the meson correlation functions by summing over the $\vec{x}$ first. The correlation functions for the mesons listed in the above table can be constructed from linear combinations of the following four independent correlation functions [115,102]:

$$M_{\mathrm{M}}(t) = \sum_{\vec{x}} \sum i,j W_{\mathrm{M}} \frac{1}{K(0,i;x,j)} \frac{1}{K(x,j;0,i)} \tag{6.23}$$

with the different combinations being

M		W_{M}	Particle(J^{PC})	Parity Doubled Particle(J^{PC})
PS	=	1	$\pi(0^{-+})$	$\epsilon(0^{+-})$
V-T	=	$(-)^{x_1} + (-)^{x_2} + (-)^{x_3}$	$\rho(1^{--})$	$b_1(1^{+-})$
PV	=	$(-)^{x_2+x_3} + (-)^{x_1+x_3} + (-)^{x_1+x_2}$	$\tilde{\rho}(1^{--})$	$a_1(1^{++})$
S	=	$(-)^{x_1+x_2+x_3}$	$\tilde{\pi}(0^{-+})$	$\sigma(0^{++})$

(6.24)

for pseudoscalar, vector tensor, pseudovector and scalar respectively.

A complete table of the operators, correlation functions with the relationship between the four independent correlation functions and the meson correlation functions on both the physical and the fine lattices is given in ref. [93].

In practice, one will make measurements of the correlation functions in a number of different gauge fields and take the average, getting the expectation value over the number of configurations. This is then fitted against an exponential to determing the mass. For the mesons one has periodic boundary conditions, and one fits to

$$M_{aa}(t) = c(e^{-mt} + e^{-m(T-t)}) \tag{6.25}$$

with t the distance from the source (Kronecker delta) in Euclidean time. The second term is due to the periodic nature of the boundary condition; the meson can propagate both forwards and backwards in time with equal probability. Thus only half of the temporal extent of the lattice is independent; the later half of the lattice is simply the time reflection of the first half.

Wilson Fermions

The formalism for Wilson fermions is essentially the same as that given above. The exception to be born in mind is that, since Wilson fermions are defined on all sites, as normal Dirac

spinors, the seperation into flavours, and the mixing of flavour and spin/parity does not occur. Furthermore, if one wants more than one flavour of quark on the lattice, one must specifically place the requisite number on the lattice in the first place.

The evaluation of the expectation value of an operator proceeds in the same fashion as given above.

The meson operator is constructed in exactly the same way as for the continuum operator, with the usual Γ_g yielding the meson quantum numbers, sans the mixing found for the Kogut-Susskind fermions. However, it must be born in mind that one will now use the Wilson fermion matrix in evaluating the propagator. Hence in eqn. 6.22 above, one will use $K^f(\alpha,i,x;\beta,j,y)$ as given by eqn. 5.131.

6.2.2 Baryon Propagators and Masses

In the same fashion as used above to obtain the meson operator, the baryon operator can be constructed from the flavoured quarks [160,115], and re-written in terms of the Kogut-Susskind variables. This yields

$$B(x) = \epsilon_{ijk}\xi_i(x)\xi_j(x)\xi_k(x) \tag{6.26}$$

and hence one obtains the baryon correlation function on the lattice to be

$$B(x,0) = \langle\bar{\chi}(x)\bar{\chi}(x)\bar{\chi}(x)\chi(0)\chi(0)\chi(0)\rangle \tag{6.27}$$

$$= \sum_{i,j,k}\sum_{i',j',k'} \epsilon^{ijk}\epsilon^{i'j'k'} \frac{1}{K(0,i;x,i')}\frac{1}{K(0,j;x,j')}\frac{1}{K(0,k;x,k')} \tag{6.28}$$

One follows the same procedure used above to determine the zero-momentum correlation function, and then fits the expectation value over the gauge configurations to an exponential

$$B(t) = c(e^{-mt} + (-)^t e^{-m(T-t)}) \tag{6.29}$$

The second term is again due to the boundary conditions leaving only half the lattice in the temporal direction independent. The sign factor reflects the fact that baryons are fermions, and hence subject to anti-periodic boundary conditions.

The same argument as given in the section on meson propagators for converting from Kogut-Susskind to Wilson fermions applies here as well.

6.3 Inherent Lattice Inaccuracies

The lattice is an approximation to reality in two cases. Firstly, one is approximating the continuum by a lattice. Secondly, one requires a finite size in order to effect an infra-red cutoff, thus approximating the infinite volume of reality. Both of these approximations introduce errors into any lattice theory.

6.3.1 Finite Size Effects

In simulations on the lattice the size used is considerably smaller than that required by the need for an infra-red cutoff. This is entirely due to the meagre computing power available. In fact, the lattices of today are still close in size to the diameter of the hadrons, a fact that renders the measurements of the masses somewhat dubious!

However, there are good estimates of the finite size effects, such that one may still place some faith in the measurements of the masses.

A comparison [120] between the masses calculated using Monte Carlo methods and the exact results for the massive Thirring/sine-Gordon model yielded a good estimate of the lattice effects on the results. In this model, the mass spectrum in the infinite volume limit is known for any lattice spacing; hence one is able to separate out the errors caused by the finite volume from those caused by the finite lattice spacing.

It was found that for a lattice of size less than, or comparable to, the Compton wavelength of the elementary particle (ie., the quark in QCD) the finite volume effects were considerable and tended to increase the mass of the particle. For a composite particle, it was found that the factor determining the importance of finite size effects was the size of the wave function relative to the lattice size. Results were the same as the infinite volume case when the lattice was large enough to completely contain the bound state wave function.

In another study of the mass shift, in the 4 dimensional Ising model, it was found that the finite size effects were low for $ML \geq 2$, and negligible for $ML \geq 5$. M is the mass gap (ie., the mass of the lowest lying state) and L the size of the lattice. Again, this indicates that lattices larger than the Compton wavelength of the particle are needed for accurate results.

A formula for the mass shift caused by the finite size has been developed by Lüscher, [152] based on the forward scattering amplitude for the infinite volume theory. This has been tested in a study based on the Gross-Neveu SU(N) model [187], which is somewhat closer to lattice QCD. The mass shifts for the elementary particles were found to be agree with the predictions, and decreased very rapidly with increasing lattice size. For the bound state, the mass was still increased ($\approx 20\%$) by the effects of the finite volume; however, the increase was less than that predicted by the formula. Thus one is still only able to estimate the effects of the finite volume by performing the calculation on lattices at different volumes, and explicitly measuring the finite size effects.

A factor contributing to the mass shifts is the fact that momenta on the lattice are quantized. The allowed momenta are all multiples of

$$\Delta p = \frac{2\pi}{a} \times \frac{1}{N} = \frac{2\pi}{L} \tag{6.30}$$

with N the number of sites, and L the physical size of the lattice. For sizes typical of the simulations presently being done ($\approx$ 2fm), this means that the momenta are quantized in units of $\approx 2\pi$MeV. Since the mass of the lowest lying state, the pion, is 139MeV, one expects considerable deviations from the continuum properties!

There is a further non-trivial problem associated with the finite size of the lattice. Any symmetry of the infinite volume continuum theory that is spontaneously broken is, unfortunately, still preserved on the lattice! Hence states that are degenerate in reality, are not so on the lattice [151]. However, the symmetry breaking still leaves some effects on the lattice — the states within a level corresponding to the 'broken' symmetry, whilst non-degenerate, are split by less than the splitting between levels.

Similarly, the periodic boundary conditions introduce symmetries; the periodic boundary condition gives a 'mirror reflection' of the first half of the lattice into the second half. These vanish in the infinite volume limit; however, they do have an effect on the mass spectrum in finite volume.

6.3.2 Finite Spacing Effects

Due to the small number of sites one can simulate on current machines, and the need to keep the physical size of the lattice reasonable, the spacing used is not close to the continuum limit.

The major effect of this is that the continuum Callan-Symanzik relation cannot be used (see section 4). This fact was not realised in the early lattice studies, and led to errors associated with linking the lattice spacing with the energy of the lattice cutoff. This can be avoided, to some extent, by using the non-perturbative β-function. This, however, is also determined 'empirically' from a lattice study, and hence is subject to similar errors!

A problem associated with the lattice spacing occurs as the lattice spacing decreases; the correlation length (for pure gauge theory) is associated with the inverse of the lattice spacing. The time taken in a simulation to reach an independent configuration is a function of the correlation length, hence smaller lattice spacings lead to larger errors associated with the Monte Carlo simulation, as well as problems obtaining sufficient configurations for good statistics.

This is lifted slightly when one moves to a simulation incorporating quarks, since the correlation length is then the inverse of the quark mass, $\xi = \frac{1}{ma}$. One then requires, for behaviour close to the infinite volume continuum limit, $a \ll \xi \ll L$. In the simulations to date, this has not been achieved; however, there are ways of improving the action according to the renormalisation group, in order to reduce the errors associated with the large spacing and small volume (see section 4 and references therein).

Chapter 7

Numerical Simulation

Since the advent of Supercomputers, such as the CRAY-1, a third branch of scientific research has emerged, complementing that of theory and experiment; that of computer modelling. There are two reasons for this. Firstly, many theories cannot be solved analytically. These involve, for example, multi-dimensional integrals, or equivalently, many degrees of freedom. A discrete functional integral is the only way to solve QCD in the non-perturbative regime. Secondly, a computer simulation can yield exact results for a model of the physical system; the parameters of the model are known, whilst those for the physical system are not. One is not required to make the many (and often unphysical) simplifications required for an analytic solution (such as taking some quantity to zero or infinity).

Thus there are many areas in which a computer simulation is better than an analytic solution at testing whether or not the theory faithfully models reality.

There are two crucial regions in which the computer simulation is lacking, however. One is the finite resolution of any simulation — for a lattice simulation, this corresponds to the lattice spacing. The other is the finite size of the configuration space explored by the simulation. Both of these limits are introduced by the finite memory and processing speed of a computer.

They can also, however, yield useful information; the manner in which a system near to a phase transition responds to the finite size of the lattice can be used, via finite size scaling theory, to extract information on the phase transition that cannot be gleaned in any other fashion. This is especially true for any phase transition in which the correlation length goes to infinity, such as a second order phase transition.

In a computer simulation one is usually after the average value of some variable governed by chance, whether it is a quantum or classical probability. The laws governing the probability can be formulated in two forms;

1. The probability for the system modelled to be at some specific point in phase-space.

2. The probability for the system to move from a given point to another point in phase-space.

The first can be illustrated by the manner in which the evolution of a gas would be modelled, if the motion and collisions of each particle were tracked. In the second, a series of independant, random configurations in phase-space would be generated, with the desired quantity being calculated by taking the average over all configurations.

In many situations it is nigh-on impossible to create new configurations according to the probability distribution in phase space, due to the prohibitively large number of the degrees of freedom. Thus one cannot model a system behaving according to probabilities of the first type. However, one may be able to re-write the probabilities such that the system is described by probabilities of the second type.

This is called a Markov Chain; one starts with a specific configuration of the system, and moves the system at random into another configuration nearby in phase space. If this is all done correctly (achieving this is the major task in this type of process), after sufficient iterations of the process the probability that the system will be in any given configuration is the same as the ab initio probability of choosing that point in phase space. Hence, by repeated iteration of the second type of probability laws one is able to return to a system described by the first type.

There are two sufficient conditions for this approach to work:

1. After some number n of steps in the Markov Chain the system reaches an equilibrium state, such that the initial starting configuration has been forgotten. Equilibrium means that the probability for the system to be in a state x after n steps is the same as the probability after infinitely many steps, $P_n(x) = P_\infty(x)$. Furthermore, the principle of detailed balance holds: $P_{tr}(x \to x')P_\infty(x) = P_{tr}(x' \to x)P_\infty(x')$.

2. Ergodicity holds. In other words, one can get to any state x' from any state x by a finite number of moves. Obviously if this requirement is not satisfied the Markov Chain will not be able to sample all configurations, and will lead to erroneous values for the averages calculated.

7.1 Monte Carlo Methods

Consider the problem of evaluating the definite integral

$$\int_{x_1}^{x_2} f(x)dx = F(x_2) - F(x_1) \tag{7.1}$$

For a single integral, or one with few dimensions at most, this can be done both algebraically, perhaps using a package such as REDUCE, or numerically with the aid of one of the multitude of numeric integration schemes. However, if one turns to the lattice one encounters an entirely different animal!

The smallest lattice that begins to give reasonable results has 10 sites in each direction; thus 10 000 sites in total. There will be a total of 36 000 links. Each link introduces 8 real dimensions in the integral for the partition function (eqn. 3.11); thus one has a 2.88×10^5 dimensional integral! This is clearly impossible to do using any algebraic technique, or any numerical integration routine such as the trapezoidal rule. However, there is another method, based on random sampling.

Now the integral above can be replace by a finite sum,

$$F(x_2) - F(x_1) \approx \sum_{x_i=1}^{n} f(x_i)\delta x_i \tag{7.2}$$

with

$$\delta x_i = x_{i-1} - x_i = \frac{x_2 - x_1}{n} \tag{7.3}$$

This is simply sampling the function at various points in the region of integration, with a suitable factor taking into account the number of samples, and the distance between samples. The latter is needed to introduce the dimensions of dx in the integral.

Now there is no reason why this sampling needs to be done at regular intervals. It may equally well be done at random points in the integration space. This is the basis of the Monte Carlo approach to evaluating integrals. One of the major advantages of choosing the points at random comes into play as the number of dimensions of the integration space increases.

With a regular lattice of sampling points, and keeping each linear dimension of the lattice constant, an increase in the number of dimensions increases the ratio of points on the surface to points in the interior. If one has N points in each direction, the number inside the volume will be $N-2$. Hence the ratio of points inside will be $(1-\frac{2}{N})^d$ where d is the dimension of the space. Thus, for a four-dimension lattice with 20 points in each direction, only 65% of the points are inside the volume. Thus, if one is after a quantity that is volume dependant, one must bias ones choice of points such that most of the points chosen lie amongst this 65%.

The other common problem in physics that can be tackled this way is that of finding the expectation value of some observable f; re-writing the mean value theorem of differential calculus [12] one gets

$$\begin{aligned} \langle f \rangle &= \frac{\int_{x_1}^{x_2} f(x)dx}{\int_{x_1}^{x_2} dx} \\ &\approx \frac{\sum_{x_i=1}^{n} f(x_i)\delta x_i}{\sum_{x_i=1}^{n} \delta x_i} \end{aligned} \tag{7.4}$$

Again, there is no reason for the sampling to be done uniformly; one can choose the points at random. Furthermore, suppose one has some idea of the shape of the function. If it is highly peaked, such as a Guassian, one can gain a very accurate estimate of the expectation value by sampling a few well-chosen points. This is the concept of importance sampling.

This is equivalent to generating points according to a non-uniform distribution $P(x)$, chosen such that the composite function $g(x) = f(x)P(x)$ is smooth and flat.

Replacing $f(x)$ by $g(x)P(x)$ in the above equation, one has

$$\langle g \rangle = \frac{\sum_{x_i=1}^{n} g(x_i)P(x_i)}{\sum_{x_i=1}^{n} P(x_i)} \tag{7.5}$$

which is $\langle f \rangle$ up to possible normalisation factors.

This looks extremely familiar, if the probability distribution is given by the Boltzmann factor, $P = \exp\left(-\frac{E}{kT}\right)$, and the function g some operator, the expectation value of which one is trying to find. Furthermore, any thermodynamic system has a large number of degrees of freedom and consequently a high value for E; thus $\exp\left(-\frac{E}{kT}\right)$ is widely variable, and peaked. Hence, if g is smooth, a few well-chosen values will yield a good estimate of the expectation value.

7.2 Dynamical Interpretation of Importance Sampling

Each iteration in a Markov chain is by no means independant from the previous one; in fact, the correlations can extend back through many previous iterations. Hence, in order to

determine the statistical error on any calculated quantity it is crucial to know how many statistically independant configurations were generated.

To do this, it is useful to understand a Markov chain in terms of a master equation describing the stochastic evolution of the system [11]. This is

$$\frac{dP}{dt}(x,t) = \sum_{x'} P_{tr}(x' \to x)P(x',t) - \sum_{x} P_{tr}(x \to x')P(x,t) \tag{7.6}$$

where t indicates Monte Carlo time; say, how many iterations have been done. One may also measure time in any other convenient unit. This equation is essentially a re-expression of the detailed balance equation above, and describes the net probability of starting in some state x' and moving to x less the probability of starting in x and moving away.

In thermal equilibrium, $P(x,t) = P_\infty(x)\forall t$, hence the probability of being in a given distribution ceases to change with time;

$$\left.\frac{dP}{dt}(x,t)\right|_{P=P_\infty} = 0 \tag{7.7}$$

For a finite system with finite potentials, one will then have ergodic simulation; however, for systems with inifinite potentials, certain configurations will be forbidden; hence one will no longer have an ergodicity.

One can regard the process of averaging in eqn 7.5 as being equivalent to integrating eqn. 7.6 along the stochastic trajectory in phase space. Thus one will have, for some observable g,

$$\langle g \rangle = \frac{\int_{t_0}^{t_f} g(t)P(t)dt}{\int_{t_0}^{t_f} P(t)dt} \tag{7.8}$$

since x is the configuration appearing at time t one can now consider g to be a function of t alone.

In order to make the notation simpler, it is convenient to normalize the differential dt; set

$$dt \mapsto \frac{P(t)dt}{\int_{t_0}^{t_f} P(t)dt} \tag{7.9}$$

which becomes, for the gluon configurations (see eqn 3.11),

$$dt = \frac{1}{Z} e^{-S_G}[dU] \tag{7.10}$$

then one has simply

$$\langle g \rangle = \int_{t_0}^{t_f} g(t)dt \tag{7.11}$$

One can also use eqn. 7.11 to study the approach of the system from the initial starting configuration to thermal equilibrium. To do this, take t_0 to be the start-time rather than the time at which thermal equilibrium is reached. One can then calculate the expectation values of the observable at various times after starting the simulation. After thermal equilibrium, these should become constant with time. One can calculate values for $\langle g(t) \rangle$ for various values of t by averaging over n runs, starting with different initial configurations and evolving according to a different set of pseudo-random numbers.

One can also use eqn. 7.11 to define correlations between observables at different simulation times, from which one can also get an idea of the amount of simulation time required to generate statistically independant configurations. The correlation can be defined as (where f and g may be the same observable):

$$\langle f(t)g(0)\rangle = \int_{t_0}^{t_f - t} f(t+t')g(t')dt' \tag{7.12}$$

For configurations that are statistically independant, the statistical error is given by

$$\sqrt{\frac{\langle g^2\rangle - \langle g\rangle^2}{n}} \tag{7.13}$$

However, in the absence of independance, one uses the expression

$$\langle(\delta g)^2\rangle = \left\langle \left[\frac{1}{n}\sum_{\mu=1}^{n}(g(\mu) - \langle g\rangle)\right]^2 \right\rangle \tag{7.14}$$

for n configurations of the system. Evaluating this expression one obtains

$$\begin{aligned}
\langle(\delta g)^2\rangle &= \left\langle \frac{1}{n^2}\sum_{\mu=1}^{n}\sum_{\nu=1}^{n}\left[g(\mu)g(\nu) - g(\mu)\langle g\rangle - g(\nu)\langle g\rangle + \langle g\rangle^2\right]\right\rangle \\
&= \left\langle \frac{1}{n^2}\sum_{\mu=1}^{n}[g(\mu)^2 - 2g(\mu)\langle g\rangle + \langle g\rangle^2] + \right. \\
&\quad \left. \frac{2}{n^2}\sum_{\mu=1}^{n-1}\sum_{\nu=\mu+1}^{n}[g(\mu)g(\nu) - g(\mu)\langle g\rangle - g(\nu)\langle g\rangle + \langle g\rangle^2]\right\rangle
\end{aligned} \tag{7.15}$$

In order to gain some idea of the time needed to generate statistically independant values for g, set $g(\nu) = g(0)$ (some point in the Markov chain at which statistical independance has been reached) and set $n - 1 = n$, which will be approximately true for n large. One then gets

$$\langle(\delta g)^2\rangle = \frac{1}{n}\left[\langle g^2\rangle - \langle g\rangle^2\right] + \frac{2}{n}\sum_{\mu=1} n(1 - \frac{\mu}{n})(\langle g(\mu)g(0) - \langle g\rangle\langle g(0)\rangle) \tag{7.16}$$

Re-writing this in terms of a continuous time $t_\mu = \delta t\mu$, with δt being the unit Monte Carlo time, one gets the integral relation

$$\langle(\delta g)^2\rangle = \frac{1}{n}(\langle g^2\rangle - \langle g\rangle^2)\left[1 + \frac{2}{\delta t}\int_{t_0}^{t_n}(1 - \frac{t}{t_n})\frac{\langle g(t)g(0) - \langle g\rangle\langle g(0)\rangle}{\langle g^2\rangle - \langle g\rangle^2}dt\right] \tag{7.17}$$

One can then define the auto correlation function;

$$C_g(t) = \frac{\langle g(t)g(0)\rangle - \langle g\rangle\langle g(0)\rangle}{\langle g^2\rangle - \langle g\rangle^2} \tag{7.18}$$

This will be 1 at $t = t_0$, and will tend to 0 as $t \to \infty$, since the configuration, and hence the observables, will become uncorrelated for t sufficiently large; hence one has $\langle g(t)g(t_0)\rangle \overset{t\to\infty}{\to}$

$\langle g(t)\rangle\langle g(t_0)\rangle$. The correlation function is, in general, a sum of exponents, each with a different parameter t_c representing the decay time of that particular mode of the correlation.

Note that the auto correlation time is only defined in the disordered phase of the system; manifestly, if an observable of the system is constrained to some constant value, then the autocorrelation based on that observable will always be one!

Now one can write, assuming only one mode in the correlation function, $t_c = \int_0^\infty C_g(t)dt$. If the total time in the Markov chain is much greater than the auto correlation time, one might as well take the upper limit of the integral in eqn. 7.17 to be infinity; this yields

$$\langle(\delta g)^2\rangle = (\langle g^2\rangle - \langle g\rangle^2)\left[\frac{1}{n} + \frac{2t_c}{n\delta t}\right] \tag{7.19}$$

where the $\frac{t}{t_n}$ term has been neglected, since the denominator tends to infinity, whilst the remainder of the integrand only contributes for t small.

Now the factor $n\delta t$ is the total time of the simulation, t_{obs}. Hence statistical independance is independant of the size of the time unit used in the Monte Carlo simulation; it could be per sweep[1], per ten sweeps or whatever. The deciding factor is how many multiples of the longest auto correlation time were executed. One then makes measurements of the value of the observable at times separated by the longest relevant correlation time.

For a local interaction, such as the Ising model described below, the longest auto correlation time will go, near a phase transition, like ξ^x (ξ the correlation length), with $x \approx 2$, in any simple algorithm. The key to present research in algorithms is to find techniques to reduce the value of x, hence reducing the total computer time needed to achieve any given statistical significance.

7.3 Ising Model

The Ising model is a very simple model of the interaction between spins. The partition function for the two-dimensional model, is given by

$$Z_I = e^{-\beta \sum_{i,j} \sigma s_i s_j} \qquad \text{i,j nearest neighbours} \tag{7.20}$$

with β the inverse temperature, σ the coupling between the spins; taken to be $\sigma = -1$ here; and s_i the value of the spin on site i.

The spins are taken to be elements of the group Z_2, hence take values of ± 1.

The Ising model has, in two dimensions, a phase transition at some value of β which is dependant on the size of the lattice, between a frozen state with all the spins aligned and a disordered state with an average spin zero. More details can be found in [140]

7.4 Problems with Simulations

One includes a configuration in the small ensemble from which one calculates physical quantities if it is independent of the previous configuration, and it is in equilibrium. (Equilibrium is essentially saying that the Boltzmann factor for that configuration is large enough for it to represent the most occupied regions of phase space.)

[1] A sweep is one update of the entire lattice.

One has a problem if the simulation gets stuck in a local minimum that has a low overall probability of occuring. This is very likely to happen in the initial iterations of the Markov chain, whilst the system is close to the relatively unrepresentative start-up configuration. (The usual start-up configurations are either cold start, in which the system is in a completely ordered state, with the variables set to some constant value over the lattice, or hot start, in which the system is in a completely random state.)

One thus needs to discard the first few iterations (often the first few 1000) in order to allow the system to 'thermalize', or forget the initial configuration and move into representative regions of phase space. If this has not happened by the time one begins to take configurations, a systematic error will be introduced into the simulation.

Another systematic error will be introduced if the algorithm does not sample all of phase space equally well, especially if it is slowed by any metastable states.

There are many varieties of Monte Carlo algorithms which attempt, using one or another devious scheme, to minimize these systematic errors; some of which will be presented below. The Ising model will be used to illustrate them, on a 64×64 lattice.

The auto correlation time for the Ising model will be calculated using the correlation between the spins on each of the sites,

$$\langle s(t)s(0)\rangle = \frac{\sum_{n-1}^{N} s_n(t)s_n(0)}{N} \tag{7.21}$$

for a lattice with N sites in total. (Note that this only has meaning in the disordered phase of the system. In the ordered phase, correlation between the spins is imposed by the fact that the system is 'frozen' at all times.) The rate at which each of the algorithms generates statistically independent configurations can then be compared.

The first, the Metropolis Algorithm, was introduced by N. Metropolis et al. in 1953 [159].

7.5 Evaluating the Fermion Determinant

One of the major tasks in any simulation of full QCD is that of evaluating the fermion determinant; this is usually done by converting the matrix to an upper triangular matrix first, and then using the diagonal elements alone. This takes of the order of n^3 operations for a matrix with n elements. Since there are $O(V)$ elements in the fermion matrix, the calculation of the fermion determinant will grow as V^3; hence the algorithm as a whole will go as V^4, since each sweep grows linearly with V!

A problem that is mathematically identical to that of finding the determinant of a matrix, but easier to implement numerically, is that of finding the inverse of a matrix. This is simply solving $Mx = y$, and can be done in a number of ways. One of the most commonly used is the conjugate gradient method.

7.5.1 Auxilliary Field Method

The relationship between the inverse and the determinant is given by the equation

$$\det M = \int \prod_n dY_n dY_n^\dagger e^{-\sum_{nn'} Y_n^\dagger M_{nn'}^{-1} Y_{n'}} \tag{7.22}$$

with $Y \in \mathbb{C}^N$ and M an $N \times N$ Hermitian matrix with positive definite eigenvalues. This is very easily proven; firstly, any Hermitian matrix has real eigenvalues and can be diagonalised.

After diagonlization, only the eigenvalues λ_n^{-1} will contribute to the integral. Since this is a standard Gaussian integral, each eigenvalue will contribute a term $\frac{\pi}{\lambda_n^{-1}}$. So the integral is the inverse of the determinant of M^{-1}, which is just the determinant of M.

One problem is that the fermion matrix is *not* positive definite Hermitian for the Wilson and Kogut-Susskind fermions. However, one can construct a positive definite Hermitian matrix M from the fermion matrix D_q for Kogut-Susskind and Wilson Fermions[2] (eqns. 5.30 and 5.131 respectively);

$$M = D_q^\dagger D_q \tag{7.23}$$

since the fermion matrix satisfies the identity $D_q^\dagger = \Gamma D_q \Gamma$, wilth $\Gamma = \gamma_5 \otimes \mathbb{1}$ for the Wilson fermions and $\Gamma = (-)^{|n|}\delta_{nn'}$ for the Kogut-Susskind fermions. This insures that the eigenvalues of D_q are either real and positive definite, or occur in complex conjugate pairs[208]. Thus M will have real positive definite eigenvalues, and is manifestly Hermitian.

Another trick that has been used for Wilson fermions is to use a factor of γ_5 in order to make the fermion matrix hermitian. Thus one gets $M = \gamma_5 D_q$.

Since the fermion action after performing the Grassmann integrals is simply a $\det D(U)$ term, one can construct an effective action for QCD using the above representation for $\det D$:

$$S_{\text{eff}}(U) = S_G(U) + \sum_{nn'} Y_n^\dagger M_{nn'}^{-1}(U) Y_{n'} \tag{7.24}$$

with S_G one of the pure gauge actions given in chapter 3. The partition function then includes an integral over the bosonic variables Y and $Y^\dagger$;

$$Z = \int [dU][dY_n][dY_n^\dagger] e^{S_{\text{eff}}(U)} \tag{7.25}$$

Since one has now replaced the original fermionic integral over Grassmannian variables with a bosonic integral over c-number variables, this method has come to be known as the 'pseudo-fermion' method.

However, the new matrix M describes double the number of fermions of the previous matrix. A technique often used to bring the fermions back to the original number is to take the square root of the determinant [207]. Furthermore, since the Kogut-Susskind fermions are independant on the even and odd sublattices, one often uses only those on the even sites; this method also reduces the spectral multiplicity to the original doubling.

Finding the inverse exactly will take $O(V^2)$ operations, a saving of V. However, one does not need the exact result, due to the inherent errors in the simulation. An approximate answer can be obtained for the inverse in comparatively few steps, whilst the determinant can only be found exactly. The overall calculation is then of the order of V^2, V^2 down from the original version.

7.5.2 Calculating the Inverse

The initial approach to calculating the inverse were based on the Gauss-Siedel iteration scheme [207]. The problem was approached as a set of coupled equations, $x = M^{-1}Y$ and the same technique used in the Heat Bath to calulate the energy minimum was used.

[2]Note that if the chemical potential is not zero, the determinant is no longer positive; this procedure is then no longer adequate to guarantee convergence of the bosonic integral.

It was soon realised that the conjugate gradient method was preferable. This is the basis of all methods in use today; however, this still takes 99% of the simulation time in a modern simulation of QCD with dynamical quarks (300 conjugate gradient iterations per inversion). One begins by making an initial guess as to the vector x, and then generates a sequence of approximations x_i.

The $i+1$th approximation is generated so as to be perpendicular to all the i vectors. Thus, for an $N \times N$ matrix the exact solution will be reached after at most N iterations, since x_{N+1} cannot be perpendicular to all the other x_i.

However, one does not need the inverse exactly; all that is required is an approximation to the inverse that differs from the exact result by less than the inherent errors of the simulation. Thus one determines some criterion for the accuracy, and performs the conjugate gradient algorithm until the norm $||Y - Dx_i||$ is less than the specified criterion.

The rate at which the algorithm approaches the desired accuracy is controlled by the ratio of the maximum and minimum eigenvalues of the matrix. Since this is independent of the lattice volume, approximately the same number of iterations are needed for any volume. This then leads to the saving of V^2.

The maximum eigenvalue is $\mathcal{O}(1)$; however, the minimum goes like $(m_q a)^2$ for the Kogut-Susskind case, and $(2Km_q a)^2$ for the Wilson fermions. Hence, as one decreases the lattice spacing or the fermion mass the number of iterations increases with the square of the product of the two.

The solution is to prepare a matrix D_0 that is closer to the unit matrix, and construct $M = D_0^{-1}D$. This preconditioning is more important for the Wilson fermions than the Kogut-Susskind fermions. A recent approach has led to a factor 15 improvement over the standard conjugate-gradient algorithm [91].

7.6 Metropolis Algorithm

The Metropolis Algorithm uses perhaps the simplest and most general way of moving from one configuration of the system to the next. Starting in a configuration x one randomly changes one or a few variables (perhaps the value of a link) resulting in a trial configuration x'. The one condition is that the probability of generating x' as trial configuration from x is the same as the probability of generating x as trial configuration from x', ie.

$$P_{tr}(x \to x') = P_{tr}(x' \to x) \tag{7.26}$$

The reason for changing no more than a few variables at each step is ergodicity; if one changes many, the chances of accepting an energetically unfavourable configuration are very small. Thus one will reach some local minimum and then stick there, unable to explore all of phase space.

So far this is merely simple sampling of the space; the next step implements the concepts of importance sampling. One compares the relative probabilities of each configuration appearing in the equilibrium limit; if

$P_\infty(x') > P_\infty(x)$ Accept the trial configuration.

$P_\infty(x') \leq P_\infty(x)$ Choose a random number R between 0 and 1. If $R < \frac{P_\infty(x')}{P_\infty(x)}$ then accept the trial configuration. If not, retain the original configuration and repeat the process for the $n+1$th step. In the situation one has with lattice QCD, the probability is given by the

Boltzmann factor; $P(x) = \exp[-S(x)]$ with $S(x)$ the action for the configuration. Thus this process amounts to choosing an energetically unfavourable change with probability

$$e^{-[S(x')-S(x)]} = e^{\delta S} \text{ if } \delta S > 0 \tag{7.27}$$

Manifestly, there are many other choices one can make for the acceptance criterion.

All that remains is to show that this satisfies the requirements of detailed balance and ergodicity. Detailed balance can be shown very simply; consider the case that $P_\infty(x') \leq P_\infty(x)$. Then one has

$$\frac{W(x \to x')}{W(x' \to x)} = \frac{P_{tr}(x \to x')\frac{P_\infty(x')}{P_\infty(x)}}{P_{tr}(x' \to x)} \tag{7.28}$$

Which gives the equation of detailed balance, after substituting eqn. 7.26

A check on ergodicity is far more problematic, and is where the major problem lies. There is no simple method that will work with all systems that can be used to check ergodicity; one needs to check each separately. In fact, one can easily devise systems with walls, such that ergodicity is not satisfied.

One further refinement of the Metropolis algorithm is to have a number of hits at each variable during each iteration. Thus one chooses a random value and decides whether to accept it or not. If not, rather than moving onto the next variable, one remains with this one until one of the trial values is accepted, or the number of hits allowed has been exceeded.

The program developed to simulate the Ising Model using the Metropolis algorithm has been listed in appendix D; the results obtained are given below.

In fig. 7.1 the auto-correlation of the Ising Model for different numbers of hits has been illustrated. This is the auto-correlation of section 7.2, with the average over the lattice of the correlation in simulation time between the spin on each site at $t = t_0$ and t. t_0 was chosen fairly arbitrarily, but away from the initial configuration to allow some time to 'forget' the cold start. Note that the time taken to reach an independant configuration is longer for 2 hits than it is for 10, as expected. However, there is little difference between the times taken for 10 and 20 hits. Since the latter takes more real time to simulate, the calculations of the average spin of the Ising model have all used 10-hit metropolis algorithms.

The average spin of the Ising Model, as calculated using the Metropolis Algorithm with 10 hits is given in fig. 7.2. Since the time to reach independant configurations is around 20 sweeps, when close to the phase transition, the 500 sweeps allowed for the initial thermalization, and seperation between samples of 100 sweeps should be sufficient to give good statistics.

The lack of any hysteresis (discrepancy in the position of the phase transition between the hot and cold start runs) indicates that the system was well thermalized at each temperature before samples were taken. This was not the case when only 100 sweeps were allowed for thermalization.

Notice how the average spin fluctuates between positive and negative values on the disordered side of the phase transition, before settling to zero. For the hot start, use was made of the symmetry between up and down; the final spin state below the phase transition was down. In order to be able to check for hysteresis, the plotted spins have all beeen flipped.

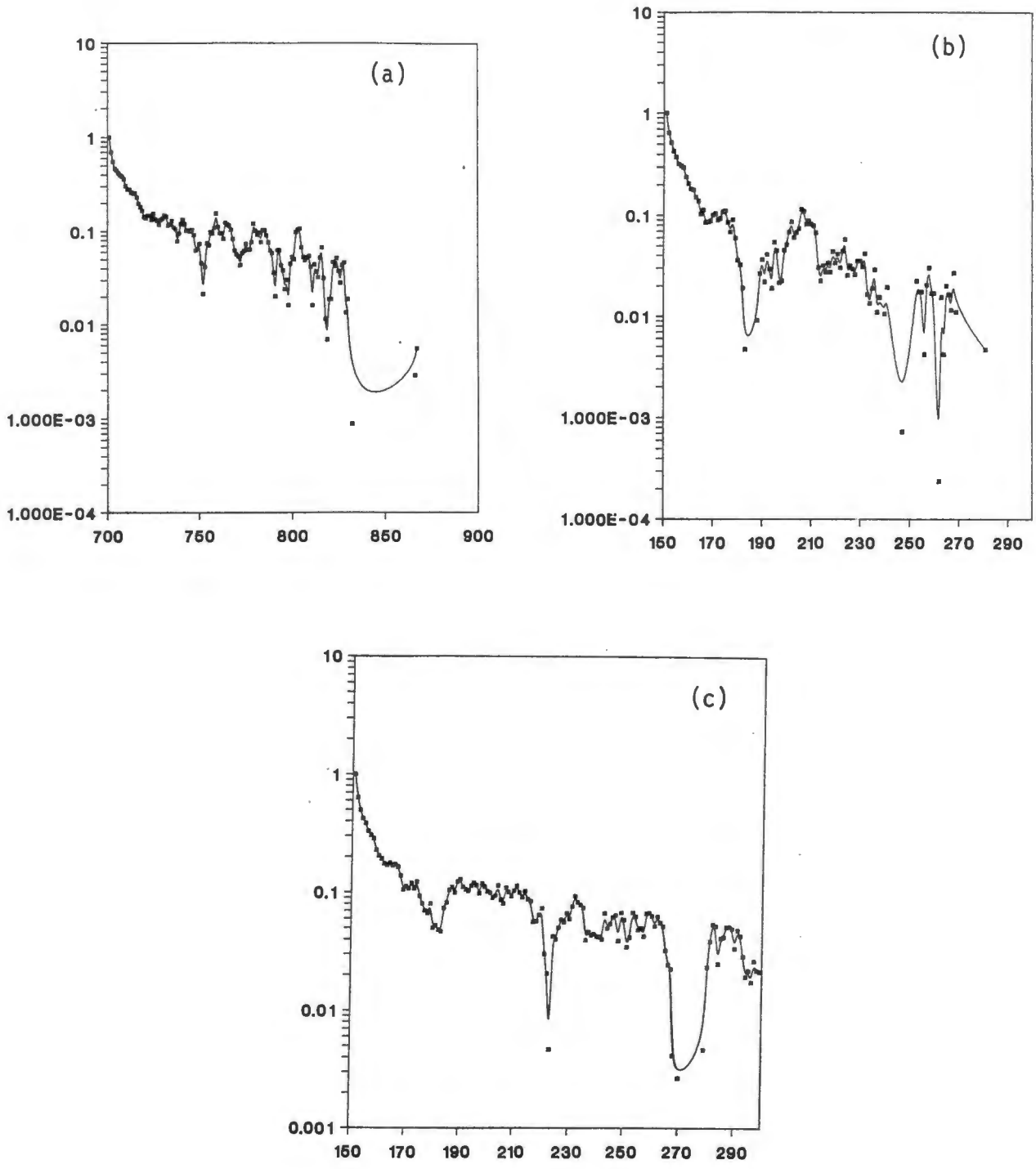

Figure 7.1: The auto-correlation of the Ising model using the Metropolis algorithm for 2 (a), 10 (b) and 20 (c) hits respectively. These were calculated in the disordered phase at a temperature $\beta = 0.5$.

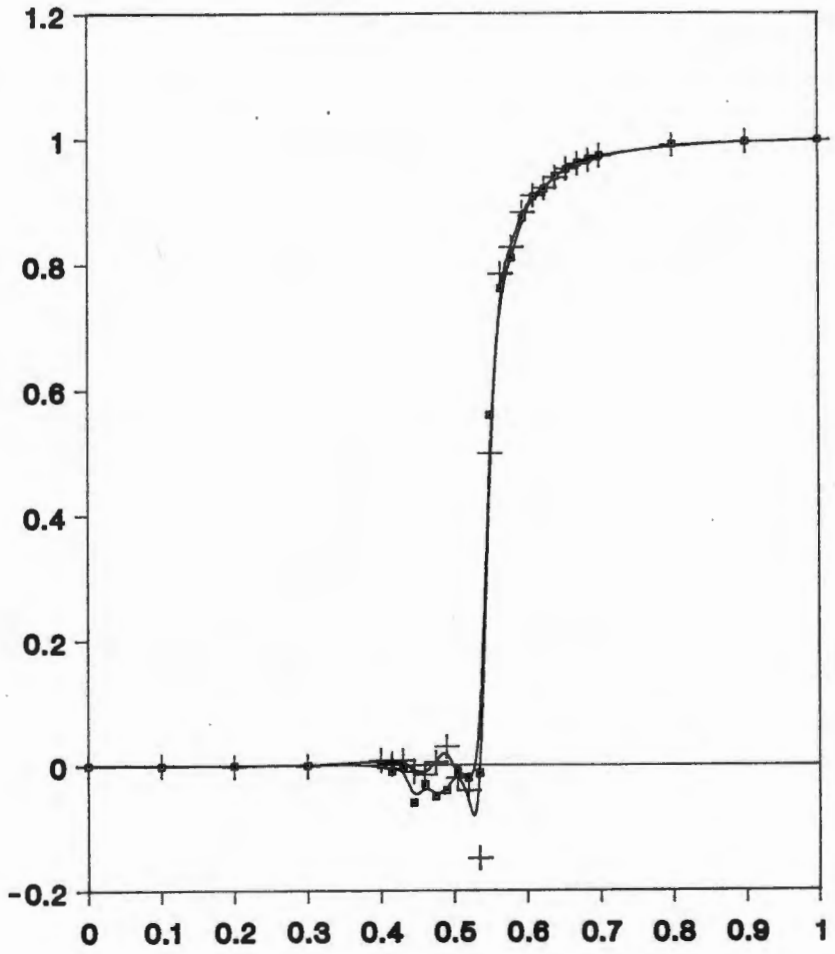

Figure 7.2: The average spin of the Ising Model using the Metropolis algorithm. The spin was calculated using both a cold and a hot start, with 500 sweeps used for the initial thermalization, with 100 sweeps between readings. A total of 5 values were obtained for the average spin at each value of β; the plotted data point is the average of those 5. The initial configuration at each new value of β was the final configuration at the previous value. The solid squares represent a cold start, the + signs a hot start.

7.7 Heat Bath Algorithm

In the Heat Bath algorithm [18,19,47], one sets each variable to a random value centered around the equilibrium value. This value is a function of the nearest neighbours, and not the variable itself, for a local interaction. This is done individually for each variable in each sweep.

In effect, one is touching a heat bath to each variable; the trial variable takes a random value, with Boltzmann distribution, around the energy minimum and is always accepted. Thus the differential probability density for the x_ith variable in the configuration x during the update to the x' configuration is given by:

$$dP(x_i') = \frac{1}{Z} e^{-S(x_{\neq i}, x_i')} \tag{7.29}$$

where the above notation makes it clear that the new value of x_i does not depend on the old value.

The Heat Bath algorithm is equivalent to a special case of the Metropolis algorithm; the Metropolis algorithm with an infinite number of hits (ie. choose the best possible trial value for the variable before accepting one) on a variable before updating the next variable.

Hence the essential difference between these two is that the Metropolis algorithm generates the trial value using a uniformly distributed random number, and then accepts it according to a biased distribution. The Heat Bath algorithm uses a biased distribution from the start to generate the trial value. Thus applying the Heat Bath algorithm to the entire lattice simultaneously would be the case of generating a new configuration at random each time, which would no longer constitute a Markov chain, as discussed in the introductory section. It thus corresponds to the type 1 probability law discussed at the start of this chapter.

In a nearest neighbour interaction, the equilibrium value for a variable will depend only on the neighbouring variables. So the new value in the Heat Bath has no memory of the old value; hence one expects the correlation time of the longest correlation to be lower than that for the Metropolis algorithm.

Thus, in terms of the number of sweeps required, the Heat Bath algorithm will reach thermal equilibrium for the entire lattice faster than the Metropolis algorithm will. (Note that the Metropolis algorithm is more likely to change the value of a variable, so will move faster through phase space.) However, one may not be able to devise a method of generating the heat bath for each link. Furthermore, the computer time needed to generate the equilibrium value for each variable may be sufficiently large that the algorithm is no faster in real time than the Metropolis algorithm is.

In the case of the Ising model, the Heat Bath algorithm is easy to implement and is faster than the Metropolis algorithm by a factor of 2. For the Ising Model one has the probability distribution for a site j

$$\Delta P(s_j) = \frac{e^{-s_j \sum_i s_i}}{e^{-\sum_i s_i} + e^{-(-1)\sum_i s_i}} \qquad \text{for } i \text{ nearest neighbour to } j \tag{7.30}$$

The algorithm is then implemented by choosing $s_j = 1$ if $\Delta P(s_j)$ is greater than some random number chosen from a uniform sequence, or choosing $s_j = -1$ if it is less than.

The program developed to simulate the Ising Model is given in appendix D.

The values of the average spin for the Heat Bath are shown in fig. 7.3. There is a discrepancy between the Metropolis and the heat bath methods in the temperature at which

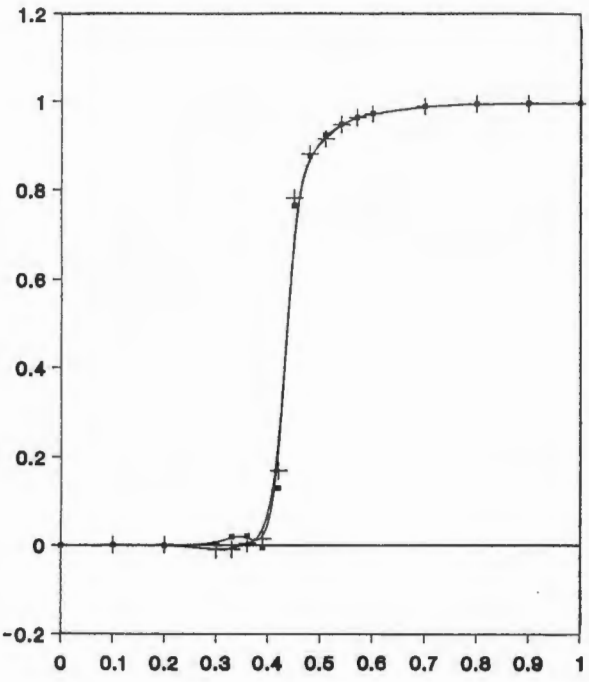

Figure 7.3: The average spin in the Ising Model, using the Heat Bath algorithm. Both hot and cold starts are shown. The first 1000 sweeps were discarded for initial thermalization, and the average spin then calculated 5 times at seperations of 100 sweeps. The average of these 5 is then plotted for each β. The initial configuration at each new value of β was the final configuration at the previous value. The solid squares represent a cold start, and the + signs a hot start.

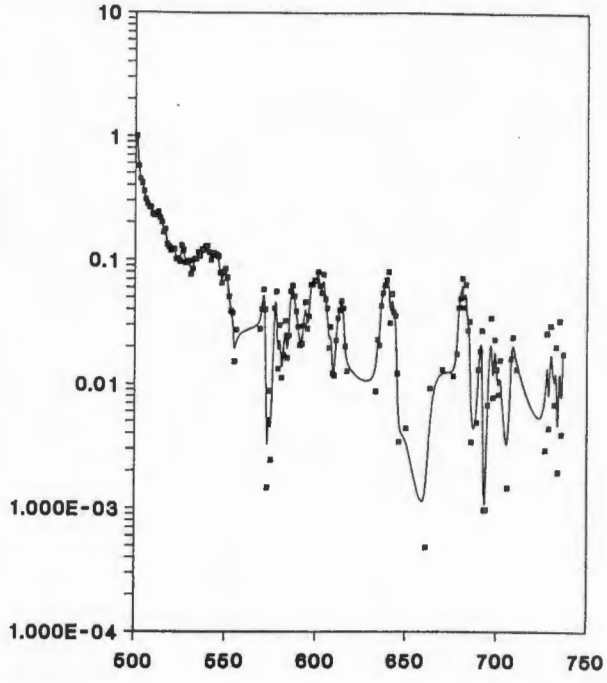

Figure 7.4: Auto-correlations between spins on each site for the Ising model using the Heat Bath algorithm at $\beta = 0.4$.

the phase transition occurs. It appears that the effective coupling in the heat bath method is greater than that in the Metropolis; the cause of this effect is unknown to me.

The auto-correlation for the Ising model is shown in fig. 7.4. The definitions are the same as for the auto-correlation in the Metropolis algorithm. Notice that the number of sweeps required to reach independant configurations is about the same as for the 10-hit Metropolis algorithm; however, in this case the processing time required is closer to that for the 2-hit Metropolis algorithm.

For the gauge groups of relevance to QCD, the technique of generating the Heat Bath proved more difficult. These were developed for SU(2) by Creutz in 1980 [72] and improved, by a factor of 4 in execution time, by Kennedy and Pendleton [135]. The SU(N) algorithm was developed by Cabibbo and Marinari in 1982 using a technique based on performing a sequence of updates of the SU(2) subgroups of SU(N). In the SU(3) case it was observed that the correlation times were reduced by a factor of 2 compared to the 10-hit Metropolis algorithms.

Now the Heat Bath algorithm is the same as a standard Gauss-Seidel minimization al-

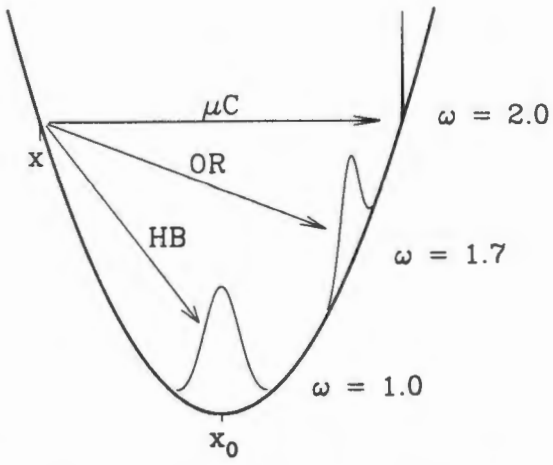

Figure 7.5: The various types of Heat Bath updates, as a function of the energy. x is the old value of the variable, the arrows indicate the position of the new value. HB = Heat Bath, OR = Over-relaxed heat Bath algorithm, and μC = Micro-Canonical algorithm. Ex. [47]

gorithm, with the addition of a Gaussian noise factor. Due to long-range coherence effects, the standard Gauss-Seidel algorithm is not the best way of minimizing a large system of variables. The overrelaxed Gauss-Seidel algorithm converges faster.

7.7.1 Overrelaxed Heat Bath Algorithm

The Overrelaxed Heat Bath algorithm was first introduced by Adler [18,19]. The difference between the Heat Bath and the Overrelaxed Heat Bath algorithms is shown in fig. 7.5. In the over-relaxed algorithm, one chooses a value of the variable with a lower energy, and on the other side of the energy minimum to the present value.

The relationship between the new and old values of a variable x is given by

$$x_i' = x_i + \omega(x_i - x_{imin}) - \left(\sqrt{\frac{\omega(2-\omega)}{4\beta}}\right)\eta_i \tag{7.31}$$

where x_{imin} is the value of x_i' that minimizes the energy, η_i is the Gaussian noise and ω is a parameter giving the amount of overrelaxation.

For this technique to work the new value of the variable must be lower than the old one; this restricts the allowed values of ω to $\omega \in [0,2]$. Note that $\omega = 1$ gives the standard Heat Bath, whilst $\omega = 2$ yields the microcanonical algorithm, in which the energy of the system remains constant.

For the standard Heat Bath the correlation time is $\sim L^2$ for a system of linear dimensions L, whilst for the Overrelaxed Heat Bath it can be reduced to $\sim L$ via judicious choice of the parameter ω. It is not possible to find the optimal parameter by any means other than empirical observation, for most systems. To give some idea of the relative merits of the Overrelaxed Heat Bath and Metropolis algorithms, the correlation times for the XY model on lattices up to 512^2 were found to be $t_c = 0.15\xi^{1.2}$ and $t_c = 5\xi^2$ respectively [106].

It was soon found that the fastest convergence times were obtained by using a hybrid version of these two algorithms, by doing a few iterations with $\omega = 1$ and then many with $\omega \approx 2$ [19]. This leads to a better covering of phase space, hence more manifest ergodicity.

Another possible hybrid algorithm is obtained by combining the Metropolis and Heat Bath algorithms, and doing a few iterations of each with some probability R and $1 - R$ respectively. This technique has been implemented by [106] for the XY model.

Since the overrelaxed heat bath algorithm is only meaningful for groups larger than Z_2, it cannot be illustrated for the Ising Model.

The previous algorithms work well for local problems; however, they are all excessively slow when it comes to calculations that are non-local in character. Now the fermion matrix potentially includes contributions from all the lattice sites, and hence is very non-local. (A considerable saving is made by the fact that the fermion matrix is sparse for the common formulations, rather than having connections between each lattice site.) Since any calculation involving fermions will include finding the determinant of the fermion matrix, one cannot use the previous simulations if one includes fermions in the simulation.

An idea of the increase in computer time needed can be obtained by considering the size of the matrix; $V \times$ Int. Symmetries $\times\, 4_{Dirac}$. (The last term is absent in the Kogut-Susskind formulation.) The calculation of the determinant will need operations of the order of V^3. In order to sweep the entire lattice, one will need V determinants, one per link; hence the total time needed for one sweep is of the order of V^4!

Manifestly, the Metropolis algorithm is no longer feasible for full QCD simulations; Some means must be found to reduce the time needed to the $O(V)$ needed for a pure gauge simulation. In other words, one needs to reduce the number of operations needed per link to some fixed number, as in the pure gauge case.

A number of methods have been proposed for this, such as the microcanonical [175], Langevin [200,26], hybrid molecular dynamics [83,84,101], and hybrid Monte Carlo [82]. These are all related to each other.

7.8 Langevin Algorithm

The Langevin algorithm [91] is based on a differential evolution equation for the variables involved. If you express the simulation time in terms of a variable t, then the position variables develop according to the Langevin, or stochastic evolution equation:

$$\frac{\Delta q_i}{\Delta t} = -\frac{\partial E}{\partial q_i} + \sqrt{\Delta t}\eta_i(t) \tag{7.32}$$

with $\eta_i(t)$ a Gaussian noise term. The configuration variable moves down the energy gradient, subject to a noise factor.

To do the same for QCD one needs to move the link variables $U_\mu(x)$ down the energy gradient, closer to the equilibrium value, with a noise factor. Since these are group elements, represented by matrices of unit determinant, one way of changing from the old to the new value of the link variable is to multiply by an exponential:

$$U_\mu(x, t + \Delta t) = U_\mu(x) e^{iX\Delta t} \tag{7.33}$$

with X some function of the energy gradient and a noise factor. Thus the differential equation must be of the form

$$\frac{-i}{U_l(t)} \frac{\Delta U_l}{\Delta t}(t) = X \tag{7.34}$$

If one is using the pseudo-fermion method of section 7.5.1 then the bosonic variables Y play the role of coordinate variables for the fermions. The Langevin equations for lattice QCD are then given by [105,91]

$$\frac{-i}{U_l(t)}\frac{\Delta U_l}{\Delta t}(t) = -i\frac{\delta S_{\text{eff}}}{\delta U_l(t)}(U(t),Y(t)) + \frac{1}{\sqrt{\Delta t}}\eta_l(t) \tag{7.35}$$

$$\frac{\Delta Y_n}{\Delta t}(t) = -\frac{1}{M_{nn'}(U(t))}Y_{n'}(t) + \frac{1}{\sqrt{\Delta t}}\xi_n(t) \tag{7.36}$$

with S_{eff} given by eqn. 7.24 and the right derivative over the group defined by:

$$\frac{\delta}{\delta U_l(t)} = t^a \sum_{ij}(t^a U)_{ij}\frac{\delta}{\delta U_{ij}} \tag{7.37}$$

The two noise vectors are $\eta_l(t) = t^a\eta_l^a(t)$ with t^a the $SU(3)$ generators, and $\xi_n(t) = \xi_n^{\alpha i}(t)$ with $\alpha \in [1,4]$ being Dirac indices (only in the Wilson formulation) and the $i \in [1,3]$ being colour indices. They satisfy the property for independent Gaussian random numbers that

$$\begin{aligned}\langle\eta_l(t)\eta_{l'}(t')\rangle &= \delta_{ll'}\delta(t-t') \\ \langle\xi_n^{\alpha i}(t)\xi_{n'}^{\alpha' i'}(t)\rangle &= \delta_{nn'}\delta^{\alpha\alpha'}\delta^{ii'}\delta(t-t')\end{aligned} \tag{7.38}$$

The evolution equation for the gauge variables can be solved, yielding

$$U(t_{n+1}) = U(t_n)e^{i\Delta t X^{(n)}} \tag{7.39}$$

where t_n represents the nth iteration of the algorithm.

The driving function for the evolution of the gauge fields is:

$$X^{(n)} = -i\frac{\delta}{\delta U_l(t)}S_{\text{eff}} + \frac{1}{\sqrt{\Delta t}}\eta_l(t) \tag{7.40}$$

The evolution equation for the variable Y becomes

$$Y(t_{n+1}) = e^{-\Delta t/M}Y(t_n) + \xi(t_n)\sqrt{\Delta t} \tag{7.41}$$

However, one does have further freedom in the choice of evolution equation for the Y, since they are not explicitly part of the physics. The general form may be written

$$Y(t_{n+1}) = [1 - \Delta t B(U(t(n))]Y(t_n) + \sqrt{\Delta t}C(U(t_n))\xi_n \tag{7.42}$$

The matrices B, C, and M satisfy the condition $BM + MB^\dagger - 2CC^\dagger = 0$, in order to obtain the correct limit for the fermion matrix as the simulation time step tends to zero.

There are two limiting cases for these matrices [26]:

$B = \frac{1}{M}$, $C = \mathbb{1}$ In this case the Y_n are treated as pseudo-fermionic variables, updated according to the fermionic matrix and an additional random vector.

$B = \frac{1}{\Delta t}$, $C = \frac{1}{\sqrt{\Delta t}}\sqrt{M}$ The so-called bilinear noise scheme, in which the Y_n do not evolve, but are merely set equal to a random number at each step in the process. This method yields lower systematic errors than the former variant [26].

The errors introduced in each of these cases, ie. the $O(\Delta t)$ term, is of the same magnitude in each case [91]; however, whilst a higher order scheme can be introduced in both cases, it is considerably less straight forward in the bilinear noise scheme.

The Langevin algorithm and the over-relaxed heat bath algorithm are also related [19]; the Langevin algorithm corresponds to the extremely underrelaxed limit of the over-relaxed heat bath algorithm.

7.9 Hybrid Molecular Dynamics

If one can reduce the number of matrix inversions required per sweep to some small constant number, approximately independant of the volume, one save a factor of V in the simulation time. Hybrid molecular dynamics (hmd) does just that. The advantages are that one has a rapid movement through phase space; one only requires one Conjugate Gradient iteration per molecular dynamics step; and the error is proportional to the square of the step size.

7.9.1 Molecular Dynamics

If one has a probability distribution of the form $e^{-E(q)}$ for a system, a function of continuous coordinates q, the expectation value (see eqn. 6.2) of an observable $\mathcal{O}$ is unchanged if one introduces a 'momentum' variable p_i conjugate to each coordinate variable q_i as follows:

$$\langle \mathcal{O} \rangle = \frac{\int [dq_i] \mathcal{O}(q_i) e^{-E(q_i)} \int [dp_i] e^{-\frac{1}{2}\sum p_i^2}}{\int [dq_i] e^{-E(q_i)} \int [dp_i] e^{-\frac{1}{2}\sum p_i^2}} \tag{7.43}$$

where an energy proportional to the squares of the momenta has been assumed.

Thus far, no real change has taken place, since one can readily integrate the momenta out, returning to the original system. One can now proceed to simulate a system according to the larger probability, $e^{-E(q_i)-\frac{1}{2}\sum p_i^2}$. One can also take over the standard Hamilton-Jacobi equations of motion;

$$\begin{aligned} \frac{dq_i}{dt} &= p_i \\ \frac{dp_i}{dt} &= -\frac{\partial E}{\partial q_i} \end{aligned} \tag{7.44}$$

in which the derivative is taken with respect to simulation time τ. Note that the 'time' in this case has a different dimension to that in the Langevin algorithm. Here, one has Newton's law, with $\ddot{q}_i = -\frac{\partial E}{\partial q_i}$ whilst previously one had $\dot{q}_i = -\frac{\partial E}{\partial q_i}$.

The connection between the two algorithms can be more easily seen if one considers the discrete solution of these two equations. One has

$$q(t_{n+1}) = q(t_n) - \frac{\partial E}{\partial q_i}\Delta t + \eta(t)\sqrt{\Delta t} \tag{7.45}$$

$$q(t_{n+1}) = q(t_n) - \frac{\partial E}{\partial q_i}(\Delta t)^2 + p(t_{n-1})\Delta t \tag{7.46}$$

for the Langevin and molecular dynamics algorithms respectively. If one sets the momenta in the molecular dynamics algorithm equal to a random number for each iteration, and relate the Langevin fictitious time t_{L} to the molecular dynamics time t_{md} by $t_{\mathrm{L}} = t_{\mathrm{md}}$ then the two methods become identical.

7.9.2 Leapfrog Integration

The technique known as Leapfrog Integration is the most common means of integrating the discrete equations of motion of both the molecular dynamics and Langevin algorithms. It has the advantage, exploited in the hybrid Monte Carlo algorithms, that it is exactly reversible.

One has a simulation time t, consisting of discrete multiples of the step length ϵ. In the Leapfrog integration scheme one evaluates the canonical coordinates at each integer multiple of ϵ, and the canonical momenta at half-integer values of ϵ.

The discrete version of the Hamilton-Jacobi equations is then

$$\begin{aligned} q_i(t+\epsilon) &= q_i(t) + \epsilon p_i(t+\frac{\epsilon}{2}) \\ p_i(t+\frac{3\epsilon}{2}) &= p(t+\frac{\epsilon}{2}) - \epsilon \frac{\partial E}{\partial q_i}(t+\epsilon) \end{aligned} \tag{7.47}$$

If the terms neglected in each of the above are of order ϵ^2, and assuming that the initial term in the series at $\tau = 0$ is exact, the error introduced at each stage will then be of order ϵ^3.

The one hiccough occurs in getting the initial value[3] of $p_i(\frac{\epsilon}{2})$. This is dependent on $q_i(0)$ and thus cannot be set to a random number. Hence one needs to apply the Hamilton-Jacobi equation once, using a half-integral step:

$$p_i(\frac{\epsilon}{2}) = p_i(0) - \frac{\epsilon}{2}\frac{\partial E}{\partial q_i}(0) \tag{7.48}$$

This will introduce an error of order ϵ^2. Since the error, after $O(\frac{1}{\epsilon})$ steps, will be ϵ^2 from the integration of the Hamilton- Jacobi equations, the final error of the simulation will go like ϵ^2.

7.9.3 QCD Molecular Dynamics

For QCD one constructs variables $P_{i,\mu}$ that play the role of momenta conjugate to the link variables $U_{i,j}$. These $P_{i,\mu}$ are $SU(3)$ matrices, defined as $P_{i,\mu} = \sum_a \lambda_a P^a_{i,\mu}$ with λ_a being the $SU(3)$ generators.

The 'Hamiltonian' used for the molecular dynamics iterations then becomes

$$\mathcal{H} = \frac{1}{2}\sum_{i,\mu} \mathrm{Tr}_c P^2_{i,\mu} + S_{\mathrm{eff}} \tag{7.49}$$

with S_{eff} as defined in eqn. 7.24. The Hamilton-Jacobi equations then become (keeping the variables Y in S_{eff} fixed)

$$\begin{aligned} \frac{-i}{U}\frac{dU}{dt} &= P \\ \frac{dP}{dt} &= -\frac{\delta \mathcal{H}}{\partial U} \\ &= -\frac{\partial S_G}{\partial U} - Y^\dagger \frac{1}{M}\frac{\delta M}{\delta U}\frac{1}{M} Y \end{aligned} \tag{7.50}$$

One can also introduce a momentum variable conjugate to Y and evolve these as well.

In order to calculate the new values of these by computer, one needs the discrete version of these equations. This can be done similarly to the method used for the Langevin algorithm. Note, however, the difference in the dimension of the 'time' in each case. Thus the discrete

[3]Note that, if the momenta correspond to some variable present in the original system, rather than being fictitious variables, one will need to repeat this step to get the final mometum.

version, using the Leapfrog integration technique, become

$$\begin{aligned} U(t+\Delta t) &= U(t)e^{iP(t+\frac{\Delta t}{2}))\Delta t} \\ P(t+\frac{\Delta t}{2})) &= P(t-\frac{\Delta t}{2})) - \left(\frac{\partial S_G}{\partial U} - \frac{Y^\dagger}{M}\frac{\partial M}{\partial U}\frac{Y}{M}\right)\Delta t \end{aligned} \tag{7.51}$$

The update for the gauge fields can then be written

$$U(t+\Delta t) = U(t)e^{iX^{(t)}\Delta t} \tag{7.52}$$

$$X^{(t)} = P(t-\frac{\Delta t}{2}) - \left(\frac{\partial S_G}{\partial U} - \frac{Y^\dagger}{M}\frac{\partial M}{\partial U}\frac{Y}{M}\right)\Delta t \tag{7.53}$$

Using these, one can take the system through the phase space in a reversible manner. Furthermore, the energy of the system is constant; hence this is known as the microcanonical, or molecular dynamics method. Since energy is conserved, it is not ergodic; however, due to the computational error introduced at each step in a simulation, the algorithm is ergodic in a sufficiently long sumulation.

7.9.4 Hybrid Molecular Dynamics

This algorithm is an hybrid consisting of both the Langevin and the molecular dynamics algorithms. Since the probability distribution of the $p_i(t)$ at a given simulation time t and site i is independant of the other p_j, $j \neq i$ and the q_i at the same time, one can apply a heat bath to each of the p_i, setting each to a random number generated from a Gaussian distribution. This is known as refreshing the momenta. It can be seen, if one looks again at the similarity between the Langevin and molecular dynamics difference equations (eqn. 7.45), that this is an obvious alteration to make to the molecular dynamics algorithm.

If one refreshes the momenta occasionally, the algorithm is ergodic. The Hamilton-Jacobi equations set up a trajectory in phase space, with the refreshing of the momenta providing a random walk component (see fig. 7.6).

One can tune the time between refreshing, such as to obtain an optimal covering of phase space. If one refreshes the momenta at each step, one has the Langevin limit, which corresponds to a random walk in phase space; one then covers a distance proportional to $\sqrt{N}$ in phase space after a simulation time of N. In the microcanonical limit of no refreshing, one loses ergodicity by travelling in loops in phase space.

The optimal time between refreshing the momenta, or, in other words, the optimal hybridisation of the two schemes, needs to be found empirically (see fig. 7.7).

The simulation time for this genre of algorithm will depend on the step size ϵ, increasing with decreasing step size. Hence, if the overrelaxed heat bath takes $O(V)$ for pure gauge, this method will take $O(\frac{V}{\epsilon})$; thus the former is better for local problems. However, since one updates all the variables simultaneously in this genre of algorithms, it will remain at $O(\frac{V}{\epsilon})$ in non-local problems. Hence it may win over the overrelaxed heat bath for those simulations, in which the latter takes $O(V^4)$!

One can define two versions of the Hybrid molecular dynamics algorithm, depending on how one tackles the fermion determinant problem [101,100].

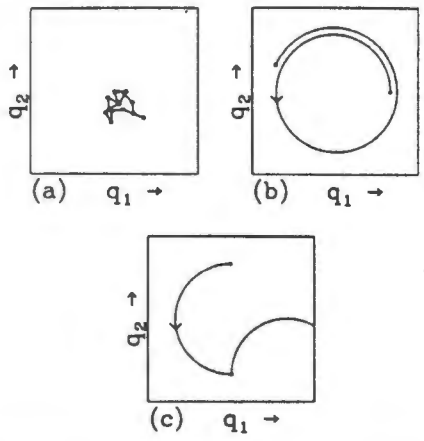

Figure 7.6: Movement of the system in phase space with (a) frequent refreshing (Langevin limit), (b) no refreshing (molecular dynamics limit) and (c) optimal refreshing. [197]

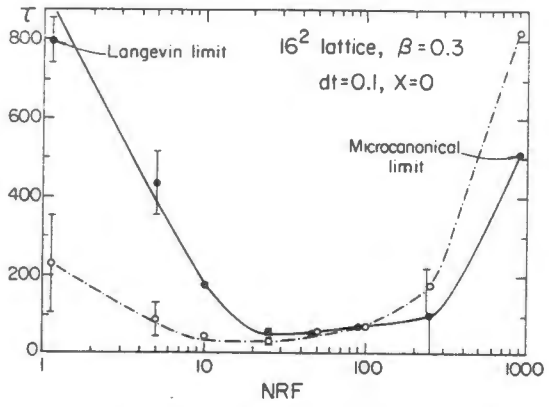

Figure 7.7: Auto correlation time versus refreshing frequency for an SU(3) × SU(3) spin model. ex [73]

7.9.5 Pseudo-fermion Method

Using the approach of section 7.5.1 one updates the fields for Y and P using the Heat Bath algorithm. This is done by mapping Gaussian random numbers $P^a_{i,\mu}$ and R_i, $R_i \in \mathbb{C}$ to each as follows:

$$P_{i,\mu} = \sum_a \lambda_a P^a_{i,\mu} \qquad \text{with} \quad \langle |P^a_{i,\mu}| \rangle = 1 \tag{7.54}$$

and

$$Y_j = \sum_i D^\dagger_{j,i} R_i \tag{7.55}$$

Where the definition for the Y yields the correct distribution ($\exp[Y^\dagger \frac{1}{M} Y]$) for them if the R are Gaussian. One needs the R on all the sites in order to calculate the Y; those on the odd sites can then be ignored if one wishes to reduce the spectral multiplicity introduced by taking the product of two fermion matrices to get M.

This is followed by $N_{\rm md}$ steps of the molecular dynamics applied to P and U, with the Y held constant. An idea of the ideal number of molecular dynamics steps required between heat bath updates can be gained from fig. 7.8

7.9.6 Random Field Method

Another method often used to determine the fermion determinant is the so-called 'fermion noise' algorithm.

If one exponentiates the determinant of M, one has $\exp[+\mathrm{Tr}\ln M]$ in the partition function. Thus the Hamilton-Jacobi equation can be written

$$\begin{aligned} \frac{dP}{dt} &= -\frac{\partial S_{\rm G}}{\partial U} + \frac{\delta}{\delta U}\mathrm{Tr}\ln M \\ &= -\frac{\partial S_{\rm G}}{\partial U} + \mathrm{Tr}\left(\frac{1}{M}\frac{\delta M}{\delta U}\frac{1}{M}\right) \end{aligned} \tag{7.56}$$

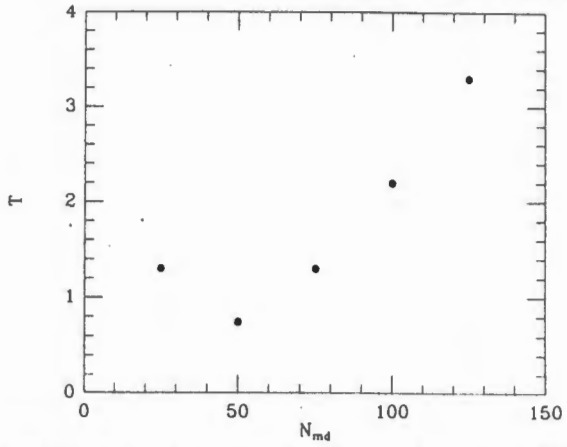

Figure 7.8: The auto correlation as a function of the number of molecular dynamics steps between heat bath updates, for a 4^4 lattice. ex. [101]

The basis of the fermion noise method is the fact that, for any variable ξ_n that is generated at random from a Gaussian Distribution,

$$\mathrm{Tr}\left(\frac{1}{M}\frac{\delta M}{\delta U}\frac{1}{M}\right) \underset{V\to\infty}{\equiv} \xi'^{\dagger}\left(\frac{\delta M}{\delta U}\right)\xi' \tag{7.57}$$

with

$$\xi' = \frac{1}{M}\xi \quad \text{and} \quad \langle \xi_n \xi_{n'} \rangle = \delta_{nn'} \tag{7.58}$$

The drawback of the pseudo-fermion method is that one can only simulate 4 Kogut-Susskind, or 2 Wilson fermions. The random field method enables one to simulate any number of fermions, including non-integer. In the case of the Kogut-Susskind fermions, if one wishes to simulate N_f continuum fermions, the determinant of the fermion matrix is raised to the power of $N_f/4$. (This can readily be understood if one recalls that, upon changing from D to M one doubled the number of fermions on the lattice. This change was effectively squaring the determinant.)

Thus the Hamilton-Jacobi equation for the momenta becomes

$$\frac{dP}{dt} = -\frac{\partial S_G}{\partial U} + \frac{1}{N_f/4}\xi'^{\dagger}\left(\frac{\delta M}{\delta U}\right)\xi' \tag{7.59}$$

7.9.7 Ising Model

Since this genre of algorithms are all designed for facilitating the simulation of systems based on more complex groups than Z_2, it is not in general possible to use the Ising Model to illustrate them. (A more realistic model would be an $SU(3) \times SU(3)$ spin system, such as used by [73].) Hence the above will be compared to the standard Metropolis and Heat Bath algorithms, in order to give an approximate idea of the relative differences.

7.10 Hybrid Monte Carlo

One can eliminate the systematic errors that arise from the finite step size, using the exact, or hybrid Monte Carlo algorithms [82,70,92]. These are known as exact because they preserve the priniple of detailed balance. In them, one uses the Hamilton-Jacobi equations, or the

Langevin algorithm etc. to construct a new configuration (x') at the end of the trajectory from the old (x) at the start of the trajectory. One can then use this final configuration as the trial configuration for the next iteration of a Metropolis simulation.

This is the essence of the exact algorithm; a Metropolis algorithm in which each successive configuration is generated from the old by a microcanonical algorithm.

The older exact algorithms, such as the auxilliary field method [207], all take computer time that grows as V^2, since the fermionic inversion needs to be performed for each site in the lattice. The major advantage of the hybrid Monte Carlo algorithms is the fact that they preserve the principles of detailed balance, whilst only needing a few fermionic inversions per sweep. These 'globally corrected' algorithms require more time than the uncorrected algorithm, but less than the other exact algorithms.

Of the two in common use, the globally corrected Langevin algorithm increases the time required by a factor of $V^{\frac{1}{3}}$, whilst the hybrid molecular dynamics algorithm uses $V^{\frac{1}{4}}$ more time than the uncorrected version.

Thus in the corrected hybrid molecular dynamics, one uses the equations of motion, with some step size Δt, to generate a new gauge configuration U' from the old. One also generates the associated canonical momentum P', this being the momentum required to reverse the process and move from the configuration U' to U.

Using the equations from the molecular dynamics section, one then gets

$$\begin{aligned} U &= U' \exp\left(-iP\Delta t + i\frac{\partial S_{\text{eff}}}{\partial U}\Delta t^2\right) \\ &= U' \exp\left(iP'\Delta t - i\frac{\partial S_{\text{eff}}}{\partial U'}\Delta t^2\right) \end{aligned} \tag{7.60}$$

and hence the equation for P', the momentum required to reverse the direction of motion;

$$P' = -P + \Delta t\left(\frac{\partial S_{\text{eff}}}{\partial U} - \frac{\partial S_{\text{eff}}}{\partial U'}\right) \tag{7.61}$$

One then applies the Metropolis acceptance criterion to the new configuration, accepting it if there is an energy drop, or if the exponent of the energy increase is less than some random number. Hence the criterion is based on the energy difference

$$\delta\mathcal{H} = \mathcal{H}(U,P) - \mathcal{H}(U',P') \tag{7.62}$$

One point to note is that one can have two different Hamiltonians; the first is used in the Metropolis accept/reject stage, the second in the molecular dynamics iterations. This leads to methods of improving the rate of decorrelation between configurations, as well as improving the acceptance rate of proposed configurations.

The one proviso that accompanies this algorithm is that the discrete numerical scheme for integrating out the Hamilton-Jacobi equations must preserve the phase space volume and be reversible, in order to satisfy the Metropolis acceptance requirements.

One scheme that does this is Leapfrog integration described earlier.

7.11 Error Analysis

This section describes the two most commonly used techniques for determining the statistical error on a quantity (eg., the propagator) calculated using a Monte Carlo algorithm.

7.11.1 Binning

This was the first technique used. In it, one splits the total set of configurations sampled into some number of subsets. One then calculates the desired quantity in each of the subsets, and finds the average and error of these. This is then taken as the quoted error.

Manifestly, this suffers from two problems. Firstly, one needs to have many subsets to get a good estimate of the error. Secondly, one needs many configurations in each subset to get the propagator accurately in each. These problems are addressed in the jacknife and bootstrap routines;

7.11.2 Jacknife

This method [109] addresses the second problem. Starting with N configurations, one generates the N possible subsets containing $N-1$ different configurations. One then gets the error from the spread of the value calculated in each of these subsets, and takes the result.

The advantage of this is that one can get a stable value for the mean with relatively few configurations in total.

7.11.3 Bootstrap

This technique is a superset of the jacknife technique; one chooses a subset of N configurations from the original set, but without any requirement of choosing each once only. (Thus there is a probability of $1/N^N$ of having any given configuration chosen N times.) If one chooses these subsets well, one gains the best approximation to N independent sets of configurations. The data are still usually not Gaussian, however; the median usually gives the most stable result, whilst the error is taken seperately on each side, such that $\delta_+ - \delta_-$ contains 63% of the range.

Naturally, there are a large number $\left(\frac{N^N}{N!}\right)$ of possible subsets one could create. In order to obtain a choice of subsets that is yields results close to those one would obtain using the total possible number of subsets, one uses a Monte Carlo routine to construct the subsets, by choosing at random from the set of configurations.

7.12 Comparison of Algorithms

Unfortunately, it is not at all clear-cut which of the above algorithms is the best choice.

One constraint is the relative importance of storage space and processing speed on the particular machine one is using. If one has memory constraints, the Langevin may be the best, since one does not need to store the values of the momenta. Furthermore, this implies that one can invent higher order schemes more easily. However, one needs more configurations than the hybrid molecular dynamics algorithm does to get the same accuracy, so the processing time required is relatively high. Long simulation times are required to gaurantee statistical independence of configurations.

Obviously, all of the algorithms based on equations of motion suffer from errors introduced by the finite step size, and the fact that the discrete approximations to the difference equations are truncated at finite order. However, they gain over the Metropolis and Heat Bath algorithms in that the fields on the lattice are updated in parallel. This is an extremely

large improvement when one is using a parallel computer, and independant parts of the lattice can be updated simultaneously

With the hybrid Monte Carlo algorithms, one has both the ease with which a molecular dynamics algorithm explores phase space, due to the simultaneous updating of the fields, as well as the absence of the truncation errors that the Metropolis algorithm has.

However, the problem with the hybrid Monte Carlo algorithm is that the change in energy grows with the volume of the lattice. Thus the acceptance rate decreases as the lattice grows larger. In order to counteract this, one needs to drop the step size in the molecular dynamics stage of the algorithm. This leads to a large increase in the auto-correlation time. It also adds to the problems associated with critical slowing down near a phase transition.

The other factor increasing the time required for an hybrid Monte Carlo algorithm is the greater precision required in the evaluation of the inverse of the fermionic matrix. Just as above, this problem is also aggravated by an increase in the lattice size.

Thus there is a compromise between hybrid molecular dynamics and hybrid Monte Carlo; the former is a factor of $V^{\frac{1}{4}}$ faster, whilst the latter has the potential for lower, and better understood, errors. Hence, for constant errors and an increasing volume hybrid molecular dynamics will eventually be faster, whilst for constant volume and decreasing error hybrid Monte Carlo will be faster.

There have been some comparisons between the Langevin and the Hybrid Monte Carlo algorithms; Gupta has presented results showing the HMC algorithm is faster [108], whilst Fukugita [91] claims the Langevin is faster. Both are still in use, and appear to be equivalent in most applications.

Since the number of operations increases rapidly with increasing lattice size, it is imperative that the errors remain under control. This means, in the first place, the avoidance of any algorithm that is biased. In addition, all sources of error must be susceptible to being monitored, and individually tuned. This implies caution in the use of any non-stochastic algorithm that may have unkown sources of error.

Another problem is that of critical slowing down. As discussed in chapter 4, as the lattice approaches a phase transition, or if the quark mass drops towards zero (in fact, any change that takes a correlation length to infinity) the time taken to reach an independent configuration increases. This is a reflection of the increasing length of time required to 'decorrelate' a given configuration.

7.13 Recent Improvements

Various schemes have been proposed recently to enable the simulation of progressively larger lattices, with smaller quark masses. Some of the recent ideas that are receiving attention are described below.

7.13.1 Percolation and Single Cluster Constructions

One proposal by Swendsen and Wang [194] based on percolation theory has recently been generalised by Wolff, in order that it may be applied to more complex systems, such as the x-y model and the $O(3)$ σ model. (The original proposal worked only for the Potts model.)

Wolff's generalisation, the Single Cluster construction, produces significantly lower autocorrelation times near the critical point of the Ising model, where the normal Metropolis

algorithms suffer from the problems of critical slowing down. Both of these models do not appear to suffer from the problems of critical slowing down.

In the single cluster construction, one forms bonds between spins $s(x)$ with a certain probability, $P[s(x), s(x+\mu)] = 1 - e^{-2\beta}$. The lattice is then composed of a set of clusters of spins, with the size of the cluster going inversely with the temperature. One can also include a parameter that regulates the strength of the correlation between site variables within the cluster. In the usual version of the construction, all of the spins in a cluster are aligned [215]. In the study of the Ising model, little volume dependence was found near the critical point for large volumes.

The interpretation of this is that the scale of the equilibrium physics and the typical size of the cluster are closely related. This is just what is required to eliminate the critical slowing down near a phase transition, in which the correlation length goes to infinity — the size of each update step must also increase without bounds.

This construction cannot be applied to lattice QCD in a trivial fashion. In the gauge sector, the 'sites' between which the bonds must be constructed are the links themselves. Hence the bonds are within the elementary plaquettes, placing restrictions on the gauge freedom at each site (corner of the plaquette). Furthermore, one can have a site such that the links emanating from it belong to different clusters; one must then choose the gauge according to one of the clusters [215].

7.13.2 Self-Avoiding Walks

It is possible that the use of a self-avoiding random walk, in place of the Langevin random walk, will improve that hybrid Monte Carlo algorithm [53]. These have been investigated on square lattices, and may lead to improved algorithms for lattice QCD.

7.13.3 Higher Order Monte Carlo Algorithms

In a recent proposal by Creutz and Gocksch [71], one generates a higher order leapfrog integration routine, allowing one to reach any desired level of accuracy. In this, one moves forward by i steps of size δ, and then back by one step of size less than $i\delta$. The sequence can be repeated until the desired level of accuracy is reached.

7.13.4 Fourier Acceleration

This technique [76] is intended to circumvent the problems associated with critical slowing down. It utilises the fact that the various momentum modes develop at different rates in the algorithms; thus an increase in overall speed will occur if one can iterate the slow-moving momenta more frequently than the fast moving momenta.

Thus one performs a Fourier Transform in momentum space, separating the high and low momentum states and then interating the low momentum states more frequently, in pure QCD, and the high momentum states more frequently in the presence of quarks (the presence of the inverse of the quark mass in the critical length leads to a reversal of the roles of high and low momenta with respect to the pure gauge case).

This can be done because it makes no difference to observables that are functions of the configuration whether we use the canonical action, as used earlier, or another function of the momentum in the extended action. Since the low (high) momenta usually correspond to

the long (short) wavelengths, weight the designated momenta accordingly. These are then Fourier transformed back into momenta for the simulation of the extended action.

7.13.5 Multigrid Techniques

Another proposal that has been put forward is to extend the lattice into another dimension, by setting up a so-called multigrid [124,153]. The intention is to replace a lattice theory near a phase transition with one far from the phase transition; it is, in essence, application of the ideas of the renormalisation group to move in a controlled manner away from the phase transition, such that the essential physics remains unchanged. In this way the problems one has with critical slowing down near a phase transition will be greatly reduced. The prediction is that the time will go as L^2 rather than as ξ^2, ξ being the correlation length.

One begins with the base lattice, Λ_N, with lattice spacing a_N. Above this successive layers of lattices $\Lambda_0, \cdots, \Lambda_{N-1}$ are added to the base, creating a 5-dimensional multigrid $\Lambda = \Lambda_0 + \cdots + \Lambda_N$. The successive layers in the multigrid have a decreasing spacing and a correspondingly increasing number of lattice sites. The lattice spacing on the ith layer is given by $a_i = L^{N-i} a_N$ with $l = 2, 3$ or 4.

In a study done for the ϕ^4 theory on a multigrid $\Lambda = \Lambda_0 + \Lambda_1 + \Lambda_2$, with the sublattices having 1, 4^4 and 12^4 respectively, it was found that the auto-correlation time was 9 times less than for the standard '1-grid' lattice using the Metropolis algorithm. Since the processing time per sweep was approximately twice as large, this results in a significant net gain. Furthermore, since the time required does not depend on the correlation length, and hence on the size of the lattice, in the manner in which the Metropolis algorithm does, the gains are expected to improve with increasing lattice size.

7.13.6 Preconditioning the Fermion Matrix

This is another area receiving much attention at the moment. The aim is to construct another matrix $\tilde{M} \approx M$, with the property that it is easy to invert $\tilde{M}$ and $\frac{M}{\tilde{M}} \approx \mathbb{1}$.

One then solves the equation $\frac{M}{\tilde{M}} Y' = \frac{1}{\tilde{M}} Y$ rather than $MY' = Y$, which will take considerably fewer conjugate-gradient iterations if the ratio $\frac{M}{\tilde{M}}$ is close to the unit matrix.

This technique has been found to work well for the Wilson fermion, in which the diagonal elements are large compared to the off-diagonal elements. One uses the incomplete Cholesky decomposition, in which the matrix M is split into upper and lower triangular matrices, L and U respectively, with $LU \approx M$. The usual choice for L is to take directly the elements of M below the diagonal, and then choose the diagonal elements such that the product LU gives the correct diagonal elements.

For the Kogut-Susskind fermions, the diagonal elements are $2m$, whilst the off-diagonal elements are $SU(3)$ matrices, and hence have a much larger magnitude for any choice of m sufficiently close to the true quark mass! There have been attempts at finding a method to precondition the Kogut-Susskind matrix [156], but so far all attempts have found that the saving gained in the conjugate-gradient algorithm is offset by the added number of steps in the algorithm.

7.13.7 Lattice Copying

This approach to getting 'something for nothing' on the lattice has been around from almost the time lattice QCD began simulations on computer. One generates a large gauge configuration by generating a smaller one and copying the small one onto a larger lattice until one has reached the requisite size. For example, a configuration will be generated on a lattice of size $11^3 \times 24$ and repeated in the time direction to give a final configuration of size $11^3 \times 48$. Note that one only repeats the gauge degrees of freedom, not the fermionic.

However, it has been shown [85] that this technique introduces systematic errors in the propagators on the lattice. This distortion was analized in the continuum Schwinger model in a finite volume, which was further subdivided into sub-boxes, the number (N) of which was a perfect square.

The fermionic fields then had anti-periodic boundary conditions over the large box, whilst the gauge fields were periodic, and were repeated over each small box.

The Schwinger model, in the infinite volume limit, leads to a fermion–anti-fermion bound state of mass e^2/π. In this calculation, no mass was generated for modes sans the periodicity of the small sub-lattices, whilst for modes with that periodicity a mass Ne^2/π was generated.

Repeating the study on a lattice, the Fourier transform of the propagator should have a pole, a function of the hopping parameter and the mass of the fermion. In the case of the copied lattice, it was found that the Fourier transform is a sum of poles, a function of the hopping parameter only, and not of the mass!

Thus it must be born in mind that this technique, whilst of value in estimating the effect increasing the volume has on the lattice results, does introduce errors itself. Propagators calculated using this method are not completely trustworthy.

Chapter 8

The Quenched Approximation

In the quenched approximation, one reduces the computation time required by setting the fermion determinant to 1 in eqn. 5.153. This implies a theory with no quark dynamics, since the background, or sea quarks, do not exist (since the number of fermions in the theory (n_f) is set to 0). Thus this is also known as the Valence approximation, in that quark loops are excluded from the calculation. Note that one still places quark sources, in the form of delta functions, on the lattice.

This is a drastic approximation, hence one should not expect physically accurate results from the calculations done in the quenched approximation. Some of the reasons for using it, however, are listed below.

- It is of benefit to isolate the effects of the sea quarks, in order to understand the role played by them. Furthermore, it is hoped that many of the quantities in QCD will be relatively unaffected by the sea quarks. Once it is understood what effect this approximations has, it is possible that one will be able to correct the quenched calculations of various observables.

- One is able to get closer to the asymptotic and finite size scaling limits than with dynamical quarks.

- One is able to get sufficiently high statistics to determine some of the systematic errors, knowledge that will be of use in the simulations involving dynamical quarks.

- The quenched approximation provides a useful tool for the development of algorithms.

The quenched calculations have been in progress for close on a decade now. It has proven to be orders of magnitude more time consuming to obtain accurate results than was first anticipated. The lattices in current use are still too coarse, ie. not in the asymptotic scaling limit; and too small, ie. not in the finite size scaling limit. None of the calculations to date have yielded a definitive answer; all merely present the 'next datum', and hope that the next generation of computers will provide a more definitive result.

That the lattices are too coarse has been shown by the fact that the lattice β-function does not yet have asymptotic behaviour (see section 4). The coupling constants used on the lattice, $\beta = \frac{2N}{g^2} = \frac{6}{g^2}$, have all been far too small (ie., g^2 too large) to be in the asymptotic scaling limit. Studies of the renormalisation group [42] have shown that, using the standard Wilson action, one will need couplings $\beta > 7.0$ to reach the asymptotic scaling limit. Most

of the simulations to date have been in the region of $\beta \approx 6.3$ or less. Note that significant improvements can be obtained by using a renormalisation-group improved action [127], in which one is closer to the continuum limit on a relatively coarser lattice. (One can determine how close one is to the continuum limit by whether or not chiral symmetry (for Wilson fermions) or flavour symmetry (for Kogut-Susskind fermions) has been restored.) Thus the calculations given below that had values of β below 7 will have errors from the use of a lattice away from the continuum limit.

The largest lattices used to date have all been less than 2fm in size, with many not much more than 1fm [150]. Now the root mean square charge radius (from the charge form factor, [14]) is 0.8fm. At low q^2 the charge has an exponential form in configuration space, with 67% of the total charge within the rms radius, and 99% within $2.4r_{\rm rms}$. Thus, in order to include 99% of the charge of the proton the lattice must have a linear dimension of at least 4fm. One can take this as a lower bound on the size required to contain the wavefunction of the proton without distortions at the walls of the box. As mentioned in section 6.3.1, calculations on fully soluble models have shown that one needs sizes larger than the size of the wave function in order to reduce the finite size effects to a negligible level. Hence, in the calculations below, those with lattice sizes below 2fm certainly have errors associated with the finite size of the lattice; in general, one expects the mass of the hadrons to increase, due to the energy associated with the particle being 'squeezed' by the lattice. Furthermore, there may well be mixing from excited states in the calculations of the masses, which will also increase the effective mass of the particles. Thus the smaller the lattice the larger the fluctuations, and the less reliable the results.

Thus the trade-off with Lattice QCD is choosing a coupling such that the lattice is large enough, yet is also as close as possible to the continuum.

Furthermore, in all of the calculations the quark masses used are at least an order of magnitude larger than the physical values. This is, in part, compensated for with the up and down quark by doing an extrapolation to zero quark mass. However, this factor does move the results away from the physical limit, a fact that is most clearly seen in the Edinburgh plots. (The Edinburgh plots were introduced by the Edinburgh group [46]. One plots the ratio of nucleon to rho mass against the ratio of the pion to rho mass, yielding a transparent comparison between the lattice results and the experimental results.)

The quenched approximation may introduce a further error; there has been some evidence that large fluctuations in the value of the fermion eigenvalues are allowed with the Wilson fermion formulation in this approximation, due to the absence of the damping factor from the fermion determinant. These lead to exceptional configurations [43] being generated more often than the continuum weighting allows, leading to deviations in the masses and propagators of the hadrons. This problem does not occur in the Kogut-Susskind formulation, since there is no r-term linking the fermions and the background gauge field.

One may construct the hadron operators in two ways. The first, described earlier, is to place the quark sources on the same site, yielding local operators. The second method involves placing the sources on adjacent sites. In this case, one needs to include the links between the quarks in the hadron operator. Despite the difficulties involved, the latter method has recently become the method of choice, since it couples less strongly to the excited states of the baryon. This means that the propagator measured on the lattice is closer to that for a pure ground state, at a given distance from the source, for non-local operators than it is for local operators.

In the remainder of the chapter, results for the hadronic spectrum obtained by various

groups are discussed. The details of each group are presented first, in no specific order.

Loft and DeGrand, 1989 [150] A lattice of size $11^3 \times 20$ was used, which yields 1.1fm for the spatial size of the lattice. 20 gauge configurations were calculated, using a heat bath algorithm [135] with anti-periodic boundary conditions. 1000 sweeps were allowed for initial thermalization, and gauge configurations were sampled at intervals of 1000 sweeps. This is a generous allowance, and should yield independent configurations[1].

This simulation used Wilson fermions, both light, for the first family, and heavy for the second family. Anti-periodic spatial boundary conditions and open (Dirichlet[2]) temporal boundary conditions (ie., the Green functions were maintained at 0) were used. The hopping parameters were $\kappa = 0.150, 0.152, 0.153$ for the light quarks, and $\kappa = 0.145, 0.130$ for the heavy quarks, with the relationship between the hopping parameter and the quark mass given by eqn. 5.141. The critical hopping parameter, found by extrapolating from the values of the hopping parameters used to the value of the hopping parameter at which the pion mass was zero, was found to be $\kappa_c = 0.1566(3)$.

The quark sources were delta-functions in space and time, sited at the centre of the lattice in space, and at $t = 4$. The propagators were then fitted out to $t = 16$. The use of local operators for the propagators means that there will be some mixing between the ground and lowest excited states for each particle.

The errors were calculated using binning. Four bins, with 5 configurations in each were set up. The masses of each hadron were calculated for each bin, and the average of these used for the final quoted mass. The quoted error is just the spread in masses over the four bins.

The fitting of the exponential curve to the propagator was only done in the section of time in which the propagator had an asymptotic form; this was $t \geq 7$ sites from the source for the mesons, and $9 < t < 13$ for the baryons.

A further source of error in this calculation is the fact that the same gauge configuration was used for each value of the quark mass. Hence the results for the different masses are correlated. No correction was made for this, and the results were assumed to be independent in the calculations.

Gupta, et al. 1987 [109] Results were calculated on a lattice of size $18^3 \times 42$ with coupling $\beta = 6.2$ using both Wilson (with $r = \frac{1}{2}$) and Kogut-Susskind fermions. With $a^{-1} = 2.5$GeV (using the rho mass as input) the spatial size of the lattice was 1.4fm. This choice was deliberate, in that the calculation was aimed at extracting information as close to the continuum limit as possible, rather than pushing for the infinite volume limit.

As an indication of the variability of the lattice spacing, a result of $a^{-1} = 2.0(5)$GeV is obtained if one uses the slope of the pseudoscalar and vector meson mass fits, as in eqn. 8.2, 1.9(1) using the nucleon to fit, and 2.1(2) using the Δ.

An optimised Metropolis algorithm was used, with 20 hits per sweep and 250 sweeps between samples. 3550 and 2500 sweeps for the Wilson and Kogut-Susskind fermions

[1] Note that correlations have been found between configurations that were only seperated by 100 sweeps.

[2] It has been found that the best fits for the hadron masses are obtained when one uses Dirichlet boundary conditions in time [46,31]. It also facilitates extending the simulation in time when necessary.

respectively were allowed to reach thermalization after a cold start. Similarly, the number of samples taken was 23 and 36. Periodic and anti-periodic boundary conditions respectively were used in all four directions. The conjugate-gradient algorithm was used to find the fermion determinant, with sufficient accuracy to insure that statistical errors dominated in the meson propagators.

For the staggered fermions, both local and non-local operators were used, with the sources placed at $t = 0$ and 1, and centred in space. This paper also provides a good introduction to the use of non-local operators on the lattice. The following quark masses were used: $m_q = 0.03, 0.025, 0.02, 0.175, 0.15, 0.0125, 0.01, 0.0075, 0.005$. Thus these ranged from 75 down to 12.5 MeV.

The hopping parameters used for the Wilson fermions were $\kappa = 0.30, 0.31, 0.32, 0.325$. The critical value was $\kappa_c = 0.3327(8)$, corresponding to quark masses from 330 to 77 MeV.

Excited states were included in the fitting procedure for the lightest mesons, where necessary.

The errors were calculated using the jacknife method (see section 7.11.2). These were then checked using binning, the results of which indicated that the configurations used were independent of each other.

The propagators were fitted to the signals in which the mass calculated was stable. The end-point was determined by eye, and was the point at which the signal was comparable to noise. The starting time was found by taking the closest time to the source that was still consistent with stable values for the mass. This was usually around $t = 8$.

Iwasaki and Yoshié, 1989 [125,127] Results were calculated on a lattices of size $16^3 \times 48$ with coupling $\beta = 2.4$, using a renormalisation group improved action, and $\beta = 5.85$ using the standard Wilson action (The latter to investigate discrepancies between the results of the rg improved action and those of the standard Wilson action). At these values of the coupling the same lattice spacing was obtained in both cases. Wilson fermions were used. With $a^{-1} = 1.81$ and 1.85GeV for the respective actions, (using the rho mass as input) the spatial sizes of the lattices were 1.77 and 1.73fm.

The renormalisation group action involved both the simple plaquette of the Wilson action, and a term involving a 1×2 loop. The form of this was determined in a study [126] using the blocking technique described in section 4. The action used was (cf eqn. 3.6)

$$S_G = \frac{1}{g^2}\left(c_0 \sum \text{Tr(elementary plaquette)} + c_1 \sum \text{Tr(1 x 2 loops)}\right) \tag{8.1}$$

with $c_1 = -0.331$ and $c_0 = 1 - 8c_1$.

15 gauge configurations were generated using the heat-bath algorithm, with 100 sweeps between samples, and 1000 sweeps used for the initial thermalization. Periodic boundary conditions were used for both the gluons and Wilson fermions. Local operators were used, with the quark sources placed at $t = 0$.

For the renormalisastion group improved action the hopping parameters used were $\kappa = 0.14, 0.145, 0.15, 0.1525, 0.154$, with the continuum hopping parameter being $\kappa_c =$

0.1569(2). Thus the quark masses ranged from 680 to 100 MeV. For the standard Wilson action (see eqn. 3.6), the following values, chosen to reproduce the physics of the corresponding values for the improved action, were used: $\kappa = 0.144, 0.149, 0.154, 0.157, 0.1585$.

No finite size effects for the mesons were observed when these results in the appropriate time slot were compared to those on lattices of size $12^3 \times 24, 16^3 \times 32, 16^3 \times 48$. This absence is interpreted as being due to the noise swamping the data close to the boundaries. Had the simulation been done with many more sweeps, the noise factor would have dropped and finite size effects would have been noticed.

In the baryon sector, the results were masked by noise for $t \geq 20$ at $K = 0.1525$, and for $t \geq 19$ at $K = 0.1540$. The fits to the masses showed that the contribution from excited states was small for $T = 48$, but not so for $T = 32$.

Using both the ground and excited states, the propagators were well fitted from the quark source. Using only the ground state, it was found that data out to $t = 24$ was needed to insure a fit that did not deviate from the 2-state fit. Using just the one-mass fit, good results were obtained using points from $t = 11$ to 37, with the fit being stable in the range $8 - 11 \leq t \leq 37 - 40$. The two-mass fits were stable in the range $4 - 5 \leq t \leq 43 - 44$. Note that, since periodic boundary conditions are used, only the points up to $t = 24$ are independent; those beyond that are a reflection of those below.

Extrapolating the pion mass to zero gave a value for the critical hopping parameter of $K_c = 0.1569(2)$. This is indistinguishable, within the errors, from the value of the physical hopping parameter at which the pion takes the experimental value for the mass.

Bowler et al. [43,45,41] In a series of calculations, results were calculated on a lattice of size $16^3 \times 24$ with coupling $\beta = 6.00, 6.15$ and 6.30 using Kogut-Susskind fermions. The lattice spacing, found using the renormalisation group equation at two-loop level (see section 4) and a value for the lattice cutoff of $\Lambda = 4.2$ MeV, was $a^{-1} = 1790, 2120, 2530$ MeV, yielding the spatial sizes of 1.8, 1.5 and 1.2 fm at the corresponding couplings. For $\beta = 6.30$ the gauge configurations were calculated on a 16^4 lattice, and extended in the time direction. (Note that, as mentioned in section 7.13.7, this technique introduces distortions in the propagators.)

A peudo-heat bath algorithm was used, with 32 gauge configurations generated. For $\beta = 6.00$ and 6.30, the first 1500 configurations were discarded, with the sample seperation being 224 sweeps. At $\beta = 6.15$, 32 configurations with periodic boundary conditions, and 24 with anti-periodic, were generated. The seperation between samples was 176 sweeps. Local operators were used, with the sources placed at $t = 5$. With the exception of the lightest pseudo-scalar, excitations were not included in the propagator fits. However, the points close to the source were omitted.

Errors were calculated by binning into 4 bins with 8 consecutive configurations. Both periodic and anti-periodic boundary conditions were used. The propagators for each were indistinguishable in the meson sector.

Quark masses $am_q = 0.5, 0.16, 0.09, 0.04, 0.01, 0.005, 0.003, 0.001$ were used; the three lightest were only used for 4 samples, and had fluctations sufficiently large that they were only of use for the pseudoscalar channel.

The calculations done at $\beta = 6.0$ showed signs of continuum behaviour, in terms of flavour symmetry restoration.For $\beta = 6.3$ finite size effects were considerable. There is then only a small region, around $\beta = 6.15$, in which one can simulate continuum physics with any hope of getting meaningful results. (At this coupling, finite size effects were not noticeable, in contradiction with the later findings of Iwasaki [127].)

In the meson sector, the signals close to the source were ignored, as were those that were indistinguishable from noise due to the distance form the source. For the low-mass mesons, the fit included the lowest excited state.

Gottlieb et al. [99] Results were calculated on a lattice of size $6^2 \times 12 \times 18$ with coupling $\beta = 5.7$ using Wilson fermions.

The Metropolis algorithm was used, with 1000 thermalization sweeps. Samples (20 in total) were taken at intervals of 500 sweeps. The hopping parameters used were $\kappa = 0.325, 0.340, 0.355$, with $\kappa_c = 0.388$. The hadronic masses were determined by fitting two of the hadron masses to experiment, and calculating the rest using the ratios.

The statistical errors in the quark masses were calculated using the jacknife method. Note that, due to the small number of points taken, and the small coupling constant (ie., large lattice spacing) this lattice is far from being near either the continuum or infinite volume limits.

APE collab., Bacilieri et al. [23] Results were calculated on a lattice of size $12^3 \times 24$ with coupling $\beta = 5.7$ and $18^3 \times 24$ with coupling $\beta = 6.0$ using Wilson fermions. With $a^{-1} = 1.44(5), 2.30(8)$ GeV at the corresponding couplings (from the rho mass) the spatial size of the lattices are 1.6 and 1.5fm.

At $\beta = 6.0$, the Metropolis algorithm was used, with 1500 sweeps to thermalize from a cold start, followed by the overrelaxed algorithm to generate the remaining configurations. Samples were taken at intervals of 300 sweeps.

The hopping parameters used at $\beta = 5.7$ were $\kappa = 0.161, 0.163, 0.165, 0.167$ with $\kappa_c = 0.169$, and $\kappa = 0.152, 0.153, 0.154, 0.155$ with $\kappa_c = 0.156$ at $\beta = 6.0$.

De Forcrand et al. [77] Results calculated on a $24^3 \times 48$ lattice, using the $\sqrt{3}$ blocking transformation twice (see section 4). This leaves a lattice of size $8^3 \times 16$ for the fermionic action. The resultant Wilson fermion action, after the blocking transformation, included both nearest neighbour and 3-space diagonal terms.

51 configurations were used, at $\beta = 6.3$, with both periodic and anti-periodic boundary conditions. The fluctuations in propagators are anti-correlated in the two different boundary conditions; a linear combination of both was used here to reduce the finite size effects.

The calculation was done at $\kappa = 0.1345, 0.1351, 0.1355, 0.1358, 0.1360, 0.1362$. The lattice spacing was found to be $a^{-1} = 4.0(3)$ GeV, using the rho mass to fit to, leading to a size of 1.2 fm.

The propagators were fitted in the range $t = 15 - 24$, using single-mass fits. Errors were calculated using the jacknife method.

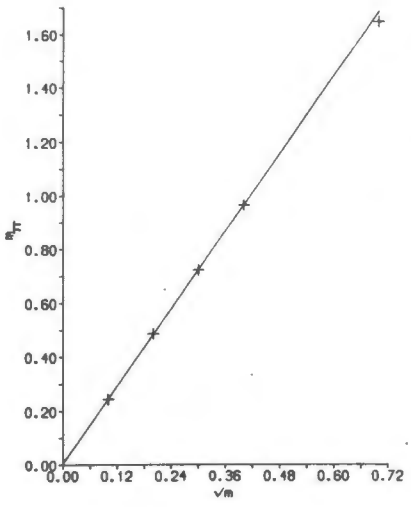

Figure 8.1: m_π vs m_q. ex.[43]

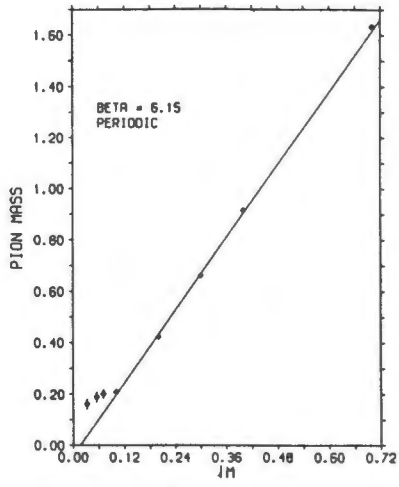

Figure 8.2: m_π vs m_q, with the line fitted to $0.01 \leq m_q \leq 0.16$. ex.[41]

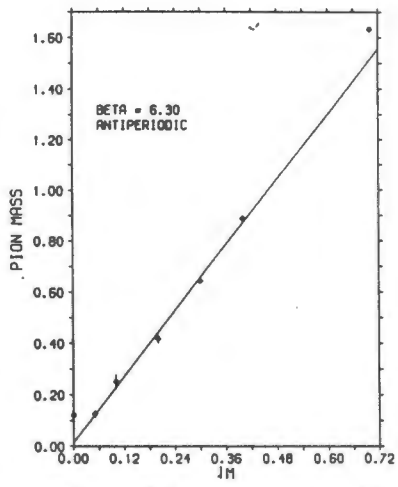

Figure 8.3: m_π vs m_q, with the line fitted to $0.01 \leq m_q \leq 0.16$. ex.[41]

8.1 Pion

Since the pion is a pseudo-Goldstone boson (see appendix B), the mass is proportional to the root of the quark mass. Thus one usually attempts to fit the pion mass to a curve of the form $a^2 m_\pi^2 = A_1^\pi m_q$, or $am_\pi = B_1^\pi \sqrt{m_q} + B_0^\pi$. One can also fit to a quadratic, $a^2 m_\pi^2 = C_\pi^2 m_q^2 + C_\pi^1 m_q + C_\pi^0$.

Bowler et al., (at $\beta = 6.0$) [43] using a fit including the excited state of the pion, found that the PS pion (see eqn. 6.24 for the notation), could be parametrised by the curve $am_\pi = 2.40(4)\sqrt{m_q}$, as in fig. 8.1. The Goldstone pion is associated with the PS channel and the pion in the scalar channel is expected to become degenerate with the Goldstone pion in the continuum limit; this gives a good test of the restoration of flavour symmetry. For low values of the quark mass, the two channels were in agreement, with the SC channel slightly above the PS.

With the pion constrained to a finite volume, the mass of the pion cannot become identically zero, even with $m_q = 0$, due to the Heisenberg uncertainty principle. Thus the deviation, as the quark mass decreases, of the pion mass data points from a linear fit in fig. 8.1 yields a good indication of the finite size effects.

At $\beta = 6.15$, [41] no difference was found between the meson propagators for the anti-periodic and periodic boundary conditions, with $m_q > 0.01$. For $m_q = 0.01$, there was a difference, indicating that finite size effects were playing a role. Below this, only periodic boundary conditions were used, since these are expected to yield results less affected by finite size effects.

Using a fit including the excited state, the pion mass points shown in fig. 8.2 were obtained. The points in the range $0.01 \leq m_q < 0.16$ are well behaved, fitting the line $m_\pi = 2.35(2)\sqrt{m_q} - 0.039(4)$. For the lower mass points, the deviation from the linear graph is indicative of the onset of finite size effects. Analysis of the propagator showed oscillations near the boundary in time. This may be due to the Dirichlet boundary condition, since these create, in effect, a source just outside the far-time edge of the lattice. It may, perhaps, be

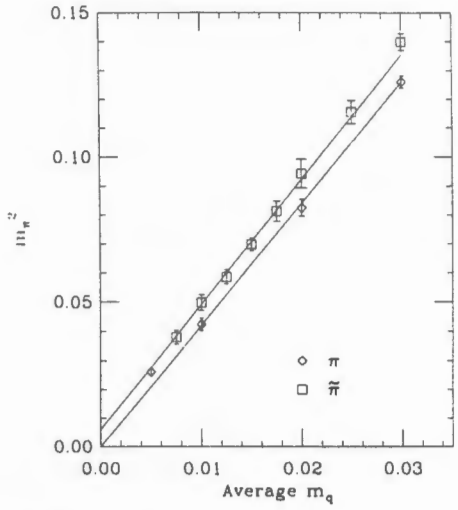

Figure 8.4: Pion mass, for both the PS (π) and SC ($\tilde{\pi}$), using Kogut-Susskind fermions. ex.[109]

unwise to impose Dirichlet boundary conditions in time with small masses.

Flavour symmetry is restored, in part, at this coupling, as shown by the proximity of the pion masses in the SC and PS channels. The former was well fitted by the curve $m_\pi = 2.42(11)\sqrt{m_q} + 0.025(34)$

The data at $\beta = 6.30$ [41] were calculated before the advantages of periodic boundary conditions was known, so used anti-periodic. The results, using a fit that included the lowest excited state, are presented in fig. 8.3. Note that the data for $m_q < 0.01$ is not fitted; these were significantly affected by the finite size effects. This is only to be expected, since the lattice is yet smaller than that at $\beta = 6.15$. The points are fitted by the line $m_\pi = 2.14(7)\sqrt{m_q} + 0.015(32)$. The SC channel is in agreement with the PS channel.

The results obtained by Iwasaki [125], using his renormalisation group improved action, can be seen in fig. 8.5. Note that the mass plots are curved, albeit by very little, with the pion data curving down and the rho data curving up. The data for the 'check' with the standard Wilson action showed no difference in the results for the pion between the two actions.

Gupta et al. [109] found, using Kogut-Susskind fermions, Goldstone behaviour for the pion, for $m_q > 0.005$. Below that, finite size effects crept in, pushing the mass of the pion above the linear mass fit. The mass of the SC pion was nigh on degenerate with it, indicating the proximity of the continuum limit via the restoration of flavour symmetry. The results can be seen in figs. 8.4. The best fit curve to the pion data is $m_\pi^2 = 4.20(15)m_q$.

The results obtained using Wilson fermions can be seen in fig. 8.13. These are consistent with those obtained for Kogut-Susskind fermions.

Loft and DeGrand [150] found the data points, and fitted the curves, as shown in fig. 8.7. The linear fit to the pion yielded $a^2m_\pi^2 = 2.47(24)m_q$, whilst the quadratic fit yielded $a^2m_\pi^2 = 1.343(8)m_q^2 + 2.202(10)m_q + 0.014(42)$.

In this case, the fits yielded the same critical hopping parameter, to within the errors. These were 0.1566(3) and 0.1570(10) for the linear and quadratic fits respectively.

Note that the convexity of the data agrees with that found by Iwasaki, shown in fig. 8.5.

The results of De Forcrand et al. using the blocking transformation improved action are

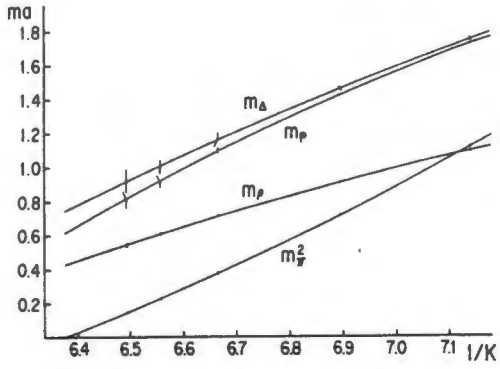

Figure 8.5: Hadron masses ex. [125]

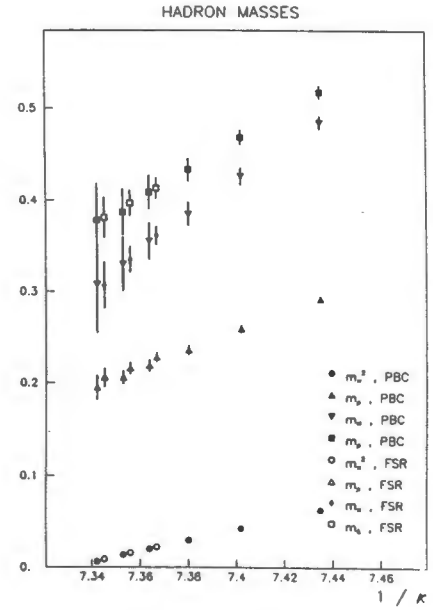

Figure 8.6: Hadron masses vs. $\frac{1}{\kappa}$. FSR represents the results calculated using a linear combination of the propagators on periodic and anti-periodic lattices. ex. [77]

shown in fig. 8.6. Note that the error bars on the pion mass are smaller than the symbol size used, and the fact that m_π^2 is a straight line.

8.2 Rho

The rho meson has a less well-behaved propagator than the pion (compare the pion and rho masses in figure 8.8), and the estimates of the mass suffer from larger errors. In simulations in which the rho is not used to fix the lattice spacing, the mass comes out low. Equivalently, when the rho mass is used to fix the lattice spacing, other masses are high, especially when compared to the same result calculated using, for example, the string tension.

Again with the rho, linear and quadratic fits are used, since there is no precise prediction as to which is correct. The fits used are: $am_\rho = A_1^\rho m_q + A_0^\rho$ and $am_\rho = C_2^\rho m_q^2 + C_1^\rho m_q + C_0^\rho$. Note that the intercept, or zero term, gives the mass of the rho in the physical (zero quark mass) limit.

One can use these fits to the masses to determine the lattice spacing. The assumption is that the slope of the fit, at the critical hopping parameter , is less prone to error than the mass of the particle [154]. The strange companion to the pion is the K meson, and the strange companion to the rho is the K*. Thus, to a linear approximation, at zero quark mass one gets $am_{K^*} = C_1^\rho m_s + am_\rho$ and $a^2 m_K^2 = C_1^\pi m_s + am_\rho^2$, with m_s the mass of the strange quark. From this one gets

$$a^{-1} = \frac{C_1^\rho}{C_1^\pi}\left(\frac{m_K^2 - m_\pi^2}{m_{K^*} - m_\rho}\right) \tag{8.2}$$

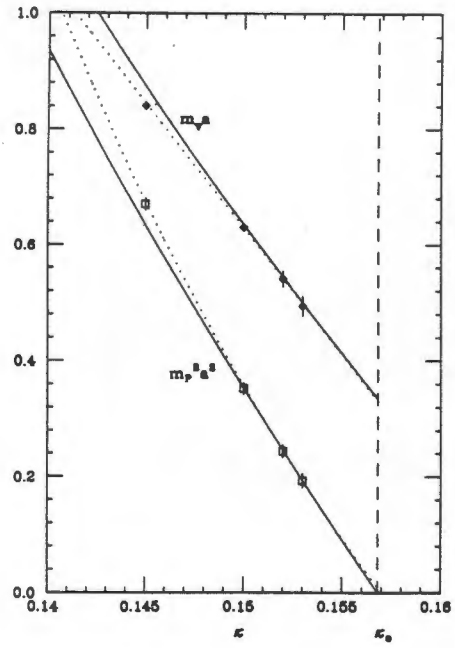

Figure 8.7: Pseudo-scalar and vector meson masses as a function of quark mass, with both linear (solid line) and quadratic (dotted line) fits. ex. [150]

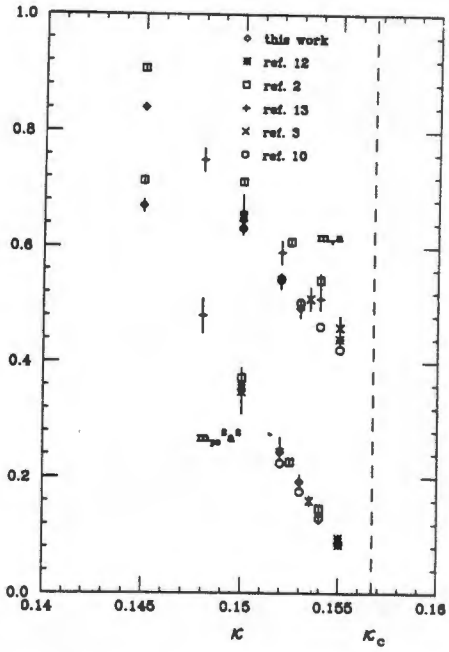

Figure 8.8: A comparison of the results of several groups, ex.[150], on comparable lattices at $\beta = 6.0$. Note how good the agreement in the pion channel is. Refs. as in [150].

The results found by Loft and DeGrand are presented in fig. 8.7. The two fits yielded

$$\begin{aligned} am_\rho &= 2.08(23)m_q + 0.338(30) \\ am_\rho &= -0.748(76)m_q^2 + 2.176(116)m_q + 0.330(96) \end{aligned} \tag{8.3}$$

Note that both fits agree on the mass, in the physical limit. (A fit of m_ρ^2 to a linear function of the quark mass was found to be far from optimal in [150].) Using the lattice spacing from the wave function, this yields a rho mass of 650 MeV, the same as was obtained by Bowler et al. at this coupling. It is, however, clearly well below the experimental result, as with most lattice rho masses.

As an example, the lattice spacing can be calculated using the slopes and eqn. 8.2. Inserting the experimental values for the masses of the respective particles, and the best-fit values for the slopes ($C_1^\rho = 2.176$ and $C_1^\pi = 2.202$), the value for the inverse lattice spacing is 1820MeV[3].

The following results were obtained by the APE collaboration (Bacilieri et al., [23]) for the fits to the rho mass:

$\beta = 5.7$;	6.0
$m_\rho^2 = 1.4(1.1)m_q^2 + 1.96(28)m_q + 0.285(18)$	$3.5(6)m_q^2 + 1.29(13)m_q + 0.112(8)$
$m_\rho = -2.7(17)m_q^2 + 3.6(4)m_q + 0.285(18)$	$-1.4(1.3)m_q^2 + 3.5(3)m_q + 0.49(2)$

(8.4)

In this case there is good agreement between the two fits at 5.7, but very bad agreement at the weaker coupling.

Gupta et al. [109] found, using Kogut-Susskind fermions, that the two types of rho were degenerate (excluding the signals at low quark mass, since these were regarded to be too noisy to fit to). The results obtained for the physical masses were:

ρ	$\tilde{\rho}$
$am_\rho = 0.31(3)$	0.32(3)
$a^2m_\rho^2 = 0.30(4)$	0.31(4)

(8.5)

Eqn. 8.2 was also used to determine the lattice spacing; this yielded $a^{-1} = 2.0(5)$GeV.

For Wilson fermions, the results were $am_\rho = 0.313(11)$ and $a^2m_\rho^2 = 0.272(17)$. Again, both fits are within the errors of each other.

Iwasaki et al., using their renormalisation group improved action [125], found $am_\rho = 0.426(15)$; since the physical mass was used as input to determine the lattice spacing, knowledge about the accuracy of this result can only be gleaned from the spectrum in general, and the fit to the different hopping parameters (see fig. 8.5). The baryons were within 10–15% of the experimental mass using their 'modest' fit, and almost spot on using a fit corrected according to phenomenological mass formulae. One can thus conclude that this is one of the more accurate lattice calculations. The mass using the Wilson action was nigh on identical to this.

Bowler et al. found that the ρ and $\tilde{\rho}$ were close to degenerate (see fig. 8.9) at $\beta = 6.0$; flavour symmetry was thus restored to within 7%. This was even better at the higher values of the coupling, indicating that these are closer to the continuum limit. This yields, for the mass, a value of 650(65) MeV [45].

[3]The value calculated by Loft and DeGrand was 1830MeV; the difference is small, and may be due to either error on their part, or to some optimising not mentioned in their article.

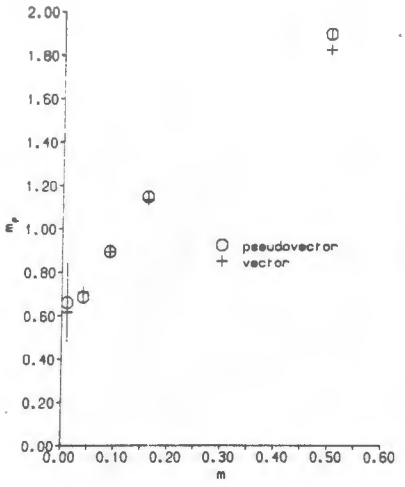

Figure 8.9: m_ρ vs m_q at $\beta = 6.0$.ex.[43]

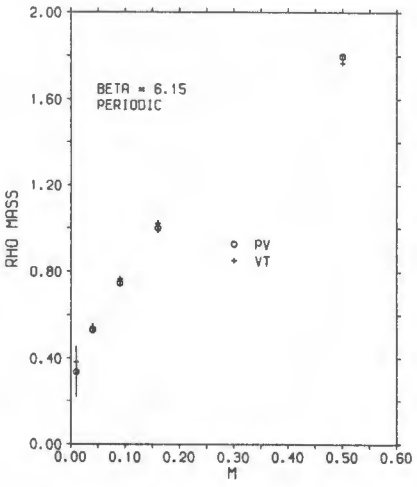

Figure 8.10: m_ρ vs m_q. ex.[41]

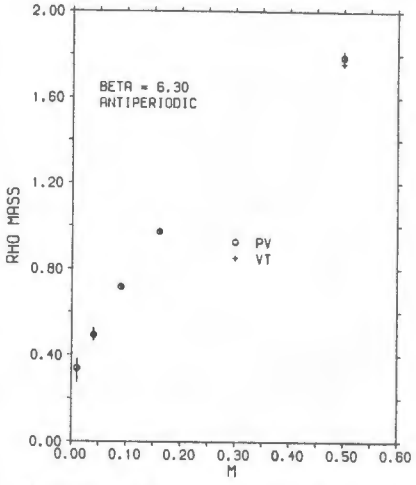

Figure 8.11: m_ρ vs m_q. ex.[41]

At $\beta = 6.15$, with both periodic and anti-periodic boundary conditions, it was possible to determine the finite size effects by a comparison of the two; there was negligible difference, implying minimal finite size effects. The mass was determined to be 650(65) MeV [45]; see fig. 8.10.

However, the results at $\beta = 6.30$ (fig. 8.11) were not good. The pion and the rho, using a fit that included the excited state, were degenerate, indicating that on a small lattice the different $q\bar{q}$ pairs were indistinguishable.

One can set up an effective coupling constant, α_{QCD}, that describes the long-range physics of mesons [167]. If one plots this against the rho mass, for both the experimental and the lattice results [150], one gets a straight line with negative slope; however, in absolute magnitude the lattice line is a factor of 3 lower than the physical line. Hence it is clear that the lattice does not reproduce the long-range physics of the meson sector very well, perhaps particularly the rho.

8.3 a & b Mesons

The a_1 and b_1 mesons are not well fitted by the simulations, in general; in most of the earlier calculations, results were not obtained for them. Also, these mesons are only obtained without any extra effort when using Kogut-Susskind quarks.

Bowler et al.[43,41] obtained the following results, using a fit that included the excited state for $\beta = 6.0$ only.

β	a_1		b_1	
	$m_q = 0.04$	$m_q = 0.01$	$m_q = 0.04$	$m_q = 0.01$
6.0		1.18(5)	1.04(10)	0.53(11)
		(2110 MeV)	(1860 MeV)	(950 MeV)
6.15	0.586(68)	0.368(53)	0.462(68)	0.289(73)
	(1240 MeV)	(780 MeV)	(979 MeV)	(612 MeV)
6.30	0.606(23)	0.370(51)	0.442(79)	0.269(89)
	(1530 MeV)	(934 MeV)	(1120 MeV)	(679 MeV)

The results at $\beta = 6.0$ are consistently too high, indicating behaviour outside the asymptotic regime. The results at the lower quark mass are not good (the data behaves well down to $m_q = 0.04$, for all three values of the coupling). The discrepancy between a_1 and b_1 at $\beta = 6.30$ indicates that the results at this coupling are dubious — as is to be expected for a lattice this small.

Bacilieri et al., [23] found, using linear fittings to the data at a coupling of $\beta = 6.0$; $m^2_{a_1} = 2.1(1.0)m^2_\rho$ and $m^2_{b_1} = 2.8(1.5)m^2_\rho$, with the experimental results being 2.7 and 2.6 respectively. Using the experimental mass of the rho as input, this yields masses of 1120 and 1290 MeV respectively.

Gupta et al. [109] found (using Kogut-Susskind fermions) that the a_1 and b_1 mesons were fairly well behaved in the simulations, yielding masses of 1320 and 1040 MeV at $m_q = 0.01$, using $a^{-1} = 2.0$ GeV. However, the parity partner of the pion, the ϵ, was found to be approximately degenerate with the a_1 for large m_q, and nowhere near the ρ, as it should be. For small quark masses, it comes out degenerate with the pion; this is manifestly wrong, since the ϵ is not a Goldstone boson, and should remain massive in the chiral limit.

This error could be due to mixing with other states on the lattice with the same parity, or it might possibly be a lattice artifact, such that the mass would stabilise at some non-zero value on a sufficiently large and fine lattice.

Finally, using Wilson fermions it was found that the mass of the a_1 (the b_1 is not found in the Wilson simulation) was 770 MeV from the linear fit ($a^{-1} = 2.1$ GeV) or 925 MeV at ($a^{-1} = 2.5$ GeV.

8.4 Strange and Charm

Loft and DeGrand were also able to calculate the masses of hadrons containing strange and charm quarks.

The hopping parameters for the strange (κ_s) quarks was determined using the theoretical prediction for the mass of a fictitious 'pure' pseudo-scalar particle, the η_s; (κ_{ch}) was determined using the η_{ch}. This route was chosen because the data for the vector mesons was very noisy. The theoretical prediction (686 MeV) [149] needs to be used, in that the pure state does not occur in nature, only mixed states with the up and down quarks. The values obtained were $\kappa_s = 0.1539(10)$ and ($\kappa_{ch} = 0.1269(9)$).

Using these values for the heavy family, and the ones given above for the light family, the meson spectrum was calculated; the results obtained are given in table 8.1. Note that the fit to the pseudo-scalar mesons is relatively good, compared to the fit of the vector mesons. Note that, for the vector mesons the masses are consistently lower than the experimental value.

	State	$q\bar{q}$	Predicted mass (MeV)	Observed mass (MeV)
Pseudoscalars	K^+	$u\bar{s}$	533(55)	493
	$\bar{D}^0$	$u\bar{c}$	1793(60)	1869
	D_s^-	$s\bar{c}$	1929(110)	1970
Vectors	ρ^+	$u\bar{u}$-$d\bar{d}$	651(65)	770
	ϕ	$s\bar{s}$	868(114)	1019
	K^{*+}	$u\bar{s}$	761(122)	892
	D^{*0}	$u\bar{c}$	1888(76)	2010
	D_s^{*-}	$s\bar{c}$	1987(76)	
	J/ψ	$c\bar{c}$	2996(141)	3070

Table 8.1: Prediction vs. experiment for strange and charm meson masses. ex. [150]

Since this is also true for the spin $\frac{3}{2}$ baryons (see table 8.3), it appears that the masses of the spin-aligned particles is suppressed. (The anti-aligned particles are not suppressed, as can be seen by the fact that the spin $\frac{3}{2}$ baryons are slightly higher in mass than the measured value.)

These results can be compared with those obtained by Gottlieb et al. in 1986 [99], presented in table 8.4. Note that in both studies, the K prediction is above experimental, whilst the K^* is below. It must be born in mind, however, that these studies were made on a small lattice outside the region in which asymptotic scaling is hoped to occur.

8.5 Baryons

The APE collaboration [23] found the following values for the mass differences between the Δ and N* at $\beta = 6.0$: $m_\Delta^2 - m_\mathrm{p}^2 = 1.1(0.2)m_\rho^2$ and $m_{\mathrm{N}*}^2 - m_\mathrm{p}^2 = 3.5(1.0)m_\rho^2$. The experimental values are 1.1 and 2.5 respectively. The proton mass was found to be $m_\mathrm{p} = 0.49(2)$; this yields a mass of 1130 MeV using the rho to fit the lattice spacing, and 1000 MeV using the string tension. Thus $m_\Delta = 1390, 1230$ MeV and $m_{\mathrm{N}*}^2 = 1830, 1630$ MeV, with the first figure coming from the rho mass fit, and the second from the string tension. It can be seen here that results closer to the physical value are obtained using the string tension as input, rather than the rho.

The values for the spin $\frac{1}{2}$ and spin $\frac{3}{2}$ baryons, including strangeness and charm, found by Loft and DeGrand [150], are given in tables 8.2 and 8.3 respectively. It is clear that these values are, in general, no closer than the 10% level to the experimental results. Furthermore, the very important hyperfine splitting between Λ and Σ of 77 MeV is not reproduced at all; the masses are degenerate.

Another systematic error occurs for the spin $\frac{3}{2}$ baryons; whilst the lowest mass Δ is close to the physical mass, for the remaining baryons the fraction by which the lattice mass is lower than the experimental mass steadily increases as the number of strange quarks increases from 1 to 3. This could be due to the mass of the strange quark being set too low; however, increasing the mass of the strange quark would result erroneously large meson masses. The second possibility is that, for the lighter baryons, the finite size of the lattice pushes the masses up. Also, in the hyperfine splitting, the lattice appears suppresses the mass of the aligned spins, and does not affect that of the anti-aligned states. These two effects may cancel

State	qqq	Lattice mass (MeV)	Observed mass (MeV)
P	uud	1098(156)	939
Λ^0	uds	1201(161)	1115
Σ^+	uus	1201(161)	1189
Ξ^0	uss	1318(169)	1315
Λ_c^+	udc	2301(79)	2281
Σ_c^{++}	uuc	2301(79)	2450
Ξ_c^+	usc	2408(82)	2459
S^+	usc	2408(82)	
T_c^0	ssc	2528(81)	
X	ucc	3498(145)	
X_s	scc	3603(150)	

Table 8.2: Calculated spin $\frac{1}{2}$ baryon masses ex. [150]

State	qqq	Lattice mass (MeV)	Observed mass (MeV)
Δ^{++}	uuu	1213(121)	1232
Σ^{*+}	uus	1300(122)	1383
Ξ^{*0}	uss	1405(131)	1532
Ω^-	sss	1512(144)	1673
Σ_c^{*++}	uuc	2341(77)	
S^{*+}	usc	2450(79)	
T_c^{*0}	ssc	2559(81)	
	ucc	3520(136)	
	scc	3623(140)	
	ccc	4642(198)	

Table 8.3: Calculated spin $\frac{3}{2}$ baryon masses ex. [150]

	Particle mass (GeV)	
	Lattice	Experiment
N	0.932 ± 0.092	0.938
Δ	1.232 (input)	1.232
Σ	1.155 ± 0.063	1.194
Λ	1.124 ± 0.068	1.115
Σ^*	1.377 ± 0.055	1.385
Ξ	1.327 ± 0.045	1.318
Ξ^*	1.523 ± 0.037	1.530
Ω^-	1.672 (input)	1.672
π	0.138 (input)	0.138
ρ	0.562 ± 0.072	0.769
K	0.605 ± 0.017	0.495
K*	0.746 ± 0.042	0.892

Table 8.4: Calculated baryon masses ex. [99]

for the lightest modes; for the heavier modes the finite size effects will not be significant, but the mass suppression of the aligned states still is.

It was mentioned in the meson sector, that if one plots the effective long-range coupling strength α against the mass, the lattice is a factor of three below the physical curve. However, the baryon sector [150] is well reproduced; the physical and lattice curves lie almost over each other.

These results can be compared with those of Gottlieb et al. [99], in which strange and charm quarks were also included[4]. Note that the splitting between Λ and Σ is reproduced here, albeit insufficiently.

Since the lattice used had relatively few points, and a coupling constant that is known to be outside the asymptotic scaling regime, one must be aware that these results are not good approximations to the physical spectrum.

Iwasaki et al. [127,125] found, using the renormalisation group improved action, the mass

[4]In fact, Loft and DeGrand claim their results are identical if the fit is restricted to a lattice of the same size as Gottlieb et al. used.

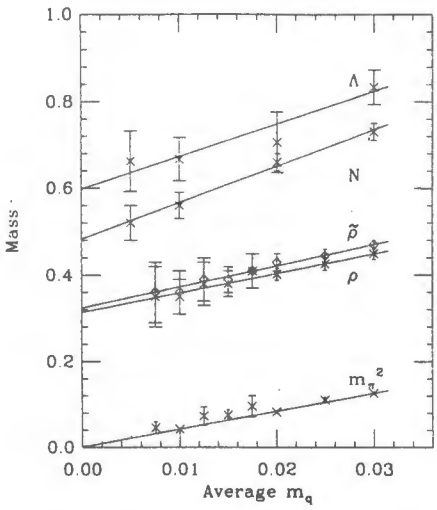

Figure 8.12: Hadron masses using Kogut-Susskind fermions. ex.[109]

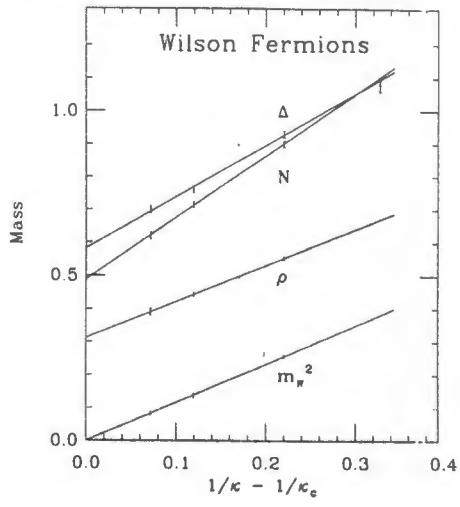

Figure 8.13: The masses for hadrons using Wilson fermions, with a linear extrapolation to κ_c. ex.[109]

of the proton and delta to be $m_p = 1080(80)$ MeV and $m_\Delta = 1370(120)$ at the physical hopping parameter.

Using, instead of the naive analysis, one based on phenomenological mass formulae from Ono [167]

$$\begin{aligned} M_{\text{baryon}} &= M_b + \sum_{i=1}^{3} + \xi_b \sum_{i>j} \frac{\mathbf{S_i} \cdot \mathbf{S_j}}{m_i m_j} \\ M_{\text{meson}} &= M_m + \sum_{i=1}^{2} + \xi_m \frac{\mathbf{S_q} \cdot \mathbf{S_{\bar{q}}}}{m_q m_{\bar{q}}} \end{aligned} \tag{8.6}$$

$$\begin{aligned} M_b &= 0.077\text{GeV} \quad M_m = -0.057\text{GeV} \\ \xi_b &= 0.02205\text{GeV}^3 \quad \xi_m = 0.0715\text{GeV}^3 \end{aligned} \tag{8.7}$$

a far better fit was obtained. Setting the masses of the quarks equal in the above equation, the only free parameter is the lattice spacing; using the spacing determined already, the fits to the lattice data yielded $m_p = 940$ MeV and $m_\Delta = 1230$ MeV! This is extremely close to the physical results!

Gupta et al. [109] found (see fig. 8.12), using Kogut-Susskind fermions, that the mass of the proton was $am_p = 0.48(3), 0.46(4)$, whilst that of the Λ was $m_\Lambda = 0.60(6), 0.59(7)$. The first figure comes from a linear fit to the data, the second from a quadratic. These can be translated into MeV; $m_p = 1200, 960$ and $m_\Lambda = 1500, 1200$, with the first using the mass of the rho as standard, and the second the slopes, as in eqn. 8.2.

Using Wilson fermions (see fig. 8.13, the following results were obtained: $am_p = 0.49(1), 0.42(2)$ and $m_\Delta = 0.58(2), 0.55(2)$. In MeV these are $am_p = 1200, 1030$ and $m_\Delta = 1450, 1220$. The ordering is as in the previous paragraph; note that the masses in MeV are taken from the linear fit only.

Bowler et al. [43,41] found, at $\beta = 6.0$, that there were large finite size effects and regarded the data as suspect. The finite size effects were thought to be due, in part, to the use of anti-periodic boundary conditions.

At $\beta = 6.15$, using periodic boundary conditions, the mass of the nucleon came out to be $m_N = 1.50(9)m_\rho = 1150$MeV. The calculation using anti-periodic boundary conditions at this coupling were regarded as suspect.

At $\beta = 6.30$, no results were quoted. The data were thought to be unreliable, due to the use of anti-periodic boundary conditions, the small size of the lattice, and the comparatively large quark masses.

The results of De Forcrand can be seen in fig. 8.6. There is again a slight negative curvature in the data for the nucleon. Notice that the use of a propagator composed of a linear combination of the propagators on lattices with periodic and anti-periodic boundary conditions leads to a decrease in the errors, as well as a small systematic shift of the results.

8.6 Quark Wave Function

A second method used by [150] to determine a^{-1}, using the value of the wave function at the origin, yielded 1926(45)MeV. This larger value for the inverse lattice spacing was then used for all the mass calculations. (This method will be described in more detail below.)

An analysis of the decay of the vector meson into an electron-positron pair yields information about the magnitude of the wave function at the origin. This is because the decay width can be written in terms of the vector-current matrix element or the quark wave function at the origin;

$$\begin{aligned} \Gamma &= \frac{4\pi\alpha^2}{3m_\rho^3}\langle\rho|\sum_{i=1}^{3}\bar{\psi}_i\gamma_\mu\psi_i|0\rangle^2 \\ \Gamma &= \frac{16\pi\alpha^2 e_q^2}{m_\rho^2}|\psi(0)|^2 \end{aligned} \tag{8.8}$$

The vector current on the lattice is related to the vector current in the continuum by a renormalisation constant [37].

If one plots the value of $|\psi(0)|^2$ at the origin for each of the vector mesons against the mass,

On the lattice, the origin is smeared over a box with sides a; for the higher mass states, this causes a large drop in the effective value of $|\psi(0)|^2$. This can be corrected for as follows: assuming the wave fuction has a Gaussian form, one can calculate the lattice wave function as the spatial average over the box of the continuum wave function. The correction factor can then be defined as the ratio of the continuum value at zero to the calculated lattice value at zero. If one then corrects the value obtained for $|\psi_L(0)|^2$ for each of the vector mesons, striking agreement with experiment is obtained (see fig. 8.14

8.7 Edinburgh Plots

The Edinburgh Plot, introduced by the Endinburgh group, provides a means of illustrating how close a lattice simulation is to reality, using mass ratios alone. It is thus relatively

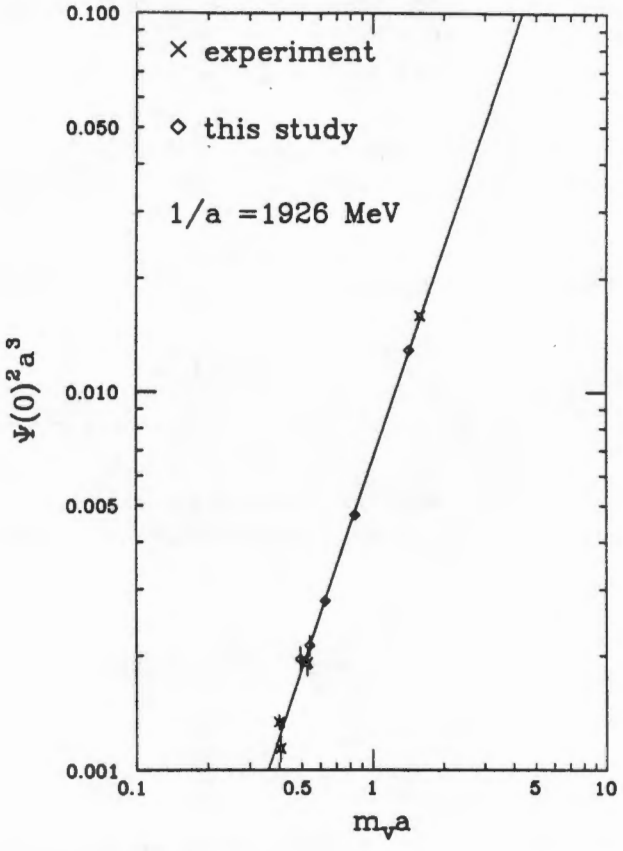

Figure 8.14: Experimental and lattice values of the wave function at the origin, including the correction factor for the lattice cut-off described in the text. ex [150]

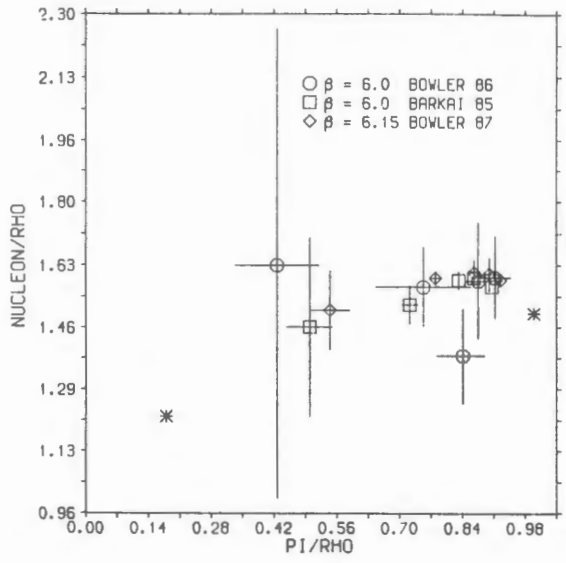

Figure 8.15: Edinburgh plot of Bowler et al. [41,43]

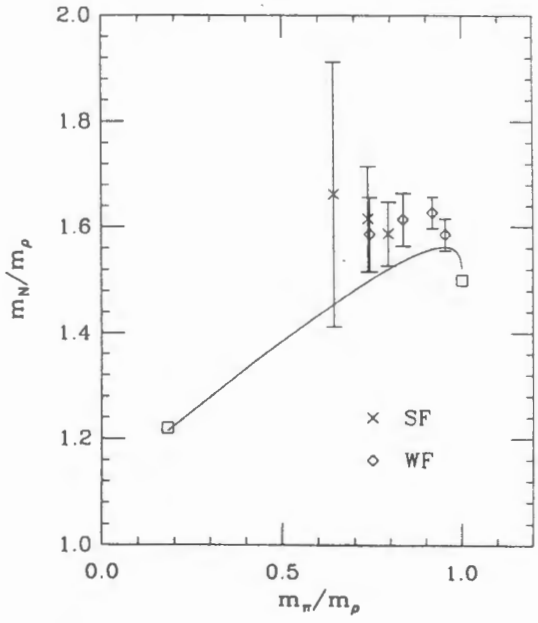

Figure 8.16: Edinburgh plot of Gupta et al. [109]

unaffected by the details of the fitting procedure, or the exptrapolation to the physical quark mass. One plots the ratio of the nucleon and rho mass to that of the pion and rho mass.

One can draw a curve, showing the result expected from a naive quark model, such as that of Ono [167]. The cross at the right-most point is the result for infinitely heavy quarks, while that in the lower left hand corner is that for the physical masses. Those lattice results lying on the curve are likely to be in the asymptotic scaling regime.

The results of Bowler et al. are illustrated in fig. 8.15 Note that the data points show some sign of approach to the physical point as the quark mass is lowered; however, they are still above the predicted curve, indicating deviations from scaling.

Looking at the results of Gupta et al., fig. 8.16, one sees that the results are reasonable, considering the large quark masses. Note, however, that if one attempts to extrapolate to zero quark mass, one lands up with a nucleon to rho ratio of about 1.6, far above the physical result of 1.22. Further problems are seen if one considers only the Kogut-Susskind fermions; the ordinates of the points *increase* with decreasing quark mass. The results of extrapolations to zero quark mass using Kogut-Susskind fermions must thus be regarded with some suspicion! The Wilson fermions are better behaved, as was to be expected from the fact that the signal was cleaner for these than for the Kogut-Susskind fermions.

In fig. 8.17 one can see the results obtained by the APE collaboration, on a relatively small lattice, at a largish coupling. The points have the correct form, and are decreasing with decreasing quark mass, but are consistently above the predicted curve. This is probably due to both finite size effects, and lack of asymtotic scaling.

The results of Iwasaki et al. using the renormalisation group improved action, fig. 8.19, showed how well the heavy quark physics is reproduced in their simulation. It remains to be seen what effect a reduction in the quark mass will have.

The plot using the standard Wilson action [127], fig. 8.20, illustrates two things. Firstly,

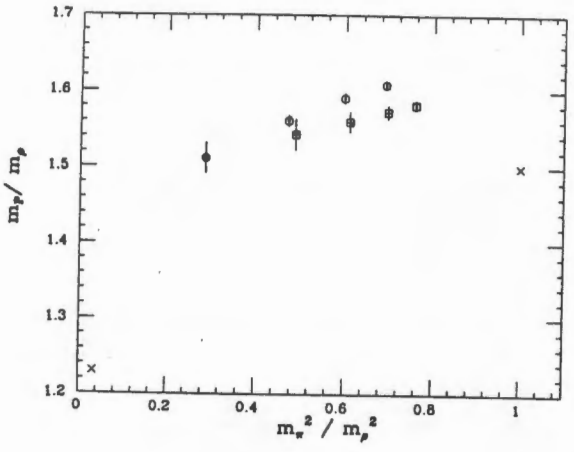

Figure 8.17: APE collaboration. Circles are for $\beta = 5.7$, squares are for $\beta = 6.0$. [23]

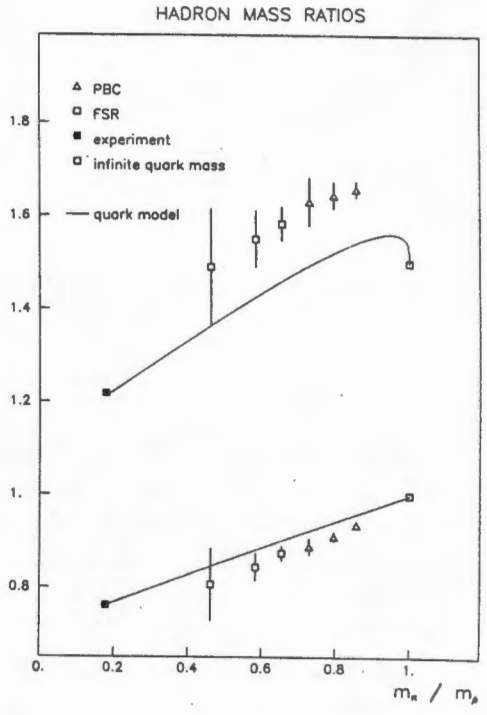

Figure 8.18: De Forcrand et al. The upper data correspond to m_N/m_ρ, whilst the lower data correspond to m_N/m_Δ. [77]

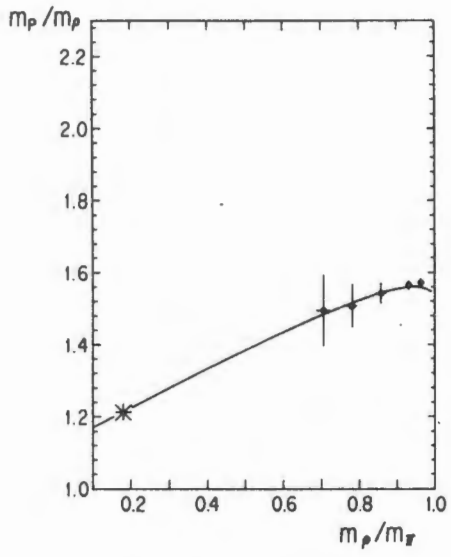

Figure 8.19: Iwasaki et al., using the improved action. [125]

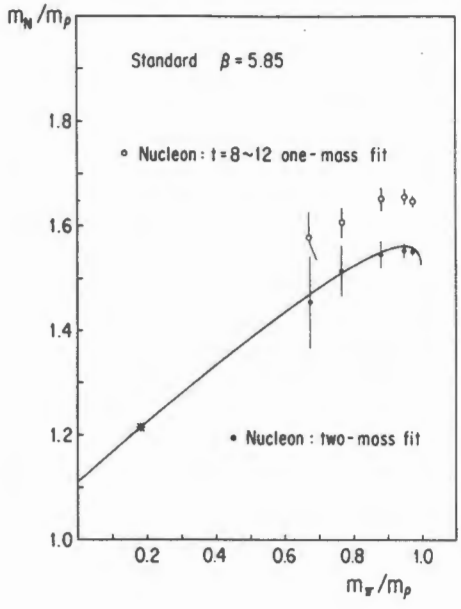

Figure 8.20: Iwasaki et al., using the standard action. The open circles represent one-mass fits over a limited range, close to the source. The closed circles are fits that included an excited state, and extended far from the source. [127]

that on a sufficiently large lattice the standard Wilson action with Wilson fermions yields results almost as good as those obtained with the improved action. Secondly, it shows how important it is to include the excited states in a fit to the mass, even when one is dealing with the heavier hadrons.

The results of De Forcrand et al. are extremely encouraging. Notice that the downward trend of the phenomenoligical model is well reproduced, due in a large part to the relatively error-free results at small quark masses. It is, however, systematically above the curve, unlike that of Iwasaki. This could be due to the former neglecting to include excited states in the fit, as well as the possible finite size effects (the lattice is only 1.2 fm in extent spatially.)

8.8 Conclusions

It should be clear from the data presented in this section that the quenched approximation is not providing us with exceptional results. In the best cases, they are within 10% of the experimental results.

With regard to scaling (which is independent of reproducing the physical masses accurately), the latest results have been encouraging. The pion, excluding the lightest quark masses, showed evidence of scaling in all of the simulations presented here. The rho also appears to be close to the asymptotic scaling regime, in those simulations with coupling $\beta > 6.0$; however, the mass of the rho usually appears to be consistently low when calculated using some other means, such as the string tension, to fix the lattice scale. This is essentially the reason for the ordinates of points in the Edinburgh plot lying above the phenomenological curve.

The baryons, however, are not so encouraging. In the case of Bowler et al., at the coupling closest to the scaling regime, the finite volume effects were so large that no value could be quoted for the baryon masses! At the higher values of β, the lack of scaling seems to be indicated in the points in the Edinburgh plot lying above the curve. However, as shown by Iwasaki et al. (fig. 8.20), one needs a large lattice and the inclusion of excited states to obtain agreement between the lattice data and the phenomenological curve.

This need is largely due to the fact that the excited nucleon state is only 50% higher in mass than the ground state is. Furthermore, the amplitude of the wave function is larger for the excited state than it is for the ground state. There is thus going to be considerable mixing between the states, a problem that will be exacerbated with small lattices or small quark masses. Hence the importance of including the excited state in any fit of the masses.

This is the origin of much of the apparent lack of scaling in the simulations to date; rather than the lattices being too coarse, they have been too small to extract good statistics about both the ground and excited baryon states. Both are required to reach agreement with the phenomenological curve. This was shown by Iwasaki, who found that the major effect of the finite lattice volume was the loss of data at large distances (along the time axis) from the quark source.

This would appear to be the major source of error in the results of Bowler et. al.; the lattice was only 24 sites long in the time direction, compared to 48 for Iwasaki. Gupta et al. used a lattice of 42 sites length; however, the use of anti-periodic boundary conditions and the fact that the lattice spacing was lower than that used by Iwasaki will have lead to loss of data. Further, excited states were not included in the baryon fits at all. Thus their conclusion that $\beta = 6.2$ is not yet in the scaling regime, whilst it may still be true, was caused

in part by the size of the lattice and lack of inclusion of excited states in the fits.

The mass of the quarks used in the simulation also play a role in determining the relative importance of finite volume vs. finite spacing effects. The UV cutoff affects the results of a propagator at small distance from the source. As a general rule, for masses around 1 in lattice units, the propagator decays sufficiently rapidly that the gauge fields on the links have minimal effect, and thus it is badly affected by the finite spacing.

The IR cutoff introduced by the finite volume will affect the results for small quark masses. This cutoff leads to discrete momentum spectra (the momentum is quantized in units of $\frac{2\pi}{aN}$, eqn 6.30, in a given direction). If the quark mass is low, the particle spectrum will be sensitive to this.

Hence it is clear that there is an optimal quark mass to use on a given lattice, as well as minimum and maximum allowable quark masses. Bowler et al. have defined criteria for the quark mass, based on the pion mass, for a given lattice size and coupling. (These were done using the Compton wavelength of the pion as a standard; this is not a good standard for a composite particle, as has been shown using the fully soluble massive Thirring/sine-Gordon model [120], see section 6.3.1. A better standard is the size of the wave function.) Remember that the pion quark masses are related through the equation $m_\pi^2 = Am_q$, from the PCAC relations (see appendix B). The slope of this curve was taken as 7 GeV in determining the constant factor in the equations below.

The optimal lattice quark mass at a given coupling was defined to be

$$M_0(\beta) = 0.66\left(\frac{9}{2\pi\beta}\right)^{\frac{4}{11}}(\Lambda a) \tag{8.9}$$

and the maximum and minimum values were defined to be

$$M_+(\beta) = 6.1\times10^{-4}\left(\frac{9}{2\pi\beta}\right)^{\frac{4}{11}}(\Lambda a)^{-1} \tag{8.10}$$

$$M_-(\beta,N) = 5.9\times10^{-3}\left(\frac{9}{2\pi\beta}\right)^{\frac{4}{11}}\frac{1}{(\Lambda a)N^2} \tag{8.11}$$

where the value for (Λa) is taken using the two-loop formula, eqn. 4.7.

To determine the minimum lattice size at a given quark mass one needs to set the optimal mass equal to the minimum mass. At couplings of $\beta = 6.15, 6.30$ this yields 47 and 56 respectively. It can thus be seen that the simulations presented here have all been woefully short in the time direction, with the exception of Iwasaki.

Another effect of the quark masses used can be seen when one considers the values used in relation to the mass of the strange quark. The lightest masses used to date for Kogut-Sussking fermions has been $m_q \approx m_s/3$, whilst the case for Wilson fermions is worse; $m_q \approx m_s$. Hence the extrapolation to zero quark mass is being done a long way from the zero mass point, and errors will be introduced at this level as well.

The advantages of using the renormalisation group techniques to improve the action is well illustrated by the results of Iwasaki, fig. 8.19 and De Forcrand, fig. 8.18. These both have the lowest errors of the calculations presented and the closest matching to the phenomenological curve of Ono. The latter case also appears relatively free of finite size effects.

In summary, the errors in the quenched approximation come from the following sources:

- β not yet sufficiently large to be in the scaling regime. This is not of great importance, since it is near to the scaling regime, and the beta-function is now known in the non-perturbative regime from lattice studies (see section 4).

- Finite volume effects; this is probably the most important source of error, especially if coupled with the absence of excited states in the fits. It appears that the use of periodic boundary conditions leads to smaller finite volume effects than those coming from the use of anti-periodic boundary conditions. Further improvement is seen if one computes hadron propagators based on a linear combination of quark propagators calculated using both boundary conditions.

- The quark mass being too large compared to the physical quark mass. Again, this is probably a large source of error, coupled with the fact that the momenta a quantized in units of $\approx 4m_\pi$.

- The quenched approximation itself. It appears that the sea quarks play a large role in determining the properties of the hadrons. For example, the strange quarks may well account for a sizeable fraction of the mass of the proton. Again, recently it has come to light that the valence quarks carry very little of the spin of the proton [64].

  Some light will be shed on this in the next section, dealing with the results obtained on the lattice using dynamical quarks.

The way ahead in the quenched approximation seems to be the use of larger lattices (Iwasaki et al. came to the conclusion that one needs $L_t > 5$ fm, and $l_s > 1.8$ fm), with periodic boundary conditions, using renormalisation group improved actions, with smaller quark masses. Furthermore, the statistics must be sufficiently good to include excited states in the fits to the propagators. Decreasing the coupling to get closer to the asymptotic scaling regime appears to be less important.

This will require an increase in computing power, or equivalently an improvement in the algorithms, sufficient to decrease the processing time by two or more orders of magnitude.

Chapter 9

Full QCD Results

In full QCD one makes no further approximations in the attempt to solve lattice QCD than those inherent in the lattice formulation itself, and those due to the use of numerical routines in the extraction of results. Hence any result in which dynamical quarks are used will be the correct prediction of QCD itself, up to these sources of error.

Owing to the enormous increase in computer time required for a full QCD simulation, there were few attempts prior to 1986. The development of more efficient algorithms has made it possible to simulate full QCD on the lattice. Sadly, the lattices used to date have been both too coarse ($a^{-1} \approx 1$ GeV, compared to the quenched approximation at 2 – 2.5 GeV) and too small (around 10 sites in each spatial direction). The lattices have had the same physical size as those used in the quenched approximation, but have had half the number of sites in any direction; and hence have had twice the lattice spacing. This is done in order to keep the computer time required to reasonable levels.

The couplings used in the full QCD simulations have been between 5.0 and 5.5, still far short of the asymptotic scaling regime. (For the quenched approximation, the scaling regime starts around $\beta = 7$. It should start slightly lower for dynamical quarks.) So the points made at the start of section 8 with regard to the problems of asymptotic scaling and finite size scaling are even more applicable here.

Secondly, the masses used for the quarks are still larger than in the quenched approximation, and these are above the physical quark masses. From the computational side, the smaller the quark mass that one uses, the longer the simulation time. This is due to the fact that the correlation length now goes as the inverse of the quark mass, and the time taken to reach an independent configuration goes like the correlation length. Hence the results using dynamical quarks are still a long way from yielding reasonable results — let alone matching the accuracy of perturbative QED!

Dynamical quarks, or in other words, quark – anti-quark pairs, are expected to affect the results of the quenched approximation in two ways;

- The sea quarks make vacuum polarization possible. This will lead to a renormalisation of the coupling constant, effectively decreasing it due to the screening effect. This leads to a given value of β being closer to the asymptotic scaling regime than that value would be in the quenched approximation. (Hence the values used in dynamical simulations, given above, are not as far from the asymptotic scaling regime as one might have thought.) This renormalisation is scale dependent.

- One is also able to split the colour electric string. This will lead to a flattening of the

quark potential at large distances, and the possibility of decays.

Decays have not been possible in lattice simulations to date, due to the high quark masses used. This has lead to the rho mass being lower than twice the pion mass. Furthermore, the lattices are to small to be able to hold two pions.

These two effects drop the mass of the hadrons, compared to the results of the quenched approximation. Increasing the number of flavours simulated also drops the mass of the hadrons. In the Wilson approximation, there is a concommitant drop in the physical hopping parameter.

The only exception is the mass of the pion, which shows the same behaviour in both approximations. This happens because chiral symmetry forces it to zero in both approximations, going as the square root of the quark mass. For large quark mass one expects no difference anyway, since sea quarks will have little effect. The pion does appear to be a Nambu-Goldstone boson, whilst the non-vanishing of the quark condensate at zero quark mass shows that the chiral U(1) symmetry is spontaneously broken in full QCD.

Flavour symmetry is not yet restored for Kogut-Susskind fermions, evidenced by the mass of the π' being considerably larger than the mass of the pion.

The reason for the success of the quenched approximation has been shown to be due to most of the effect of the dynamical quarks on the mass spectrum going into renormalisation of the coupling. Thus the results of the mass spectrum here agree with those of the quenched approximation to within 10 to 20%. The sea quarks do, however, play a large role in the long-range behaviour of QCD, so such factors as the masses of excited states, or P-states with the wave function peaking away from the origin are changed.

Although the precision of the results falls far short of that found in the quenched approximation, they are useful, and, as the lattices slowly approach the infinite volume continuum limit with low-mass quarks, so the predictions of the lattice should approach the experimental values. Sadly, the most noticeable feature of the full QCD results, when compared to the quenched approximation results, is the paucity of decent results.

The following summarizes the details of some of the recent simulations of QCD with dynamical quarks.

Born et al., 1989 [39] Results were calculated on a lattice of size $12^3 \times 24$ with coupling $\beta = 5.20$ and 5.35 using Kogut-Susskind fermions, in the pseudofermion approach. With $a^{-1} = 1$ GeV the spatial size of the lattice was 2.4fm. Quark masses of 0.075, 0.050 and 0.025 were used.

The Metropolis algorithm was used for the gauge fields, and a heatbath for the pseudo-fermions. 5000 iterations were used to thermalize, and 100 to 150 configurations were sampled at the different quark masses, seperated by 50 sweeps. 75 to 100 sweeps were used in the heat bath to bring the pseudo-fermions into equilibrium with the gauge fields.

The fits were in a single variable, and symmetric due to the periodic boundary conditions, over a range t_{min} to $T - t_{\text{min}}$ (see eqn 6.25). The fits took into account both ground and excited states for most of the particles. The error estimates were obtained from two sources; firstly, MINUIT was used to get the error from the fitting, and secondly errors were calculated using the standard jacknife procedure. The errors from each were comparable.

Gottlieb et al., 1988 [102] Results were calculated on lattices of size $6^3, 8^3, 10^3 \times 24$ with two different couplings, Kogut-Susskind fermions. The couplings were not set beforehand; in this simulation, the couplings were varied such that a physical length scale was kept constant. This was chosen to be the crossover temperature, as measured on lattices at temperatures of $\frac{1}{4a}$ $\frac{1}{6a}$. This was done because the renormalised coupling is a function of both the bare coupling and the bare quark mass. From this, the size of the lattice used was chosen such that there was no chance of any traces of the deconfinement transition affecting the results.

The hybrid molecular dynamcics algorithm developed by Gottlieb et al. [101] was used. 100 trajectories were used for the initial thermalization, and between 200 and 500 sample configurations were taken at each quark mass ($m_q = 0.1, 0.05, 0.025$), seperated by 2 to 5 trajectories.

A single quark source was used, but repeated for each of the three colours. Periodic boundary conditions were used for the mesons, and anti-periodic for the baryons. Correlations between the configurations were taken into account in the fits. The data at points t and $T - t$ were averaged, and the average was then used in the fit, from some t_{min} to $T/2$.

Patel et al., 1989 [173] Results were calculated on a lattice of size $8^4 \mapsto 8^3 \times 24$ with coupling $\beta = 5.30$ using Wilson fermions. With $a^{-1} = 1.4$ GeV, from the average of fits using the rho and nucleon respectively, the spatial size of the lattice was 1.1 fm.

The hybrid Monte Carlo algorithm was used, with 150 to 190 trajectories used for the initial thermalization. Hopping parameters of $\kappa = 0.162, 0.165, 0.167$ were used, with 30, 30, 60 samples seperated by 50, 60, 40 sweeps at the corresponding hopping parameters. The critical hopping parameter was $\kappa_c = 0.1686(3)$.

Periodic boundary conditions were used for the gauge fields, whilst anti-periodic spatial and periodic temporal boundary conditions were used for the quarks. Since local operators were used, there was some contamination of the ground states.

The interesting feature of this study is that different hopping parameters (masses) were used for the sea and valence quarks, leading to a good estimate of how the mass spectra should change as the masses used in the simulations approach the physical quark masses.

Hamber, 1988 [114] Results were calculated on a lattice of size $^3\times$ with coupling $\beta =$ using both Wilson and Kogut-Susskind fermions. With $a^{-1} = 2.5, 1.1$ GeV respectively, the spatial sizes of the lattices were 0.8 and 1.8 fm.

Three quarks were simulated, representing u, d, and s. At $\beta = 5.3$ hopping parameters of $\kappa = 0.177, 0.178, 0.179, 0.180$ were used, and at $\beta = 5.4$ hopping parameters of $\kappa = 0.156, 0.158, 0.160, 0.162, 0.163$ were used.

The masses of the hadrons were then fitted to an equation of the general form

$$m_H = A + B_u m_u + B_d m_d + B_s m_s + C m^2 \tag{9.1}$$

where m is the average of the three quark masses. Periodic boundary conditions were used. The errors were calculated using binning and the jacknife procedure.

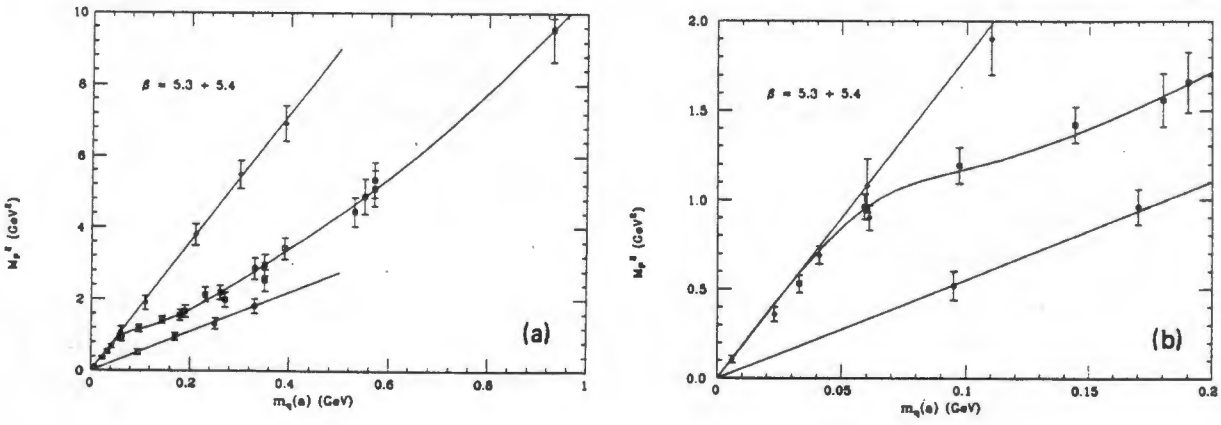

Figure 9.1: (a) Pion mass squared, in $(\mathrm{GeV})^2$ vs m_q. (b) Same, illustrating the small quark mass region in more detail. [113]

9.1 Pion Results

All of the studies qouted have found the expected PCAC pion behaviour. Hamber [113] found that the pion mass data could be fitted to a curve $m_\pi^2 = 12.6(10)m_q$ at $\beta = 5.3$, and 6.5(6) at 5.4 (see fig. 9.1). These fits were done over a range of masses from 330 MeV to 2600 MeV. The physical slopes are the same for each coupling; the change in lattice spacing accounts for the change in the coefficient of the quark mass.

Born et al. [39] found no evidence for the 0^{+-} partner to the pion in the Kogut-Susskind formulation. Flavour symmetry was restored to some extent, but not as well as in the quenched approximation. Gottlieb et al. [102] found no evidence of flavour symmetry restoration; the pion mass tended to zero, but the π' tended to a constant, close to the mass of the other mesons. The flavour symmetry did improve, however, at the higher value of β. The pion masses could be fitted to a curve of the form $m_\pi = 2.728(9)\sqrt{m_q} - 0.542(31)m_q$ at $aT_c = \frac{1}{4}$ and
$m_\pi = 3.027(130\sqrt{m_q} - 1.313(46)m_q$ at $aT_c = \frac{1}{6}$.

9.2 Rho, a_1 and b_1 Mesons.

Hamber [113] obtained reasonable results for the rho meson. Fitting to the difference between the rho and pion masses, he obtained

$$\sqrt{m_\rho^2 - m_\pi^2} = \begin{cases} 0.67(3) \\ 0.29(2) \end{cases} \Rightarrow m_\rho = \begin{cases} 757(34) \\ 754(52) \end{cases} \quad \text{MeV}, \quad \text{at } \beta = \begin{cases} 5.3 \\ 5.4 \end{cases} \tag{9.2}$$

Using Kogut-Susskind fermions, Gottlieb et al. [102] obtained results in for the rho that were far inferior to those obtained for the pion mass. The mass was only stable if the data between times 4 and 9 were used. Both before and after these the rho mass rose. This has its origin in the comparatively large fluctuations in the rho propagator.

Due to these, the statistics began failing below the midpoint in time of the lattice. Thus a lattice of larger temporal extent would not improve matters. The best option is probably to increase both the temporal extent and the number of independent configurations.

The a_1, which is the opposite parity partner to the ρ', was not well fitted. Results for the ground state could only be obtained if the excited states of both the rho and a_1 were included. The b_1, in the ρ channel, could not be fitted at all; the data were just too poor.

The results obtained by Patel et al. [173] were good. These are given in table 9.1, and the mass ratios plotted in the Edinburgh plot in fig. 9.2. No data on the other meson types was extracted, partly due to the use of Wilson fermions. Note, in table 9.1, the effect of the sea vs. the valence quarks on the masses. More detail will be paid to this in the section below on the Edinburgh plots.

Finally, the results of Born et al. [39] were slightly better than those of Gottlieb et al. The a_1 and ρ' channel was dominated by the ρ', but the signal, whilst very noisy, was such that some data was obtained on the a_1. In the b_1/ρ channel, the only effect of the b_1 was to perturb the rho data. No fit to the b_1 was possible.

Flavour symmetry, measured by the proximity of the ρ and ρ' masses, was found to be restored to within 5%. The following results were obtained for the rho mass and thus the lattice spacing:

$$m_\rho^2 = \begin{cases} 0.960(28) \\ 0.695(35) \end{cases} \Rightarrow a = \begin{cases} 0.25(1) \\ 0.18(1) \end{cases} \text{ fm} \quad \text{at } \beta = \begin{cases} 5.20 \\ 5.35 \end{cases} \tag{9.3}$$

9.3 Baryons

The results for the baryon spectrum are similar to those for the rho mass; far from stunning.

Hamber [113] used an indirect method to calculate the baryon masses; a fit to $\sqrt{m_N^2 - 2.8m_\pi^2}$. Results were only obtained for the nucleon and delta masses, since two-flavour Wilson fermions were used. The results for the nucleon mass, taking $m_N^2 \propto m_q$ were

$$m_N = \begin{cases} 970(140) \\ 970(210) \end{cases} \text{ MeV at } \beta = \begin{cases} 5.3 \\ 5.4 \end{cases} \tag{9.4}$$

whilst taking a linear relationship between the two gave

$$m_N = \begin{cases} 980(180) \\ 1130(200) \end{cases} \text{ MeV at } \beta = \begin{cases} 5.3 \\ 5.4 \end{cases} \tag{9.5}$$

The following results were obtained for the mass splitting between the delta and the nucleon:

$$\sqrt{m_\Delta^2 - m_N^2} = \begin{cases} 800(100) \\ 860(180) \end{cases} \text{ MeV} \tag{9.6}$$

As can be seen, the errors are considerably larger than those in the quenched approximation. Furthermore, the quark masses used are considerably larger than those used in the quenched approximation, so the extrapolation to zero quark mass is even more prone to errors.

Gottlieb et al [102] obtained good results for the large quark mass of 0.1, with the propagator being fitted from $t = 4 - 12$. At the lowest quark mass of 0.025, the data was swamped by noise from $t = 8$ onwards. As an indication of how far the quark masses were from the physical values, they calculated that values of $am_q = 0.0084(6)$ were required at $aT_c = \frac{1}{4}$ to yield the physical value for the pi to rho mass ratio. At $aT_c = \frac{1}{6}$ a mass of 0.0017(4) is required to yield the physical result. More details will be given in the section dealing with the Edinburgh plots for dynamical quarks.

κ_{val}	κ_{sea}	π	ρ	N	Δ	M_π/M_ρ	M_N/M_ρ
0.167	0.162	0.89(1)	1.03(1)	1.75(6)	1.80(8)	0.86	1.70
0.165	0.162	0.96(1)	1.08(1)	1.80(6)	1.84(7)	0.89	1.67
0.162	0.162	1.05(1)	1.15(1)	1.87(5)	1.89(6)	0.91	1.63
0.165	0.165	0.79(1)	0.93(1)	1.52(7)	1.61(8)	0.85	1.63
0.167	0.167	0.49(2)	0.68(2)	1.12(7)	1.22(7)	0.72	1.65
0.165	0.167	0.58(1)	0.74(2)	1.19(7)	1.26(7)	0.78	1.61
0.162	0.167	0.71(1)	0.83(1)	1.29(7)	1.34(7)	0.86	1.55

Table 9.1: Hadron masses, ex. [173]

9.4 Edinburgh Plots

Shown here is the Edinburgh plot of Born et al., fig. 9.3 [38], and that of Patel et al., fig. 9.2.

In the results of Patel et al., one notes that the quark mass is still, for the lightest value, no smaller than the strange quark mass. Also, since there are no strange quarks, the results need not be the same as the experimental points, since it is known that the strange quarks have a large effect on the proton mass (see section 9.5). The calculation is also being done at a strong coupling, such that the proton correlation length is still less than one lattice spacing.

The encouraging feature of these results is the effect that lowering the sea quark mass has on the nucleon to rho ratio. Examining the three results around $\frac{m_\pi}{m_\rho} = 0.85$ in table 9.1 one sees that $\frac{m_N}{m_\rho} = 1.70, 1.63, 1.55$ in order of decreasing sea quark mass. Clearly, as the sea quark mass is lowered, the nucleon/rho mass ratio moves in the correct direction. Since the quenched approximation has already proven that dropping the valence quark mass moves both mass ratios in the correct direction, it is certain that lower masses will yield results ever closer to the experimental results.

This conclusion is supported by those of Born, especially the preliminary result at $m_q = 0.010$. This is the result with dashed error bars, and is certainly moving in the correct direction.

In the case of Gottlieb et al. the mass ratios obtained were good only at the highest mass; this is almost certainly due to the very poor propagator statistics at the lower masses.

9.5 Sea Quarks

This is the major feature, inaccessible in the quenched approximation, to come out of the dynamical quark simulations. Tentative calculations have been made to determine the strange quark content of the proton, and the relative importance of the sea and valence quarks for pions and nucleons. The accuracy is still to low to enable the determination of, for example, the the correction in the quark mass due to the virtual pion cloud surrounding it.

With the inclusion of the sea quarks, it is possible to assign a different mass to the sea and valence quarks. This can be done because the sea quarks are described by the $\det M$ factor, whilst the valence quarks are described by a Delta function at some point on the lattice.

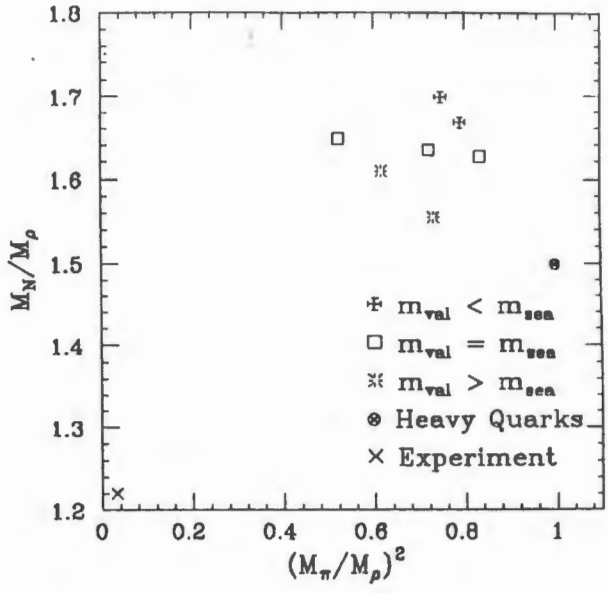

Figure 9.2: Edinburgh Plot ex. [173]

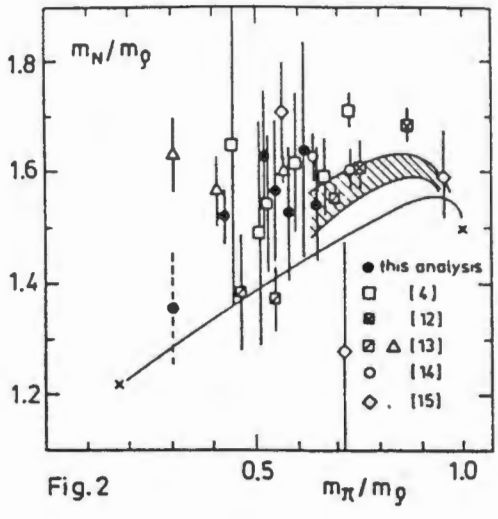

Figure 9.3: Edinburgh Plot ex. [38]

Once one has a set of values for each, it is possible to calculate the slope of a given hadron mass, written as a function of the respective quark mass.

Hamber [113] found

$$\frac{\partial m_{\rm p}^2}{\partial m_{\rm sea}} = \begin{cases} 21.3(4.2)a^{-1} \\ 9.2(2.2)a^{-1} \end{cases} \quad \frac{\partial m_{\rm p}^2}{\partial m_{\rm v}} = \begin{cases} 14.3(2.7)a^{-1} \\ 8.7(1.2)a^{-1} \end{cases} \quad \text{at } \beta = \begin{cases} 5.3 \\ 5.4 \end{cases} \tag{9.7}$$

Thus one can find the fraction of strange quarks in the proton,

$$\begin{aligned} \frac{\langle {\rm p}|\bar{s}s|{\rm p}\rangle}{\langle {\rm p}|\bar{u}u + \bar{d}d + \bar{s}s|{\rm p}\rangle} &= \frac{21.3}{3 \times 14.3 + 3 \times 21.3} \\ &= 0.20(5) \end{aligned} \tag{9.8}$$

at $\beta = 5.3$, and 0.17(5) at $\beta = 5.4$. This can be compared with the experimental result of 0.21.

These slopes were looked at by Patel et al. who obtained the following results:

$$\begin{aligned} \frac{\partial m_\rho}{\partial m_{\rm sea}} &= 2.5(1)\frac{\partial m_\rho}{\partial m_{\rm val}} \\ \frac{\partial m_{\rm p}}{\partial m_{\rm sea}} &= 4(1)\frac{\partial m_{\rm p}}{\partial m_{\rm val}} \end{aligned} \tag{9.9}$$

Two things are clear from this; namely that changing the sea quark mass affects the hadron mass more than changing the valence quark mass does, and secondly that the rho is affected less than the nucleon is. This leads to the hope that the Edinburgh plot will improve as the mass of the sea quark approaches the physical limit. Further, since the two hadrons are affected to a different extent by the sea quarks, it is clear that one cannot simply absorb the effect of the sea quarks into a global renormalisation of the coupling.

9.6 Random Lattices

Some work has been done using a formulation of fermions on random lattices. On these, one no longer has any remnant of translational or rotational invariance before one reaches the continuum limit; hence the Nielsen Ninomiya theorem does not predict the spectral doubling that plagues the regular tesselations of space-time.

Since the random lattice is takes time to generate, and requires considerably more processing time to generate the gauge and fermion field configurations, they have been little used, despite the fact that the formalism was developed in the early 80s [62].

There have, however, been some good results of late. The propagators have been calculated on a random lattice in 4 dimensions [169], for both the quarks and composite baryons. The results obtained are close to the continuum limits; see fig. 9.4 for the propagators for the scalar and pseuso-scalar bosons.

In the case of the random block lattice (see section 5.6) the results obtained by Chiu [60] for the fermion propagator in the two dimensional Schwinger model are presented in fig. 9.5.

This indicates that the random lattice could be the solution to the problem of spectral multiplicity, in that one is able to have an undoubled chiral fermion coupled to the gauge field that appears to have the correct continuum limit.

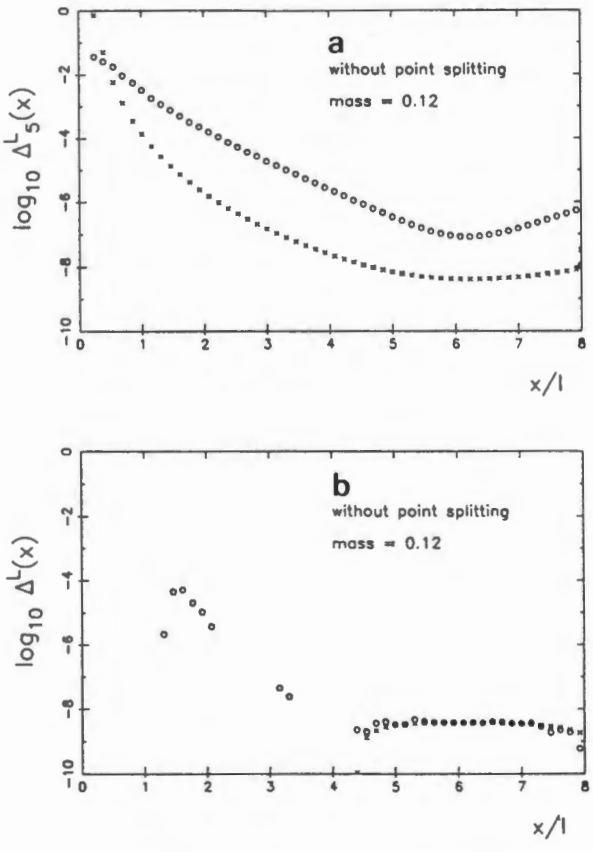

Figure 9.4: (a) Composite pseudo-scalar propagator. (b) Composite scalar propagator. Crosses represent continuum calculations, dots the averages over a random lattice. ex [169]

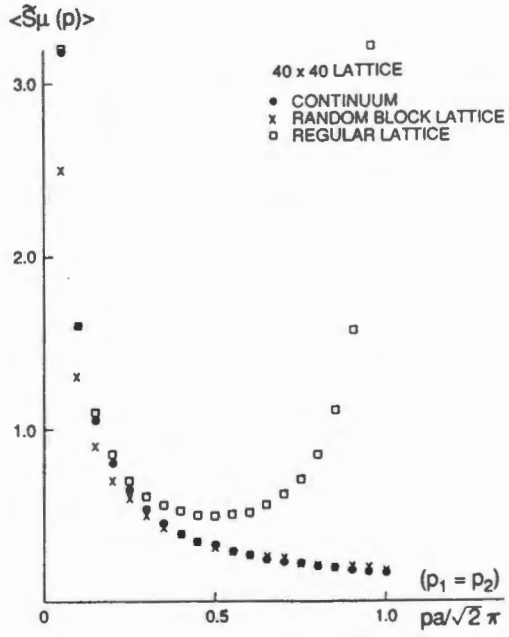

Figure 9.5: Massless fermion propagator, in the zero coupling, or $\beta = \infty$ limit. [60]

9.7 Conclusion

The conclusions drawn in the previous chapter about the various sources of error can be taken over directly, with the only modification being the increase in the magnitude of the error. (This excludes one source of error in the quenched approximation; viz., that introduced by ignoring the sea quarks!)

So to avoid repetition, this section will concentrate on those aspects that are different, and especially those that are encouraging.

One encouraging point is that these studies have validated the use of the quenched approximation for many of the calculated quantities. A good idea of the effect of the sea quarks on the mass of the proton, say, has been obtained; it is small, and at the higher quark masses used, indistinguishable from the numerical errors involved.

Information that is unobtainable in the quenched approximation has been gained as well. The strange quark content of the proton, due entirely to the sea quarks, has been measured, and found to be very close to the experimental value.

Whilst the lattices are, as yet, too small to allow for decays to occur, information on these will be generated on larger lattices. This expectation is borne out by the fact that the inter-quark potential flattens out, due to the screening effect of dynamical quarks, on the larger lattices.

The prodigous amount of processing time required for the inversion of the fermion matrix (90%) is the major reason for the lack of accuracy here. The time required is due to the non-locality of the matrix, which reflects the time required to propagate a change through the lattice. This problem will be exacerbated by larger lattices, as well as by smaller fermion masses. It is the most important area in which significant savings of processing time can be made by the discovery of more efficient algorithms.

The use of excited states in the fits to the signals seems to be required. This necessitates the use of larger lattices, with longer runs and better statistics. The results of Iwasaki in the quenched approximation illustrated the consequences of using excited states.

However, one must come to the final conclusion that these dynamical results are not definitive calculations, but merely a hopeful indication that, given a sufficiently accurate simulation, lattice QCD is capable of yielding meaningful results.

Chapter 10

The Future in Lattice QCD

The previous chapters have illustrated, I believe, the power of lattice QCD in extracting numbers that are unobtainable by using other methods.

However, the results presented here have all, to a greater or lesser degree, suffered from the constraints imposed by both computing speed and computer memories. To obtain results at better than the 10% accuracy of today, an increase of 3 orders of magnitude in the speed and memory is required. This will require a machine with processing speed around 100 Gflops to 1 Tflop. This machine will, in all likelyhood, be a massively parallel machine based on connected computing units, (such as transputers) and custom-built for the task of lattice calculations. The APE collaboration has already announced plans to construct a machine of this nature, to use in about 4 years from now [180]. For a review of the current status of the supercomputer side of lattice QCD, consult [63].

This speed will allow both the quark mass and the lattice spacing to drop, and the physical lattice size to increase, by an order of magnitude. This should be sufficient to place the calculations just within the asymptotic and finite size scaling regimes.

With improved computing power will also come better error analysis. It should also be possible to accurately compare molecular dynamics and exact algorithms, in order to check the former for any inherent biases. Manifestly, the use of unbiased algorithms is a pre-requisite to any accurate calculation.

All this assumes no change in the algorithms and techniques used. The single most important factor in full QCD sumulations is the inversion of the fermion matrix; this consumes 90% of the computing time used. Another avenue for improvement lies in the use of renormalisation group improved actions. It has been demonstrated that these yield results closer to the continuum limit, without much change in the processing time required.

The major stumbling block for lattice QCD is the problem of fermion spectral multiplicity. To date, the only reliable results have come from either Wilson or Kogut-Susskind fermions. There have been many other proposals over the years, without any improvements. Possibilities for improvement still exist, though; one being the use of 'fuzzy mathematics' or perhaps a smearing of the lattice operators. These are intuitivlely appealing as they explixitly re-introduce to the lattice some of the continuity of space-time.

The current question about whether to use compact or non-compact actions for U(1) and SU(2) may well continue into SU(3). Should it do so, many of the results in the pure gauge sector will need amending. However, it seems unlikely that the results presented here on the hadron spectrum will be negated by a new calculation involving a non-compact action. It

may well be, however, that the quarks play a vital role in the confinement mechanism.

The best signal of the status of lattice QCD is the Edinburgh plot. As has been shown, the data still have large errors, which will be reduced with larger lattices and better statistics. At present, the results are moving closer to the experimental point. It has been shown that the sea quarks move the datum in the correct direction, as does a decrease in the quark mass. The use of strange quarks in the Wilson simulations also move the datum in the correct direction.

Thus, despite the fact that the lattice calculations have proven to be orders of magnitude more difficult than was anticipated at first, it is perfectly reasonable to hope for good results on the hadron spectrum from future calculations.

These calculations will have quark masses of $am_q = 0.001$, with lattices of size 100^4, and β at 7.0 or above. Probably renormalisation group improved actions will be used as well. The quenched approximation will also start to yield better results. (Full QCD uses two orders of magnitude more processing time than the quenched approximation does. However, since the results in the quenched approximation are correct to within 10 – 20% for some questions in QCD, the calculations are still well worth doing).

The calculation of hadronic weak matrix transtition elements will also receive attention with the advent of faster computers. Much work has already been done in this area in the quenched approximation, and it remains to be seen what effect the inclusion of dynamical quarks will have on this calculation.

One caveat, however; so far the lattice has yielded no new insight into the problem of confinement. It is possible that the confinement-deconfinement transition that has been observed is simply a lattice artifact. However, even if the lattice does prove the presence of confinement in $SU_c(3)$, it is debatable whether or not one can glean a better insight into the physics involved from the impressive manipulation of numbers by a CRAY alone. In this sense, the lattice approach is still unsatisfactory.

The lattice approach to understanding the strong interaction is clearly imperfect; but it is the best available to us today.

Acknowledgements

The work presented here is due, in a large part, to the patient understanding and encouragement of my supervisor, Prof. J. Cleymans. His assistance is greatly appreciated.

In addition, the comments of Dr J. Seixas of LAPP during his all too brief visit to UCT have been of great benefit to me.

I also wish to thank my family, and those friends and fellow physicists who have helped me in my endeavour to savour life and physics to the full.

This work has been partially supported by the FRD in the form of a postgraduate grant; my thanks go to them for the generous support.

Appendix A

The Nielsen-Ninomiya Theorem

The Nielsen-Ninomiya Theorem [164,165] proved that there are fundamental restrictions on placing a fermionic field onto a lattice. An explanation of the effects of this No-Go Theorem is given on page 31. Below is the proof of the theorem, based on the Poincaré-Hopf theorem, first given by Karsten [131].

A.1 NN Theorem

Take a left-handed fermion field ψ with N spinor components, defined on an infinite lattice in Euclidean 4-space, and transforming under some symmetry group, say $SU_c(3) \otimes SU(2) \otimes U_{chiral}(1)$. The following generic action is invariant under this symmetry group:

$$S = -\sum_{x,y}\sum_{\mu=1}^{4} \bar{\psi}(x)\gamma^{\mu}H_{\mu}(x,y)\psi(y) \tag{A.1}$$

One then makes the following reasonable assumptions about the action:

1. Locality of the interaction.
2. Translational Invariance under multiples of one lattice spacing in any of the four directions. This implies that $H_{\mu}(x,y)$ cannot depend on x and y individually, but only on the distance between them, viz. $H_{\mu}(x-y)$.
3. Hermiticity of the momentum operator H_{μ}. This is required for the action to be real, and gives $H_{\mu}^{*}(z) = H_{\mu}(-z)$.

One also makes the following assumptions about the charges (e.g., fermion number, electric etc.:)

1. Exact conservation, even at the scale of the fundamental lattice. This means that energy and momentum eigenstates will also be charge eigenstates.
2. The charge is locally defined, i.e. a bounded set of lattice points completely defines the charge.
3. The charge is quantized.
4. The charge is bilinear in the fermion field ψ.

The Nielsen-Ninomiya Theorem states that, under the above assumptions, the requirements of Chiral Symmetry and no Fermion Doubling are mutually exclusive.

The proof of the No-Go theorem rests on the Poincare-Hopf theorem in algebraic topology. Before covering this, a short introduction to the relevant concepts in geometry and topology would be useful.

A.2 Manifolds

The definitions of a manifold, connected manifold, tangent manifold, tangent bundle etc. have been omitted for brevity; information on these can be found in any elementary text on differential geometry, topology etc. A good text for the physicist is Dodson and Poston [5]. With regard to notation, a manifold is refered to as M, and a specific point in it as m.

A.2.1 Orientation of a Manifold

A connected manifold with a choice of basis has an orientation defined as well [3, p103]. If dim M>0, the bases all fall into one of two equivalence classes, called positive and negative; two bases are equivalent if the matrix mapping one into the other has positive determinant. A clear picture can be gained in $\Re^3$; the set of all right-handed coordinate systems forms the positive class, the set of all left-handed coordinate systems forms the negative class.

A rotation matrix has positive determinant, and the coordinate system remains Right or Left-Handed under rotation. A reflection has negative determinant and changes the coordinate system from Right to Left-Handed, and vice-versa. This is equivalent to chirality; a rotation leaves a left-handed neutrino unchanged, whilst a reflection changes it to a right-handed neutrino.

A.2.2 The Derivative of a Mapping

The derivative one first encounters is that of a function mapping the real line into the real line; $f : \Re \mapsto \Re : y \rightsquigarrow x^2$, mapping a 1-manifold into a 1-manifold. The derivative is another mapping from a 1-manifold to a 1-manifold; $f' : \Re \mapsto \Re : y \rightsquigarrow 2x$. The derivative of the function at a point x, f'_x, is the linear approximation to the function at the point x in question.

This notion [5, p213ff] can be extended to a general map from one manifold to another, $F : \mathrm{M} \mapsto \mathrm{N}$. The derivative of F at a point $m \in \mathrm{M}$ (written $\underset{\sim}{\mathrm{D}}_m F$) is the flat approximation of the manifold N at the point n, where $F : m \rightsquigarrow n, F(m) = n$. Flat approximation means the linear part of the affine space approximating N at the point n. Thus we have a map from the tangent space at m to the tangent space at n; $\underset{\sim}{\mathrm{D}}_m F : \mathrm{T}_m\mathrm{M} \mapsto \mathrm{T}_{F(m)}\mathrm{N}$.

These tangent spaces, assuming they are connected and have bases defined on them, will be oriented. Hence the derivative at m can map the coordinates of $\mathrm{T}_m\mathrm{M}$ into those of $\mathrm{T}_n\mathrm{N}$ in one of two ways: orientation preserving, or orientation reversing.

Since the map may vary over the pre-image manifold, $\underset{\sim}{\mathrm{D}}_m F$ may map one part of $\mathrm{T}_m\mathrm{M}$ for some $m \in \mathrm{M}$ and preserve orientation, and reverse the orientation at other $m \in \mathrm{M}$.

A.2.3 Homological Euler Number

Manifolds have some quantities that are invariant under a topological transformation. For example, the number of holes is conserved (so a doughnut is topologically identical to a

tea-cup).

Certain of these topological characteristics of a space X can be given in terms of the *Cohomology Groups* ($H^i(X)$) of the space [1, p1]. This is the higher-dimensional analogue of the number of connected pieces that constitute the space. The cohomology groups are usually some $\Re^n$; thus each cohomology group has a number, the dimension of $\Re^n$, associated with it. This number is called the Betti number; $\beta_i = \dim(H^i(X))$.

These are all topological invariants of the space. If the space X is a compact n-manifold, one can define a further topological invariant, the *Homological Euler Number* $\chi'(X)$, as the alternating sum of the Betti numbers; $\chi'(X) = \sum_{i=0}^{n}(-)^i\beta_i$.

There are two results that are needed later [1, p279];

1. A surface[1] M has Euler Number $\chi(\mathrm{M}) = 2 - 2g$, where g is the genus of the surface. The genus is defined to be the number of 'handles' one must add to the 2-sphere to get the surface M. A tea-cup has $g = 1$, as does the torus.

2. The Euler Number of a manifold formed by taking the product of two other manifolds is given by $\chi(\mathrm{M}\times\mathrm{N}) = \chi(\mathrm{M}).\chi(\mathrm{N})$.

A.3 Vector Fields on Manifolds

A.3.1 Definition

One can define a vector field [1, p281] V on the manifold by choosing a vector v in $\mathrm{T}_x\mathrm{M}$ (the tangent bundle of the manifold M) at each x in the manifold These chosen vectors define trajectories on the manifold, from any given starting point. Note that, in order for the choice of vectors to define a field, one adds the restriction that the trajectories must be C^∞. The vectors then define a smooth path in the manifold; with differential equation $\dot{c}(t) = V(c(t))$ for trajectories $c : \Re \mapsto \mathrm{M}$. The vector field is a map from the manifold M to a sub-manifold N, or section, of the tangent bundle $V : \mathrm{M} \mapsto \mathrm{N}$.

A.3.2 Equilibrium Points

A point $x \in \mathrm{M}$ at which the vector $\mathrm{v} \in V$ is zero is called an equilibrium point, the stationary solutions of the differential equation ($c(t) = x$.) Information on the nature of an equilibrium point is provided by the index $I_v(x)$ [1, p219, 230] (winding number in 2 dimensions [2]) of the point . This is found as follows (the manifolds M and N are as defined in the previous sub-section).

Consider an equilibrium point x in an n-manifold M; construct a ball around x. The vector field defines a map from the surface of the ball in M to a surface in N; replacing V by $g = \frac{V}{|V|}$ one gets a map from the surface of the ball in M to the surface of a ball in N; $g : \mathrm{S}^{n-1} \mapsto \mathrm{S}^{n-1}$. Approximate g by a differentiable map h. Choose a point in general position[2] in the image space of the map h. The index of the equilibrium point x is the number of pre-image points that are mapped by h into this image point, counted algebraically. By algebraically, one means $+1$ if the differential (the map $\underset{\sim}{\mathrm{D}}_m h$) preserves orientation, and -1 if the differential reverses orientation.

[1] A surface is a 2-manifold.

[2] A point with no distinguishing feature, such as it being a point of intersection.

This can easily be seen in a surface; say the complex plane, and we are considering the origin as the point to find the index of. The mapping from a plane Z into a plane W by $w = z$ has index 1, since any image-point on the unit circle in w has only one pre-image point in z. If the mapping is $w = z^2$, however, the index is 2 since 2 pre-image points, π apart, are mapped into the same image point.

A.3.3 Euler Number

The sum of the indices of all the equilibrium points in the manifold is a constant, the *Euler Number* $\chi(\mathrm{M})$.

$$\chi(\mathrm{M}) = \sum_i I_v(x_i) \tag{A.2}$$

This constant depends only on the manifold M, and is independant of the vector field V chosen on the manifold. The proof of this relies on algebraic topology, and is a restricted form of the Atiyah-Singer Index Formula [1, p218]

A.4 Poincaré-Hopf Theorem

This is a very simple result, first shown for 2 dimensions by Poincaré in 1895, and in general by Hopf in 1925. This states that *The homological Euler Number equals the Euler Number for any compact manifold without boundary* [3, p164] [4, p126]. The proof rests on Morse Theory, and can be found in [3].

A.5 Proof of the NN Theorem

On an infinite lattice, the momentum space forms a compact manifold[3]. Choosing a Brillouin Zone $p_\mu \in (-\frac{\pi}{a}, \frac{\pi}{a}]$, one gets the circle S^1 as the momentum manifold for each dimension. Thus the momentum space is a 4-manifold, the torus $\mathrm{T}^4 = \mathrm{S}^1 \times \mathrm{S}^1 \times \mathrm{S}^1 \times \mathrm{S}^1$. The surface of a doughnut is just the 2-torus T^2.

Using the two results in section A.2.3 one can calculate the Euler Number of T^4. Firstly, $\chi(\mathrm{T}^2) = 2 - 2 = 0$. Thus one gets

$$\begin{aligned} \chi(\mathrm{T}^4) &= \chi(\mathrm{T}^2 \times \mathrm{N}^2) \\ &= \chi(\mathrm{T}^2) \times \chi(\mathrm{T}^2) \\ &= 0 \end{aligned}$$

A continuous function F defined on the manifold T^4 gives rise to another manifold, the vector space V (a C^∞ section of TT^4;)

$$F : \mathrm{T}^4 \mapsto \mathrm{V} : p \rightsquigarrow F(p) = v \in \mathrm{V}$$

As T^4 is a compact manifold without boundary, the Poincaré-Hopf theorem states that the sum of the indices of the indices of the vector field must be 0;

$$\sum_p I_v^{(p)} = \chi(T^4) = 0$$

[3] A finite lattice has a discrete momentum space, rather than continuous; the proof still holds, however. Details can be found in most good solid state texts, as Bloch's Theorem.

Pole	Pre-Image Point	Image Point	Index	No. of poles
$(0,0,0,0)$	$(0,0,0,\varepsilon)$	$(0,0,0,\varepsilon)$	1	1
$(0,0,0,\frac{\pi}{a})$	$(0,0,0,\frac{\pi}{a}-\varepsilon)$	$(0,0,0,\varepsilon)$	-1	4
$(0,0,\frac{\pi}{a},\frac{\pi}{a})$	$(0,0,\frac{\pi}{a},\frac{\pi}{a}-\varepsilon)$	$(0,0,0,\varepsilon)$	1	6
$(0,\frac{\pi}{a},\frac{\pi}{a},\frac{\pi}{a})$	$(0,\frac{\pi}{a},\frac{\pi}{a},\frac{\pi}{a}-\varepsilon)$	$(0,0,0,\varepsilon)$	-1	4
$(\frac{\pi}{a},\frac{\pi}{a},\frac{\pi}{a},\frac{\pi}{a})$	$(\frac{\pi}{a},\frac{\pi}{a},\frac{\pi}{a},\frac{\pi}{a}-\varepsilon)$	$(0,0,0,\varepsilon)$	1	1

Table A.1: Poles of Naive Fermions, Demonstrating the Poincaré-Hopf Theorem.

Hence, for each 0 of the vector field V with $I_v = 1$ (orientation preserving), there is one with $I_v = -1$ (orientation reversing).

The origin of the fermion doubling problem lies in the fact that the momentum space is a compact manifold with Euler Number 0; there is no way of removing the problem without losing some physics; or adding some fermions!

A.6 Illustration of the Consequences

The generic fermion propagator will be of the form $S^{-1}(p) = \sum_\mu \gamma^\mu F(p_\mu)$. For the naive derivative one gets

$$F(p_\mu) = \sin p_\mu a$$

Thus $F : \mathrm{T}^4 \mapsto \mathrm{T}^4$, and

$$\underset{\sim}{\mathrm{D}}_p F(p_\mu) = \cos p_\mu a$$

is a map $\underset{\sim}{\mathrm{D}}_p F(p_\mu) : \mathrm{TT}^4 \mapsto \mathrm{TT}^4$. The basis vectors in p-space, T^4, are $\hat{e}_\mu = (\delta_{1\mu}, \delta_{2\mu}, \delta_{3\mu}, \delta_{4\mu})$, and in the direction of increasing p_μ. The basis vectors in the function space at some point $F(p_\mu)$, say $\hat{e}'_\mu(p_\mu)$, are in the direction of increasing $\sin p_\mu a$, and are given by $\underset{\sim}{\mathrm{D}}_p F(\hat{e}_\mu)$.

Hence the map F will preserve orientation at a point p if;

- $\cos p_\mu a > 0 \ \ \forall \mu$
- $\cos p_\mu a < 0 \ \ \forall \mu$
- $\cos p_\mu a > 0$ for 2 of the μ, and < 0 for 2

and will reverse orientation if

- $\cos p_\mu a < 0$ for 1 or 3 of the μ only.

One can now calculate the index of each of the sixteen zeroes of the vector field F.

Consider the point $p = (0,0,0,0)$; $F(p) = (0,0,0,0)$. Constructs a sphere S^3 around p, radius ε. $F(p)$ then gives an image ball of radius $\approx \varepsilon$, $F : \mathrm{S}^3 \mapsto \mathrm{S}^3$. Consider the image point $(0,0,0,\varepsilon)$); this has one pre-image point, $(0,0,0,\varepsilon)$. Since $\cos p_\mu a$ is positive for all μ, the map is orientation preserving and gives the index $I_v(0,0,0,0) = 1$.

Repeating this for the other fifteen poles, one gets the following result;

There are 8 poles of index 1 and 8 of index -1; thus the Poincaré-Hopf theorem is satisfied. The other significant point to realise is that a pole of index 1 is a massless particle of positive

helicity, one of index -1 has negative helicity. (The index essentially tells one about the behaviour of the propagator at that point under the reflection operator.) There is thus explicit chiral symmetry!

One can compare this with the Wilson Fermion; here one removes the 15 unwanted fermions by adding a mass-like term that is irrelevant in the continuum limit. Unfortunately, this completely destroys the chiral symmetry!

The inverse propagator for the Wilson Fermions (chapter5.5) is;

$$S^{-1} = \sum_{\mu} i\gamma^{\mu} \frac{\sin p_{\mu} a}{a} + 4\frac{r}{a} - \frac{r}{a} \sum_{\mu} \cos p_{\mu} a$$

In the Wilson theory, especially if the parameter r is less than 1, (see section 5.5) the extra fermions are not removed; hence table A.1 still applies, as does the Poincaré-Hopf theorem. The Wilson term simply adds to the mass of the unwanted fermions, removing the mass degeneracy. These terms decouple in the continuum limit; since the continuum limit is what one is interested in, this is sufficient.

Appendix B

Symmetries of Continuum QCD

This is intended as a short summary of the basics of the symmetries of continuum QCD. Further details may be found in, for example, Pascual and Tarrach, [8].

Denote a quark field by $\psi_\mu^{cf}(x)$ with colour index $c \in \{1,2,3\}$, flavour index $f \in \{1,\cdots,N_f\}$ and Dirac Index μ. The covariant QCD Lagrangian for this quark field is given by

$$\mathcal{L}(x) = \sum_{cf}\left\{\frac{i}{2}\left[\bar{\psi}_\alpha^{cf}(x)(\gamma_\mu)^{\alpha\beta}D^\mu\psi_\beta^{cf}(x) - \left(D^\mu\bar{\psi}_\alpha^{cf}(x)\right)(\gamma_\mu)^{\alpha\beta}\psi_\beta^{cf}(x)\right] + m_f\bar{\psi}_\alpha^{cf}(x)\psi_\alpha^{cf}(x)\right\} + \frac{1}{2g^2}\mathrm{Tr}[F^{\mu\nu}F_{\mu\nu}] \tag{B.1}$$

This Lagrangian is invariant under a local $SU(N_c)$ colour transformation. It also has the following Global symmetries:

1. $U_V(1)$ (Baryon Number)
   This is invariance under a set of 1-parameter transforms $\exp\{-i\theta\mathbb{1}_{cf4}\}$ where $\mathbb{1}_{cf4}$ denotes the identity matrix in Dirac, colour and flavour space.

2. $U_1(1)\otimes\cdots\otimes U_{N_f}(1)$ Conservation of quark types
   Invariance under set of 1-parameter transforms $\exp\{-i\theta_f\mathbb{1}_{c4}\}$, with one per flavour. (This symmetry is not respected by the weak force.) This is enlarged to the symmetry group $SU(N_f)$ if all the masses are equal, ie. if one is also able to mix the flavours whilst leaving the Lagrangian invariant.

   If all the masses are equal to nought, one enlarges this vector symmetry to include an axial vector symmetry, giving $SU_V(N_f)\otimes SU_A(N_f)$. The vector and axial vector symmetries are given by the following 1-parameter transformations;

   - Vector: $u_V : \psi(x) \mapsto e^{(-i\theta^a T^a)\mathbb{1}_4}\psi(x)$ for $u_V \in SU_V(N_f)$.
   - Axial Vector: $u_A : \psi(x) \mapsto e^{(-i\theta^a T^a)\gamma_5}\psi(x)$ for $u_A \in SU_A(N_f)$.

   This symmetry can be re-written as a chiral symmetry, $SU_L(N_f)\otimes SU_R(N_f)$, using $T^a(\mathbb{1}_4-\gamma_5)$ and $T^a(\mathbb{1}_4+\gamma_5)$ as generators for the left-handed and right-handed quarks respectively. One then has the correspondence $SU_V(N_f) = SU_{L+R}(N_f)$ and $SU_A(N_f = SU_{L-R}(N_f)$[1].

[1] A good review of Chiral symmetry can be found in [168].

3. $U_A(1)$
   For massless quarks, one has the following axial symmetry in addition to the vector symmetry given in the first item;

$$u_A : \psi(x) \mapsto e^{-i\theta\gamma_5}\psi(x) \tag{B.2}$$

   for $u_A \in U_A(1)$.

4. Poincare Invariance
   The Lagrangian, since it is covariant, is also symmetric under the full Poincarè group, ie the combination of translations, relflections, rotations and Lorentz Boosts in the continuum.

B.1 Axial Anomaly

The Axial symmetry appears in the theory due to the fact that the particles have spin $\frac{1}{2}$ and thus are described by $2^{d/2}$ spinor components in a d-dimensional theory. This is the number of components required to have Poincare invariance, and is given by dimensions of the matrices generated in the fundamental representation of the Clifford group generated by the Clifford algebra of the Dirac matrices. It is worth noting that the parity operation, which mixes the components of the Dirac spinor, anti-commutes with the γ_5 responsible for generating the axial symmetry:

$$\{P, \gamma_5\}_+ = 0 \qquad \text{with} \quad P = i\gamma^\nu\gamma_5, \quad x_\nu \mapsto -x_\nu \tag{B.3}$$

The $U_A(1)$ axial symmetry is responsible for one of the more troublesome aspects of the standard model, the so-called axial anomaly. This was first pointed out by Adler, Bell and Jackiw in a pair of independant papers [20,27] It is an approximate symmetry, that only holds for the Lagrangian in the limit of massless quarks. Since the quarks have a mass, this symmetry is broken explicilty (as is the higher chiral symmetry, $SU_V(N_f) \otimes SU_A(N_f)$).

With massless fermions, the Lagrangian is invariant under $U_A(1)$; however, the symmetry is broken by the vacuum! This is shown by the experimental fact that the vacuum expectation value of $\bar{\psi}\psi$ is non-zero[2]

Since the symmetry is broken by the vacuum, one expects either a Nambu-Goldstone boson, if the symmetry is broken by the Nambu-Goldstone mechanism, or, if it is broken by the Wigner-Weyl mechanism, that all massive hadrons appear as parity doublets. The latter is manifestly untrue, which rules out that option. For the first option, we need a massless, spinless, negative parity particle; the eta is the natural candidate. This would then be equivalent to the pion, the Goldstone boson generated when the vacuum breaks the larger chiral symmetry, $SU_L(N_f) \otimes SU_R(N_f)$ down to $SU_{L+R}(N_f)$. The three pions observed correspond to the three generators of the broken axial group, $SU_{L-R}(N_f)$

Now, neither the pion nor the eta are massless; the pion is an approximate Goldstone boson, with a mass generated by the fact that the quarks are not massless in nature; in other words, chiral symmetry is broken in the Lagrangian as well as by the vacuum. Since the same term would generate the mass of the eta if it were a Goldstone boson, this implies that the

[2]Invariance under γ_5 means that $\langle 0|\bar{\psi}\psi|0\rangle = \langle 0| - \bar{\psi}\gamma_5\gamma_5\psi|0\rangle$ which can only be satisfied if the chiral condensate, $\langle\bar{\psi}\psi\rangle$, is identically zero.

two should have the same mass. (In fact, it can be rigorously proven that $m_\eta < \sqrt{2}m_\pi$ [206] for the eta to be a Goldstone boson). However, it is experimentaly known that $m_\eta/m_\pi \approx 4$; this rules out the former realization of the symmetry breaking!

One thus has the Axial Anomoly, or $U_A(1)$ problem; a current, with an associated charge, which is conserved by the Lagrangian is not conserved by nature; however, neither of the mechanisms that can be used by the vacuum to break the symmetry are observed!

One begins with the current generated by the axial symmetry ($J_5^\mu = \sum_{cf} \bar{\psi}(x)\gamma^\mu\gamma_5\psi(x)$). This not conserved[3] due to the triangle anomaly[4] giving anomalous terms in the Ward identities associated with the Axial current. If there is no conserved charge, there is no axial anomaly.

However, the current generated by subtracting another term from J_5^μ *is* conserved in the absence of instantons. This is $\bar{J}_5^\mu = J_5^\mu - \frac{g^2}{8\pi^2}N_f\epsilon^{\mu\rho\sigma}[A_\nu^a\partial_\rho A_{a\sigma} + \frac{g}{3}f^{abc}A_{a\nu}A_{b\rho}A_{c\sigma}]$ with summation implied, and A the chromoelectric vector potential. Whilst the current is gauge-variant, the associated charge is not-and hence is conserved! This implies the unobserved Goldstone boson is required to break the conservation.

The resolution of the problem was provided by t'Hooft [196] who showed that, in the presence of instantons, the required Goldstone boson appears as a massless pole in the gauge-variant Green functions alone, and not in the gauge-invariant one that is relevant to observable physics; this then provided a mechanism for breaking the symmetry, yet not having any observable consequence of the mechanism used. (Note that one of the requirements for this proof to hold is that there exists equal numbers of complete lepton and quark families, which provides some understanding of those present, and shows the importance of finding the truth quark.)

[3] Even though it is conserved in the classical limit.

[4] This is present in flavour-changing decays, for example, as well as the famous 'VVA' diagram, in which the quark triangle gives an infinite contribution, since there is no limit on the momentum that may circulate within it.

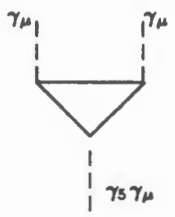

Vector, Vector, Axial Vector Boson interaction

Appendix C

Explicit Euclidean Representation of the Clifford Group

Using the Euclidean Dirac matrices defined in section 2.4 the 16 linearly independent elements of the Clifford Group, composed of all possible products of the Dirac matrices can be constructed as follows.

The notation of eqn.5.54 and those immediately following is used to label the independent elements of the Clifford Group; thus all lower case letters represent an element of the group $\mathcal{G}$.

The following useful identities for the Euclidean representation of the Clifford group hold true:

$$\Gamma_a^\dagger = (-)^{A.\bar{A}}\Gamma_a \tag{C.1}$$

$$\Gamma_{a+b} = (-)^{A\bar{B}}\Gamma_a\Gamma_b \tag{C.2}$$

$$\Gamma_a\Gamma_b = (-)^{A\bar{B}}\Gamma_b\Gamma_a \tag{C.3}$$

where $a, b, \cdots, z \in G$, and the relationship between the group element and the corresponding vector (written in upper case) is given by:

$$A_\mu = \begin{cases} 1 & \mu \in a \\ 0 & \text{otherwise} \end{cases} \tag{C.4}$$

One can define two related quantities that are of use:

$$\bar{A} = (0, A_1, A_1 + A_2, A_1 + A_2 + A_3)$$

$\bar{A}$ was used in the definition of the η sign factors for the Kogut-Susskind fermions, see eqn. 5.25

$$\tilde{A} = (A_2 + A_3 + A_4, A_1 + A_3 + A_4, A_1 + A_2 + A_4, A_1 + A_2 + A_3)$$

The 16 linearly independant elements of the Clifford group are explicitly given in the

following form:

$$\Gamma_0 = \mathbb{1}$$

$$\Gamma_1 = \gamma_1 = \begin{pmatrix} 0 & 0 & 0 & -i \\ 0 & 0 & -i & 0 \\ 0 & i & 0 & 0 \\ i & 0 & 0 & 0 \end{pmatrix} \quad \Gamma_3 = \gamma_2 = \begin{pmatrix} 0 & 0 & 0 & -1 \\ 0 & 0 & 1 & 0 \\ 0 & 1 & 0 & 0 \\ -1 & 0 & 0 & 0 \end{pmatrix}$$

$$\Gamma_6 = \gamma_3 = \begin{pmatrix} 0 & 0 & -i & 0 \\ 0 & 0 & 0 & i \\ i & 0 & 0 & 0 \\ 0 & -i & 0 & 0 \end{pmatrix} \quad \Gamma_{12} = \gamma_4 = \begin{pmatrix} 1 & 0 & 0 & 0 \\ 0 & 1 & 0 & 0 \\ 0 & 0 & -1 & 0 \\ 0 & 0 & 0 & -1 \end{pmatrix}$$

$$\Gamma_2 = \begin{pmatrix} i & 0 & 0 & 0 \\ 0 & -i & 0 & 0 \\ 0 & 0 & i & 0 \\ 0 & 0 & 0 & -i \end{pmatrix} \quad \Gamma_5 = \begin{pmatrix} 0 & i & 0 & 0 \\ i & 0 & 0 & 0 \\ 0 & 0 & 0 & i \\ 0 & 0 & i & 0 \end{pmatrix}$$

$$\Gamma_7 = \begin{pmatrix} 0 & -1 & 0 & 0 \\ 1 & 0 & 0 & 0 \\ 0 & 0 & 0 & -1 \\ 0 & 0 & 1 & 0 \end{pmatrix} \quad \Gamma_{10} = \begin{pmatrix} 0 & 0 & i & 0 \\ 0 & 0 & 0 & -i \\ i & 0 & 0 & 0 \\ 0 & -i & 0 & 0 \end{pmatrix} \tag{C.5}$$

$$\Gamma_{13} = \begin{pmatrix} 0 & 0 & 0 & i \\ 0 & 0 & i & 0 \\ 0 & i & 0 & 0 \\ i & 0 & 0 & 0 \end{pmatrix} \quad \Gamma_{15} = \begin{pmatrix} 0 & 0 & 0 & 1 \\ 0 & 0 & -1 & 0 \\ 0 & 1 & 0 & 0 \\ -1 & 0 & 0 & 0 \end{pmatrix}$$

$$\Gamma_4 = \begin{pmatrix} 0 & 0 & 1 & 0 \\ 0 & 0 & 0 & 1 \\ -1 & 0 & 0 & 0 \\ 0 & -1 & 0 & 0 \end{pmatrix} \quad \Gamma_9 = \begin{pmatrix} 0 & i & 0 & 0 \\ i & 0 & 0 & 0 \\ 0 & 0 & 0 & -i \\ 0 & 0 & -i & 0 \end{pmatrix}$$

$$\Gamma_{11} = \begin{pmatrix} 0 & -1 & 0 & 0 \\ 1 & 0 & 0 & 0 \\ 0 & 0 & 0 & 1 \\ 0 & 0 & -1 & 0 \end{pmatrix} \quad \Gamma_{14} = \begin{pmatrix} i & 0 & 0 & 0 \\ 0 & -i & 0 & 0 \\ 0 & 0 & -i & 0 \\ 0 & 0 & 0 & i \end{pmatrix}$$

$$\Gamma_8 = \gamma_5 = \begin{pmatrix} 0 & 0 & 1 & 0 \\ 0 & 0 & 0 & 1 \\ 1 & 0 & 0 & 0 \\ 0 & 1 & 0 & 0 \end{pmatrix}$$

with the entries coming from the product of no, one, two, three and four of the Dirac matrices respectively.

Appendix D

Programs

D.1 Metropolis

Listed below is the program developed for the simulation of the Ising Model using the Metropolis et al. algorithm; see section 7.6. Included are the lines of code used for the evaluation of the correlations. (The Metropolis sub-routine was developed in collaboration with Dr J. Seixas of LAPP, Annecy during his visit to UCT.)

```
      PROGRAM ISING_METROPOLIS
      PARAMETER(LS=64,NSC=LS*LS,NITER=1000)
      INTEGER IS(LS,LS),ISN(LS,LS),TAU,T,IS1(LS,LS)
      REAL STP(LS,LS),ACTO(LS,LS),ACTN(LS,LS),TOTAV,PLQ(LS,LS),
     C     APLQ(NITER)

C     IS,ISN -- Current and new spin array
C     NITER -- Number of Iterations


      OPEN (4,FILE='test.DAT')
      OPEN (5,FILE='test1.DAT')
      WRITE(5,*) 'CORRELATIONS IN THE METROPOLIS ALGORITHM'
      WRITE(5,*) 'METROPOLIS CONFIGURATION 64*64, BETA = 0.5, '
     C ,NITER,' ITER ',
     C 'COLD START, SAMPLING EVERY ITERATION AFTER 700 TO THERM'
      WRITE(5,*) 'TAU   NORMCORR       CORRCON         COR'

1     CALL DATIME(ID,IT)
      SEED = ((IT*10000) + IT)/1.0e8 {Seed for random number generator
      WRITE(6,*) 'SEED = ',SEED
      WRITE(4,*) 'SEED = ',SEED
      CALL RANSET(SEED)          {Initialize random number generator; CERN library

      BETAI = 0.7
      BETAF = 0.4                {Initial and final values for the inverse temperature
      NSTEP = 20                 {No of temperature values sampled
       STEP = (BETAF-BETAI)/NSTEP
      NAV=100                    {Number of sweeps between averaging and printing
```

```
      NMEAS=500                 {Number of sweeps allowed for initial thermalizing
      NCTHM = 700               {Number of iterations before taking correlations
      ASPIN=0.                  {Sum of the average spin for 50 sweeps
      ERPIN=0.                  {Statistical error
      NHIT = 10                 {No of hits before remaining with the old spin
      TOTAV = 0.
      WRITE (4,*) 'BETAI = ',BETAI,';    BETAF = ',BETAF

      DO 10 I=1,LS
        DO 10 J=1,LS
          IS(I,J)=1             {Cold start, init. spins
C          R = RANF()
C          IF(R.LE.0.5) IS(I,J) = -1  {Hot start.
C          WRITE(4,*) 'HOT START'
          ACTO(I,J)=0.          {Init. local action for each site
10    CONTINUE

C     Main routine
C
      DO 60 BETA = BETAI,BETAF,STEP  {Execute from cold to hot
        WRITE (6,*) 'BETA = ',BETA
        WRITE (4,*) 'BETA = ',BETA

        EPT = 0.                {Expectation value of the average plaquette
        EPT2 = 0.               {Expectation value of the average plaquette squared
        EPTTAU = 0.             {Expectation value of the average plaquette at T times at TAU

        DO 50 ITER=1,NITER
          DO 30 J=1,LS
          DO 30 I=1,LS

            I1=I-1
            J1=J-1
            I2=I+1
            J2=J+1

            IF(I.EQ.1) I1=LS    {Implement boundary conditions
            IF(J.EQ.1) J1=LS
            IF(I.EQ.LS) I2=1
            IF(J.EQ.LS) J2=1

            STP(I,J)=IS(I1,J)+IS(I,J1)+IS(I2,J)+IS(I,J2)
            STP(I,J)=BETA*STP(I,J)  {value of staple excluding I,J site
            ACTO(I,J)=-IS(I,J)*STP(I,J)  {Action of site
            PLQ(I,J) = IS(I,J)*IS(I2,J)*IS(I2,J2)*IS(I,J2)

            DO 20 IH=1,NHIT     {Begin metrop.
              IR=1
              R=RANF()
              IF(R.LT.0.5) IR=-1
              ISN(I,J)=IS(I,J)*IR           {Trial spin
              ACTN(I,J)=-ISN(I,J)*STP(I,J)  {New action
              IF(ACTN(I,J).LT.ACTO(I,J)) THEN
```

```
                IS(I,J)=ISN(I,J)
                GOTO 20
              ENDIF              {Metrop. criterion: choose the best of NHIT hits
              R=RANF()
              E=EXP(ACTO(I,J)-ACTN(I,J))
              IF(E.GE.R) IS(I,J)=ISN(I,J)
20          CONTINUE
            IF(ITER.EQ.(NCTHM+1)) THEN
               IF((I.EQ.1).AND.(J.EQ.1)) PRINT*,'ITER = ',ITER
               IS1(I,J) = IS(I,J)
               EPT = EPT + IS1(I,J)
               EPT2 = EPT2 + IS1(I,J)*IS1(I,J)
            ENDIF
            EPTTAU = EPTTAU + IS(I,J)*IS1(I,J)
30        CONTINUE

          IF(ITER.EQ.(NCTHM+1)) THEN
            EPT = EPT/(64*64)
            EPT2 = EPT2/(64*64)
            WRITE(5,*) 'EPT = ',EPT,' EPT2 = ',EPT2
          ENDIF
          IF (ITER.GT.NCTHM) THEN
            EPTTAU = EPTTAU/(64*64)
            COR = EPTTAU
            CORCON = EPTTAU - EPT*EPT
            CORNRM = CORCON/(EPT2 - EPT*EPT)
            WRITE(5,'(I4,3F13.8)') ITER,CORNRM,CORCON,COR
          ENDIF
          EPTTAU = 0

        IF (ITER.LE.NMEAS) GOTO 50    {Thermalized?
        AI=0.
        DO 40 J=1,LS
         DO 40 I=1,LS               {Total spin
          AI=AI+IS(I,J)
40      CONTINUE
        ASPIN=ASPIN+AI/NSC
        ERPIN=ERPIN+(AI/NSC)**2
        IF(MOD(ITER,NAV).EQ.0) THEN
          AVPIN=ASPIN/NAV           {Average Spin
          ERROR=SQRT((ABS(AVPIN**2-(ERPIN/NAV)))/NAV)
          WRITE (4,*) 'ITER= ',ITER,    {Output average spin for NAV iterations
     1                '    AVERAGE SPIN :',AVPIN,' +/- ',ERROR
          TOTAV = TOTAV + AVPIN         {Block average
          ASPIN=0.
          ERPIN=0.
        ENDIF
50      CONTINUE
        WRITE(4,*) 'FINAL AVERAGE = ',TOTAV/((NITER - NMEAS)/NAV)
        TOTAV = 0.
60    CONTINUE
```

```
      TEMP = BETAF
      BETAF = BETAI
      BETAI = TEMP
      STEP = (BETAF-BETAI)/NSTEP
      DO 65 BETA = BETAI,BETAF,STEP  {Execute from hot to cold
```

The section of the program in the DO 65 loop is identical to that in the DO 60 loop, and has been omitted for brevity.

```
65    CONTINUE
      STOP
70    END
```

D.2 Heat Bath

The program listed below was used to simulate the Ising Model using the heat bath algorithm; see section 7.7.

```
      PROGRAM ISING_HEAT_BATH
      PARAMETER(LS=64,NSC=LS*LS,NITER=1500)
      INTEGER IS(LS,LS),ISN(LS,LS),TAU,T,IS1(LS,LS)
      REAL STP(LS,LS),ACTO(LS,LS),ACTN(LS,LS),NORM,TOTAV
     C     ,PLQ(LS,LS),APLQ(NITER)

C     IS,ISN -- Current and new spin array

      OPEN (4,FILE='HTBATH.DAT')
      OPEN (5,FILE='HTB_COR.DAT')
      WRITE(5,*) 'CORRELATIONS IN THE heat bath ALGORITHM'
      WRITE(5,*) 'METROPOLIS CONFIGURATION 64*64, BETA = 0.4, '
     C ,NITER,' ITER ',
     C 'COLD START, SAMPLING EVERY ITERATION AFTER 100 TO THERM'
      WRITE(5,*) 'TAU   NORMCORR       CORRCON         COR'
1     CALL DATIME(ID,IT)
      SEED = ((IT*10000) + IT)/1.0e8
      WRITE(6,*) 'SEED = ',SEED
      WRITE(4,*) 'HEAT BATH'
      WRITE(4,*) 'SEED = ',SEED
      CALL RANSET(SEED)
      BETAI = 0.6              {Initial and final values for the inverse temperature
      BETAF = 0.3
      WRITE (4,*) 'BETAI = ',BETAI,';    BETAF = ',BETAF
      NSTEP = 10               {No of temperature values sampled
      STEP = (BETAF-BETAI)/NSTEP
      STEP = 1
      NAV=100                  {Number of sweeps before averaging and printing
```

```
      NMEAS=1000                {Number of sweeps allowed for initial thermalizing
      NCTHM = 500               {Number of iterations before taking correlations
      ASPIN=0.                  {Sum of the average spin for 50 sweeps
      ERPIN=0.                  {Statistical error
      TOTAV = 0.                {Final block average

      DO 10 I=1,LS
        DO 10 J=1,LS
          IS(I,J)=1             {Cold start, init. spins
C          R = RANF()
C          IF(R.LE.0.5) IS(I,J) = -1  {Hot start.
C          WRITE(4,*) 'HOT START'
          ACTO(I,J)=0.          {Init. local action for each site
          PLQ(I,J) = 0.
          APLQ(J) = 0.
10    CONTINUE



C     Main routine
C
      DO 60 BETA = BETAI,BETAF,STEP  {Execute from cold to hot
        WRITE (6,*) 'BETA = ',BETA
        WRITE (4,*) 'BETA = ',BETA

        EPT = 0.            {Expectation value of the average plaquette
        EPT2 = 0.           {Expectation value of the average plaquette squared
        EPTTAU = 0.         {Expectation value of the average plaquette at T times at TAU

        DO 50 ITER=1,NITER
          DO 30 J=1,LS
          DO 30 I=1,LS

            I1=I-1
            J1=J-1
            I2=I+1
            J2=J+1

            IF(I.EQ.1) I1=LS    {Implement boundary conditions
            IF(J.EQ.1) J1=LS
            IF(I.EQ.LS) I2=1
            IF(J.EQ.LS) J2=1

            STP(I,J)=IS(I1,J)+IS(I,J1)+IS(I2,J)+IS(I,J2)
            STP(I,J)=BETA*STP(I,J)  {value of staple excluding I,J site
            ACTO(I,J)=-IS(I,J)*STP(I,J)  {Action of site
            PLQ(I,J) = IS(I,J)*IS(I2,J)*IS(I2,J2)*IS(I,J2)

            R = RANF()                              {Choose a random number
            NORM = EXP(-1*STP(I,J))+EXP(1*STP(I,J)) {Normalize
            DPUP = (EXP(-1*STP(I,J)))/NORM          {Probability density for the spin to
            IF(DPUP.LE.R) THEN
               IS(I,J) = 1
```

```
            ELSE
              IS(I,J) = -1
            ENDIF
C       PRINT*, 'R = R',R,'   NORM = ',NORM,'  DPUP = ',DPUP,'   IS = ',IS(I,J)
            IF(ITER.EQ.(NCTHM+1)) THEN
              IF((I.EQ.1).AND.(J.EQ.1)) PRINT*,'ITER = ',ITER
              IS1(I,J) = IS(I,J)
              EPT = EPT + IS1(I,J)
              EPT2 = EPT2 + IS1(I,J)*IS1(I,J)
            ENDIF
            EPTTAU = EPTTAU + IS(I,J)*IS1(I,J)
30        CONTINUE


          IF(ITER.EQ.(NCTHM+1)) THEN
            EPT = EPT/(64*64)
            EPT2 = EPT2/(64*64)
            WRITE(5,*) 'EPT = ',EPT,' EPT2 = ',EPT2
          ENDIF
          IF (ITER.GT.NCTHM) THEN
            EPTTAU = EPTTAU/(64*64)
            COR = EPTTAU
            CORCON = EPTTAU - EPT*EPT
            CORNRM = CORCON/(EPT2 - EPT*EPT)
            WRITE(5,'(I4,3F13.8)') ITER,CORNRM,CORCON,COR
          ENDIF
          EPTTAU = 0

          IF (ITER.LE.NMEAS) GOTO 50          {Thermalized?
          AI=0.
          DO 40 J=1,LS
           DO 40 I=1,LS          {Total spin
            AI=AI+IS(I,J)
40        CONTINUE
          ASPIN=ASPIN+AI/NSC
          ERPIN=ERPIN+(AI/NSC)**2
          IF(MOD(ITER,NAV).EQ.0) THEN
              AVPIN=ASPIN/NAV   {Average Spin
              ERROR=SQRT((ABS(AVPIN**2-(ERPIN/NAV)))/NAV)
              WRITE (4,*) 'ITER= ',ITER,
     1                    '    AVERAGE SPIN :',AVPIN,' +/- ',ERROR
              TOTAV = TOTAV + AVPIN
              ASPIN=0.
              ERPIN=0.
              NPRI = NPRI + 1
          ENDIF
50      CONTINUE
        WRITE (4,*) 'FINAL AVERAGE = ',TOTAV/NPRI
        WRITE (6,*) 'FINAL AVERAGE = ',TOTAV/NPRI
        TOTAV = 0.
        NPRI = 0
60    CONTINUE
```

```
      TEMP = BETAF
      BETAF = BETAI
      BETAI = TEMP
      STEP = (BETAF-BETAI)/NSTEP

      DO 61 BETA = BETAI,BETAF,STEP
```

The section of the program in the DO 65 loop is identical to that in the DO 60 loop, and has been omitted for brevity.

```
61    CONTINUE
      STOP


70    END
```

Bibliography

[1] Bleeker, David. **Atiyah-Singer Index Formula and Gauge-Theoretic Physics.** Springer-Verlag New York Inc., 1985.

[2] Jordan, D.W. and Smith, P. **Nonlinear Ordinary Differential Equations.** Oxford University Press.

[3] Hirsch, Morris W. **Differential Topoplogy.** Springer-Verlag New York Inc.

[4] Bott, Raoul and Tu, Loring W. **Differential Forms in Algebraic Topology.** Springer-Verlag New York Inc., 1982.

[5] Dodson, and Poston, **Tensor Geometry.** Pitman Publishing Limited, London. 1979.

[6] Cheng, Ta-Pei and Li, Ling-Fong, **Gauge theory of elementary particle physics.** Oxford University Press, 1984.

[7] Richter, R.D. *Principles of Advanced Mathematical Physics VII*, Springer-Verlag, New York, 1981.

[8] Pascual, P. and Tarrach, R. **QCD: Renormalization for the Practitioner.** Springer-Verlag, Heidelberg, 1984.

[9] Amit, Daniel J. **Field Theory, the Renormalization Group, and Critical Phenomena.** World Scientific, Singapore, 1984.

[10] Muta, Taizo **Foundations of Quantum Chromodynamics.** World Scientific Lecture Notes in Physics — Vol. 5, Singapore, 1987.

[11] K. Kawasaki, in **Phase Transitions and Critical Phenomena**, ed. by C. Domb, M.S. Green, vol. 2. Academic Press, New York 1972.

[12] T. M. Apostol, **Mathematical Analysis** Addison-Wesley Publishing Company, Reading, Massachusetts, 1957.

[13] Ph. de Forcrand et al. in **Lattice Gauge Theory 86**, H. Satz, I Harrity and J. Potvin (eds.), Plenum Press, New York, 1987.

[14] Halzen and Martin **Quarks and Gluons.** John Wiley and Sons, New York, 1984.

[15] DeWitt, Bryce **Dynamical Theory of Groups and Fields.** Gordon and Breach New York, 1965.

[16] Butkov, E. **Mathematical Physics.** Addison-Wesley, Mass., 1968.

[17] AMY Collaboration ; KEK 88-109 (1989)

[18] Adler, Stephen L ; Phys. Rev. D 23 (1981) 2901

[19] Adler, Stephen L ; Phys. Rev. D 37 (1988) 458

[20] Adler, Stephen L ; Phys. Rev. 177 (1969) 2426

[21] Allasia, D et. al. ; Z. Phys. C 28 (1985) 321

[22] Aubert, J.J. et. al. ; Nucl. Phys. B272 (1987) 740

[23] Bacilieri, P. ; Phys. Lett. B 214 (1988) 115

[24] Barad, K.M. ; Phys. Rev. D 30 (1984) 1306

[25] Bartels, Jochen and Chang, Shau-Jin ; ILL-TH-89-#32 (1989)

[26] Batrouni, G.G. et al. ; Phys. Rev. D 32 (1985) 2736

[27] Bell, J.S. and Jackiw, R. ; Il Nuovo Cimento (1969) 47

[28] Bender, Carl M. et. al. ; Phys. Rev. Lett. 51 (1983) 1815

[29] Bender, Carl M et. al. ; Phys. Rev. Lett. 56 (1986) 2445

[30] Berg, Bernd A. and Billoire, Alain H. ; FSU-SCRI-88-136 (1988)

[31] Bernard, C. et al ; Phys. Rev. D 27 (1983) 227

[32] Bernaschi, M. et al. ; Phys. Lett. B 228 (1989) 383

[33] Bhanot, G. and Creutz, M. ; Phys. Rev. D 24 (1981) 3212

[34] Bilensky, S.M. and Hosek, J. ; Phys. Rep. 90 (1982) 73

[35] Billoire, A. et al. ; Nucl. Phys. B251 (1985) 581

[36] Billoire, A., Decker, K. and Henzi, R. ; Phys. Lett. B 211 (1988) 124

[37] Bochicchio, M. ; Nucl. Phys. B262 (1985) 331

[38] Born, K.D. et al. ; PITHA 88/19 (1988)

[39] Born, K.D. et al. ; Phys. Rev. D 40 (1989) 1653

[40] Born, K.D. et al. ; Phys. Rev. D 40 (1989) 1664

[41] Bowler, K.C. et. al. ; Nucl. Phys. B296 (1988) 732

[42] Bowler, K.C. ; Phys. Lett. B 161 (1987) 375

[43] Bowler, K.C. et al. ; Nucl. Phys. B284 (1987) 299

[44] Bowler, K.C. et al. ; Nucl. Phys. B296 (1988) 431

[45] Bowler, K.C. et al. ; Nucl. Phys. B301 (1988) 304

[46] Bowler, K.C. et al. ; Phys. Lett. B 162 (1985) 354

[47] Brown, Frank R. and Woch, Thomas J. ; Phys. Rev. Lett 58 (1987) 2394

[48] Cabibbo, Nicola and Marinari, Enzo ; Phys. Lett. B119 (1982) 387

[49] Cahill, Kevin ; ANL-HEP-PR-89-58 (1989)

[50] Cahill, Kevin ; ANL-HEP-PR-89-77 (1989)

[51] Cahill, Kevin ; Lattice 88, Batavia (1988)

[52] Caracciolo, Sergio et al. ; Phys. Lett. B 228 (1989) 375

[53] Caracciolo, Sergio et al. ; SNS 23-88 (1988)

[54] Caselle, M., Fiore, R. and Gliozzi, F. ; Phys. Lett. B 224 (1889) 153

[55] Caswell, William E. ; Phys. Rev. Lett. 33 (1974) 244

[56] Catterall and Wheater, J.F. ; Oxford Preprint (1988)

[57] Celmaster, William ; Phys. Rev. D 26 (1982) 2955

[58] Celmaster, William and Maloof, D. ; Phys. Rev D 24 (1981) 2730

[59] Celmaster, William and Krausz, Frank ; Nucl. Phys. B220 (1983) 434

[60] Chiu, Ting-Wai ; Phys. Lett. B 217 (1989) 151

[61] Chodos, A and Healy, J.B. ; Nucl. Phys. B127 (1977) 426

[62] Christ, N.H. et al. ; Nucl. Phys. B210 (1982) 310

[63] Christ, N.H. ; *1988 Symposium on Lattice Field Theory*, Nucl. Phys. B (Proc. Suppl.)

[64] Clement, Gerard and Stern, Jacqueline ; CERN-TH.5216/88 (1988)

[65] Cleymans, J. Gavai, R. V. and Suhonen, E. ; Phys. Rep. 130 (1986) 217

[66] Cleymans, J. et al. ; Phys. Rev D 39 (1989) 323

[67] Close, F.E. ; (Academic Press, New York, 1979)

[68] Creutz, Michael ; BNL-42028 (1988)

[69] Creutz, Michael ; Phys. Rev. D 36 (1987) 515

[70] Creutz, Michael ; Phys. Rev. D 38 (1988) 1228

[71] Creutz, Michael and Gocksch, Andreas ; BNL – 42601 (1989)

[72] Creutz, Michael ; Phys. Rev. D 21 (1980) 2308

[73] Dagotto, E. and Kogut, J.B. ; Nucl. Phys. B290 (1987) 451

[74] Daniel, David and Kieu, T.D. ; Phys. Lett. B175 (1986) 73

[75] Das, A. ; Z. Phys. C 41 (1988) 505

[76] Davies, C. et al. ; Phys. Rev. D 37 (1988) 1581

[77] De Forcrand, Philippe et al. ; Phys. Lett. B 200 (1988) 143

[78] De Forcrand, Philippe et al. ; Nucl. Phys. B304 (1988) 628

[79] DeTar, Carleton and Kogut, John B. ; Phys. Rev. D 36 (1987) 2828

[80] Dong, Shao-Jing ; ITP-SB-88-59 (1988)

[81] Drouffe, J.M. and Zuber, J. ; Phys. Rep 102 (1983) 1

[82] Duane, S. et al. ; Phys. Lett. 195B (1987) 216

[83] Duane, Simon ; Nucl. Phys. B257 (1985) 652

[84] Duane, Simon and Kogut, John B. ; Phys. Rev. Lett. 55 (1985) 2774

[85] Duncan, A. and Roskies,R. ; Phys. Lett. 126B (1983) 255

[86] Elze, Hans-Thomas and Heinz, U. ; CERN-TH.5325/89 (1989)

[87] Eriksson, K.E. Svartholm, N Skagerstam, B.S. ; J. Math. Phys. 22 (1981) 2276

[88] Espriu, D. et al. ; Nucl. Phys. B275 (1986) 39

[89] Fucito, F. Solomon, S. and Rebbi, C. ; Phys. Rev. D 31 (1985) 1460

[90] Fukugita, M. et. al. ; Phys. Lett. B 191 (1987) 165

[91] Fukugita, M., Oyanagi, Y. and Ukawa, A. ; Phys. Rev. D 36 (1987) 824

[92] Gausterer, H. and Sanielevicie, S. ; Phys. Rev. D 38 (1988) 1220

[93] Gilchrist, J.P. et al. ; Nucl. Phys. B248 (1984) 29

[94] Gliozzi, F ; Nucl. Phys. B204 (1982) 419

[95] Golterman, Maarten ; Nucl. Phys. B273 (1986) 663

[96] Golterman, Maarten and Smit, Jan ; Nucl. Phys. B245 (1984) 61

[97] Golterman, Maarten and Smit, Jan ; Nucl. Phys. B255 (1985) 328

[98] Gottfried, K. ; Phys. Rev. Lett. 18 (1967) 1154

[99] Gottlieb, Steven et al. ; Nucl. Phys. B263 (1986) 704

[100] Gottlieb, Steven et al. ; Phys. Rev. D 36 (1987) 3797

[101] Gottlieb, Steven et. al. ; Phys. Rev. D 35 (1987) 2531

[102] Gottlieb, Steven et. al. ; Phys. Rev. D 38 (1988) 2245

[103] Gottlieb, Steven et. al. ; Phys. Rev. Lett. 59 (1987) 1513

[104] de Groot, E.H. ; Act. Phys. Pol. B16 (1985) 627

[105] Guha, Arunabha and Lee, S.C. ; Phys. Rev. D 27 (1983) 2412

[106] Gupta, Rajan et al. ; Phys. Rev. Lett. 61 (1988) 1996

[107] Gupta, Rajan et al. ; Phys. Lett. B 211 (1988) 132

[108] Gupta, Rajan et al. ; Phys. Rev. D 40 (1989) 2072

[109] Gupta, Rajan et al. ; Phys. Rev. D 36 (1987) 2813

[110] Gusken, S. et al. ; CERN-TH-5304/89 (1989)

[111] Gusken, S. et al. ; CERN-TH-5094/88 (1988)

[112] Hamber, H.W. et al. ; Phys. Lett B 124 (1983) 99

[113] Hamber, Herbert ; Phys. Rev. D 39 (1989) 896

[114] Hamber, Herbert ; UCI 88/11 (1988)

[115] Hamber, Herbert and Parisi, Giorgio ; Phys. Rev. D 27 (1983) 208

[116] Hasenfratz, Anna and Hasenfratz, Peter ; Nucl. Phys. B193 (1981) 210

[117] Hasenfratz, Anna and Hasenfratz, Peter ; Phys. Lett. 93B (1980) 165

[118] Hasenfratz, Peter ; Proc. XXIII HEP Conf., Berk. (1986) 169

[119] Hetrick, James E. and Hosotani, Yutaka ; IASSNS-HEP-89/26 (1989)

[120] Hochberg, David and Thacker, H.B. ; Nucl. Phys. B257 (1985) 729

[121] Hoek, Jaap ; RAL 88-092 (1988)

[122] Hoek, Jaap ; RAL-89-023 (1989)

[123] Horn, D. et al. ; SLAC-PUB-4880 (1989)

[124] Hulsebos, Arjan, Smit, Jan and Vink, Jeroen ; ITFA-88-52 (1988)

[125] Itoh, S., Iwasaki, Y. and Yoshié, T ; Phys. Lett. B 183 (1987) 351

[126] Iwasaki, Y. ; Nucl. Phys. B258 (1985) 141

[127] Iwasaki, Y. and Yoshié, T. ; Phys. Lett. B 216 (1989) 387

[128] Jaffe, R.L. ; CTP 1617 (1988)

[129] Johnson, K. ; Act. Phys. Pol. B6 (1975) 865

[130] Jones, D.R.T. ; Nucl. Phys. B75 (1974) 531

[131] Karsten, Luuk ; Phys. Lett. B104 (1981) 315

[132] Karsten, Luuk and Smit, Jan ; Nucl. Phys. B183 (1981) 103

[133] Kawai, H et al. ; Nucl. Phys. B189 (1981) 40

[134] Kawamoto, N and Smit, J ; Nucl. Phys. B192 (1981) 100

[135] Kennedy, A.D. and Pendleton, B. J. ; Phys. Lett. B156 (1985) 393

[136] Kieu, T.D. ; Phys. Rev. D 38 (1988) 636

[137] Kilcup, G.W. and Sharpe, Stephen R. ; Nucl. Phys. B283 (1987) 493

[138] Kluberg-Stern,H Morel,A and Napoli,O ; Nucl. Phys. B220 (1983) 447

[139] Kogut, John et. al. ; Nucl. Phys. B225 (1983) 326

[140] Kogut, John ; Rev. Mod. Phys. 51 (1979) 659

[141] Kogut, John and Susskind, Leonard ; Phys. Rev. D 11 (1975) 11

[142] Koike, Yuji ; Phys. Lett. B 216 (1989) 184

[143] LaCock, Pierre ; UCT-TP 95/1988 (1988)

[144] Lang, C.B. et al. ; Phys. Lett. B 101 (1981) 173

[145] Lang, C.B. et al. ; Phys. Rev. D 26 (1982) 2028

[146] Langacker, Paul ; DESY 88-076 (1988)

[147] Leutwyler, H. ; BUTP-88/27 (1988)

[148] Lipkin, Harry J. ; ANL-HEP-CP-86-81 (1986)

[149] Lipps, H. et al. ; Phys. Lett. 126B (1983) 250

[150] Loft, R.D. and DeGrand, T.A. ; Phys. Rev. D 39 (1989) 2678

[151] Lüscher, M. ; DESY 88–156 (1988)

[152] Lüscher, M. ; Commun. Math. Phys. 104 (1986) 177

[153] Mack, Richard and Meyer, Steffen ; DESY 89-009 (1989)

[154] Maiani, L. and Martinelli, G. ; Phys. Lett. B 178 (1986) 265

[155] Manton, N.S. ; Phys. Lett. B96 (1980) 328

[156] McCarthy, J.F. ; Phys. Rev. D 39 (1989) 3167

[157] McLerran, Larry ; Rev. Mod. Phys. 58 (1986) 1021

[158] Menotti, P. and Pelissetto, A. ; Phys. Rev. D 35 (1987) 1194

[159] Metropolis, N. et al. ; J. of Chem. Phys. 21 (1953) 1087

[160] Morel, A and Rodrigues, J.P. ; Nucl. Phys. B247 (1984) 44

[161] Negele, J.W. ; CTP#1611 (1988)

[162] Negele, J.W. ; CTP#1623 (1988)

[163] Nielsen, H.B. ; NBI–HE–87–61 (1987)

[164] Nielsen, N.B. and Ninomiya, M. ; Nucl. Phys. B185 (1981) 20

[165] Nielsen, N.B. and Ninomiya, M. ; Nucl. Phys. B193 (1981) 173

[166] Oneda, Sadao and Terasaki, Kunihiko ; Prog. Th. Phys. Suppl. 82 (1985) 1

[167] Ono, S. ; Phys. Rev. D 17 (1978) 888

[168] Pagels, Heinz ; Phys. Rep. 16 (1975) 221

[169] Pang, Yang and Ren, Hai-cang ; Phys. Lett.B 195 (1987) 223

[170] Parisi, Giorgio and Zhang, Yi-Cheng ; Phys. Lett. B132 (1983) 130

[171] Park, I.H. (AMY Collab.) ; AMY 89-12 (1989)

[172] Patel, Apoorva and Gupta, Rajan ; Phys. Lett. B 183 (1987) 193

[173] Patel, Apoorva et al. ; CERN-TH-5379/89 (1989)

[174] Perantonis, S.J. and Wheater, J.F. ; Nucl. Phys. B300 (1988) 443

[175] Polonyi, J. and Wyld, H.W. ; Phys. Rev. Lett. 51 (1983) 2257

[176] Polyakov, A.M. ; Phys. Lett. B 59 (1975) 79,82

[177] Prokhorov, L.V. ; Ottawa-Carleton Inst.for Phys.89-03 (1989)

[178] Rebbi, Claudio ; Sci. Am. Feb. (1983) 36

[179] Reisz, T. ; MPI–PAE/PTh 79/88 (1988)

[180] Remiddi, E. ; *1988 Symposium on Lattice Field Theory*, Nucl. Phys. B (Proc. Suppl.)

[181] Ren, Hai-Cang ; Nucl. Phys. B300 (1988) 531

[182] Samuel, Stuart ; J. Math. Phys. 21 (1980) 2806

[183] Samuel, Stuart ; J. Math. Phys. 21 (1980) 2806

[184] Satz, Helmut ; Nucl. Phys. A400 (1983) 541c

[185] Sharatchandra, H.S. Thun, H.J. Weisz, P ; Nucl. Phys. B192 (1981) 205

[186] Sharpe, Stephen R. ; SLAC Report 336 (1988) 271

[187] Sheikholeslami-sabzevari, Bijan ; Phys. Lett B. 227 (1989) 439

[188] Sloan, T., Smadja, G. and Voss, R. ; Phys. Rep. 162 (1988) 45

[189] Smit, Jan ; Act. Phys. Pol. B17 (1986) 531

[190] Sohnius, Martin F. ; Phys. Rep. 128 (1985)

[191] Stephenson, D.B. ; Nucl. Phys. B295 (1988) 511

[192] Susskind, Leonard ; Les Houches, Session XXIX (1976) 206

[193] Susskind, Leonard ; Phys. Rev. D 16 (1977) 3031

[194] Swendsen, R.H. and Wang, J.-S. ; Phys. Rev. Lett. 58 (1987) 86

[195] Tarasov, O.V. et al. ; Phys. Lett. 93B (1980) 429

[196] 'T Hooft, G. ; Phys. Rev. Lett. 37 (1976) 8

[197] Toussaint, D. ; AZPH-TH/89-6 (1989)

[198] Trivedi, Anil K. ; Phys. Lett. B 230 (1989) 113

[199] Trivedi, Anil K. ; Phys. Rev. Lett. 61 (1988) 907

[200] Ukawa, A. and Fukugita, M. ; Phys. Rev. Lett. 55 (1985) 1854

[201] Ukawa, Akira ; CERN-TH-5245/88 (1988)

[202] Ukawa, Akira ; CERN-TH.5244/88 (1988)

[203] Ukawa, Akira ; CERN-TH.5266/88 (1988)

[204] Van Den Doel, Cees and Smit, Jan ; Nucl. Phys. B228 (9183) 122

[205] Villain, J ; J. Phys. (Paris) 36 (1975) 581

[206] Weinberg, Steven ; Phys. Rev. D 11 (1975) 3583

[207] Weingarten, D. and Petcher, D. ; Phys. Lett. 99B (1981) 333

[208] Weingarten, D.H. and Challifour, J.L. ; Ann. Phys. 123 (1979) 61

[209] Weingarten, D. ; IBM-RC 14378 (1989)

[210] Weisz, P. ; Nucl. Phys. B212 (1983) 1

[211] Wilczek, Frank ; Phys. Rev. Lett. 59 (1987) 2397

[212] Wilson, Kenneth G. ; Phys. Rev. D 10 (1974) 2445

[213] Wilson, Kenneth G. ; Rev. Mod. Phys. 55 (1983) 583

[214] Wilson, Kenneth G. and Kogut, John ; Phys. Rep. 12C (1974)

[215] Wolff, Ulli ; DESY 87-082 (1987)

[216] Wolff, Ulli ; Phys. Lett. B 228 (1989) 379

[217] Wu, S.L. ; Phys. Rep. 107 (1984) 59